Monte Carlo treatment planning with modulated electron radiotherapy: framework development and application

Andrew William Alexander

Doctor of Philosophy

Department of Physics

McGill University

Montréal, Quebec

2011-12-1

A thesis submitted to McGill University in partial fulfillment of the requirements of the degree of Doctor of Philosophy

DEDICATION

For all patients receiving radiotherapy.

&

For my family and friends, who offered me love and support throughout the course of my work.

ACKNOWLEDGEMENTS

I would like to thank my two supervisors, Dr. Jan Seuntjens and Dr. François DeBlois for their guidance and enthusiastic encouragement for this work. I have enjoyed my time while working on this project and gained a wealth of information in the process. The success of this project is largely due to their support, patience, and teachings.

I especially thank Sarah Finch for her constant support of my work. She was always there to provided help with my presentations, abstracts, and papers.

I would also like to express my gratitude to the staff of the McGill Medical Physics Unit. The infrastructure and research tools available to me are due to the timeless efforts of various people throughout the department. I especially thank Margery Knewstubb and Tatjana Nisic for their administrative support of my work.

Support from individuals was truly appreciated. In particular: Magdalena Bazalova for her expertise in Monte Carlo applications, Emilie Soisson for her expertise in clinical medical physics and treatment planning, Tanner Connell and Wamied Abdel-Rahman for their dedication to maintaining the research cluster, John Kildea for his encouraging words of support, Dr. Tarek Hijal for his dedication to the breast boost study and teachings about clinical radiation oncology. Line Comeau for volunteering to be the first dosimetrist MMCTP user and for providing high quality feedback on the usability of MMCTP. Tanya Bradley and Christophe Furstoss for reviewing this thesis.

My sincere thanks to my friends at McGill: Arman, Eunah, Tanner, Pavlos, Marc-André, Kyu, Steve, Emilie, John, Danielle, Erika, Derek, Christophe, Magdalena, Emily, Ismail, Guillaume, Jonathan, Marc, Ellis, Gabriella, and Joseph. A special thanks to Lina and Rasha for sticking through the early development of MMCTP.

Funding in support of the research presented in this thesis has been provided by the Terry Fox Foundation Strategic Initiative for Excellence in Radiation Research for the 21st Century (EIRR21) at CIHR and CIHR grant MOP 79448 and NCIC TFF grant # 016298.

ABSTRACT

Within the field of medical physics, Monte Carlo radiation transport simulations are considered to be the most accurate method for the determination of dose distributions in patients. The McGill Monte Carlo treatment planning system (MMCTP), provides a flexible software environment to integrate Monte Carlo simulations with current and new treatment modalities. A developing treatment modality called energy and intensity modulated electron radiotherapy (MERT) is a promising modality, which has the fundamental capabilities to enhance the dosimetry of superficial targets. An objective of this work is to advance the research and development of MERT with the end goal of clinical use. To this end, we present the MMCTP system with an integrated toolkit for MERT planning and delivery of MERT fields. Delivery is achieved using an automated "few leaf electron collimator" (FLEC) and a controller. Aside from the MERT planning toolkit, the MMCTP system required numerous add-ons to perform the complex task of large-scale autonomous Monte Carlo simulations. The first was a DICOM import filter, followed by the implementation of DOSXYZnrc as a dose calculation engine and by logic methods for submitting and updating the status of Monte Carlo simulations. Within this work we validated the MMCTP system with a head and neck Monte Carlo recalculation study performed by a medical dosimetrist. The impact of MMCTP lies in the fact that it allows for systematic and platform independent large-scale Monte Carlo dose calculations for different treatment sites and treatment modalities. In addition to the MERT planning tools,

various optimization algorithms were created external to MMCTP. The algorithms produced MERT treatment plans based on dose volume constraints that employ Monte Carlo pre-generated patient-specific kernels. The Monte Carlo kernels are generated from patient-specific Monte Carlo dose distributions within MMCTP. The structure of the MERT planning toolkit software and optimization algorithms are demonstrated. We investigated the clinical significance of MERT on spinal irradiation, breast boost irradiation, and a head and neck sarcoma cancer site using several parameters to analyze the treatment plans. Finally, we investigated the idea of mixed beam photon and electron treatment planning. Photon optimization treatment planning tools were included within the MERT planning toolkit for the purpose of mixed beam optimization.

In conclusion, this thesis work has resulted in the development of an advanced framework for photon and electron Monte Carlo treatment planning studies and the development of an inverse planning system for photon, electron or mixed beam radiotherapy (MBRT). The justification and validation of this work is found within the results of the planning studies, which have demonstrated dosimetric advantages to using MERT or MBRT in comparison to clinical treatment alternatives.

ABRÉGÉ

La technique Monte Carlo de transport de particules est considéré la méthode la plus précise pour calculer la distribution de dose dans les patients. La plateforme de planification de traitement Monte Carlo de McGill (MMCTP) offre un environnement de logiciels flexibles pour intégrer des simulations Monte Carlo avec les modalités de traitement actuelles et nouvelles. Une nouvelle modalité de traitement surnommée MERT devrait améliorer la dosimétrie sur des cibles superficielles. Un des objectifs de ce travail est d'avancer la recherche et le développement de MERT à des fins d'usage clinique. Ainsi, nous présentons la plateforme MMCTP avec une boite à outils intégrée pour la planification et l'administration de plans MERT. Ces plans sont administrés à l'aide d'un collimateur automatisé surnommé FLEC et d'un contrôleur. En plus des outils de planification MERT, la plateforme MMCTP a nécessité plusieurs ajouts pour effectuer les taches complexes impliquées dans l'automatisation des simulations Monte Carlo à large échelle. La première addition était un filtre d'importation DICOM, suivie par l'implémentation de DOSXYZnrc comme outil de calcul de dose puis l'implémentation des méthodes logiques pour soumettre et mettre à jour le statut des simulations Monte Carlo. Dans ce travail, nous avons validé la plateforme MMCTP en recalculant avec le code Monte Carlo un plan tête et cou réalisé initialement par un dosimétriste médical. L'impact de MMCTP réside dans le fait qu'il permet des calculs de dose Monte Carlo à grande échelle avec une plateforme indépendante et systématique pour différents sites et différentes

modalités de traitement. En plus des outils de plannification MERT, différents algorithmes d'optimisation ont été créés indépendamment de MMCTP. Ces algorithmes produisent des plans de traitement MERT basés sur des contraintes dose volume en utilisant des kernels pré-générés Monte Carlo de patient spécifiques. Les kernels Monte Carlo sont générés à partir des distributions de dose Monte Carlo de patient spécifique dans MMCTP. La structure des algorithmes d'optimisation et du logiciel de la boite d'outils de planification sont démontrées. Nous avons également étudié l'impact clinique de MERT sur les irradiations de la colonne, les irradiations accélérées de sein, les irradiations de la tête et des sarcomes du cou en utilisant plusieurs paramètres pour analyser les plans de traitement. Finalement, nous avons cherché à combiner des plans de traitement photons avec d'autres d'électrons. Les outils d'optimisation du plan de traitement en photon ont été inclus dans la boite à outils de planification de MERT dans le but d'optimiser la combinaison des faisceaux. En conclusion, le travail de cette thèse a permis de développer une plateforme avancée pour les études de planification de traitement Monte Carlo en photons et en électrons. Il a également permis de développer un système de planification inverse pour photon, électron ou la radiothérapie de faisceaux combinés (MBRT pour "Mixed Beam RadioTherapy"). La justification et la validation de ce travail sont démontrées à travers les résultats des études de planification, qui ont déterminées les avantages dosimétriques d'utiliser MERT ou MBRT par rapport aux alternatives cliniques de traitement.

TABLE OF CONTENTS

LIST OF FIGURES

LIST OF TABLES

STATEMENT OF ORIGINALITY

The complexity of modulated electron radiotherapy (MERT) has so far limited its clinical applications. High quality MERT plans require an automated beam shaping system, an accurate dose calculation engine, and an inverse optimization algorithm. In light of this we have developed an advanced treatment planning system (MMCTP) which employs Monte Carlo codes for dose calculation. The MMCTP system is unique as it allows for autonomous dose calculations for a wide array of treatment techniques and machines. This includes Varian CL21EX accelerators from electron cutout fields to photon RapidArc fields, Siemens conformal photon therapy, and tomotherapy volumetric modulated arc therapy. Although others have developed Monte Carlo treatment planning systems, none appear to have developed an autonomous system to convert clinical DICOM data to treatment planning data with full access to edit planning parameters and maintain the ability to convert planning data to Monte Carlo input data with full access to edit Monte Carlo parameters. In addition, the MMCTP system is designed to be used by non-Monte Carlo specialists such as a dosimetrist, as highlighted in our head and neck IMRT study. The autonomous job control logic within MMCTP overcomes the tedious process of generating, transferring, submitting, and tracking of the hundreds or thousands of Monte Carlo input and output files required in the generation of beamlet dose distributions for inverse plan optimization. We have developed a phase-space database within MMCTP to further reduce the calculation time associated with our Monte Carlo simulations.

The database automatically reuses and links previous simulations of the same type with new ones.

We have developed an inverse plan optimization toolkit for MMCTP to streamline the process of MERT planning. The toolkit makes use of the DICOM structure data to identify and rank potential external beam angles based on the target and external contour positions. We have investigated the effect of subfields on overall plan quality with the use of raster or feathered beamlets. Additionally, beamlets may be collimated based on target depth. We have linked the toolkit with three C optimization codes developed for MERT. Optimization runs can be saved within an output database to visualize and compare two or more competing plans. We have integrated photon and electron optimization within the planning toolkit to examine mixed beam radiotherapy plans. We have developed an advanced few leaf electron collimator (FLEC) controller to efficiently drive the FLEC field and linac settings. The controller acquires a sequence of aperture settings from an optimization run to automatically deliver a FLEC plan. None of the previously reported investigations addressed existence of a Monte Carlo treatment planning system with inverse optimization tools for the purpose of MERT that is practical, autonomous, and connects to an automated MERT delivery system. So far very little research has examined the reproducibility of the dosimetric advantages of MERT particularly with advanced photon techniques such as volumetric arc therapy, as presented in our breast boost MERT planning study. Previous research on the topic is often purely theoretical because means of delivery were not established or focused on the dosimetric characteristics of an

electron collimator. We present a comprehensive evaluation of FLEC-based MERT planning. We show that it provides a valuable addition to the current photon or electron treatment planning techniques when applied to superficially located tumours. In addition, we show the dosimetric benefit of producing mixed beam treatments using photons and electrons.

CONTRIBUTIONS OF AUTHORS

This thesis consists of five manuscripts, three published and two submitted. I was responsible for writing the manuscripts and performing the experimental work. Several authors have contributed to the manuscripts.

The work presented in the paper entitled "MMCTP: A radiotherapy research environment for Monte Carlo and patient-specific treatment planning", was initiated by Dr. Jan Seuntjens and early versions of the code by Dr. François DeBlois. At the time of publication, the percentage of MMCTP code developed by myself was over eighty-percent. Dr. Gabriela Stroian, Dr. Khalid Al-Yahya, and Dr. Emily Heath were involved in the initial testing of MMCTP and the manuscript review.

The work presented in the paper entitled "Patient comparison between the Analytic Anisotropic Algorithm and Monte Carlo dose calculation for head and neck patients treated with simultaneous integrated boost intensity-modulated radiation therapy", was initiated by Dr. Emilie Soisson and Line Comeau as a feasibility test of the clinical installation of MMCTP. Line Comeau collected the DICOM patients and recalculated them in MMCTP. Analysis of the results and the manuscript was done by myself and reviewed by all the co-authors.

The work presented in the paper entitled "Towards automatic field selection and planning using Monte Carlo-based direct aperture optimization in modulated electron radiotherapy" was carried out by myself under the supervision of my

supervisors. Dr. Jan Seuntjens assisted in the C optimization programs and carefully revised the manuscript.

The work presented in the paper entitled "Comparison of modulated electron radiotherapy to conventional electron boost irradiation and volumetric modulated photon arc therapy for the treatment of tumour bed boost in breast cancer" was initiated by Dr. Emilie Soisson, Dr. Tarek Hijal, and myself. Dr. Emilie Soisson and Dr. Tarek Hijal were responsible for creating the clinical treatment plans with the assistance of Dr. Arman Sarfehnia, while I created the modulated electron plans, analyzed the results, and wrote the manuscript. The manuscript was reviewed by all co-authors.

The work presented in the paper entitled "Dynamic jaw optimization" was initiated by myself under the supervision of Dr. Jan Seuntjens. Dr. Emilie Soisson was responsible for creating the clinical treatment plans within this study. Marc-André Renaud assisted with the optimization code and provided thoughtful programming insight. I wrote the manuscript and the co-authors reviewed the manuscript.

CHAPTER 1
Introduction

Contents

1.1 Radiotherapy

Radiotherapy uses radiation for the treatment of a variety of diseases. The aim of radiotherapy is to deliver an accurate dose of radiation to a precise location of interest with minimal damage to surrounding healthy tissues. This results in the eradication of the disease, the prolongation of life, and the improvement in the quality of life [1]. Radiotherapy as a cancer treatment modality is used to relieve symptoms and control the progression of cancer cells in curative treatments (including adjuvant therapy), and palliative care. If a patient is to receive radiotherapy, the tumour volume, location, and cell type dictate the type of treatment chosen. Clinical application of radiotherapy commenced shortly after the discovery

of x-rays by Wilhelm Conrad Röntgen on 8 November 1895; the first reported case in the literature occurred in January 1896 [2]. Today about 50% of cancer patients are treated with radiation [3] and in Canada, the Canadian Cancer Society predicted 173,800 new cases of cancer for 2010 with 76,200 deaths [4]. In an effort to increase the effectiveness of their treatment, cancer patients commonly receive a combination of treatments concurrently or sequentially that may include surgery, chemotherapy, and radiotherapy.

Radiotherapy sources for cancer treatments produce ionizing radiation. Ionizing radiation is capable of ionizing matter, as the radiation energy is above the ionization potential of atoms. As ionizing radiation travels through matter, such as the human body, it deposits energy along its path length to the medium. This deposited energy can cause single and double strand DNA breaks within cells along the path of radiation. The cell will attempt to repair and correct the DNA damage through DNA repair. When DNA repair fails, the cell may enter apoptosis, also known as programmed cell death. The probability of cell death is correlated to the amount of dose (D), defined as the energy absorbed (dE) per unit mass (m) of tissue with SI units for J/kg and symbol Gy.

$$D = \frac{dE}{dm} \tag{1.1}$$

The primary challenge in radiotherapy is the trade off between destroying cancer cells and damaging healthy tissue. In an ideal world, radiation would only cause damage to the cancer cells. However, normal cells or healthy tissues are affected by exposure to ionizing radiation. All disease free tissue is classified or

labeled as: healthy tissue or normal tissue or normal cells. Radiotherapy relies on precise delivery of radiation to the tumour volume, while sparing as much as possible, healthy tissues. Radiation fields conform to the dimensions of the tumour or lesion to minimize the dose to healthy tissue, but the irradiation of some tissue is unavoidable. A second complication arises from the dose response curves. In an ideal world, the tumour is more sensitive or has less ability to repair damage than the surrounding tissue. Ideal dose response curves for tumour control probability (TCP) and normal tissue complication probability (NTCP) are illustrated in figure 1–1. The sigmoidal property of the tumour control curve reveal a threshold dose, a steep gradient, and an asymptotic plateau nearing 100% response. Due to the steep dose response gradient a 2% difference in dose could translate into a larger than 2% difference in TCP. The dose response curves in figure 1–1 have been drawn with the TCP curve to the left of the NTCP curve. With this convention, the optimum choice of radiation dose is one that maximizes TCP and minimizes NTCP. It should be noted however, that the classical ideal picture in figure 1–1 is not always correct. Normal tissue complications may occur at lower doses than tumour control. In addition, for some cases, tumour control never reaches 100% for a variety of reasons [1](such as radiosensitivity). Thus it is through advanced treatment planning and the 4-R's of radiotherapy (Repair, Reoxygenation, Redistribution, and Repopulation) that the TCP can be kept above the NTCP. In order to achieve 95% TCP, a radiation oncologist will prescribe a lethal tumour dose. A lethal dose depends on the radiation type, cell radiosensitivity, and hypoxia.

In general, the data that is used to generate TCP and NTCP curves, is typically derived from literature and from "clinical experience". Much of the dataset is not complete as many of these TCP curves only contain data at the top of the curve while the NTCP curves only contain data at the bottom of the curve [1]. Animal experimentation has added insight to these dose response curves. However, due to the remaining uncertainty in TCP and NTCP curves and the variations within clinical datasets, clinical radiation oncology relies on large-scale multi-centered treatment protocols for advancing our understanding of the effects of radiation on the human body. In 2005, El Naqa developed a comprehensive software package for researchers to computer their own TCP and NTCP models based on their own clinical data [5].

In radiotherapy, the dose given to the tumour is limited by the dose given to surrounding tissues. Some of the side effects of radiotherapy include fatigue, skin reactions or hair loss. These effects are primarily due to the loss of normal tissue. Recent advances in radiotherapy aim at minimizing the dose to normal tissue while maintaining or escalating the tumour control [6]. Some of these techniques include external 3D conformal radiation therapy (3D-CRT) or intensity modulated radiation therapy (IMRT) with multiple isocentric beams.

In today's modern cancer centre hospital, a radiotherapy department can administer radiation to a patient using a number of methods. Radiotherapy is divided into two types, external and brachytherapy. External radiotherapy involves a radiation source which is external to the patient. Brachytherapy involves internal or external radiation, where radioactive sources on the order of millimetres in size,

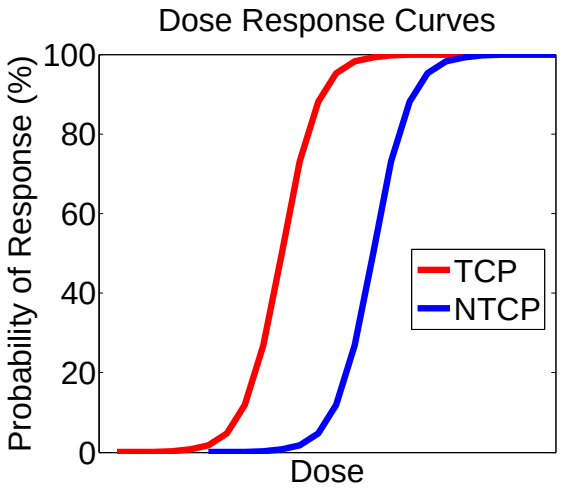

Figure 1–1: Ideal dose response curves for tumour control probability (TCP) and normal tissue complication probability (NTCP). The sigmoidal shape and position of these curves varies in different clinical circumstances depending on the radiosensitivity of the tumour and normal tissue cells.

are placed in proximity of the tumour or lesion. The particle type and energy varies between these methods from electrons, positrons, photons, protons, carbon ions and alpha particles within the energy range from keV to MeV. Distinctions in particle type and energy define the properties of the lateral and depth dose profiles. Linear accelerator based external beam radiotherapy typically consists of electrons within the energy range from 4 to 20 MeV and a photon spectrum produced within a metallic target within the following photon energies 6, 10, 15, 18, and 20 MV. Radiation treatments are tailored to ensure that the physical properties of the radiation beam are appropriate for the treatment goals. In general, linear accelerator produced electrons are used in superficial treatments due to the average energy loss of 2 MeV/cm in water that limits the penetration depth

of therapy electrons, while photons are used in deep-seated treatments. In current practice, linac photon treatments are the most common radiotherapy modality. As such, various methods have been developed to calculate the total energy deposited within a patient undergoing photon irradiation.

1.2 Radiotherapy Research

Radiotherapy research can involve many disciplines of science and engineering. Historically, the main three were physics, radiobiology, and radiation oncology. Innovative research in these disciplines has translated into the development of new treatment machines, techniques, and protocols for improved radiation therapy. In today's multidisciplinary research centres, radiotherapy research projects may involve molecular radiation biology, human tumour translational studies, precision radiation therapy deliveries, computational biology, clinical trials, and population-based health outcome research. The work developed within this thesis fits within the following areas of radiotherapy research: physics dosimetry, development of novel treatment techniques, and precision of radiotherapy deliveries.

1.3 The Role of External Beam Treatment Planning in Radiotherapy

All applications of radiotherapy require some form of treatment planning. By definition, radiotherapy treatment planning is an optimization problem where the aim is to find a plan, which maximizes the probability of target eradication and minimizes the damage to surrounding healthy tissues. The optimization process must be considerate of the radiation particle type, energy, radiation source location, and field collimation, in addition to the human side whereby the target location may be affected by motion (internal and external). For example, there

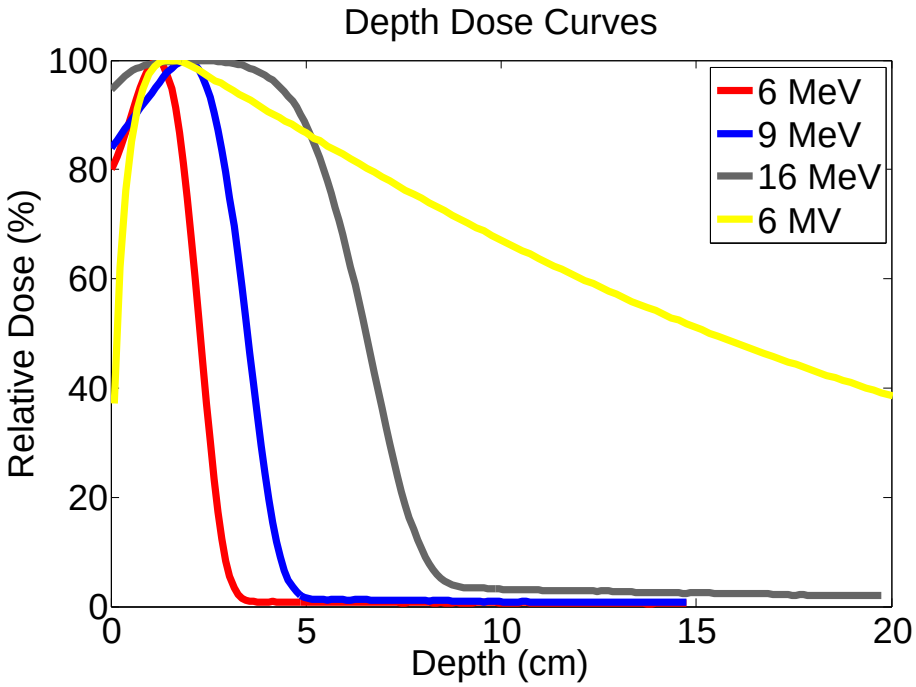

Figure 1–2: 10×10 cm^2 field sized depth dose curves in water for three electron beam energies (6, 9, and 16 MeV) and one photon beam energy (6 MV).

are distinct differences between the depth dose curves from electrons and photons. Particle energy will also affect the depth dose curve. Percentage depth dose curves (PDD) for various radiotherapy beams are plotted in figure 1–2.

The planning process has evolved with the introduction of computers and imaging modalities. Computers have allowed radiotherapy departments to calculate dose distributions for individual patients within a complex treatment planning system (TPS). In today's TPS, computerized tomography (CT) images are the standard image dataset required for 3D treatment planning and dose distribution calculations. The 3D image dataset has enabled accurate localization of the tumour and critical tissues. In addition, the 3D dose calculation has enabled

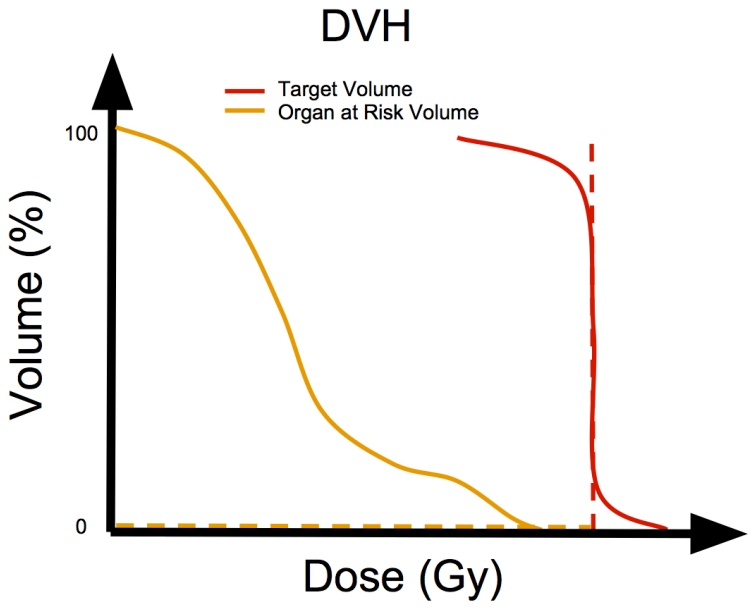

Figure 1–3: Dose volume histogram (DVH) graph for ideal and realistic scenario. The dashed lines represent the ideal situation where a uniform dose is given to the target volume and zero dose is given to the organ at risk. The solid lines represent reality.

accurate dose volume statistics for the tumour and critical tissues. During dose calculation, the 3D images are down-sampled to a typical dose scoring voxel resolution of $0.25 \times 0.25 \times 0.3$ cm^3. A dose distribution is simply a 3D matrix of dose voxels. A dose volume statistic, such as a dose volume histogram (DVH), is created by analyzing the dose voxels within a volume of interest. The DVH curve plots the fraction of volume, which receives a specific dose value. In clinical radiation oncology, the DVH is often expressed as a cumulative DVH plot. The cumulative DVH plots the fraction of volume, which receives at least a specific dose value. For example, the cumulative DVH is plotted in figure 1–3 for an ideal

and realistic radiotherapy plan. Notice that the ideal plan delivers a single dose value to the entire volume of interest without depositing any dose within the organ at risk. The DVH graphs of the target volume, organs at risk (OAR), and healthy tissues allow for quick assessment of overall plan quality. As such, the DVH is often the first quantitative metric used to critique a radiotherapy plan. Consequently, DVH graphs of multiple plans may be overlaid for quick assessment of the trade-offs between competing plans.

1.4 Hypothesis

This thesis work focuses on the development of external beam energy and intensity modulated electron therapy (MERT) for applications in clinical radiotherapy. It is hypothesized that there exists a range of clinical scenarios where MERT treatment plans can out-compete the current standard of care in terms of dosimetric plan quality, as well as out-compete even the most advanced photon intensity modulated treatment plans. The prerequisites for this work involved the development of an advanced treatment planning system for the generation of modulated electrons plans and the development of a motorized electron collimator.

1.5 Objectives

The main objectives of the thesis are:

1. The development of an electron Monte Carlo treatment planning system (MMCTP) for accurate, large scale electron dosimetry.
2. The development of an inverse optimization system for FLEC-based MERT.
3. The development of motion control software for a motorized electron collimator.

4. To demonstrate the dosimetric advantages of FLEC-based MERT.

1.6 Thesis Outline

The thesis consists of five manuscripts, three of which were published and the remaining two have been submitted. The thesis is organized as follows: Chapter 2 introduces the historical, physical, and clinical aspects of external beam radiotherapy treatment planning. In Chapter 3, the MMCTP system (McGill Monte Carlo Treatment Planning) is described as presented in its published form. Chapter 4, describes a number of instrumental updates to MMCTP for its use as an intuitive, independent Monte Carlo treatment planning system. The motivation for these updates was to enable non-Monte Carlo specialists access to a clinical Monte Carlo TPS. A detailed discussion on the modulated electron radiotherapy toolkit is also provided. The clinical installation and use of MMCTP is described in Chapter 5, with the IMRT head and neck recalculation study. Chapter 6 presents a manuscript which describes the integrated planning approach to FLEC-based MERT. The manuscript presents and contrasts two competing beamlet arrangements techniques for MERT. Chapter 7 describes an in-depth study on the quality of MERT plans for breast boost irradiation. The clinical advantages of MERT versus photon IMRT are discussed. Chapter 8 describes a third approach to FLEC-based MERT optimization, which dynamically optimizes the aperture shapes and beamlet weights. The approach yields MERT plans with less beamlets and larger aperture shapes. Appendix A describes the FLEC control software (FLOC), which manages the workflow in delivering FLEC-based MERT

sequences. The FLOC software interfaces with the FLEC, linac, and treatment planning system. The thesis conclusions are presented in Chapter 9.

1.7 Other manuscripts

There are four other manuscripts (currently under review) I participated in during my studies; I was not the main investigator and these manuscripts are not directly related to my thesis work.

1. T Connell, A Alexander, M Evans and J Seuntjens *An experimental feasibility study on the use of scattering foil free beams for modulated electron radiotherapy*
2. E Conneely, A Alexander, G Stroian, J Seuntjens and M Foley *An investigation into a simplified method to tune Monte Carlo accelerator source parameters and testing its clinical application*
3. E Conneely, A Alexander, R Ruo, M Foley and J Seuntjens *Monte Carlo investigation of collapsed versus rotated IMRT plan verification*
4. M Serban, J Seuntjens, E Roussin, A Alexander, J Tremblay and W Wierzbicki *Modular patient-specific compensation for Co-60 TBI treatments based on Monte Carlo design: A feasibility study*

1.8 References

[1] J V Dyk. *The Modern Technology of Radiation Oncology.* Medical Physics Publishing, Madison, Wisconsin, 1st edition, 1999.

[2] GT Beatson. On the treatment of inoperable cases of carcinoma of the mamma: suggestions for a new method of treatment, with illustrative cases. *Lancet*, 148(3803):104–107, 1896.

[3] Adrian C Begg, Fiona A Stewart, and Conchita Vens. Strategies to improve radiotherapy with targeted drugs. *Nature reviews. Cancer*, 11(4):239–253, 2011.

[4] Canadian Cancer Society. Canadian cancer statistics 2010. Technical report, Canadian Cancer Society, Statistics Canada, 2010.

[5] I El Naqa, G Suneja, P E Lindsay, A J Hope, J R Alaly, M Vicic, J D Bradley, A Apte, and J O Deasy. Dose response explorer: an integrated open-source tool for exploring and modelling radiotherapy dose-volume outcome relationships. *Phys. Med. Biol.*, 51(22):5719–5735, 2006.

[6] SA Bhide. Recent advances in radiotherapy. *BMC medicine*, 8(25):1–5, 2010.

CHAPTER 2
Introduction to External Beam Radiotherapy Treatment Planning

Contents

Figure 2–1: Typical linac for external beam radiotherapy. [Author Dina Wakulchik. Reprinted with permission under Creative Commons Attribution 2.0 Generic license]

Once a patient has been diagnosed with cancer, the oncologist assigns a therapy based on a wide range of variables. Their therapy will often include a treatment of external beam radiotherapy. A typical treatment unit as shown in figure 2–1 uses a radiation source or linear accelerator (linac) mounted on a 360° rotating gantry. The patient lies on a moveable treatment couch with 6 degrees of freedom. A typical patient setup would place the position of the treatment volume at isocentre with respect to motion of the gantry, couch, and linac collimator.

Well before a patient enters the treatment room for his/her first treatment, a radiotherapy department has finalized the complex process of radiation treatment planning for said patient. The process involves the following steps [1]:

1. Diagnosis and 3D imaging: 3D images are acquired typically from CT simulators to reconstruct the 3D volumes of interest. This includes delineation of the tumour volume and healthy tissues, which are in close proximity to the tumour location.
2. Treatment guidelines: Tumour dose prescription and healthy tissue dose tolerances are recorded by a physician with a suggested treatment technique.
3. Treatment unit and technique selection: A treatment machine and technique is selected based on the complexity of the treatment, active treatment protocols, and departmental policies.
4. Treatment planning: A dosimetrist or physicist generates a treatment plan using 3D treatment planning software.
5. Plan evaluation: The physician reviews the plan with the dosimetrist or physicist. If the plan does not meet the objectives of the prescription, the process may jump back to step 1 or 2.
6. Plan approval: The physician approves the plan and assigns a prescription dose. The treatment plan is now normalized to the prescription dose and is ready for delivery.
7. Treatment verification and delivery: Once the plan has been approved, a physicist verifies the accuracy of the treatment planning software in

determining the dose to the patient, and precision of the treatment machines in delivering the planned dose.

Depending on a number of clinical and practical issues, the planning process may take anywhere from a few days to a few weeks. This chapter introduces the concepts and challenges in current radiotherapy treatment planning.

2.1 Treatment Planning

Treatment planning has evolved from the use of tables and charts to predict patient dose, to complex 3D software capable of modelling patient specific dose distributions. The planning process begins with a 3D x-ray CT dataset. Afterwards, the 3D images are imported into a TPS, where a physician delineates the volumes of interest. Volumes include the planning target volume (PTV) and identifying the various organs at risk (OAR) volumes. These volumes are required within the treatment planning software to enable dose volume statistics for the PTV and OAR. Typical dose volume statistics include the DVH and specifically the following points: maximum dose (D_{max}), minimum dose (D_{min}), mean dose (D_{mean}), 'near minimum dose' [2] received by 98% of the volume ($D_{98\%}$), dose received by 95% of the volume ($D_{95\%}$), and 'near maximum dose' [2] received by 2% of the volume ($D_{2\%}$). These dosimetric endpoints are used to evaluate and critique the merits of one plan versus another. The standard goal for treatment planning is to cover the PTV with at least 95% of the prescription dose while minimizing the dose to the OAR [3, 4]. The challenge for treatment planners is to find the right balance between target coverage and normal tissue complication. Proper target coverage is essential for eradicating the tumour cells and minimizing the risk of

tumour recurrence; however, radiation toxicity to normal tissue can drastically alter patient quality of life.

2.1.1 Conformal Treatment Planning

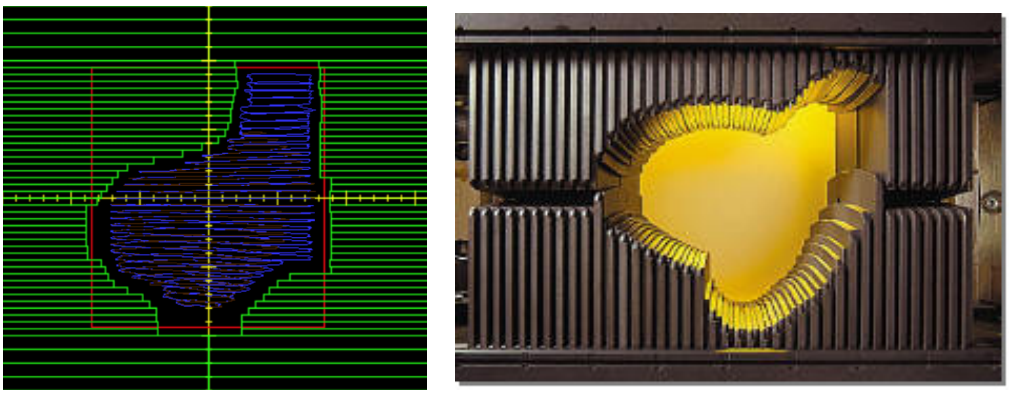

(a) (b)

Figure 2–2: MMCTP image of MLC field adjusted to the shape of the tumour volume (blue object) (a). Photo of a Varian 120 leaf Millennium MLC (b) [Reprinted with permission from Varian Medical Systems, Palo Alto, CA].

Before the advent of CT images for 3D treatment planning, plans were produced using less accurate methods such as the use of bony landmarks, soft tissue edges, and skin-topography to define the field shapes. Treatment machines were designed to produce large flat fields for uniform tumour radiation. In order to compensate for beam obliquity, due to the irregular shape of a patient's body, wedged beam modifiers were placed in the beam [5]. With the advent of CT images for 3D planning, planners were now able to shape the prescription dose volume to the PTV, while at the same time, keeping the dose to the organs at risk at or below their tolerance dose [1]. Over the years, the need to adjust beam collimation to the shape of the cross-sectional area of the tumour led to

the development of a high resolution double-focused multileaf collimator (MLC). Figure 2–2 shows an example of a MLC defined field and photograph of a MLC. The MLC together with 3D images were used to produce 3D conformal treatments (3D-CRT). A 3D-CRT plan will typically produce a homogeneous dose region within the tumour volume. Conformal treatments are ideal for convex tumour sites; however, they inherently overdose normal tissue for concave tumour sites. To overcome this issue, Brahme [6] proposed a new type of treatment technique using intensity modulated beams (IMRT) to create a homogeneous dose pattern for concave tumour sites. Shaping the dose to the structure of the tumour volume was made possible through the use of a large number of independent small sized radiation beams collimated by the MLC. With the use of a large number of independent beams, the potential for creating highly conformal treatments is greatly improved versus conformal 3D therapy.

2.1.2 Inverse Treatment Planning

IMRT provides the treatment planner with more control than conformal radiotherapy to shape the structure of the dose distribution for PTV coverage and OAR avoidance. IMRT allows us to push the dose conformation potential to the physical limits; the penumbra between the target and the OAR can be made as narrow as the boundary of a single fixed field [7]. The first commercially available inverse-planned IMRT planning system (MiMiC MLC and Peacock, NOMOS Corporation, Pittsburgh, PA) was released in 1993. Since then, IMRT has become a standard technique in radiotherapy departments for a variety of tumour sites. In photon IMRT, field intensity is modulated through the movement of MLC leaves.

There are two types of MLC deliveries: dynamic, and step and shoot. A dynamic delivery entails movement of the MLC leaves while the beam is on, whereas a step and shoot delivery entails a series of static MLC apertures. Inverse treatment planning involves the use of a mathematical function to express the priorities of a plan during an iterative optimization search of the available solution space. The optimization run produces a fluence map per gantry angle, which represents the relative intensity weight of each spatially independent beamlet. Beamlets represent the discretization of the MLC aperture into hundreds or thousands of discrete beams. These beamlets are typically on the order of 0.5×0.5 cm^2 and are visible in the fluence maps of a prostate IMRT plan as shown in figure 2–3. A typical optimization system will produce an ideal fluence map which will require a translation into a deliverable MLC pattern for treatment delivery.

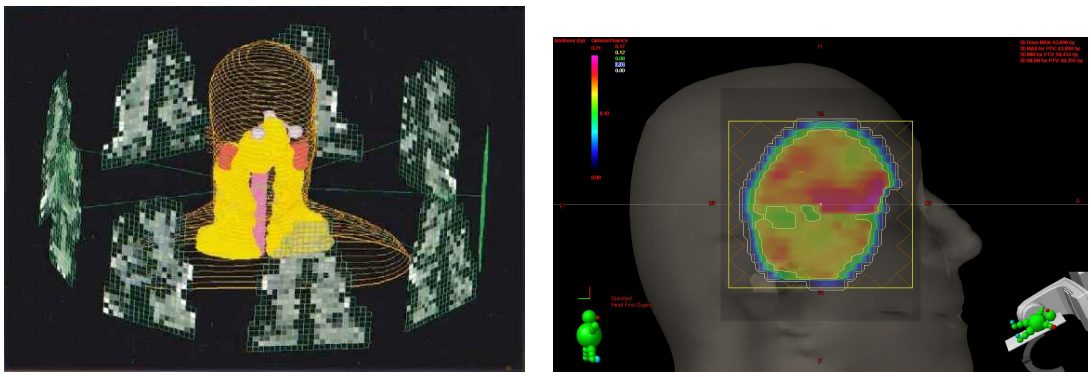

(a) (b)

Figure 2–3: 3D illustration of the IMRT fluence maps per gantry angle for a 7 beam IMRT prostate plan (a) [8], 2D colour map illustration of fluence for one IMRT beam (b). Source http://www.drrajurao.com

Today there is widespread interest in the use of inverse treatment planning for radiotherapy as evident in the growing number of available systems on the

market. Inverse treatment planning systems for external beam therapy at the McGill University Health Centre include: TomoTherapy (TomoTherapy, Madison, WI), Varian's RapidArc and IMRT (Varian Medical Systems, Palo Alto, CA), and BRAINLAB (Brainlab, Munich, Germany). However, due to the complexity of generating inverse plans, treatment planning systems often employ various time saving measures which affect the quality and accuracy of treatments [9]. Approximations in the dose calculation algorithms and subsequent post-optimization procedures lead to dose prediction errors (DPEs) and optimization-convergence errors (OCEs) [10]. To minimize these errors, Dogan *et al* [9], emphasized the importance of using the most accurate available dose calculation algorithm during optimization.

2.1.3 Electron Treatment Techniques

Electron treatments are reserved for superficial or subcutaneous disease, and are regarded as simple due to the use of a single field for treatment. A cutaway view of an electron field shown in figure 2–4 illustrates the electron applicator and cutout plane. The cutout plane defines the shape of the electron field and is typically situated 5 cm from the patient's skin. The 5 cm distance is a compromise to include a safety margin between the patient and cutout, as well as to reduce electron air scattering. Typical electron applicator sizes are: 6×6 cm^2, 10×10 cm^2, 15×15 cm^2, 20×20 cm^2, and 25×25 cm^2. The therapeutic range ($R_{90\%}$ (cm)) of an electron field defines the depth of dose of the 90% isodose level. $R_{90\%}$ is a function of electron beam energy and should coincide with the distal edge of the tumour volume. The electron energy chosen for treatment depends on the distal

tumour depth and to some extent on the cutout geometry, due to lateral electron scattering. A modern high energy linac provides electron beam energies in the range of 4-22 MeV.

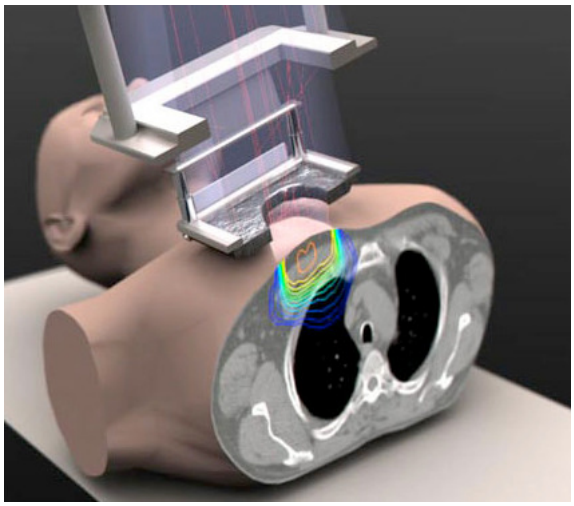

Figure 2–4: Cutaway view of electron applicator and mannequin subject to electron beam radiotherapy. [Image source, NRC, Ottawa, ON]

Clinical electron treatment planning has not evolved past the use of bolus to flatten out irregular surfaces, increase surface dose or to reduce the electron beam penetration depth in regions of the treatment field at the McGill University Health Centre (Montreal, QC, Canada). The lack of an advanced electron treatment planning and delivery system may be due in part to the complexity of electron particle transport in oblique surfaces and tissue boundaries. Historically, conventional electron treatment planning systems have used look-up table type algorithms, which lack dosimetric accuracy in predicting patient dose [1]. More recently commercial Monte Carlo treatment planning systems for electron monitor unit calculations have been available for use [11]. Aside from the dose calculation method, the

creation of the metal alloy cerrobend (also known as Lipowitz's alloy 50% bismuth, 26.7% lead, 13.3% tin, and 10% cadmium by weight [12]) cutout used to define the electron field, and the bolus material used to shape isodose lines to conform to the tumour volume is time-consuming and consists of only one segment [6, 1]. Electron treatments could be improved with the use of multiple segments and energies, however this would require an automated collimation device and accurate electron dosimetry [13]. Current practice at the McGill University Health Centre is to generate one electron field for treatment within an electron treatment planning system and perform an output measurement to validate the electron dosimetry. In addition, patients that require only one dose of radiation, may have their treatment plans created while lying on the treatment couch through the use of palpation of the treatment site to determine field edges and depth of treatment with the use of ultrasound imaging. A suitable electron energy is determined based on the treatment depth and the plan is considered complete. These real-time treatments are generally considered to be coarse with large margins and leave much to be desired in terms of target conformality and OAR sparing. Without the use of 3D treatment planning systems and trusted electron dose calculation accuracy, the chances of one creating an optimal electron plan is low [14]. In essence, there is currently a large potential to improve the quality of electron treatment plans. In addition, these poor quality electron plans do a disservice to the perceived beliefs of the "usefulness" of clinical electron radiotherapy. Minor improvements could be as simple as changing the electron dose calculation algorithm and performing 3D forward treatment planning for electron plans. The most accurate method

to calculate electron dose distributions is through Monte Carlo techniques, now available in many of the commercial treatment planning systems. With the use of trusted dose calculation engines such as Monte Carlo, the number and quality of electron plans may increase. Subsequently, the necessity for output validation decreases with trusted calculation engines, which will reduce the overall workload for electron planning.

In 1996, Hyödynmaa *et al* [15] published their work on optimization of conformal electron therapy using energy and fluence-modulated beams. The published technique used electron pencil beams generated from a spot scanning racetrack microtron of energies from 5-25 MeV to modify the energy deposition with depth in a controlled manner as an alternative to bolus. Since 1996 there have been many attempts to adapt this technique on a clinical radiotherapy accelerator as an advanced alternative to bolus; however, these attempts have remained in research and development. The community is still waiting for the first commercially available advanced energy and intensity modulated electron radiotherapy system.

2.2 Radiotherapy Optimization

The optimization algorithm is an integral component of inverse treatment planning. This section introduces optimization aspects applied to radiotherapy. A standard optimization algorithm, classified as "physical optimization", uses dosimetric values as endpoint criteria. The relative weights of a set of beams or beamlets is typically the only treatment parameter used to meet these endpoints. Optimization algorithms were developed as forward planning techniques could not

be applied to the enormous number of beamlets and endpoint criteria used within IMRT. The concept of physical optimization may be intuitive to the medical physics community for solving the problem of treatment planning; however, the radiation oncology community is still struggling to find the optimal clinical treatment plan. It is likely that the optimal clinical plan involves patient specific biological optimization in addition to physical dose optimization. The combination of physical and biological criteria for radiotherapy optimization has been suggested by Niemierko and others [16, 17]. Unless specified, the remainder of this thesis will focus on physical dose optimization.

Optimization implies a mathematical representation of a problem. In radiotherapy today, treatment planners use DVH points to evaluate and score treatment plans based on an objective function. The cumulative DVH is often used as a means to prioritize dosimetric endpoints within the optimization process. The DVH constraint is an input parameter to the optimization algorithm and is most useful to manage dose volume limits to parallel critical structures [18, 16, 19]. DVH constraints, as well as maximum and minimum dose limits are all carefully chosen before each optimization run. The goal of an optimization algorithm is to find a solution to the problem which meets the input constraints. The number and type of dose constraints are designed for sufficient flexibility to overcome and ease the difficult task of quantifying an optimal plan [20] based on limited input parameters. In practice, oncologists will likely review a number of optimized plans in their search for the clinically optimal plan. Depending on the complexity of the planning parameters, this process may consume a significant amount of time [21].

There is often some degree of disconnect between the optimization algorithms and treatment machines delivering the optimized plan. For example, the planning system may not take physical limitations of the treatment machine into consideration in the creation of an optimal plan. Consequently, beam optimization may be significantly diminished if the results must be approximated due to hardware limitations imposed by the delivery device [22]. In addition, the algorithms are not capable of providing *a priori* information on the trade-offs between conflicting treatment goals. As a result, a planner is often forced to perform many trial and error simulations to deduce trade-offs. As such, an important requirement on optimization criteria is therefore to allow for a high degree of steerability of the plan [23].

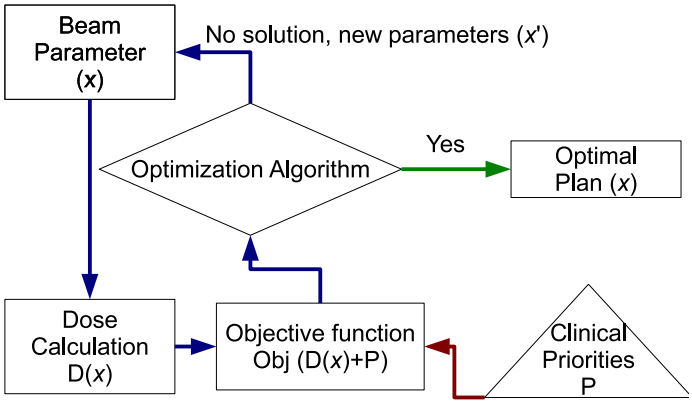

Figure 2–5: The optimization loop (blue) for iterative physical optimization. Treatment parameters x are defined and used to produce a patient specific dose distribution $D(x)$. The dose distributions and plan priorities are feed into the objective function for optimization. If the solutions is not acceptable the loop continues with new parameters x'.

The basic optimization loop is displayed in figure 2–5. The starting point typically requires the planner to choose a set of isocentric fields separated by gantry angle. The TPS splits these fields into beamlets and calculates a patient-specific dose distribution. Next, the objective function uses the dose distributions and dosimetric priorities to calculate a single value. The value scores the quality of the current plan, which allows for inter-plan evaluation. The optimization algorithm is effectively a search of the global minimum to arrive at the optimal plan. The search is most often performed iteratively. Convergence of the loop is achieved when certain criteria are met. Otherwise, the next iteration begins with a modified version of previous beam parameters.

The following subsections explain the basics of an optimization algorithm.

2.2.1 Inverse Problem

The inverse problem in radiotherapy is conceptually simple and can be summarized as a set of linear equations:

$$\mathbf{d} = \mathbf{D}\mathbf{w} \tag{2.1}$$

where $\mathbf{d}$ is a vector representing n samples of 3D dose distributions, $\mathbf{w}$ is a vector representing the weights of m elemental dose distributions, and $\mathbf{D}$ is a matrix representing the fractional dose contribution to the ith dose sample from the jth elemental dose distribution having weight w_j [24]. In matrix notation:

$$\begin{bmatrix} d_1 \\ \vdots \\ d_n \end{bmatrix} = \begin{bmatrix} D_{11} & \cdots & D_{1m} \\ \vdots & \ddots & \vdots \\ D_{n1} & \cdots & D_{nm} \end{bmatrix} \begin{bmatrix} w_1 \\ \vdots \\ w_m \end{bmatrix} \tag{2.2}$$

The objective of an optimization algorithm is to determine the vector of beamlet weights, $\mathbf{w}$, which meet the goals of the planning parameters. Typically, this type of optimization problem would be solved using matrix inversion to determine $\mathbf{w}$.

$$\mathbf{w} = \mathbf{D}^{-1}\mathbf{d} \tag{2.3}$$

In practice, an approximation for $\tilde{\mathbf{D}}^{-1}$ is used for the inverse dose calculation matrix because it is impractical to directly invert $\mathbf{D}$ due to its size [24]. However, due to the boundary condition that all values of $\mathbf{w}$ must be greater than zero (as we can not subtract dose) and that the samples n must be equal to the number of weights m, matrix inversion or direct calculation methods have been largely abandoned in favour of iterative methods [25].

Iterative methods are particularly computationally challenging due to the large number of variables (beamlet dose distributions and optimization constraints). For each iterative adjustment in $\mathbf{w}$, an optimization algorithm will recalculate a new value of $\mathbf{d}$, a new cost function value, and possibly new direction gradients. For example, the number of TomoTherapy photon beamlets can exceed 10,000 and the number of optimization constraints can exceed 10. Each constraint consists of a number of constraint points which are calculated from their respective volume on a $256\times256\times n$ CT image resolution (where n is the number of CT slices). Due to the sizeable amount of data and the large number of computational operations, it is essential to recognize the importance of computational speed for each optimization technique.

2.2.2 Linear Programming

Linear programming approaches have been used for constrained optimization in radiation therapy [26, 27, 28, 18, 29, 30]. The condition of a linear program is that the set of constraints must be expressed as linear relationships among the variables [31]. In addition, a non-negativity constraint is placed on the beamlet weight variables. The objective of the linear program is to find the values of variables that collectively minimize a linear objective function. A typical linear constraint would be to set maximum and minimum dose limits for the points within a target volume. The primary advantage of the linear programming approach is the speed and ease of formulation [20]. However, there are a few deterrents to the linear approach. The first is that approximate solutions do not exist with linear programming. A linear programming method will either find a solution or fail [29]. The second is that the format of the linear constraint is restrictive. With the linear programming formulation, it is unlikely that a physician could always achieve an acceptable result [20].

2.2.3 Nonlinear Programming

Nonlinear programming (NLP) approaches allow for an extended range of possible objective functions and constraints [32]. A typical nonlinear approach uses a weighted least square objective function. The task of the optimizer is to minimize the square difference between the prescribed dose and the total dose summed over all beamlets. The flexibility of NLP allows for dose-volume constraints within the objective function [20]. A dose-volume constraint consists of both a dose and volume limit that specifies the maximum amount of volume

that can receive a specific dose value. Graphical representation of a dose-volume constraint is illustrated in figure 2–6. However, it has been suggested that dose-volume constraints can introduce local minima in radiotherapy optimization [33]. Due to the complexity of a NLP objective function, investigators often employ specialized large-scale optimization algorithms [34, 35]. A drawback to these algorithms is the increased computational time with complex objective functions and the fact that they do not guarantee that the solution is globally optimal [20].

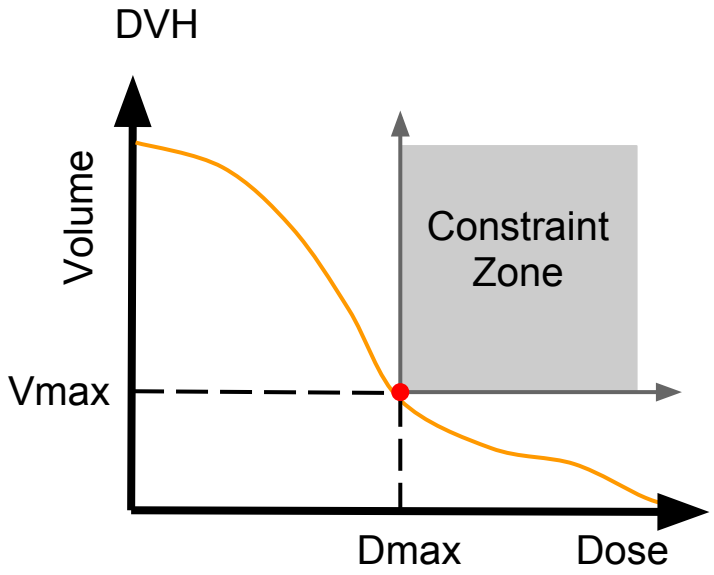

Figure 2–6: Dose volume constraints prevent the cumulative DVH from going above the point D_{max},V_{max}

2.2.4 Objective Function and Dose Constraints

As mentioned above, optimization algorithms require a mathematical formulation of the optimization problem. In radiotherapy, the problem is to deliver precise amounts of dose to specific locations of tissue. The mathematical representation

of the problem is reduced to a set of desired dose constraints for tissue volumes. The value of each constraint is often based on clinical experience and correlation between clinical observation and characteristic dose value [36]. In radiotherapy the problem can be simplified by grouping volumes of interest into targets or OARs. Dose constraints for targets usually include D_{max} and D_{min} and are applied to the whole target volume. The values chosen for D_{max} and D_{min} are typically close to the prescription dose to enforce dose homogeneity and to represent a realistic clinical experience. OARs may also include a D_{max} tolerance dose to the volume, in addition to D_{max} tolerance doses to fractional volumes. These dose constraints form the mathematical measure $F^{DV}(\mathbf{w})$ of a given treatment plan solution with dose weights $\mathbf{w}$. A typical cost function $F^{DV}(\mathbf{w})$, is the sum of the target cost $F^{D}_{TV}(\mathbf{w})$ and OAR cost $F^{V}_{OAR}(\mathbf{w})$.

$$F^{DV}(\mathbf{w}) = F^{D}_{TV}(\mathbf{w}) + F^{V}_{OAR}(\mathbf{w}) \tag{2.4}$$

$$\begin{aligned} F^{D}_{TV}(\mathbf{w}) &= \frac{\pi^{min}_{TV}}{N_{TV}} \sum_{i=1}^{N_{TV}} \left[\Theta_{min}\left(D^{TV}_{min} - D^{TV}_{i}(\mathbf{w})\right)\right]^2 \\ &\quad + \frac{\pi^{max}_{TV}}{N_{TV}} \sum_{i=1}^{N_{TV}} \left[\Theta_{max}\left(D^{TV}_{max} - D^{TV}_{i}(\mathbf{w})\right)\right]^2 \end{aligned}$$

$$\Theta_{min} = H\left(D^{TV}_{min} - D^{TV}_{i}(\mathbf{w})\right)$$

$$\Theta_{max} = H\left(D^{TV}_{i}(\mathbf{w}) - D^{TV}_{max}\right)$$

$$F_{OAR}^{V}(\mathbf{w}) = \sum_{l} \pi_{OAR_l} \left[\frac{\Theta_{OAR_V}(\sum_{i \in OAR_l} \Theta_{OAR_D} \Delta V_i - V_{max}^{OAR_l})}{V_{OAR_l}} \right]^2$$

$$\Theta_{OAR_D} = H(D_{OAR_l, i(\mathbf{w})} - D_{max}^{OAR_l})$$

$$\Theta_{OAR_V} = H(\sum_{i \in OAR_l} \Theta_{OAR_D} \Delta V_i - V_{max}^{OAR_l})$$

Where π_{TV}^{max} and π_{TV}^{min} refer to the penalty parameters of the target maximum and minimum dose constraint. Θ_{min} and Θ_{min} define the Heaviside functions (H) at D_{min}^{TV} and D_{max}^{TV}, and $D_i^{TV}(\mathbf{w})$ is the dose deposited to point i of the target (denoted by TV), which contains a total of N_{TV} dose points. The dose to the target volume is constrained by the user-specified maximum and minimum dose D_{max}^{TV} and D_{min}^{TV}. The dose-volume relations for critical organs are specified by the dose-volume constraints of ($D_{max}^{OAR_l}, V_{max}^{OAR_l}$), where l labels the organ constraint and ΔV_i is the elemental volume in the OAR. The Θ_{OAR_D} and Θ_{OAR_V} Heaviside functions filter the total number of volume elements ΔV_i to the number of volume elements that violate the dose-volume constraint. The Θ_{OAR_D} function identifies volume elements that exceed $D_{max}^{OAR_l}$, while the Θ_{OAR_V} function determines if the sum of volume elements exceed $V_{max}^{OAR_l}$. Each OAR constraint is assigned a penalty value π_{OAR} that weighs the individual penalty contribution to the overall objective function. This type of cost function is summarized as the square difference from a given dose constraint and results in a mathematically convex function [37] for

$F_{TV}^{D}(\mathbf{w})$ and a non-convex function for $F_{OAR}^{V}(\mathbf{w})$. Convex functions are ideal as they allow for fast gradient search optimization. The π parameter allows the planner to introduce "steering parameters" that effectively drives the algorithm to an acceptable solution. As mentioned above, it is common practice to perform many trial and error simulations to deduce trade-offs between various values of π. Unfortunately, the values of π have no intuitive meaning. According to the optimization algorithm, an optimum treatment is the one with the smallest overall deviation from the prescription (cost function). However, the prescription and cost function are input parameters to the optimization process and will drastically influence the results. In the end, an optimized solution may not even be close to the "best" optimal solution.

2.2.5 Optimization Algorithm

There have been a number of optimization algorithms written for radiotherapy applications over the last 30 years [38]. The function of an algorithm is to determine the beam weights for a given set of constraints. As such, the algorithm and objective function are closely related. In general there are two types of algorithms. The first type is deterministic, such as a gradient algorithm that can be applied to convex objective functions for a fast global minimum search. However, when gradient algorithms are applied to multiple local minima problems, there is an increased risk in suboptimal termination of the algorithm due to it being trapped in the wrong local minima [33]. The second algorithm type is stochastic, such as simulated annealing, which can be applied to non-convex objective functions or multiple local minima problems. The advantage of a stochastic method is

that the global minimum can be found even if local minima exist. The cost of stochastic methods is a significant increase in optimization time in comparison to deterministic algorithms.

Gradient Algorithm

A common gradient method is steepest decent [39, 40, 41, 17, 42]. This method calculates the gradient of the objective function. The gradient ∇ determines the steepest direction along the surface of the objective function and is used to update the values of the beam weights $\mathbf{w}$ for each step of the iteration x.

$$\mathbf{w}_{x+1} = \mathbf{w}_x - \alpha \nabla F^{DV}(\mathbf{w}_x) \tag{2.5}$$

The j^{th} component of the gradient is the partial derivative of $F^{DV}(\mathbf{w})$ with respect to w_j. The j^{th} component of the target maximum dose is calculated below with,

$$\frac{\partial F^{D}_{TV}}{\partial w_j} = \frac{2\pi^{max}_{TV}}{N_{TV}} \sum_{i=1}^{N_{TV}} \left[\Theta_{max} \left(D^{TV}_{max} - D^{TV}_{i}(\mathbf{w}) \right) D^{TV}_{i,j} \right] \tag{2.6}$$

where $D^{TV}_{i,j}$ is the dose at voxel i from beamlet j. A gradient is calculated on each parameter of the objective function ($F^{DV}(\mathbf{w})$) for each beamlet j. The sum of these gradients for each beamlet j, determines the direction of the new beamlet weight w_j for $\mathbf{w}_{x+1}$. Each iteration x generates a new set of beamlet weights $\mathbf{w}$. In the event that a negative beamlet weight is calculated, the weight is reset to zero. After the new set of weights have been calculated, the objective function is updated and the process continues with the next iteration. The iterations continue until the minimum is found or exit conditions are met. In general, gradient algorithms differ by their determination of step size α throughout the search. The

value of α can be constant or variable and determines the size of the iterative step. Advanced algorithms may make use of the second partial derivative (Hessian matrix) to determine the curvature of the solution. For quadratic objective functions, it has been shown that one can reach the optimal minimal in just one step that equals the product of the gradient and the inverse Hessian matrix [7]. Classical optimization methods such as "Newton's method" [43] function in a similar manner. Although, due to the difficulties in calculating the inverse Hessian matrix, reductions are usually employed to find an approximate inverse.

Simulated Annealing Algorithm

The basic strategy behind an annealing algorithm is to escape from the trap of local minima [44]. There are two methods, one called "climbing uphill" and the other "tunneling". Within the context of radiotherapy optimization, both methods have been illustrated by Webb [37]. Mathematically, the method involves the use of random numbers to sample a step size α for beam weight $\mathbf{w}$ changes. A random sample of the step size allow the solution to "tunnel" from one solution space to another. The step size width is dynamically decreased as the solution approaches the global minima. The decision on whether or not to accept a new solution is approached in a different manner than deterministically. If the new solution lowers the objective function value then the solution is accepted. However, if the new solution increases the objective function value then the new solution is accepted with a probability P_x. The P_x probability allows the system to accept worse solutions in an effort to sample neighbouring sections of the solution space. The P_x function is carefully tuned to the optimization problem and appropriately

decreased in probability as the solution approaches the global minima. A slow decrease in P_x function values allows the system to reach steady state values, which increase the change of finding solutions with lower cost function values. A typical P_x function is as follows:

$$P_x = \exp\left(\frac{-\Delta F_x^{DV}}{k_B T(x)}\right) \tag{2.7}$$

The term $T(x)$ represents temperature, and it is dynamically adjusted to smaller values with iteration number x. The initial value of T is set high enough to increase the probability for a large number of "wrong" or "uphill" solutions. Gradually decreasing the value of T "cools" the system until only "downhill" solutions are accepted. The method of temperature cooling, step size reduction, step size sampling, complexity of the objective function F^{DV}, and the initial condition of the beam weights $\mathbf{w}$ all affect the ability of an algorithm to arrive at the global minimum solution. The annealing schedule should be carefully chosen such that at each temperature the system can reach a steady state for a given step size. It is important to keep in mind that the step size and step size sampling algorithm dominate the change in objective function between iterations. This imposes a strict relationship between the temperature value and step size.

Simulated annealing algorithms are useful as they can find the global minimum of convex and nonconvex functions. They are typically implemented for large-scale inverse treatment planning [45, 46] where there is concern for being trapped in local minima [33]. However, due to their lengthy computation time [47] clinical TPS prefer to use fast deterministic approaches. Nonetheless a simulated

annealing algorithm could be used as a benchmark with which to test the accuracy of other inverse algorithms [48].

2.2.6 Beam Orientations

Beam orientation optimization is often external to standard radiotherapy inverse planning techniques. A planner typically chooses a predefined beam configuration based on current treatment policies and leaves the optimization software to compute intensity maps for each beam. This is done to increase the efficiency of generating and delivering IMRT plans. In addition, experienced planners can often chose a close-to-optimal configuration of beams and there is often not much gain in the additional step required to search for optimal beam orientations. However, this approach ignores a degree of freedom, which could be exploited [36]. The number of treatment beams and their direction of incidence could be used within the optimization loop to find the optimal treatment plan.

The lack of beam orientation optimization is likely a consequence of the non-convex problem of orientation optimization [49]. As mentioned above, non-convex problems are computationally difficult to solve and require advanced optimization algorithms to avoid local minima. In addition, the number of beams to be used to create the optimal plan can increase without bounds. Although in practice it has been observed that there exists a saturation point beyond which only marginal improvements are observed with additional beams. The required number of beams to generate an acceptable plan depends on the anatomy, the desired level of dose homogeneity in the target, and the OAR dose tolerances [19]. In general, the community has adopted the use of anatomic site specific classes of five to seven

evenly spaced beams [36]. Optimization of beam orientation is not considered to be an important issue.

With the recent advent of volumetric modulated arc therapy (VMAT), the importance of beam orientation optimization is even further reduced. The VMAT technique utilizes a large number of regularly spaced beam orientations. For the sake of TomoTherapy VMAT, the beam arraignment consists of 51 equispaced beams. In a simple comparison to a seven field static beam arraignment, the TomoTherapy technique would be able to utilize seven times more beamlets than the static beam technique. This greatly reduces the importance of initial beam orientation by increasing the degree of freedom in the number and placement of beamlets such that the optimization process governs if a beamlet is to be discarded rather than observation or experience.

2.2.7 Direct Aperture Optimization

Direct aperture optimization (DAO) proposed by Shepard *et al* [50] is a technique that is designed to reduce the uncertainty in intensity modulated treatment plans by avoiding the post-optimization of intensity maps. As mentioned above, subsequent post-optimization procedures ("leaf sequencing") may lead to sub-optimal plans. The procedure for DAO is as follows:

1. A number of apertures (MLC shapes) are defined per beam direction;
2. Patient-specific dose is calculated per aperture;
3. The optimization may either adjust the aperture weights, or be extended to adjust the aperture shapes (followed by a dose calculation) and weights;

4. Once the optimization has finished, the solution is dosimetrically exact and deliverable.

Aperture shapes may be based on the patient's anatomy or systematically adjusted within the optimization algorithm to produce complex patterns. The advantage of DAO plans is that they are free from DPE and OCE. In addition, DAO has been shown to improve IMRT efficiency by reducing the number of IMRT delivery segments without sacrificing plan quality [50, 51, 52].

2.2.8 Multi-Criteria Optimization

In general, radiotherapy plan optimization is a tedious process. This is due to the fact that most optimization systems operate such that there is no reward for reducing the dose in the critical structures below the constraint [7]. At times it may be possible to reduce the dose to a critical structure without compromising the dose to any other structure. As a result, it is extremely useful to know the sensitivity of the dose relationship between two or more structures [53]. Typically the relationship is masked by the use of a single objective score, which oversimplifies the complexity of radiation treatment planning. However, multi-criteria optimization (MCO) [54, 55, 56] allows the planner to control objectives (target and critical structures) separately and simultaneously. MCO effectively removes the trial and error simulations and provides the treatment planner with an array of best clinical trade-off plans to choose from. The MCO approach searches the feasible parameter space for the Pareto surface solutions. A Pareto optimal solution is defined as a solution, which cannot be further improved in any volume of interest without worsening another volume of interest. A graphical

representation of a Pareto surface for two competing end-points can be seen in figure 2–7. The three main advantages to this type of optimization are [7]:

1. This removes the artificial weight factors (which have no real clinical meaning).
2. Unnecessarily high doses in the organs at risk are avoided as all solutions are Pareto optimal.
3. Once the solutions are calculated, the final plan can be tuned in real-time by an oncologist, where the sensitivity and dependency of dose limits are instantly apparent.

Despite the benefits of this approach, there are currently very few TPS that provide this type of optimization. One exception would be RayStation (RaySearch Laboratories, Stockholm). One reason could be the lengthy calculation time required to build a database of Pareto solutions.

2.3 Dose Calculation Algorithms

The dose calculation algorithm defines the accuracy of the TPS. Due to the sigmoidal shape of dose response curves, dosimetric difference of as little as 5% can drastically alter the probability of tumour control and normal tissue complication [57]. In the application of inverse treatment planning such as IMRT, candidate beamlet dose distributions are used to evaluate the clinical acceptability of a plan during iterative beamlet intensity optimization. This process is contingent on the dose calculation accuracy. In practice, dose calculation accuracy is in competition with dose calculation speed [36]. In a clinical setting,

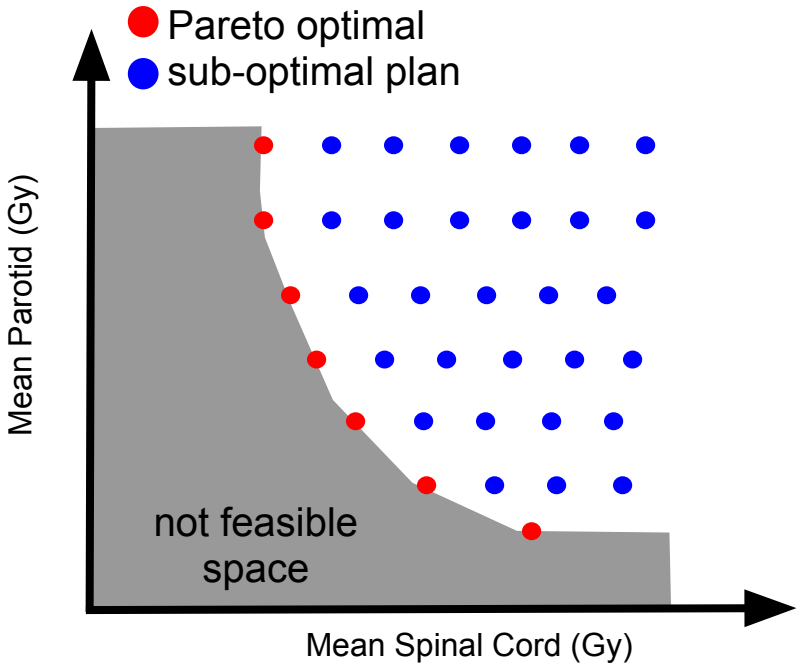

Figure 2–7: Two dimensional Pareto front for two trade-offs mean parotid and spinal cord dose. Each dot represents a solution; the red dots represent Pareto optimal solutions.

an IMRT plan might have required thousands of iterations in a complex multi-parameter optimization problem. However it is the dose calculation speed, which is often the rate-limiting component affecting the overall optimization time [36]. As a result, many clinical systems use severe approximations within the dose calculation algorithms to allow for a solution in an acceptable time frame at the cost of dosimetric accuracy.

This section describes two clinically used dose calculation algorithms, the photon pencil beam convolution algorithm (PBC) and the Analytical Anisotropic Algorithm (AAA). Following this is a section on Monte Carlo dose calculation,

which is considered the gold standard in radiation dosimetry and has historically been used by researchers within medical physics. Clinical physicists are now just beginning to use Monte Carlo dose engines for patient dosimetry. The following sections will not go into explicit depth into these dose calculation methods. Moreover, they are introduced here for the purpose of a basic understanding of the approximations within each technique. Let us first discuss the basic concept of energy transferred from a photon to medium, which forms the basis of dose.

2.3.1 KERMA and Dose

There are two subprocesses that describe energy transfer from a photon to medium:

1. Interaction of the photon field with atoms in the medium, resulting in a transfer of energy (dE_{tr}) and setting charged particles (electrons) in motion.
2. Transfer of energy from charged particles to the medium through excitations and secondary ionizations.

KERMA (K) is an acronym for Kinetic Energy Released per unit MAss. In the case of indirectly ionizing radiation such as photons, K represents the average amount of energy transferred from indirectly ionizing radiation to directly ionizing radiation (subprocess 1):

$$K = \frac{dE_{tr}}{dm} \tag{2.8}$$

where dE_{tr} is the energy transferred from photons to the primary electrons or positrons in an elemental mass of the medium dm. dE_{tr} depends on the incident photon energy and atomic number of the medium.

Subprocess 2 describes absorbed dose with units of J/kg or Gy (gray). The absorbed dose D is defined at a point inside a volume as the mean energy imparted by ionizing radiation to matter of mass m. The energy imparted is determined by taking the sum of energy entering the volume and subtracting the energy leaving the volume [5].

2.3.2 Pencil Beam Algorithms

A typical photon pencil beam model consists of a primary beam model, first scatter, and multiple scatter component. These types of models were first introduced in radiotherapy by Boyer *et al* [58] and Mohan *et al* [59]. Pencil beam models use the following form to calculate dose:

$$D(r) = \int_{V'} \phi(r') \cdot k(r - r') \cdot dV' \tag{2.9}$$

In the previous equation, $\phi(r')$ is considered to be the photon fluence distribution and k the interaction kernel, which describes the spread of radiation from a point r' to r. In a homogeneous medium, k can be calculated for the entire radiation dose transport process and is considered to be spatially invariant. The Fourier transform of $k(r)$ is the modulation transfer function for the deposition of dose by fluence.

Consider ϕ_0 to be the fluence of mono-energetic E_0 photons (number of photons/cm^2) impinging on a normal water surface at distance SSD cm. The primary fluence can be calculated by ray tracing from the original source, applying the inverse square and exponential attenuation. The water phantom is divided into a three dimensional array of calculation voxels represented by index i. The formula

for fluence becomes:

$$\phi_p(r) = \phi_0 \times \left(\frac{SSD}{SSD+d}\right)^2 \prod_i e^{-\mu \Delta d_i} \tag{2.10}$$

where d cm is the depth into the phantom and μ cm^{-1} is the linear attenuation coefficient for E_0 at voxel i along the path length from the source. The value of K at the point r is calculated with the fluence $\phi_p(r)$ and mass energy absorption coefficient μ_{en}/ρ. K energy is not the absorbed dose at the point r, as this energy will spread out to surrounding points by secondary electron transport. The transport of energy by electrons is very difficult to model analytically. Thus, Monte Carlo simulations are used to create a kernel, k_e for electron transport. In addition to an electron kernel, there are scattering kernels for first scatter k_s and multiple scatter $k_{s,m}$ events. The sum of these kernels $k_t(r)$ forms the impulse response or point spread function which operates on the primary fluence $\phi_p(r)$. The Fourier transform of $k_t(r)$,

$$H = \mathcal{F}[k_t(r)] \tag{2.11}$$

becomes the modulation transfer function for radiation dose transport. H can be calculated once for the entire simulation and stored for later multiplication with the Fourier transform of the primary fluence P. The inverse Fourier transform of the product of $\mathcal{F}^{-1}[P \cdot H]$ yields dose $D(r)$.

The pencil beam (PB) algorithm as described above has been shown to work reasonably well in homogeneous phantoms [58]. In regions of heterogeneity, the attenuation coefficients and electron densities would have to be included

in the convolution. Scattering elements from point r' to r requires path length scaling between the two points by an effective density, which tend to break down for extreme conditions such as air cavities [59]. The accuracy of clinical PB algorithms has been thoroughly investigated since their introduction in commercial treatment planning systems [60, 58, 61, 62, 63, 64, 65]. Ma *et al* [66] investigated the accuracy of the Corvus (Nomos Corp., Sewickley, PA) PB algorithm and reported discrepancies of more than 5% in the target region and over 20% in the OAR regions. In summary, PB inaccuracies are isolated to regions involving heterogeneities such as air-tissue, lung-tissue, and bone-tissue interfaces. Despite these inaccuracies, many of the IMRT treatment-planning systems still employ pencil beam algorithms because they use iterative optimization procedures and therefore require fast dose calculation algorithms [64].

2.3.3 Analytical Anisotropic Algorithm

The Analytical Anisotropic Algorithm (AAA) was implemented into Varian's Eclipse treatment planning system to replace the PB algorithm for photon dose calculation [67]. AAA was developed to improve the PB accuracy in regions of tissue heterogeneities. The algorithm consists of two photon sources (primary and secondary) an electron contamination source and Monte Carlo precalculated scatter kernels, scaled according to the electron density. During AAA commissioning, an optimization algorithm determines the parameters characterizing the multiple sources by maximizing the agreement between measured and calculated depth dose curves and profiles [68]. The algorithm uses a set of precalculated monoenergetic

Monte Carlo scattering kernels to develop an analytical scattering kernel expression per voxel, which is weighted by the energy spectrum of a beamlet. Next, the calculation model separates depth dependent dose and lateral dose components. Heterogeneities are accounted for in each spatial dimension by scaling the depth dependent and lateral scattering components by the inverse relative electron density in water. Splitting the photon interactions into depth and lateral components affects the accuracy of the heterogeneity correction since it does not take the divergent scatter of heterogeneities of upper levels correctly into account [68]. In addition, the lateral corrections are applied in a limited number of angular sectors. These two approximations are the main sources of error between measured and calculated profiles in heterogeneous media.

Researchers who reported on the accuracy of AAA have found significant improvements compared with PB particularity within the beam penumbra, build-up dose, and tissue interfaces [69, 70, 71, 72, 73] . Unfortunately, these improvements come at the cost of computation time and ultimately result in the use of PB dose calculation during IMRT optimization. Thereafter, AAA is used to calculate the optimized plan dose. AAA accuracy has also been compared with Monte Carlo calculations in a number of investigations. Gagne *et al* [70] demonstrated that AAA inaccuracies can be as high at 12% near isolated MLC leaf edges and up to 5% at leaf ends. Ding *et al* [71] concluded that AAA does not predict the dose in lung-tissue interface for higher energy photon beams such as 10 MV. Ottosson *et al* [73] studied dose differences between AAA and MC for non-small cell lung cancer cases and concluded there to be clinically significant

differences. In addition, Ottosson cautions the use of higher energy (>10 MV) photons in favour of 6 MV, which has proven to be more accurate.

2.3.4 Monte Carlo

Monte Carlo is a technique that uses pseudo random numbers to simulate naturally random processes based on statistical probabilities. The idea was developed in the 1940's and its use has spread to many fields including medical physics [74]. The technique uses random numbers to sample a probability distribution function to arrive at a solution. The statistical uncertainty in the solution is directly related to the number of histories or events. In radiotherapy, MC methods are employed to solve the Boltzmann transport equation for electrons and photons. This approach yields an exact solution to particle transport through matter. The sole disadvantage of MC techniques is the long computational time required for low statistical noise. Although, the use of the word "long" could be misleading as advancements in computer hardware technology and intelligent variance reduction techniques can considerably reduce the simulation time. In fact, due to the independence of particle histories, the MC technique is inherently more efficient in the calculation of dose for complex simulations such as VMAT [75]. To summarize, there is widespread interest in the use of MC techniques today, as evident in the large number of fast commercial MC algorithms available to the clinic.

Radiation Particle Transport

Particle transport refers to the transportation of each original particle and its entire offspring to determine the dose deposited in media [76]. As a particle travels through a medium, it creates a shower of secondary particles through

interactions. These interactions follow specific probability distributions based on initial particle type and energy. For every particle, the Monte Carlo transport algorithm determines the location and type of interaction. These interactions lead to the deposition of energy along the particle's path. As the particles interact, the information pertaining to the interaction type and location is saved as the particle history. The main components of a Monte Carlo algorithm include cross-section data for the interaction probabilities, the transport algorithm, and geometry specifications. The transport algorithm defines the characteristics and efficiency of any algorithm. A Monte Carlo transport algorithm for radiotherapy details the coupled transport of photons and electrons through the media. Parameters such as charge, energy, position, and direction are recorded at each interaction point. The cross-section data for different interactions provides the statistical probability for each interaction type. Photon interactions involve the following effects:

1. Photoelectric effect
2. Compton effect
3. Rayleigh Scattering
4. Pair and Triplet production

Photon particle transport begins with the mean free path for a photon and a random number. The state of a particle is defined by its position, energy, and direction cosines. The change in a particle's state from position "A" to "B" depends on the mean free path, scattering mechanisms, the change of direction, and the energy loss that are all sampled from probability distribution functions. The simulation of a particle history is processed by repeating this step. Particle

transport is terminated when the particle leaves the geometric boundary of the system or when the energy becomes smaller than a cutoff value or variance reduction.

Statistics and Efficiency

The statistics of a MC calculation consists of type A and B uncertainties. Type A are statistical in nature while type B are estimated by non-statistical methods. In the application of MC calculations, programming errors, cross-section data, and general modelling inaccuracies belong to type B uncertainty and are not usually expressed in a MC calculation. An exception to the rule would be type B dimension and position tolerances, which are often included in MC brachytherapy simulations. In order to define a type A uncertainty let's first examine how we arrive at the expectation value $< x >$ of a certain quantity of interest. For example, dose deposition in a voxel is estimated by means of the average $\bar{x}$:

$$\bar{x} \equiv \frac{1}{N} \sum_{i=1}^{N} x_i \tag{2.12}$$

where x_i is the dose contribution to x from the i^{th} statistically independent history and N is the number of histories. By virtue of the central limit theorem, which permits the mean of a large number of independently random variables to be approximated normally (equation 2.12), we arrive at an expression for the variance of type A, such as dose [77]:

$$s^2_{<x>} \equiv \frac{1}{N-1} \left[\frac{1}{N} \sum_{i=1}^{N} x_i^2 - \left(\sum_{i=1}^{N} \frac{x_i}{N} \right)^2 \right] \tag{2.13}$$

In the limit of a large number of histories (N), the quantity Ns^2 can be considered constant and the uncertainty can be approximated to $N^{-0.5}$. This leads to the following Monte Carlo definition of efficiency ϵ:

$$\epsilon \equiv \frac{1}{Ts^2} \tag{2.14}$$

T is the computing time required to obtain the variance s^2. The efficiency equation states that the efficiency of a particular simulation is constant. Therefore, a decrease in the statistical uncertainty by a factor of 10 requires an increase in the computation time by a factor of 100. Variance reduction techniques reduce the statistical uncertainty while maintaining the same computational time and without affecting the physics of the simulation. These techniques attempt to increase the relative occurrence of certain events, which minimize the number of required histories. There are a number of variance reduction techniques available for each Monte Carlo package. Forced interactions, particle splitting, cross-section enhancement, bremsstrahlung splitting, and range rejection are some examples [78].

2.3.5 EGSnrc Codes

The EGSnrc (Electron Gamma Shower) system was developed from EGS4 [79] and is maintained by researchers within the Institute for National Measurement Standards, Ionizing Radiation Standards, NRC (National Research Council, Ottawa, ON). The system is a powerful package for Monte Carlo simulations of coupled electron-photon transport within the energy range of 1 keV to 10 GeV. The demand for accuracy in radiotherapy has escalated the profile of EGSnrc and spurred new developments in the code. EGSnrc is very popular amongst

radiotherapy researchers and was used throughout this thesis with user codes BEAMnrc and DOSXYZnrc.

BEAMnrc

BEAMnrc [80] is a EGSnrc user code developed at the NRC in collaboration with Rock Mackie *et al* in Madison through the OMEGA project (Ottawa Madison Electron Gamma Algorithm), to develop a Monte Carlo dose calculation algorithm for electron beam radiotherapy [81]. BEAMnrc performs the particle transport through the complex geometry of radiotherapy treatment units including linear accelerators, orthovoltage units, and cobalt-60 units. Since its original release in 1995, the system has been in continuous development with the latest version released in May 2011.

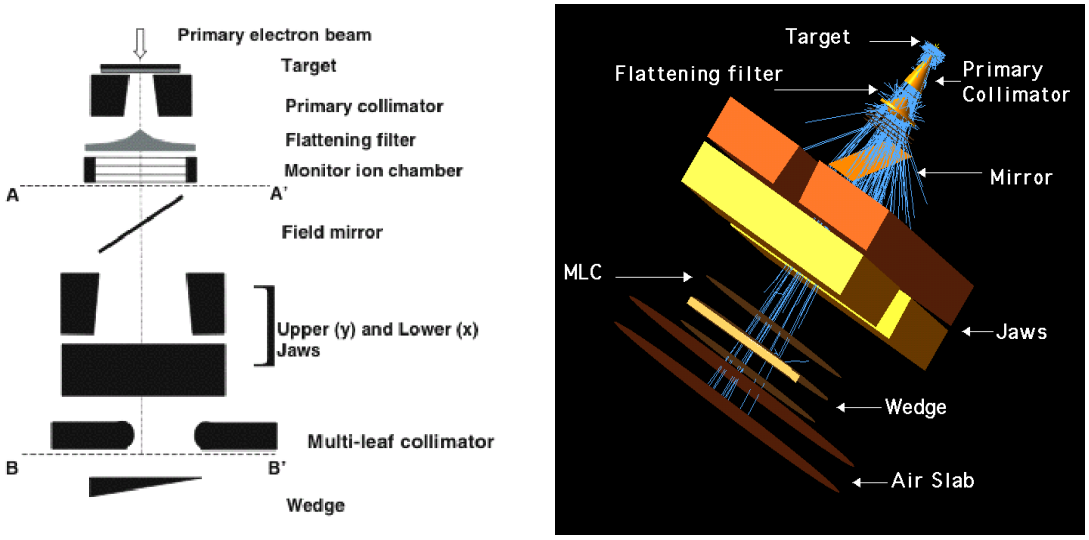

(a) (b)

Figure 2–8: Schematic drawing of linac component modules in BEAMnrc [82] (a), BEAMnrc simulation of a Varian CL21EX 18 MV photons (blue) through linac head (b).

BEAMnrc uses the concept of component modules (CM) to model each component of a treatment unit. A modelled treatment unit consists of a series of CMs stacked perpendicular to the beam axis with a top and bottom surface. An axial cross-sectional view of a typical linac model with eight CMs is shown in figure 2–8(a). There are currently 20 CMs each designed to model a specific type of geometry. Users often develop their own CM to handle unique complex geometry. The values and properties of each CM are specified within a BEAMnrc input file. These values include transport parameters such as the energy cutoff limits for electrons (ECUT) and photons (PCUT), minimum energy required for knock on electrons (AE) and bremsstrahlung photons (AP). The energy source and variance reduction options are defined within the input file header section.

BEAMnrc output is typically a phase-space file containing information on the physical characteristics of all particles crossing the scoring plane. These characteristics include position (x, y, z), direction (u, v, w), particle energy (E), charge (Q), and particle weight (wt). The phase-space can be used as a source for another simulation, or analyzed to calculate physical quantities such as particle energy spectra, fluence, angular distributions, and spatial distributions.

In this thesis, BEAMnrc is used for linac simulations of electron and photon beams.

DOSXYZnrc

DOSXYZnrc [83] is another EGSnrc user code developed at the NRC for 3D absorbed dose calculations. DOSXYZnrc simulates the transport of photons and electrons and scores energy deposition (dose) in a voxelized rectilinear Cartesian

volume. The simulation geometry and energy source arrangements are entered into the simulation via an ASCII formatted input file. The voxelized volume is most often used to model the patient anatomy. After a calculation, dose and statistical uncertainty are scored per voxel.

The energy source and beam geometry for a dose calculation are defined using various default source models contained within DOSXYZnrc. Throughout this thesis, a number of source models were used to calculate patient dose: source 1 - parallel rectangular beam, source 2 - full phase-space, source 3 - point source from front, source 9 - BEAMnrc treatment head simulation. In addition, a McGill-developed source, source 11, was created to model dynamic BEAMnrc treatment head simulations. The DOSXYZnrc coordinate system positions these beam source types on the phantom set at the location of the phantom isocentre. The isocentre is defined by an x, y, z position while the angles of incidence are defined with θ, ϕ, ϕ_{col}. In terms of the linac coordinates, these angles define the gantry, couch, and collimator angle. A patient geometry model is often created from CT images of the patient along with a CT-to-density curve. These models are formatted into an EGSPhant file and used as input to DOSXYZnrc. Voxels are assigned by material and density. See figure 2–9 for a planar view of an EGSPhant patient model.

In this thesis, DOSXYZnrc is used to simulate patient dose from linac simulations and other radiotherapy sources.

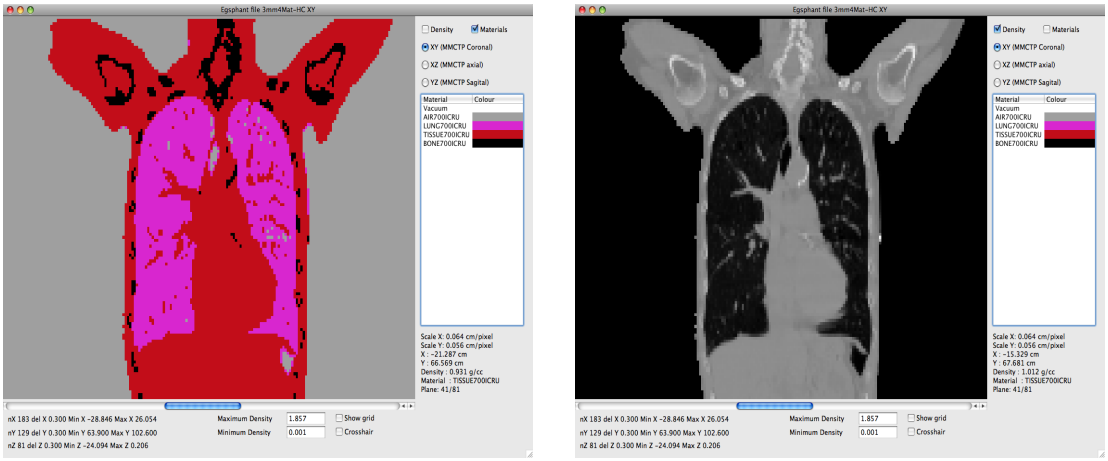

(a) (b)

Figure 2–9: DOSXYZnrc EGSPhant geometry of coronal view plane illustrating material voxel assignment (a) and density voxel assignment (b). Materials included air (gray), lung (pink), tissue (red) and bone (black). Density from 0.001 to 1.857 g/cm^3.

PEGS Data

PEGS (preprocessor for EGS) data provides material cross-sections for a range of photon and electron energies [84]. Cross-sectional data is created from theoretical and empirical formulas for each element or compound used within a calculation. The energy cutoffs used within the PEGS data must be compatible with the cutoffs within the BEAMnrc or DOSXYZnrc simulation.

2.3.6 XVMC Code

XVMC is a unique MC code designed to minimize all the unnecessary computations found within the EGSnrc system for efficient particle transport through the human body [85]. The improved simulation efficiency is due to a fast electron transport algorithm and ray tracing techniques. For photon beams, the ray tracing technique is used to calculate the number of electrons created in each

voxel by the primary photon beam. Electron beam transport uses the following approximations to help speed up the calculation: multiple history technique and step size restriction for electron transport. The multiple history technique reuses the same electron history in different regions of the simulated volume; this reduces the number of histories required to achieve a certain statistical uncertainty. Step size restrictions decrease the number of electron steps per history by increasing the step size [78].

XVMC sources may be monoenergetic electrons or photons, a spectrum, a beam model, or a phase-space file. The user specifies a geometric volume as a matrix of voxels, where each voxel is assigned a specific density. The voxel dimensions represent the spatial resolution and the dose scoring volume. Voxel densities may be assigned by manual input or based on CT images. In XVMC particle transport, the material data source is based on the density provided within the DMX file. A particle is first transported in water at a density of 1 g/cm^3. Secondly, the path length, energy losses, and scattering angles are re-evaluated based on the actual voxel density. The path length is scaled by the ratio of unrestricted stopping powers of the material to that of water. This ensures that at the end of each step, the electron in material x has the same energy as an electron transported through one-step of water. Stopping powers are determined from a linear relationship relating physical density and mass stopping power, as shown in ICRU Report 37. The scattering powers are also related to the physical densities. Particles are transported until a cutoff energy or the particle exits the geometry

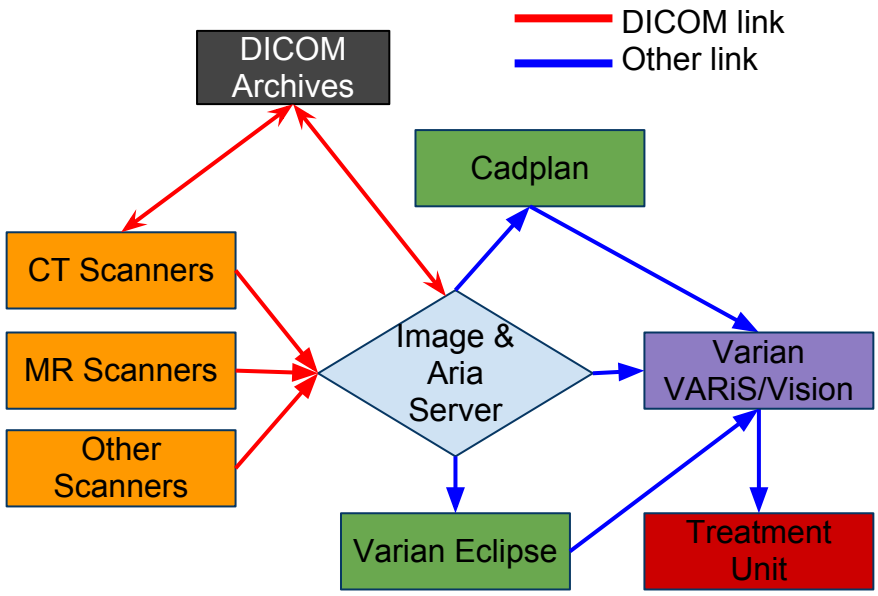

Figure 2–10: Flow of DICOM data within a Varian cancer centre

volume. XVMC output is a dose matrix with the same dimensions as the DMX file.

In this thesis, XVMC is used to simulate patient dose from linac simulations and other radiotherapy sources.

2.4 DICOM RT

DICOM (Digital Imaging and Communications in Medicine) is a standard for handling, storing, and transmitting information in medical imaging [86]. DICOM RT is an extension of DICOM for radiotherapy information. The format is constantly evolving as the demand for more detailed patient information increases. Security of patient data is always a concern in addition to the integrity of data transfers across a network. However, data transfers between systems implies a

level of compatibility and conformance, which is left up to system manufactures to ensure. There are many examples of different systems implementing the same feature in different ways. As such, the interoperability of DICOM RT is not guaranteed.

The RT extension includes the following new data sets:

1. RT Structure Set: Patient-related structures including target volumes and organs at risk
2. RT Plan: Geometric and dosimetric data relating to the treatment plan including external beam treatment unit, isocentre, gantry couch and collimator angles
3. RT Image: Images relevant to the RT Plan, treatment and acquisition details
4. RT Dose: 2D or 3D dose distributions calculated by TPS and dose volume histograms if calculated and exported by the TPS

DICOM RT is heavily used within the radiation oncology department at the McGill University Health Centre and throughout this thesis. The flow of DICOM data in a Varian cancer centre is illustrated in figure 2–10. DICOM RT is most often used to transfer data between devices from independent manufacturers whereas, a manufacturer dependent format may be used to transfer data between devices originating from one vendor.

2.5 References

[1] E B Podgorsak and International Atomic Energy Agency. *Radiation Oncology Physics: A Handbook for Teachers and Students*. International Atomic Energy Agency, 2005.

[2] International Commission on Radiation Units and Measurements (ICRU). *Prescribing, Recording, and Reporting Photon Beam Intensity Modulated Radiation Therapy.* ICRU Report 83, 2010.

[3] International Commission on Radiation Units and Measurements (ICRU). *Prescribing, Recording, and Reporting Photon Beam Therapy.* ICRU Report 50, 1993.

[4] International Commission on Radiation Units and Measurements (ICRU). *Prescribing, Recording, and Reporting Photon Beam Therapy.* ICRU Report 62, 1999.

[5] H E Johns and J R Cunningham. *The physics of radiology.* Charles C Thomas, 4th edition, 1983.

[6] A Brahme. Design principles and clinical possibilities with a new generation of radiation therapy equipment. A review. *Acta. Oncol.*, 26(6):403–412, 1987.

[7] Jatinder Palta and T Rockwell Mackie. *Intensity-Modulated radiation therapy, the state of the art Physical optimization.* AAPM, 2003.

[8] Intensity Modulated Radiation Therapy Collaborative Working Group. Intensity modulated radiotherapy current status and issues of interest. *Int. J. Radiat. Oncol. Biol. Phys.*, 51(4):880–914, 2001.

[9] N Dogan, J V Siebers, P J Keall, F Lerma, Y Wu, M Fatyga, J F Williamson, and R K Schmidt-Ullrich. Improving IMRT dose accuracy via deliverable Monte Carlo optimization for the treatment of head and neck cancer patients. *Med. Phys.*, 33(11):4033–4043, 2006.

[10] P Keall, J Siebers, R Jeraj, and R Mohan. The effect of dose calculation

uncertainty on the evaluation of radiotherapy plans. *Med. Phys.*, 27(3):478–484, 2000.

[11] J E Cygler, C Lochrin, G M Daskalov, M Howard, R Zohr, B Esche, L Eapen, L Grimard, and J M Caudrelier. Clinical use of a commercial Monte Carlo treatment planning system for electron beams. *Phys. Med. Biol.*, 50(5):1029–1034, 2005.

[12] G W A Milne. *Gardner's Chemical Synonyms and Trade Names*. Wiley, 1999.

[13] E E Klein, Z Li, and D A Low. Feasibility study of multileaf collimated electrons with a scattering foil based accelerator. *Radiother. Oncol.*, 41(2):189–196, November 1996.

[14] B Faddegon, J Balogh, R Mackenzie, and Daryl Scora. Clinical considerations of Monte Carlo for electron radiotherapy treatment planning. *Radiat. Phys. Chem.*, 53:217–227, 1998.

[15] S Hyödynmaa, A Gustafsson, and A Brahme. Optimization of conformal electron beam therapy using energy- and fluence-modulated beams. *Med. Phys.*, 23(5):659–666, 1996.

[16] A Niemierko. Random search algorithm (RONSC) for optimization of radiation therapy with both physical and biological end points and constraints. *Int. J. Radiat. Oncol. Biol. Phys.*, 23(1):89–98, 1992.

[17] X H Wang, R Mohan, A Jackson, S A Leibel, Z Fuks, and C C Ling. Optimization of intensity-modulated 3D conformal treatment plans based on biological indices. *Radiother. Oncol.*, 37(2):140–152, 1995.

[18] M Langer and J Leong. Optimization of beam weights under dose-volume

restrictions. *Int. J. Radiat. Oncol. Biol. Phys.*, 13(8):1255–1260, 1987.

[19] J Stein, R Mohan, X H Wang, T Bortfeld, Q Wu, K Preiser, C C Ling, and W Schlegel. Number and orientations of beams in intensity-modulated radiation treatments. *Med. Phys.*, 24(2):149–160, 1997.

[20] D M Shepard, MC Ferris, GH Olivera, and TR Mackie. Optimizing the delivery of radiation therapy to cancer patients. *Siam Rev*, 41:721–744, 1999.

[21] M Oliver, W Ansbacher, and W A Beckham. Comparing planning time, delivery time and plan quality for IMRT, RapidArc and Tomotherapy. *J Appl Clin Med Physs*, 10(4):3068–131, 2009.

[22] P S Cho and R J Marks. Hardware-sensitive optimization for intensity modulated radiotherapy. *Phys. Med. Biol.*, 45(2):429–440, 2000.

[23] T Spalke, D Craft, and T Bortfeld. Analyzing the main trade-offs in multi-objective radiation therapy treatment planning databases. *Phys. Med. Biol.*, 54(12):3741–3754, 2009.

[24] T Holmes and T R Mackie. A comparison of three inverse treatment planning algorithms. *Phys. Med. Biol.*, 39(1):91–106, 1994.

[25] T Bortfeld. Optimized planning using physical objectives and constraints. *Seminars in radiation oncology*, 9(1):20–34, 1999.

[26] G Bahr, J Kereiakes, H Horwitz, R Finney, J Galvin, and K Goode. The method of linear programming applied to radiation treatment planning. *Radiology*, 91:686–693, 1968.

[27] L Hodes. Semiautomatic optimization of external beam radiation treatment planning. *Radiology*, 110:191–196, 1974.

[28] A T Redpath, B L Vickery, and D H Wright. A new technique for radiotherapy planning using quadratic programming. *Phys. Med. Biol.*, 21(5):781–791, 1976.

[29] S Morrill, R Lane, JA Wong, and II Rosen. Dose-volume considerations with linear programming optimization. *Med. Phys.*, 18(6):1201–1210, 1991.

[30] I Rosen, R Lane, SM Morrill, and J Belli. Treatment plan optimization using linear programming. *Med. Phys.*, 18(2):141–152, 1991.

[31] G L Nemhauser and L A Wolsey. *Integer and Combinatorial Optimization*. Wiley, New York, 1988.

[32] P E Gill, W Murray, and M H Wright. *Practical Optimization*. Academic Press London, 1981.

[33] JO Deasy. Multiple local minima in radiotherapy optimization problems with dose-volume constraints. *Med. Phys.*, 24(7):1157–1161, 1997.

[34] SG Nash and J Nocedal. A numerical study of the limited memory bfgs method and the truncated-newton method for large scale optimization. *SIAM J. Optim*, 1(3):358–372, 1991.

[35] A Conn, N I M Gould, and P L Toint. *LANCELOT: a Fortran package for large-scale nonlinear optimization (Release A)*. Springer, 1992.

[36] T Bortfeld, R Schmidt-Ullrich, W De Neve, and D E Wazer. *Image-Guided IMRT*. Springer, 2005.

[37] S Webb. The physical basis of IMRT and inverse planning. *Br. J. Radiol.*, 76(910):678–689, 2003.

[38] S Webb. *Intensity-modulated radiation therapy*. Institute of Physics, 2001.

[39] B Lind. Properties of an algorithm for solving the inverse problem in radiation therapy. *Inverse Problems*, 6(3):415–426, 1990.

[40] P Källman, B K Lind, and A Brahme. An algorithm for maximizing the probability of complication-free tumour control in radiation therapy. *Phys. Med. Biol.*, 37(4):871–90, 1992.

[41] A Gustafsson, B K Lind, and A Brahme. A generalized pencil beam algorithm for optimization of radiation therapy. *Med. Phys.*, 21(3):343–356, 1994.

[42] Q Wu, R Mohan, A Niemierko, and R Schmidt-Ullrich. Optimization of intensity-modulated radiotherapy plans based on the equivalent uniform dose. *Int. J. Radiat. Oncol. Biol. Phys.*, 52(1):224–235, 2002.

[43] W H. Press. *Numerical Recipes The Art of Scientific Computing*. Cambridge University Press, 2007.

[44] S Kirkpatrick, C Gelatt, and M Vecchi. Optimization by simulated annealing. *Science*, 1983.

[45] S M Morrill, R G Lane, and I I Rosen. Constrained simulated annealing for optimized radiation therapy treatment planning. *Comput Methods Programs Biomed*, 33(3):135–144, 1990.

[46] G S Mageras and R Mohan. Application of fast simulated annealing to optimization of conformal radiation treatments. *Med. Phys.*, 20(3):639–647, 1993.

[47] S Webb. Optimization by simulated annealing of three-dimensional, conformal treatment planning for radiation fields defined by a multileaf collimator: Ii. inclusion of two-dimensional modulation of the x-ray intensity. *Phys. Med.*

Biol., 37(8):1689–1704, 1992.

[48] R Jeraj and P Keall. Monte Carlo-based inverse treatment planning. *Phys. Med. Biol.*, 44(8):1885–1896, 1999.

[49] T Bortfeld and W Schlegel. Optimization of beam orientations in radiation therapy: some theoretical considerations. *Phys. Med. Biol.*, 38(2):291–304, 1993.

[50] D M Shepard, M A Earl, X A Li, S Naqvi, and C Yu. Direct aperture optimization: a turnkey solution for step-and-shoot IMRT. *Med. Phys.*, 29(6):1007–1018, 2002.

[51] Z Jiang, M A Earl, G W Zhang, C X Yu, and D M Shepard. An examination of the number of required apertures for step-and-shoot IMRT. *Phys. Med. Biol.*, 50(23):5653–5663, 2005.

[52] A M Bergman, K Bush, M Milette, I A Popescu, K Otto, and C Duzenli. Direct aperture optimization for IMRT using Monte Carlo generated beamlets. *Med. Phys.*, 33(10):3666–3679, 2006.

[53] M Alber, M Birkner, and F Nüsslin. Tools for the analysis of dose optimization: II. Sensitivity analysis. *Phys. Med. Biol.*, 47(19):N265–N270, 2002.

[54] Y Yu. Multiobjective decision theory for computational optimization in radiation therapy. *Med. Phys.*, 24(9):1445–1454, 1997.

[55] C Cotrutz, M Lahanas, C Kappas, and D Baltas. A multiobjective gradient-based dose optimization algorithm for external beam conformal radiotherapy. *Phys. Med. Biol.*, 46(8):2161–2175, 2001.

[56] HW Hamacher and KH Kufer. Inverse radiation therapy planning - a multiple

objective optimization approach. *Discrete Applied Mathematics*, 118(1-2):145–161, 2002.

[57] S Dische, M I Saunders, C Williams, A Hopkins, and E Aird. Precision in reporting the dose given in a course of radiotherapy. *Radiother. Oncol.*, 29(3):287–293, 1993.

[58] A Boyer and E Mok. A photon dose distribution model employing convolution calculations. *Med. Phys.*, 12(2):169–177, 1985.

[59] R Mohan, C Chui, and L Lidofsky. Differential pencil beam dose computation model for photons. *Med. Phys.*, 13(1):64–73, 1986.

[60] T R Mackie, J W Scrimger, and J J Battista. A convolution method of calculating dose for 15-MV x rays. *Med. Phys.*, 12(2):188–196, 1985.

[61] L Wang, C S Chui, and M Lovelock. A patient-specific Monte Carlo dose-calculation method for photon beams. *Med. Phys.*, 25(6):867–878, 1998.

[62] A Ahnesjo, M Saxner, and A Trepp. A pencil beam model for photon dose calculation. *Med. Phys.*, 19(2):263–273, 1992.

[63] T Bortfeld, W Schlegel, and B Rhein. Decomposition of pencil beam kernels for fast dose calculations in three-dimensional treatment planning. *Med. Phys.*, 20(2 Pt 1):311–318, 1993.

[64] W U Laub, A Bakai, and F Nusslin. Intensity modulated irradiation of a thorax phantom: comparisons between measurements, Monte Carlo calculations and pencil beam calculations. *Phys. Med. Biol.*, 46(6):1695–1706, 2001.

[65] L Wang, E Yorke, and C Chui. Monte Carlo evaluation of 6 MV intensity modulated radiotherapy plans for head and neck and lung treatments. *Med.*

Phys., 29(11):2705–2717, 2002.

[66] C M Ma, T Pawlicki, S Jiang, and J Li. Monte Carlo verification of IMRT dose distributions from a commercial treatment planning optimization system. *Phys. Med. Biol.*, 45(9):2483–2495, 2000.

[67] W Ulmer, J Pyyry, and W Kaissl. A 3D photon superposition/convolution algorithm and its foundation on results of Monte Carlo calculations. *Phys. Med. Biol.*, 2005.

[68] Varian Medical Systems, Varian Medical Systems, Inc., Palo Alto, CA, UAS. *Reference Guide for Algorithms Eclipse*, 2004.

[69] A Van Esch, L Tillikainen, J Pyykkonen, M Tenhunen, H Helminen, S Siljamaki, J Alakuijala, M Paiusco, M Lori, and D P Huyskens. Testing of the analytical anisotropic algorithm for photon dose calculation. *Med. Phys.*, 33(11):4130–4148, 2006.

[70] I Gagne, W Ansbacher, and S Zavgorodni. A Monte Carlo evaluation of RapidArc dose calculations for oropharynx radiotherapy. *Phys. Med. Biol.*, 53(24):7167–7185, 2008.

[71] G Ding, D Duggan, B Lu, D Hallahan, A Cmelak, A Malcolm, J Newton, M Deeley, and C W Coffey. Impact of inhomogeneity corrections on dose coverage in the treatment of lung cancer using stereotactic body radiation therapy. *Med. Phys.*, 34(7):2985–2994, 2007.

[72] I Fotina, P Winkler, T Künzler, J Reiterer, I Simmat, and D Georg. Advanced kernel methods vs. Monte Carlo-based dose calculation for high energy photon beams. *Radiat. Oncol.*, 93(3):645–653, December 2009.

[73] R O Ottosson, A Karlsson, and C F Behrens. Pareto front analysis of 6 and 15 MV dynamic IMRT for lung cancer using pencil beam, AAA and Monte Carlo. *Phys. Med. Biol.*, 55(16):4521–4533, 2010.

[74] D Rogers. Fifty years of Monte Carlo simulations for medical physics. *Phys. Med. Biol.*, 51:R287–R301, 2006.

[75] I Kawrakow. Recent code developments in Monte Carlo Treatment Planning. In *Proceedings of the 2009 European Workgroup on Monte Carlo Treatment Planning*, Cardiff, UK, 2009.

[76] A Kling, F J C Barao, M Nakagawa, L Tavora, and P Vaz, editors. *Advanced Monte Carlo for Radiation Physics, Particle Transport Simulation and Applications*. Springer, 1st edition, November 2001.

[77] J Sempau, A Sánchez-Reyes, F Salvat, H O ben Tahar, S B Jiang, and J M Fernández-Varea. Monte Carlo simulation of electron beams from an accelerator head using PENELOPE. *Phys. Med. Biol.*, 46(4):1163–1186, 2001.

[78] I Kawrakow and M Fippel. Investigation of variance reduction techniques for Monte Carlo photon dose calculation using XVMC. *Phys. Med. Biol*, 45(8):2163–2183, 2000.

[79] W R Nelson, H Hirayamall, and D W Rogers. The EGS4 code system. *SLAC Stanford Linear Accelerator Center*, 265:1–206, 1985.

[80] D W O Rogers, B A Faddegon, G X Ding, C M Ma, J We, and T R Mackie. BEAM: A Monte Carlo code to simulate radiotherapy treatment units. *Med. Phys.*, 22(5):503–524, 1995.

[81] D W O Rogers. Fifty years of Monte Carlo simulations for medical physics.

Phys. Med. Biol., 51:R287–R301, 2006.

[82] F Verhaegen and J Seuntjens. Monte Carlo modelling of external radiotherapy photon beams. *Phys. Med. Biol*, 48(21):107–164, 2003.

[83] B Walters, I Kawrakow, and D W O Rogers. *DOSXYZnrc Users Manual*. Ionizing Radiation Standards, National Research Council of Canada, 2007.

[84] W R Nelson and Y Namito. The EGS4 Code System: Solution of gamma-ray and electron transport problems. *SLAC PUB*, 1990.

[85] F Hasenbalg, M Fix, E Born, R Mini, and I Kawrakow. VMC++ versus BEAMnrc: A comparison of simulated linear accelerator heads for photon beams. *Med. Phys.*, 35(4):1521, 2008.

[86] O S Pianykh. *Digital Imaging and Communications in Medicine (DICOM): A Practical Introduction and Survival Guide*. Springer, 2nd edition, 2011.

CHAPTER 3
Paper I: MMCTP: A radiotherapy research environment for Monte Carlo and patient-specific treatment planning

Andrew Alexander, François DeBlois, Gabriela Stroian, Khalid Al-Yahya, Emily Heath, and Jan Seuntjens

Phys. Med. Biol., 52(13):N297-308, 2007

Contents

At the McGill Medical Physics Unit, there was a strong desire to utilize developed Monte Carlo codes for the purpose of large scale Monte Carlo patient recalculations. Monte Carlo packages such as BEAMnrc and DOSXYZnrc became

tools for researchers to perform Monte Carlo simulations, however there was a disconnect between the patient DICOM data and the Monte Carlo packages. Researchers were forced to develop a large number of scripts to automate this process. Despite these efforts, the process still relied on user interaction, as was the case within the McGill Medical Physics Unit. The procedure was inefficient and relied on an experienced Monte Carlo user. As a result, this prompted the development of a framework environment for efficient Monte Carlo patient recalculations. The following manuscript describes the McGill developed Monte Carlo treatment planning system which is an integral component of this thesis.

Abstract

Radiotherapy research lacks a flexible computational research environment for Monte Carlo (MC) and patient-specific treatment planning. The purpose of this study was to develop a flexible software package on low cost hardware with the aim of integrating new patient specific treatment planning with MC dose calculations suitable for large-scale prospective and retrospective treatment planning studies. We designed the software package "McGill Monte Carlo treatment planning" (MMCTP) for the research development of MC and patient specific treatment planning. The MMCTP design consists of a graphical user interface (GUI), which runs on a simple workstation connected through standard secure-shell protocol to a cluster for lengthy MC calculations. Treatment planning information (e.g., images, structures, beam geometry properties and dose distributions) is converted into a convenient MMCTP local file storage format designated, the McGill RT format. MMCTP features include: (a) DICOM_RT, RTOG and

CADPlan CART format imports; (b) 2D and 3D visualization views for images, structure contours, and dose distributions; (c) contouring tools; (d) DVH analysis, and dose matrix comparison tools; (e) external beam editing; (f) MC transport calculation from beam source to patient geometry for photon and electron beams. The MC input files which are prepared from the beam geometry properties and patient information, (e.g., images and structure contours) are uploaded and run on a cluster using shell commands controlled from the MMCTP GUI. The visualization, dose matrix operation and DVH tools offer extensive options for plan analysis and comparison between MC plans and plans imported from commercial treatment planning systems. The MMCTP GUI provides a flexible research platform for the development of patient-specific MC treatment planning for photon and electron external beam radiation therapy. The impact of this tool lies in the fact that it allows for systematic, platform-independent, large-scale MC treatment planning for different treatment sites. Patient recalculations were preformed to validate the software and ensure proper functionality.

3.1 Introduction

The impact of improvements in dose calculation algorithms need to be established using realistic treatment plans and comparisons of these plans must be made using a common platform. Clinical impact of treatment plan evaluation and comparisons with different treatment planning systems using commercial software is often not reproducible since these packages use their own plan evaluation algorithms such as DVH and data storage format. Results between packages are typically not reproducible and these platform dependent effects could lead

to inconsistent results between researchers. Inconsistency amongst researchers may be partially due to the lack of a widely available graphical data analysis and programming environment which could be used to read, review, and compare dose, contours, and image data from a wide range of clinical and academic planning systems [1]. There is a need for an accessible software platform that combines different forms of treatment planning and analysis tools with ease specifically for large-scale retrospective research studies. Two software environments, CERR [1] (Division of Bioinformatics and Outcomes Research, Dept. of Radiation Oncology, Washington University School of Medicine) and MINERVA [2] (Idaho National Engineering and Environmental Laboratory (INEEL), Montana State University (MSU), Lawrence Livermore National Laboratory (LLNL) and the University of California Davis School of Medicine) were designed for radiotherapy research. However, these software environments require additional (commercial) packages to be installed, use interpreted and slow language tools, lack MC capabilities or are not easily available.

We describe a radiotherapy research environment for MC and patient-specific treatment planning, "McGill Monte Carlo treatment planning" (MMCTP), to facilitate comparison of MC dose calculations and the evaluation of treatment plans from different platforms. MMCTP provides a flexible software environment to integrate MC planning and to support the development of new treatment modalities. The aim of this project is to build a patient specific treatment planning system, with (1) MC treatment planning (external beam electron and photon planning),

(2) the use of multi modality and multi instance imaging, and (3) analysis tools for plan evaluation and studies of outcome correlations.

3.2 Materials and Methods

3.2.1 Programming Environment

The MMCTP platform was designed using REALBasic® (RealSoftware Inc., Austin Texas). REALBasic® runs on Macintosh, Windows and Linux operating systems and includes built-in 3D graphics tools for visualization effects. It is a rapid application development environment (RAD) meaning one can quickly design applications and GUIs with full fledge Object Oriented Programming (OOP) offering great flexibility for programming changes.

3.2.2 Monte Carlo Software

There are many MC codes available for radiation transport simulations. In this work, we have interfaced MMCTP with BEAMnrc [3] and the voxel Monte Carlo code XVMC [4, 5]. These codes are used in succession to calculate patient dose. BEAMnrc simulates the particle phase-space data at 70 cm from the source while XVMC transports the simulated phase-space file through the patient geometry to calculate patient dose. The patient geometry is defined within the XVMC density matrix (DMX) file. The DMX voxel densities may be assigned either by manual input through assigning a density value to a structure volume or through an algorithm which assigns densities based on CT numbers, as shown by [6]. The dose distribution uncertainty is an important detail in treatment planning. No more is this apparent than in the stochastic nature of MC dose distributions where the uncertainty is closely related to the number of histories.

XVMC simulations report the statistical uncertainty for dose values within the dose distribution. All MC codes including BEAMnrc and XVMC require commissioning before one can trust the simulation results. The commissioning process for BEAMnrc includes fine-tuning of the virtual linac configurations and adjusting the source energy within the BEAMnrc input files so that the dose calculations under controlled conditions are in agreement with measurements. [7].

3.2.3 MMCTP Features

MMCTP version 1 features are summarized in table 3–1. The MMCTP design consists of a GUI, which runs on a simple workstation connected through standard secure-shell protocols to a cluster for lengthy MC calculations. As the local station controls the shell, this strategy enables the use of an off-site cluster that does not require specific software (e.g., daemons, etc) to be installed. In addition, the design allows for anonymous patient information on the calculation cluster and a minimal amount of data interchanged between calculation cluster and workstation.

3.2.4 MMCTP Validation Steps

MMCTP validation involved DVH verifications, measurement comparisons and patient dose recalculations to check the consistency of coordinate transformations and the implementation of beam settings (e.g., wedge orientations, etc). DVH testing included DVH comparisons with commercial treatment planning systems and DVH calculations of simplistic dose distributions for which the DVH was manually calculated for comparison. Patient recalculations under simplified conditions (e.g., heterogeneous patient density replaced by homogeneous water density)

Table 3–1: MMCTP version 1, features.

Features	Summary
Import formats	DICOM_RT, RTOG, CADPlan CART
Export formats	RTOG
Visualization options	2D axial, sagittal or coronal view for images, contours and dose distributions 3D beam's eye view and room's eye view for images, contours, and beam geometry settings (e.g., jaws, MLC, couch, table and gantry rotation)
Treatment planning	Add and delete external beams, edit beam properties (e.g., treatment unit, energy, jaw settings and MLC leafs) Structure contouring and editing tools
Monte Carlo	Generation of input files and simulation submission for BEAMnrc and XVMC
Dose analysis	DVH calculator and dose distribution operations (e.g., addition, subtraction, multiplication and division of dose distributions)

and comparison of the MMCTP dose distribution against dose distributions from conventional planning systems verified many consistency features.

3.3 MMCTP Development

The initial programming task was to develop an organized object class structure to store treatment planning information within memory. The RTOG format, a well-documented and widely available radiotherapy archiving mechanism, was used as a model to base the REALbasic® objects. This not only helps to organize the variables but also ensures native reading and writing to RTOG. In addition, new MMCTP programmers will benefit from a simple RTOG object based GUI.

3.3.1 McGill RT Characteristics

While the RTOG format provides a convenient object class, it does not provide a flexible file storage format. A new file format "McGill RT" was introduced for saving patient plans on the workstation as an internal format. The file system resembles the RTOG format but includes efficiency improvements. The RTOG format was designed for exporting and importing patient plans and thus, there is no simple method for saving small changes. The McGill RT format, on the other hand, was developed to minimize redundant information and minimize the number of files edited to save changes. Figure 3–1 shows a schematic diagram of the McGill RT file format. McGill RT format uses a specific organization of folders containing files which are either binary or text. Images and dose distributions are stored as binary files while structures and beam information are stored as text files. The file structure of the McGill RT format contains a main McGill folder, under which folders for each patient are located. The patient folders are titled with the patient name and ID number. Within a patient's folder there can be multiple image sets (CT, magnetic resonance imaging (MRI), ultrasound (US)) and each set has its own folder. Under each image set, there are folders for multiple plans as well as a folder for the images and structures. The plan folders store beams, doses, and MC control files. The McGill RT file storage format is flexible enough to allow for future adaptation to include image data sets such as, image fusion between MRI, US, positron emission tomography (PET), CT and time phased computed tomography (4D CT). The McGill RT format should not be considered as yet another radiotherapy storage format. The MMCTP design uses McGill RT

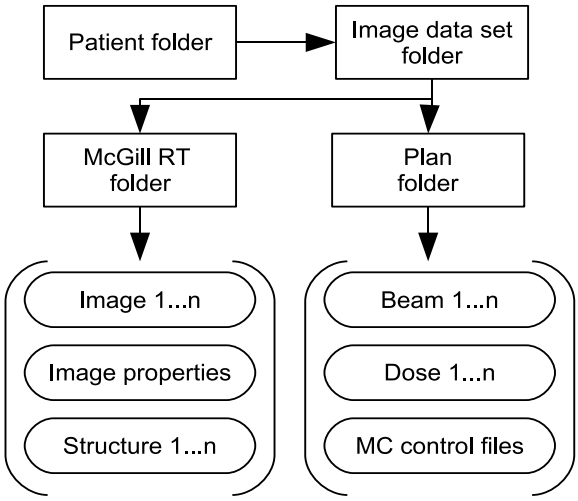

Figure 3–1: McGill RT file structure, folders and files. The image data set includes one McGill RT folder for the image and structure files and one or more plan folders for the various plans associated to an image data set. Plan folders contain beam geometry files, Monte Carlo control files and dose distribution files.

as an internal format, but also includes export functions to standard radiotherapy formats such as RTOG.

Image files are stored individually under the McGill RT folder and these files define the image set for a MMCTP patient. The image data files are binary files containing the slice position and pixel data. In order to properly read these files, there is an image properties text file which stores the image dimension size, the bytes per pixel value and the (x, y) origin of the patient coordinate system. Generally, the (x, y) origin of the patient coordinate system is at the centre of the image. Additional parameters to the properties file are required for the future implementation of MRI, US, PET or 4D data sets.

Structure files contain a sequence of three-dimensional coordinates which define a volume of interest including target volumes and organs at risk. Coordinates are defined on each CT image slice. Within a given slice, a structure may consist of one or more segments where each segment is a sequence of at least four points which define a closed curve. Structure files are found under the McGill RT folder since they are associated with the image files. Each structure file contains a header section followed by the structure coordinates. The header information contains the structure name and colour while the structure coordinates points are arranged in order per slice number. Coordinate points are written relative to the patient coordinate system.

Plans

Patient plans are assigned folders within an image set folder. The files found within a patient plan folder include: beam files, dose distribution files and MC control files.

Beam geometry files contain the information defining an external radiation beam. These include various properties such as: treatment unit, beam energy, beam applicators, number of monitor units (MU), number of fractions, aperture type, wedge angle and orientation, collimator gantry and couch angle, isocentre distance, isocentre coordinates (x, y, z), and X, Y jaw positions. The MLC leaf positions are not included within the beam file. Instead, there is a MLC file which contains the MLC fields for all beams of a plan.

Dose distribution files store a matrix of dose values at one or more points throughout a volume. The format allows for a regularly spaced grid in which a two

dimensional array of points is defined on one or more evenly spaced parallel planes. This format permits the computation of dose on a two-dimensional array of points on each CT image plane. The coordinate system for the array of dose points is defined with the patient coordinate system. Within one plane, a two-dimensional array of points is defined with the x, y position of the top left hand corner point, the number of points in x, y and the grid spacing in x, y. Each axial plane is identified with its z position, which normally corresponds to an axial CT image.

Monte Carlo control files store specific properties and the simulation progress for each MC simulation. The BEAMnrc properties file stores the number of initial particles, job split number and the simulation status. The XVMC properties file records the DMX settings, the XVMC calibration dose and the simulation progress for each beam. The DMX settings describe the specific properties of the DMX file since there are a few ways to generate the DMX file, either from CT numbers or assigning density values based on structure volumes or using a combination of both methods.

3.3.2 MMCTP Description

MMCTP is comprised of individual task windows and a main program window which is subdivided into tabs. A flow chart of MMCTP windows and tabs is shown in figure 3–2.

The external beam window is the main program window which opens after one loads a patient. The window as shown in figure 3–3 is comprised of a listbox, three graphic canvases and a tab menu. The listbox displays the patient plans and available dose distributions associated to each plan. The three canvases display

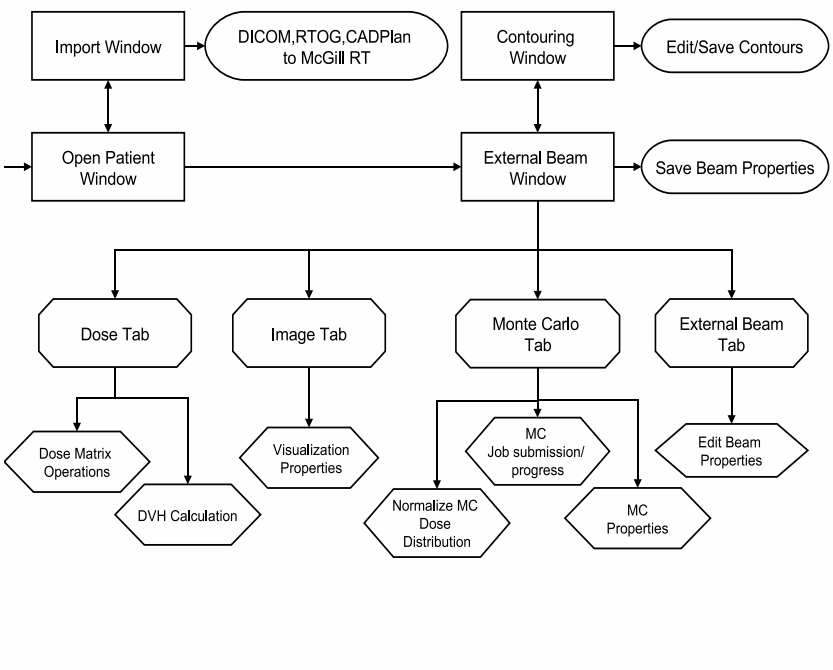

Figure 3–2: MMCTP flow chart. MMCTP opens with the open patient window; the user may then navigate to the main program windows for importing, contouring or external beam editing. The tab menu groups MMCTP features into common categories.

images, contours and dose distributions where each canvas can display three views: axial, sagittal or coronal. The tab menu splits the bottom portion of the beam window into four sections: external beams, Monte Carlo, image and dose.

The external beam tab lists the beams associated to a plan within a listbox. The listbox also displays various beam properties for each beam. Most of these properties are editable within the listbox. There is also a beam properties window which allows access to all the beam properties. A right click on the listbox allows the user to add or delete a beam.

The image tab lists various canvas display options. These options include window and level adjustments, scale settings, contour display options, colour-wash dose distributions options, isodose lines, display image and display cross-hairs. The contours and colour-wash dose distribution options include a transparency setting to view overlapping objects. Contour options include the structure colour and check boxes to fill-in the area and or show the edges.

The Monte Carlo tab handles the simulation properties for BEAMnrc and XVMC. Simulations are run on a remote cluster using a shell terminal which requires properties such as login IP, user name and password. MMCTP periodically checks the status of the simulation for both BEAMnrc and XVMC. Once a simulation is complete, the shell sends commands to add phase-space files or download dose distribution files. A second sub-tab menu separates the BEAMnrc and XVMC properties. The BEAMnrc tab includes BEAMnrc simulation properties, a run button and a simulation progress listbox. The BEAMnrc properties include the job split number and the number of initial particles. The run button generates

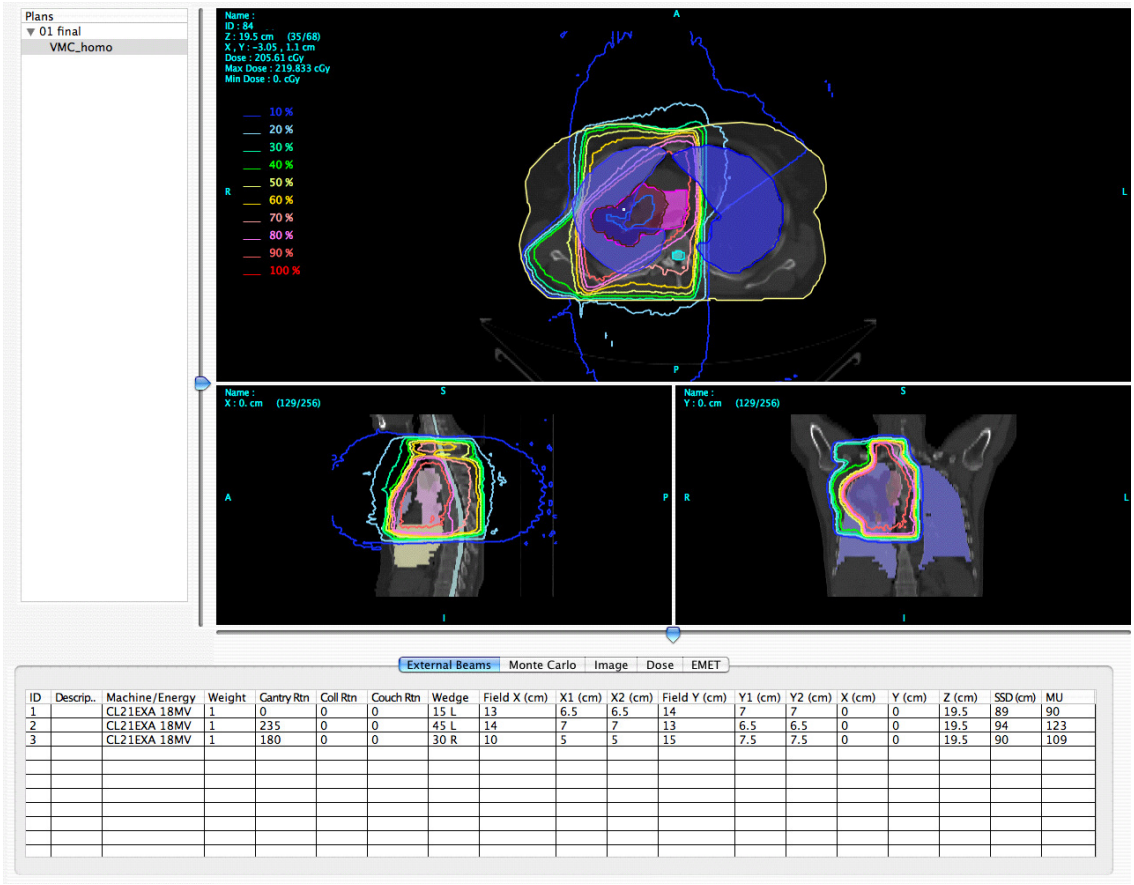

ID	Descrip..	Machine/Energy	Weight	Gantry Rtn	Coll Rtn	Couch Rtn	Wedge	Field X (cm)	X1 (cm)	X2 (cm)	Field Y (cm)	Y1 (cm)	Y2 (cm)	X (cm)	Y (cm)	Z (cm)	SSD (cm)	MU
1		CL21EXA 18MV	1	0	0	0	15 L	13	6.5	6.5	14	7	7	0	0	19.5	89	90
2		CL21EXA 18MV	1	235	0	0	45 L	14	7	7	13	6.5	6.5	0	0	19.5	94	123
3		CL21EXA 18MV	1	180	0	0	30 R	10	5	5	15	7.5	7.5	0	0	19.5	90	109

Figure 3–3: The external beam window showing patient plans on the left, three canvas views for axial, sagittal and coronal display and the tab menu. The external beam tab is selected which displays a properties listbox of the external beams for the selected plan.

the BEAMnrc input file, uploads the input file to the cluster and submits the job to the queue. The XVMC tab includes the DMX generation setting, XVMC normalization properties, run button and a progress listbox. The DMX generation settings define how the patient geometry will be modelled within XVMC. DMX generation settings include an option to generate the density values either from CT numbers (e.g., using a CT to density calibration curve) or assigning density values based on structure volumes or using a combination of both methods. Changes to these settings are saved within the XVMC properties file. If there are significant artefacts in the CT data set (patients with dental fillings or prostheses), one may choose to omit the CT images with artefacts. In this action, the CT to density algorithm will average over the omitted CT images. Alternatively, one may assign density values based on structure volumes to deal with artefacts. Both the DMX file and XVMC input file are automatically generated and uploaded to the cluster while the XVMC dose distribution files are downloaded to the workstation after a simulation is complete. Once all XVMC simulations are complete (one dose distribution per beam), MMCTP normalizes and adds the dose distribution file(s) to generate one McGill RT dose file. The XVMC normalization property includes the energy specific calibration value, which is used to properly normalize the MC dose distribution into dose per monitor unit. The uncertainty of the normalized dose distribution is spatially dependent and as such requires careful analysis of the voxel uncertainties. Uncertainties for each voxel will eventually be available within MMCTP. Although, the current version of MMCTP does not make use of

the XVMC uncertainties to generate an uncertainty map of the normalized dose distribution.

In general, a three field plan with MLC and wedged fields will take about 30 hours of CPU time on a single 1.8 GHz 64 bit AMD processor. With the use of a cluster, the total CPU time remains the same but the CPU time on the individual nodes is significantly decreased depending on the number of nodes. Within MMCTP, BEAMnrc and XVMC simulations are currently run using a high number of histories to achieve a low statistical uncertainty. This is inefficient and undesirable since the goal of MCTP is to simulate a dose distribution to a specific uncertainty [5]. Future versions will attempt to use statistical uncertainty as the cutoff point for simulations.

The dose tab contains the DVH calculator and the dose comparison tools. DVHs are calculated and stored in memory for all contours and can be viewed in differential or cumulative mode. Once calculated, DVHs are displayed in the DVH window, as shown in figure 3–4. The dose comparison tools allow the addition, subtraction, multiplication and division of two dose distributions. The second dose distribution may be replaced with a constant. This operation generates a new dose distribution based on the selected operation. The newly generated dose distribution is automatically saved under the appropriate plan folder. Currently, MMCTP does not use the dose distribution uncertainty information. In future releases, propagation of uncertainties needs to be handled properly for dose distribution manipulations. MMCTP also includes a "paint" dose distribution tool where the user can generate a grid and manually paint dose values one plane at a

time. This tool has been used to quantify the DVH calculation accuracy but its future role can be to define dose constraints for inverse planning techniques.

The contouring window was designed for structure contouring where the user may create, edit or delete structures. This window is shown in figure 3–5 and includes a main canvas for editing contours, thumbnail image preview, a list of structures and some basic display options. Structures are edited individually on axial planes where a structure may have multiple contour segments per axial plane. Segment editing options include: add point, move point, delete point, scale segment, move segment, and copy segment to superior or inferior slice. There also exists an auto-contouring tool which contours objects based on CT number constraints. The display options allow the user to change the image window and level, the scale size, the contour transparency settings and boolean check boxes to show the CT image and or the contours.

3.4 MMCTP Results

3.4.1 MMCTP Validation

Preliminary validation focused on the DVH calculator and patient recalculations. Within MMCTP, DVHs are calculated by interpolating a dose value at the center of each pixel for all pixels within a structure where the structure pixels refer to the pixels within a contoured CT image. Dose distributions of simple objects for which the DVH can be manually calculated were created to assess the accuracy of the DVH calculator. The MMCTP DVHs were within an upper limit of 1% to the manually calculated DVHs. The interpolation of the dose distribution grid onto the pixel grid is the main source of discrepancy.

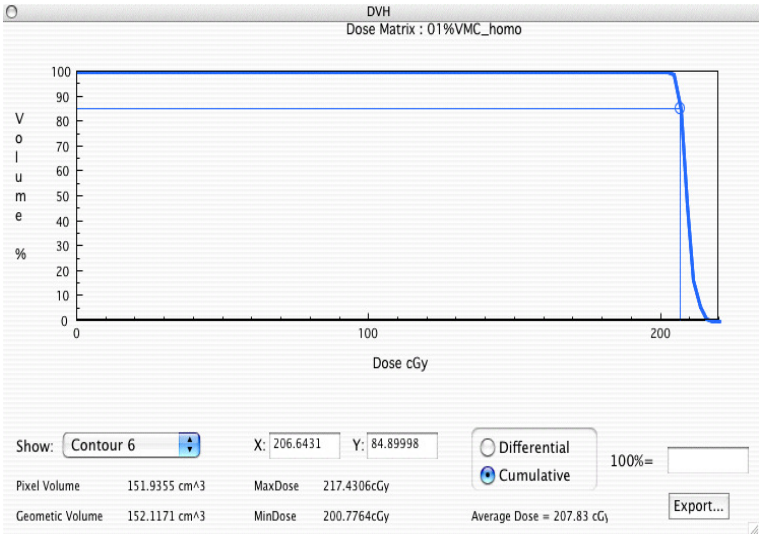

Figure 3–4: MMCTP DVHs are displayed as differential or cumulative within the DVH window. The window includes a summary of the contour volume, maximum and minimum dose, as well as an option to show multiple or single DVH graphs.

The DVH calculation accuracy is also dependent on the structure volumes. If the volume is not accurate then the DVH is not accurate. The structure volumes are determined from the following process. The structure x, y cm coordinate points are used to paint a 2D polygon onto an image with the native CT resolution. The number of pixels within the painted polygon determines the structure volume. If the structure volume is large compared to the volume of one voxel then there is excellent agreement between the MMCTP calculated volumes and the manually calculated volumes. Smaller structure volumes have greater error as there is a higher ratio of edge voxels versus internal voxels. The structure error is a result of the approximation in transferring a curve onto a finite pixel resolution image. Table 3–2 demonstrates this effect.

Figure 3–5: Contour window for editing and creating new contours. The contouring tools include: add point, move point, delete point, scale, move segment, copy sup and copy inf.

Table 3–2: Real and MMCTP calculated volumes. As expected, the volume error becomes significant with small volumes. In addition to the volume size, the error also depends on the image resolution (pixel width, height, and depth). The pixel width × height × depth is the elementary unit of volume. As the unit volume decreases, the error in volume decreases. The volumes in this table were calculated on a 256×256 image with pixel dimensions of 0.164×0.164 cm^2 and an image depth of 0.5 cm.

Volume	MMCTP	
cm^3	cm^3	error (%)
700	699.6	0.1
175	174.9	0.1
87.5	87.4	0.1
25	25.01	0.1
14	12.3	12.1

Conventional Planning Systems

Lung cancer patients were recalculated using MMCTP as an extensive test to identify problems throughout MMCTP job control and submission mechanics. These patients were originally planned using CADPlan version 6.2 (Varian Medical Systems Inc., Palo Alto, CA) and thus, the dose distribution was calculated using a pencil beam algorithm with the patient geometry set to homogeneous water. Patient plans were imported within MMCTP for MC dose recalculation. The MMCTP-generated MC input files were compared with manually created MC input files and differences between these files indicate errors within the MC module. It should be noted that the XVMC patient specific density matrix was set to homogeneous water to test the agreement between CADPlan calculated dose distribution for homogeneous water patients and the MC dose distribution. Once the MC dose distribution was calculated, a visual isodose comparison and a

DVH comparison was performed. A patient DVH comparison between MMCTP and CADPlan is shown in figure 3–6 and as expected, the two DVH curves are similar. There is a 1% difference separating the DVH curves for the CTV contour dose at 90% of the volume, although this difference increases to 3% at maximum dose. At first glance, a maximum dose difference suggests a problem with the XVMC normalization factor. However, the normalization factor was ruled out after verifying its accuracy under standard 10×10 cm^2 fields. In addition, the structures in figure 3–6 all have volumes above 90 cm^3 and thus the DVH volume error is negligible. With proper normalization and an accurate DVH calculator, the maximum dose difference is attributed to a small difference in dose distributions at high dose values and not a result of the analysis process. Within figure 3–6 there is a noticeable difference throughout the heart DVH. This is a three-field plan with MLC shaped fields where the heart is tangential to the fields. Since the heart is a tangential organ, it is expected that the observed difference is primarily due to beam modeling between MC and pencil beam algorithms. This has been demonstrated by the fact that good agreement was obtained between MLC shaped profiles calculated with MC and experimental profiles in the penumbra of the field whereas penumbra was systematically underestimated with CADPlan [7].

3.5 Conclusions

Monte Carlo treatment planning (MCTP) has only now made a slow entry in the clinical environment taking considerably longer than envisioned. [8] The main objective of this project was to build a flexible computational radiotherapy research environment which allows for MCTP, outcome analysis and other future

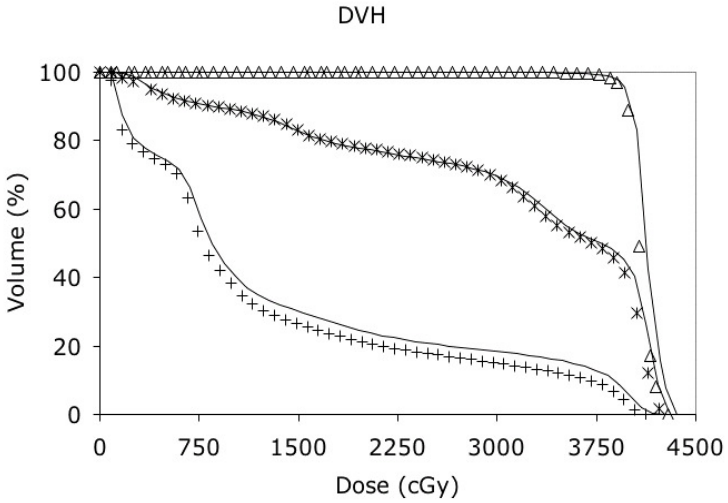

Figure 3–6: MMCTP patient recalculation with patient geometry set to the density of water; CADPlan DVH ($\triangle$ CTV, $*$ lung and + heart). MMCTP CTV DVH is slightly right shifted, resulting in a less than 1% dose difference at 90% volume.

research implementations. It is well known that DVHs and outcome analysis must be compared on the same platform to avoid platform dependent effects. A research environment of this type opens the possibility of large-scale retrospective and prospective MC studies.

MMCTP was built as a research platform for the development of patient specific MC treatment planning for external beam radiation therapy. The MMCTP design consists of a GUI which remotely connects to a computer cluster for MC simulations. MMCTP uses an internal storage format that is flexible in that it allows for future implementation of multi-instance and multi-modality image information. The visualization options, dose matrix operations and DVH tools offer extensive possibilities for plan analysis and comparisons. Plans are imported within MMCTP from commercial treatment planning systems through

well-documented storage protocols such as DICOM_RT and RTOG. MMCTP features a MCTP architecture that uncouples the private patient data from remote calculation engines. This philosophy allows MMCTP to connect to large university-based computer grids so there is no need for expensive computer hardware. Ideally, MMCTP can offer clinics access to MCTP by providing non-specialist people (dosimetrist) a simple interface for MCTP.

MMCTP validation tested cluster communications, MC results, DVH calculations and patient recalculations. Patient recalculations were performed as a validation step to identify potential problems throughout the MC process such as wedge orientations, coordinate systems, couch, gantry and collimator angles. Patient recalculations with the patient geometry set to water should produce similar dose distributions with the conventional heterogeneity uncorrected imported dose distributions. MMCTP DVHs from the MC and conventional dose distribution agreed well for the CTV target.

The MMCTP package will be released for use as a download from our webpage. It is intended that this package be used for radiotherapy research, and not as a clinical application. Improvements, updates and bug fixes are expected and new versions will be posted on our website

`http://www.medphys.mcgill.ca/~mmctp/`. MMCTP is designed to run on low cost hardware and as such, the minimum system requirements are a 1 GHz processor with at least 512 MB of ram.

3.6 Acknowledgements

This work has been supported in part by the Canadian Institutes of Health Research through Grant No. MOP 79448 and through the National Cancer Institute of Canada, Terry Fox Foundation Grant No. 016298.

3.7 References

[1] J O Deasy, A I Blanco, and V H Clark. CERR: a computational environment for radiotherapy research. *Med. Phys.*, 30(5):979–985, 2003.

[2] J Lehmann, C H Siantar, D E Wessol, C A Wemple, D Nigg, J Cogliati, T Daly, M Descalle, T Flickinger, D Pletcher, and G DeNardo. Monte Carlo treatment planning for molecular target radiotherapy within the MINERVA system. *Phys. Med. Biol.*, 50(5):947–958, 2005.

[3] D W O Rogers, B A Faddegon, G X Ding, C M Ma, J We, and T R Mackie. BEAM: A Monte Carlo code to simulate radiotherapy treatment units. *Med. Phys.*, 22(5):503–524, 1995.

[4] I Kawrakow, M Fippel, and K Friedrich. 3D electron dose calculation using a Voxel based Monte Carlo algorithm (VMC). *Med. Phys.*, 23(4):445–457, 1996.

[5] I Kawrakow and M Fippel. Investigation of variance reduction techniques for Monte Carlo photon dose calculation using XVMC. *Phys. Med. Biol*, 45(8):2163–2183, 2000.

[6] C Constantinou, J C Harrington, and L A DeWerd. An electron density calibration phantom for CT-based treatment planning computers. *Med. Phys.*, 19(2):325–327, 1992.

[7] I J Chetty and J P Seuntjens. Monte-Carlo-based Clinical Treatment Planning:

Issues for Consideration. In *Integrating New Technologies into the Clinic: Monte Carlo and Image-Guided Radiation Therapy*, Windsor, Ontario, Canada, June 2006. AAPM, Medical Physics Publishing.

[8] F Verhaegen and J Seuntjens. International Workshop on Current Topics in Monte Carlo Treatment Planning. *Phys. Med. Biol.*, 50(5):20, 2005.

CHAPTER 4
Updates to MMCTP

Contents

The previous chapter has introduced the MMCTP software package as outlined in the original 2007 publication. Since then, there has been an enormous

amount of development in all aspects of the code. The following chapter summarizes the main features and additions not included in the previous published paper.

4.1 DICOM Class

DICOM import was the last import format added to MMCTP. The first versions of MMCTP DICOM import were limited as they were transcribing individual files into a text file and then converting into McGill RT. The procedure was contained within two methods, read DICOM and convert DICOM. It was soon realized that this approach was not robust enough to handle DICOM interoperability. DICOM import was then split into three methods: DICOM to text parser, DICOM class reader, and DICOM to McGill RT converter.

The DICOM parser was written to read all types of DICOM files. The parser populates an array of DICOM elements. Each element contains two tags, element type (VR), size, and data set value. The complication with DICOM is that data sets can contain other nested data sets, which are encoded as sequences. In radiotherapy, these nested data sets can reach five or six layers. Elements contain a layer variable, which defines the sequence level of each element. Upon completion of the DICOM parser, these elements are viewable within the MMCTP DICOM listbox viewer. The first section of a TomoTherapy DICOM plan file is shown in figure 4–1.

The DICOM class reader builds radiotherapy specific classes from the generalized element parser class. MMCTP contains four DICOM RT classes: image, structure, plan, and dose. Each class contains variables pertinent to the function

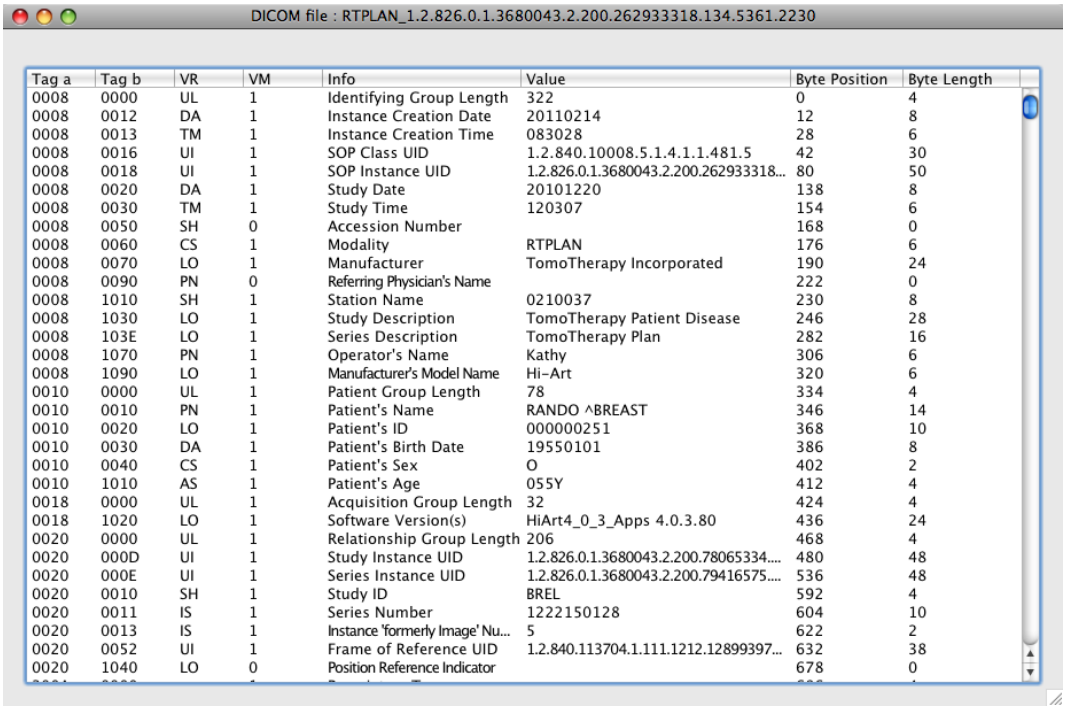

Tag a	Tag b	VR	VM	Info	Value	Byte Position	Byte Length
0008	0000	UL	1	Identifying Group Length	322	0	4
0008	0012	DA	1	Instance Creation Date	20110214	12	8
0008	0013	TM	1	Instance Creation Time	083028	28	6
0008	0016	UI	1	SOP Class UID	1.2.840.10008.5.1.4.1.1.481.5	42	30
0008	0018	UI	1	SOP Instance UID	1.2.826.0.1.3680043.2.200.262933318...	80	50
0008	0020	DA	1	Study Date	20101220	138	8
0008	0030	TM	1	Study Time	120307	154	6
0008	0050	SH	0	Accession Number		168	0
0008	0060	CS	1	Modality	RTPLAN	176	6
0008	0070	LO	1	Manufacturer	TomoTherapy Incorporated	190	24
0008	0090	PN	0	Referring Physician's Name		222	0
0008	1010	SH	1	Station Name	0210037	230	8
0008	1030	LO	1	Study Description	TomoTherapy Patient Disease	246	28
0008	103E	LO	1	Series Description	TomoTherapy Plan	282	16
0008	1070	PN	1	Operator's Name	Kathy	306	6
0008	1090	LO	1	Manufacturer's Model Name	Hi-Art	320	6
0010	0000	UL	1	Patient Group Length	78	334	4
0010	0010	PN	1	Patient's Name	RANDO ^BREAST	346	14
0010	0020	LO	1	Patient's ID	000000251	368	10
0010	0030	DA	1	Patient's Birth Date	19550101	386	8
0010	0040	CS	1	Patient's Sex	O	402	2
0010	1010	AS	1	Patient's Age	055Y	412	4
0018	0000	UL	1	Acquisition Group Length	32	424	4
0018	1020	LO	1	Software Version(s)	HiArt4_0_3_Apps 4.0.3.80	436	24
0020	0000	UL	1	Relationship Group Length	206	468	4
0020	000D	UI	1	Study Instance UID	1.2.826.0.1.3680043.2.200.78065334....	480	48
0020	000E	UI	1	Series Instance UID	1.2.826.0.1.3680043.2.200.79416575....	536	48
0020	0010	SH	1	Study ID	BREL	592	4
0020	0011	IS	1	Series Number	1222150128	604	10
0020	0013	IS	1	Instance 'formerly Image' Nu...	5	622	2
0020	0052	UI	1	Frame of Reference UID	1.2.840.113704.1.111.1212.12899397...	632	38
0020	1040	LO	0	Position Reference Indicator		678	0

Figure 4–1: MMCTP DICOM element viewer.

of each type. Sequences and nested sequences are contained within their own class. With a total of twenty seven unique classes, MMCTP is able to store DICOM RT data into native DICOM class structures. These DICOM classes greatly simplified the transformation of data from DICOM to McGill RT. For example, there are two common DICOM techniques to define the z slice thickness and z slice position for axial dose planes. A serial DICOM reader and transcriber would assume the first read technique to be correct. With the use of a DICOM class, interchangeable elements can be evaluated simultaneously to determine which is the correct z slice thickness. In addition, DICOM classes also simplify the transformation of McGill RT data back into DICOM format. This transformation is split into three

steps: creation of DICOM class from McGill RT, creation of DICOM elements from DICOM class, writing binary DICOM elements to disk, which is universal to all classes. DICOM dose export is currently the only DICOM export filter within MMCTP.

4.2 MMCTP Classes

There are a few main MMCTP classes, which greatly increase the flexibility of MMCTP. The following sections describe their importance.

4.2.1 Shells

The shell class stores the information required to login and submit a simulation to a remote or local user account. The following properties are required to allow MMCTP to login and navigate the system: IP address, user name, password, line feed prompt, list files command, and file transfer protocol. Windows systems require additional properties, the location paths of plink and pscp. These two third-party Windows software packages establish the remote connection. The following properties allow MMCTP to submit a remote simulation: bash, maximum number of jobs, EGSnrc folder, XVMC folder and bin path. Together, these two groups of properties facilitate compatibility between MMCTP and remote computers. Ultimately, these shell classes allow MMCTP to switch simulations between remote computers independently of any user interference. The details and benefits of this process are discussed below.

4.2.2 Linacs

The linac class structure allows the user to define multiple treatment machines within MMCTP. The main properties of a treatment machine are beam mode,

linac name, and beam energy. The beam mode can be Photon or Electron while the linac name and energy are defined by the user. Additional physical machine properties such as MLC type, electron applicators, dynamic wedges, and physical photon wedges can all be assigned to the linac class. These physical properties set limits to the beam line configuration of a linac.

MC settings are also included in the linac definition class. MC settings include: BEAMnrc input file, BEAMnrc pegs file, desired phase-space particle density, BEAMnrc folder name, DOSXYZnrc normalization value, and XVMC normalization value. MC settings pair the linac with a BEAMnrc linac model in addition to providing instructions on how to modify the BEAMnrc linac model to the beam line configuration of a user specific orientation. The creation of a BEAMnrc input file from a user defined beam line configuration is a fundamental feature of MMCTP. The linac type property specifies the linac manufacturer. Linac specification is used to guide the creation of a new BEAMnrc input files as the linac design varies between manufacturers such as Varian, Siemens, and TomoTherapy. As a result, MMCTP must separate BEAMnrc configuration scripts between manufacturers. It should also be noted that the BEAMnrc folder, DOSXYZnrc and XVMC dose normalization values are defined per MMCTP login shell. Separating these parameters per shell allows the user to use a shell specific normalization value, which may be necessary in the event of differences between BEAMnrc versions, operating systems, and compilers.

The linac class is fundamental to the function of MMCTP and is heavily used throughout the code. The class pairs BEAMnrc input files to treatment machine

names and guides the creation of new BEAMnrc input files. It is this class that enables MMCTP to be a universal treatment planning system for all types of external beam treatment machines.

4.2.3 MLCs

The MLC class holds an array of available MLC types for assignment into a linac class. The class consists of the MLC name, type (binary or leaf pairs), number of leaves, leaf end gap, leaf direction, and leaf boundaries. The class is first used during the initialization of a McGill RT beam. The initialization process transfers the geometric properties of the MLC class to a specific beam MLC class. Once initialized, the user may visualize the projected MLC leaf pattern with respect to the target volume or any contoured volume.

The class properties are also used during the creation of a BEAMnrc input file. Physical properties, such as the number of leaves, are used to ensure that the MLC CM of the BEAMnrc input file is compatible with the McGill RT beam MLC. The MLC type (binary or leaf pairs), in addition to the linac manufacturer type, guide the creation of new MLC CM properties.

MLC classes are defined by the user or created automatically during DICOM patient import. DICOM plan files specify the properties of a MLC within the beam limiting device sequence. During DICOM import, MMCTP will attempt to link a DICOM MLC class with an existing MLC class. If the DICOM MLC class is unmatched, a new MLC class is defined within MMCTP. Once defined, the user may then link this MLC class to an existing linac class.

4.2.4 CT to Density Curves

CT to density curves are defined within the CT2D class. The class allows the user to create, modify, and delete CT to density curves. The CT curve associates a Hounsfield unit (HU) range with a material name and density range. During the creation of a patient specific EGSPhant file, the user has the option of assigning material and density values to EGSPhant voxels based on the HU of the patient's CT image.

It is necessary to be able to switch between CT curves for the creation of individual types of EGSPhant files. For instance, the material names are linked to a pegs file, which is only valid for a predefined range of energies. The user may then define a high energy CT curve for higher energy beams and low energy curve for lower energy beams. In addition, the user may want to define a heterogeneous water EGSPhant file as opposed to a heterogeneous material EGSPhant file.

Each curve is defined with a unique name, pegs file, and the number of linear segments and materials. For example, the CT curve illustrated in figure 4–2 is defined by 4 lines. As a rule, the HU range must increase from lowest (first material) to highest (last material). In addition, the HU high value should equal the HU low value on the following line. The density values do not need to be continuous. Lastly, the material names do not need to be unique; the user may define a CT curve with 4 lines and only one material.

4.3 BEAMnrc

The BEAMnrc structure tree contains an enormous amount of code and variables. The main branches of the tree are shown in figure 4–3. Each level of

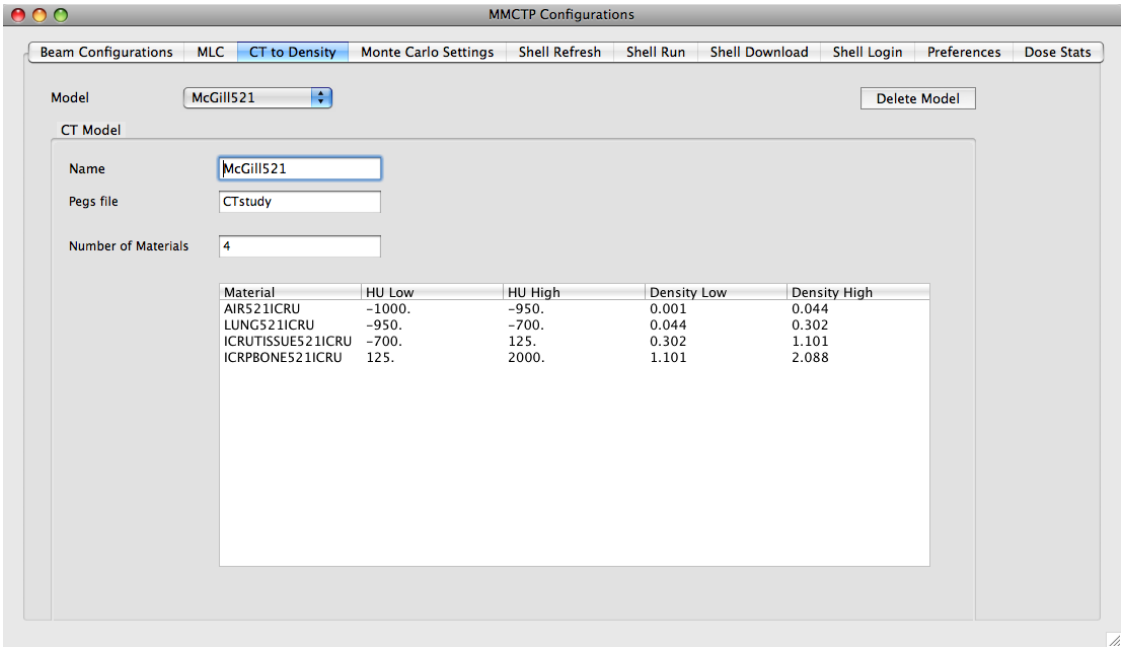

Figure 4–2: CT to density configuration tab, creation/modification of CT to density curves

the tree contains a large number of methods to act upon the variables within that level. The BEAMnrc thread sits atop of the tree as it is the control box, which processes BEAMnrc tasks within MMCTP. These tasks range from reading in an input file to determining the size of a phase-space file. The main properties of the BEAMnrc class include an array of BEAM classes (one for each McGill RT beam), a few default BEAMnrc class settings such as auto run and refresh, remove w files, default number of BEAMnrc jobs, default values for IDAT (controls output of the .egsdat file) and IZLAST (controls whether or not ZLAST is recorded in phase-space files), and the phase-space Real SQL database.

The BEAM class level stores the BEAMnrc methods and properties associated to one McGill RT beam. The properties can be divided into native BEAMnrc

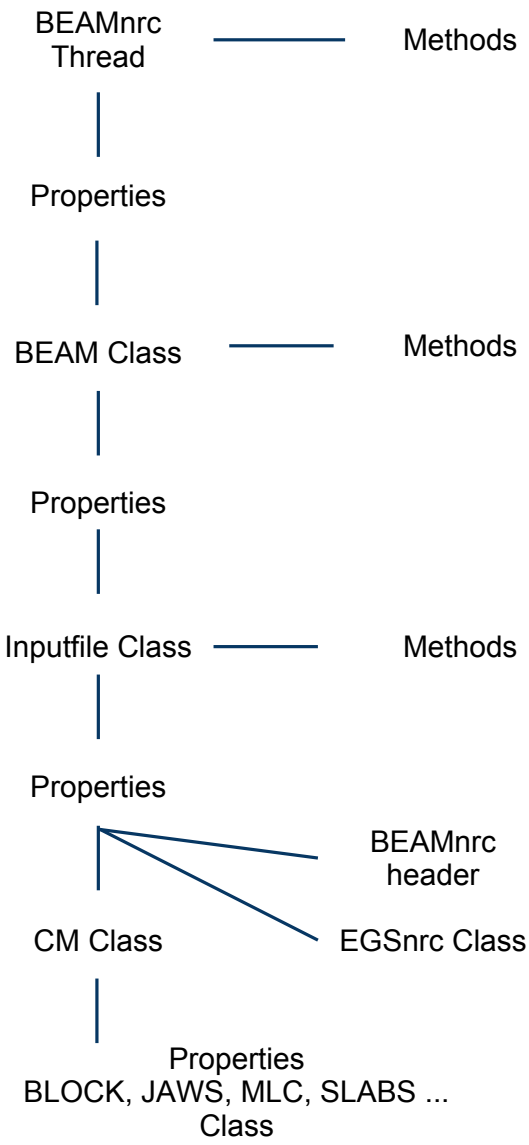

Figure 4–3: Flow chart of BEAMnrc class

properties and MMCTP defined BEAMnrc properties. For example, the properties that define a BEAMnrc input file are all native to BEAMnrc while the properties such as the simulation start time, status of a simulation, and number of phase-space particles are MMCTP add-ons. The main methods within the BEAM class are read, auto-edit, and write BEAMnrc input files. These BEAMnrc structure methods include sub-methods for the header, EGSnrc section, and CM sections. The auto-edit methods dictate how a specific CM section should be modified based on the associated McGill RT beam and linac type. The current version of MMCTP auto-edits the following list of CMs: APPLICAT, BLOCK, DYNJAWS, JAWS, PYRAMID, MLC, SLABS, TOMOMLC, VARMLC, and WEDGE.

The input file class level stores the main methods for parsing the CM modules of an input file, the array of CM classes, the header, and EGSnrc properties. This level stores BEAMnrc data in its native format for easy data manipulation within the auto-edit methods or manually within the BEAMnrc CM GUI windows. The philosophy behind this is to simplify future adaptations and modifications to MMCTP. One only has to generate a new auto-edit method to customize MMCTP to their needs. Reading and writing of the CM is already handled. In addition to editing the CMs, the header section of the input file is available for modification. A current feature of MMCTP makes use of this access to automatically determine the DBS radius based on the McGill RT beam settings. Other uses could be to view or edit the scoring plane, or modify the electron splitting plane.

The final layer of the BEAMnrc class structure rests with the CM classes. These classes contain properties specific to a BEAMnrc CM and methods to read

and write. The current version of MMCTP reads and writes the following list of CMs: APPLICAT, BLOCK, FLATFILT DYNJAWS, JAWS, PYRAMID, MLC, SLABS, TOMOMLC, VARMLC, and WEDGE. Many of these CMs can be viewed and edited within the BEAMnrc CM GUI of MMCTP.

4.3.1 BEAMnrc GUIs

The BEAMnrc GUIs within MMCTP allow the user to verify the settings within the BEAMnrc input file in addition to providing an intuitive interface to make changes to the input file. The implantation of BEAMnrc GUIs within MMCTP is a large extension from the original idea of simply modifying a few key lines of the BEAMnrc input file. It was soon realized that advanced users required more control of the BEAMnrc simulations and would benefit from having this control within MMCTP. The first level of the GUIs is the advanced BEAMnrc GUI, shown in figure 4–4.

The advanced BEAMnrc GUI displays the header information, listbox of CMs, an option to open the EGSnrc inputs and an option to open the egslst/egslog file. A number of the header properties with pulldown menus open-up additional GUIs for more options. For example, source GUIs are included with sources: 0, 1, 3, 19, and 21. A number of CM GUIs have also been coded to allow the user to view and edit CM specific properties. The list of CM GUIs includes: APPLICAT, SLABS, BLOCK, JAWS, DYNJAWS, DYNVMLC, MLC, WEDGE, and TOMOMLC. This list of sources and CMs have been sufficient for the needs of the McGill Medical Physics department, however, additional GUIs may be needed for other

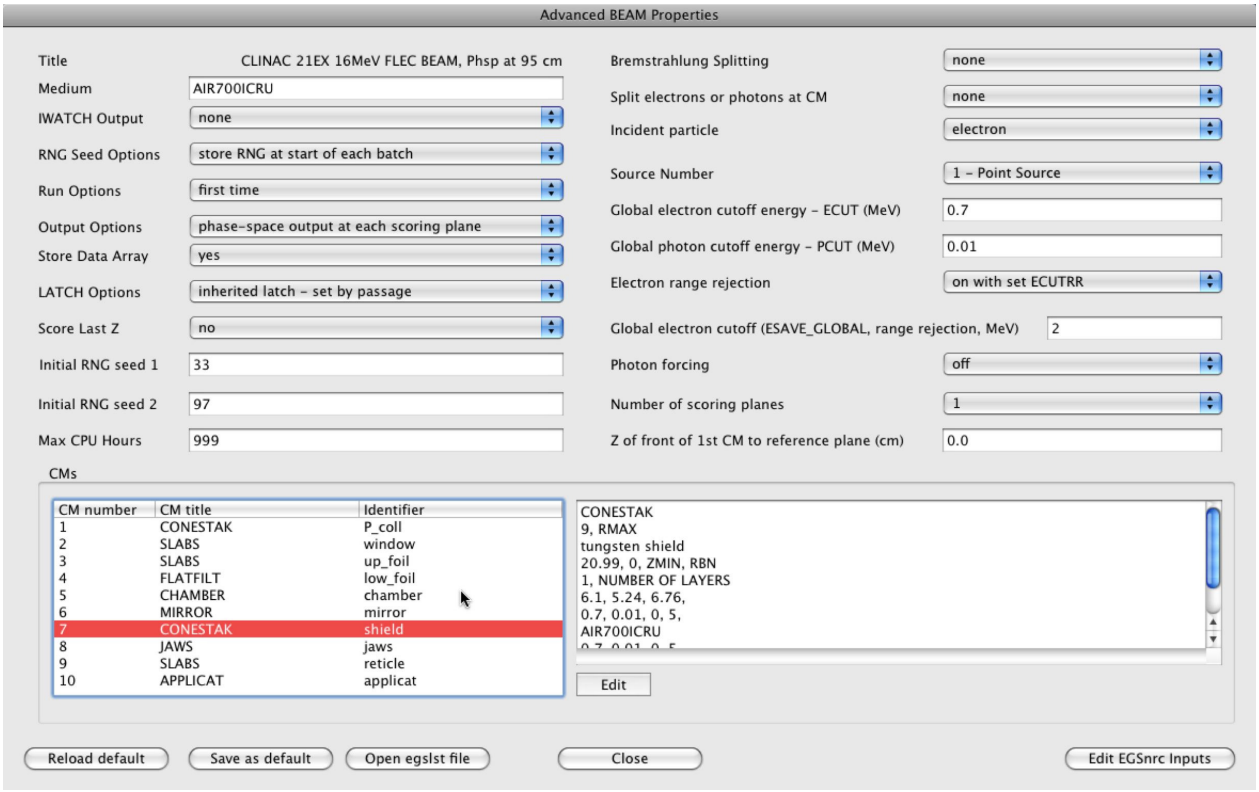

Figure 4–4: Advanced BEAMnrc GUI

departments. The development of an additional CM GUI is simplified by the separation of native BEAMnrc components within MMCTP.

4.4 DOSXYZnrc

DOSXYZnrc was not included in the original versions of MMCTP, as XVMC was used to model patient radiation transport. The addition of DOSXYZnrc constitutes a major advancement to the flexibility of MMCTP. The implementation of DOSXYZnrc followed the approach taken with BEAMnrc, with options to view and edit DOSXYZnrc parameters. The DOSXYZnrc structure tree consists of the DOSXYZ thread, DOSXYZ class, EGSPhant class and input file class.

The main DOSXYZ thread is the control box, which processes DOSXYZnrc tasks within MMCTP. These tasks range from creating an EGSPhant file to determining the progress of a simulation. The main properties of the DOSXYZ thread include an array of DOSXYZ classes (one for each EGSPhant file), a large list of default DOSXYZnrc settings, such as auto run and refresh, remove w files, default number of DOSXYZnrc jobs, default source value, and average percent uncertainty. Additional configuration options allow users to customize basic functions within MMCTP. These functions refer to importing downloaded 3ddose files and automatically generating EGSPhant files based on predetermined instructions.

The DOSXYZ class is specific to an EGSPhant file. This class contains a number of methods, an EGSPhant file class, and an array of DOSXYZ input file classes (one for each McGill RT beam). The EGSPhant file class contains the EGSPhant file in its native format. This class enables MMCTP to load and visualize any EGSPhant file created within MMCTP or otherwise. Visualization is a key feature to verify the generation of a proper EGSPhant file. The EGSPhant GUI is shown in figure 2–9. The input class stores the DOSXYZnrc input file in its native format and contains a read and write method. This allows users to modify the input file within the DOSXYZnrc GUIs without concern for reading and writing these changes.

4.4.1 DOSXYZnrc GUIs

MMCTP contains a number of DOSXYZnrc GUIs, which enable the user to visualize and modify many of the parameters within the input file and EGSPhant

file. The advanced DOSXYZnrc GUI, shown in figure 4–5, provides the first level of options. Additional source GUIs are provided for sources: 1, 2, 3, 8, 9, and 11 (source 11, a shared library for volumetric radiotherapy). The advanced GUI provides access to the log files, non-CT phantoms, and EGSnrc inputs.

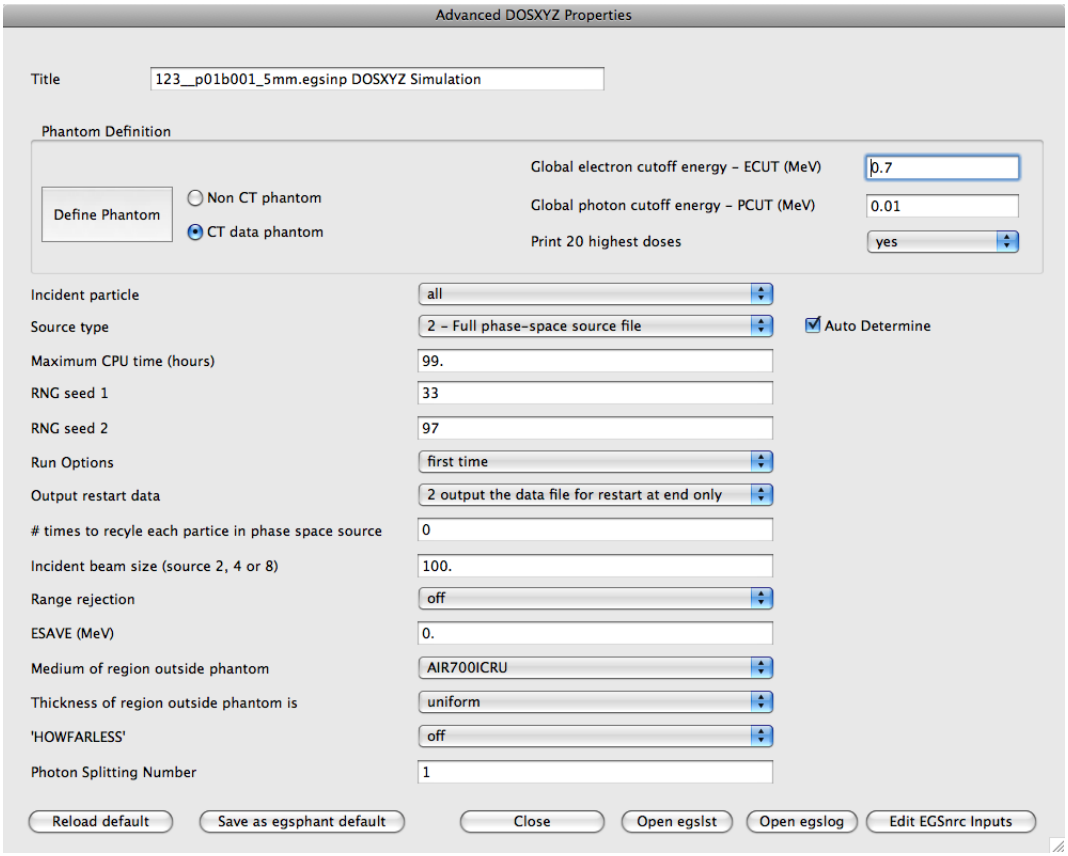

Figure 4–5: Advanced DOSXYZnrc GUI, provides access to the DOSXYZnrc input file, phantom, and EGSnrc inputs.

DOSXYZnrc Phantom GUI

The DOSXYZnrc phantom GUI allows the user to create a commissioning phantom in Cartesian space. Typical commissioning phantoms would include

various PDD profiles and x, y axis profiles. The user can assign materials and density values to the phantom voxels. Phantoms are designed using a combination of voxel groups in the direction of the profile and three individual voxels in the dimensions orthogonal to the profile. For example, the x and y voxel boundaries for a PDD profile in the z direction would be set at -15 cm, -0.5 cm, 0.5 cm, 15 cm. This creates a 30×30 cm^2 phantom in x and y with a 1 cm^2 in-plane resolution for the central axis PDD voxel point. The use of large volume voxel outside the area of interest and limiting the number of high resolution voxels to the volume of interest greatly increase the simulation efficiency. In addition, homogeneous commissioning profiles may use "HOWFARLESS", an option that removes the restriction that charged particle steps must stop at voxel boundaries. For photon beams, "HOWFARLESS" improves efficiency by roughly 30% [1] when PRESTA-I boundary crossing algorithm is used. Proper use of "HOWFARLESS" and voxel boundaries allows the generation of high quality profiles in an efficient time frame.

4.5 MMCTP Commissioning

MMCTP contains a commissioning analysis toolkit to provide a framework for the user to compare and track changes in the beam profiles. Commissioning tools are essential for any treatment planning system in radiotherapy. The commissioning tools in MMCTP allow the user to import RFA watertank measurements, Eclipse treatment planning (Varian Medical Systems, Palo Alto, CA) profile data and spread-sheet data. MC profiles produced in MMCTP are imported into the

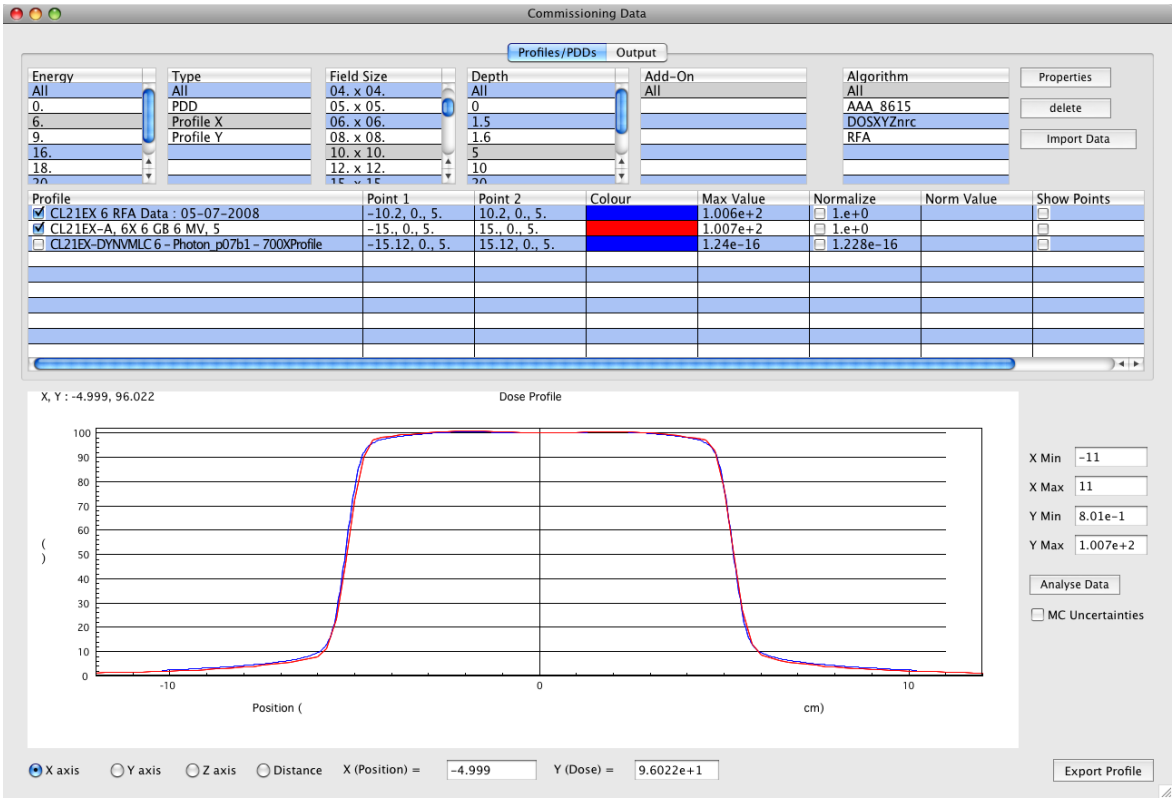

Figure 4–6: Main commissioning window. The window consists of a listbox to filter the list of profiles. Profiles can be displayed below, as shown with an x axis profile comparison between 6 MV water tank measurements (blue) and DOSXYZnrc dose profile (red).

commissioning toolkit for PDDs and profiles generated from DOSXYZnrc non-CT phantoms. Commissioning data is housed within the commissioning folder in *.Profile text files. Each text file contains a header section, which describes the properties of the simulation or measurement. The header is followed by a series of data points. Profile files are loaded into MMCTP at start-up and viewed within the commissioning window (shown in figure 4–6). The top section of the commissioning window allows the user to filter the listbox of profiles to specific

beam energies, field sizes, profile depths, and algorithms. Profiles that match the filtering options are displayed in the listbox below. The user may select and plot any number of profiles in the canvas below. A comparison can be easily made between measurements and simulations within the canvas plots or within the profile analysis data window. The analysis window allows for a 2D gamma [2] analysis and dose difference plot. The dose-difference (%) and distance-to-agreement (cm) are adjustable parameters for each gamma calculation. Each calculation returns the percentage of profile points that pass the criteria. The dose-difference tool generates a new dose-difference profile viewable within the list of profiles and a Chi-square distribution χ^2 value to quantify the difference between the plots.

Output tables are also included within the commissioning window. The output tables are saved within *.Output files housed within the commissioning folder. An output table can be generated manually or imported from an Eclipse output file. Each output value is normalized to the 10×10 cm^2 field size value. Each column and row index defines a specific X and Y field size. There are a number of properties associated to each table, such as detector depth, SSD, add-on, beam energy, and calculation algorithm. These properties are displayed within the main output table listbox. Tables are opened simultaneously for comparison purposes. MC output data produced in MMCTP is automatically imported into an output table when generated from a DOSXYZnrc non-CT output phantom. Output phantoms are defined with the label "output" within the phantom name and through the use of a three voxel phantom in x, y, z. MMCTP assumes that the output voxel is the second voxel in x, y, z.

4.6 MMCTP Job Control Logic

Clinical TPS enable radiotherapy planners to calculate patient dose at the click of a button. In the research world of BEAMnrc and DOSXYZnrc, the user is left to generate input files, transfer them to a calculation computer, probe simulation status, and link completed simulations together. These tasks are a tax to the overall efficiency of MCTP. In order to increase the overall efficiency of large scale MC calculations using BEAMnrc and DOSXYZnrc, a number of logic scripts are included within MMCTP to simplify the calculation process to the end-user as well as maximize CPU utilization. The logic scripts are governed by a number of user settings with MMCTP. These settings define when, where, and which type of simulation should be processed. The scripts are triggered by timers and separated into two groups: refresh and run.

4.6.1 Auto Refresh

The auto refresh scripts are quite simple and self explanatory. The main function of auto refresh is to determine the number of running BEAMnrc, DOSXYZnrc, and XVMC jobs on a computer and to launch subsequent processes after the completion of a simulation. The tasks required for each process forms a sequence of events, which relies on a successful simulation. Interruptions to this sequence can be caused by a simulation error within the MC code or within a host computer affecting as little as a single parallel job. The frequency of interruption is low, however, they can cause a significant decrease in calculation efficiency as the user is required to investigate the problem. At the McGill Medical Physics Unit, the frequency of interruption is on the order of 1%.

BEAMnrc

The base level of auto refresh for BEAMnrc simulations is the status of the lock file. The lock file provides information such as the number of split jobs running and the progress of the simulation. At the completion of a simulation, BEAMnrc removes the lock file and generates log files for each split job. If the lock file is not found within the auto refresh search, the second level of auto refresh is to search for the log files. The log file search examines each $*\_w(job\#).egslog$ file to determine if the simulation had successfully completed. If all log files exist and contain the phrase "Finished simulation", then the simulation is considered to have properly finished. If this check is successful for all logs files, the number of running jobs is reinitialized to zero and add phase-space is triggered. The status of add phase-space is checked and if complete, auto refresh runs BEAMDP on the phase-space file to report the total number and number of photon particles within. Lastly, auto refresh updates the phase-space database and downloads the simulation log files.

DOSXYZnrc

The base level of auto refresh for DOSXYZnrc simulations is the status of the lock file or the status of the egslst file. The second level of auto refresh is to check the status of the 3ddose file. If the 3ddose file exists, a subsequent command downloads the 3ddose and accompanying log files. The log files provide useful information such as the simulation CPU time and the simulation uncertainty within the high dose region (voxels >50% D_{max}). This information is used to predict simulation time and uncertainty for future simulations.

XVMC

The XVMC auto refresh checks the simulation status of a log file, downloads the d3d files and accompanying log files, as well as updates the number of running jobs.

4.6.2 Auto Run

The auto run scripts are more complex and are unique to the type of simulation. The main function of auto run is to determine when, where, and what number of parallel jobs to submit. One of the main features of MMCTP is the ability of MMCTP to submit jobs to multiple computer clusters. The configured shells allow MMCTP to generate, transfer, and submit shell-specific input files. Within the properties of each shell there exists a variable, which sets the maximum number of running jobs. Once the maximum number of jobs has been reached, MMCTP will switch shells and begin submitting jobs to shells with remaining openings. In addition, the script will reduce a parallel job submission to the number of available job slots. This would occur in the event that the sum of the original parallel job split number plus the number of current running jobs would be higher than the maximum job limit. As such, the script requires an accurate number of running jobs per iteration. This number is constantly updated within auto run and refresh. The flexibility to switch shells within auto run is controlled with a user variable "Auto Shell". If this variable is off, then auto run will submit to the selected shell when job slots become available.

BEAMnrc

Auto run for BEAMnrc simulations consist of three events. The first phase will attempt to link the current simulations with an existing phase-space file. The matching process consists of the following steps:

1. A search is performed for the phase-space file within the selected shell. If found the new beam is linked with the previous simulation.
2. Otherwise, if not found and if auto shell is on, a search is performed for the phase-space file within all online shells. If found the new beam is linked with the previous simulation and the shell variable is updated.
3. Otherwise the search returns nil and the simulation advances to the second phase.

The second phase will run a test simulation to determine the number of particles per history, CPU time per history, and verify that the input file is free of errors.

The output from the test run is used to populate MMCTP BEAMnrc variables, which characterize the simulation. Their main function is to determine the number of histories to simulate in order to arrive at a desired particle density as well as provide an estimate of the simulation time. If the test run was successful, the next event submits the production run. A production run consists of the following steps:

1. If auto shell is on, then a suitable shell is selected for the run and the job split number is updated. Otherwise the job split number is updated based on the selected shell.

2. MMCTP removes any previous simulation files with the same job identification on the shell.
3. MMCTP creates new input files and transfers them to the shell.
4. MMCTP submits the job to the queuing system.

In the event that an error occurs within these steps, the process is terminated and an error message is displayed within the treatment planning window. Once submitted, the number of running jobs is updated.

DOSXYZnrc

The auto run scripts for DOSXYZnrc simulations are dependent on the DOSXYZnrc source type and beam mode. In a similar fashion to the BEAMnrc scripts, all DOSXYZnrc simulations begin with a test simulation to determine voxel uncertainty per history and CPU time per history. This information is used to determine the number of histories required to arrive at a desired statistical uncertainty. A production run consists of the following steps:

1. Upload EGSPhant file to shell if necessary.
2. Remove previous simulation files with same job identification on shell.
3. Create new input files and transfer them to the shell.
4. Submit the job to the queuing system.

Prior to job submission, the auto run script performs a series of checks. In the event that the DOSXYZnrc source is 2 (phase-space), the existence of the phase-space file is checked and shell consistency between DOSXYZnrc and BEAMnrc is also checked. A simulation is submitted when job slots become available on the shell in question. In the event that the DOSXYZnrc source is 1 or 3, the

simulation can run on any shell and is submitted on the first available shell. In the event that the DOSXYZnrc source is 9 or 11, the simulation can run on the selected shell when job slots are available, or on any shell when auto shell is on.

A special set of rules are followed for modulated electron radiotherapy (MERT) beam mode using DOSXYZnrc source 2. The rules allow the DOSXYZnrc scripts to switch the BEAMnrc shell under two conditions. The first condition makes use of the phase-space database, which was designed for MERT due to the frequent reuse of identical fields. For example, consider if there are two shells (a, b) configured within MMCTP and the same phase-space file exists on both shells. Under normal conditions, if shell a was selected within the BEAMnrc phase-space search then DOSXYZnrc would have to wait until job slots became available on a. However, if there are job slots available on b then DOSXYZnrc can switch the BEAMnrc shell to b and continue with the DOSXYZnrc simulation. This rule allows MMCTP to dynamically change shells based on load to maintain maximum simulation efficiency. The second condition was designed for the following event: If the phase-space file exists only on shell a, then a would have been selected within the BEAMnrc phase-space search and DOSXYZnrc would have to wait until job slots became available on a. In the event that there are job slots available on b after the first condition was checked, then DOSXYZnrc can switch the BEAMnrc shell to b and begin a new phase-space simulation on b. It is important to note that the second condition must be followed by the first condition in order to minimize additional phase-space simulations.

4.7 Modulated Electron Radiotherapy Toolkit

The majority of TPS include optimization tools, which ease the process of creating quality plans. The MERT toolkit within MMCTP was designed with this goal in mind. This section describes the three main components of the MERT toolkit.

The first step to MERT planning is choosing a suitable isocentre and gantry angle. In forward electron beam planning, this task can be performed manually through iterative adjustments of the isocentre, gantry angle, and cutout shape to tweak plan quality. Quality assessment requires a dose calculation for each adjustment. The time required for each dose calculation is minimal for clinical TPS however, a combined BEAMnrc and DOSXYZnrc simulation for each adjustment would be impractical. As such, an automated method has been developed to choose a suitable isocentre and gantry angle based on the target geometry, body contour and three parameters. These parameters include target depth, target projection width per gantry angle, and target symmetry. For each axial image slice in z, the algorithm steps along the body contour to calculate a distance between the body contour and the 2D center of mass of the target area per body contour pixel. Each calculation point represents a tentative x, y isocentre position and gantry angle. Points are scored by minimizing the target depth, maximizing the projection width and maintaining target symmetry in isocentre z position. In addition, points are rejected if the cutout plane, located at 95 cm from the electron source, crosses the boundary of the body contour. The results of one run are shown within the external beam positioning tab of the MERT beam

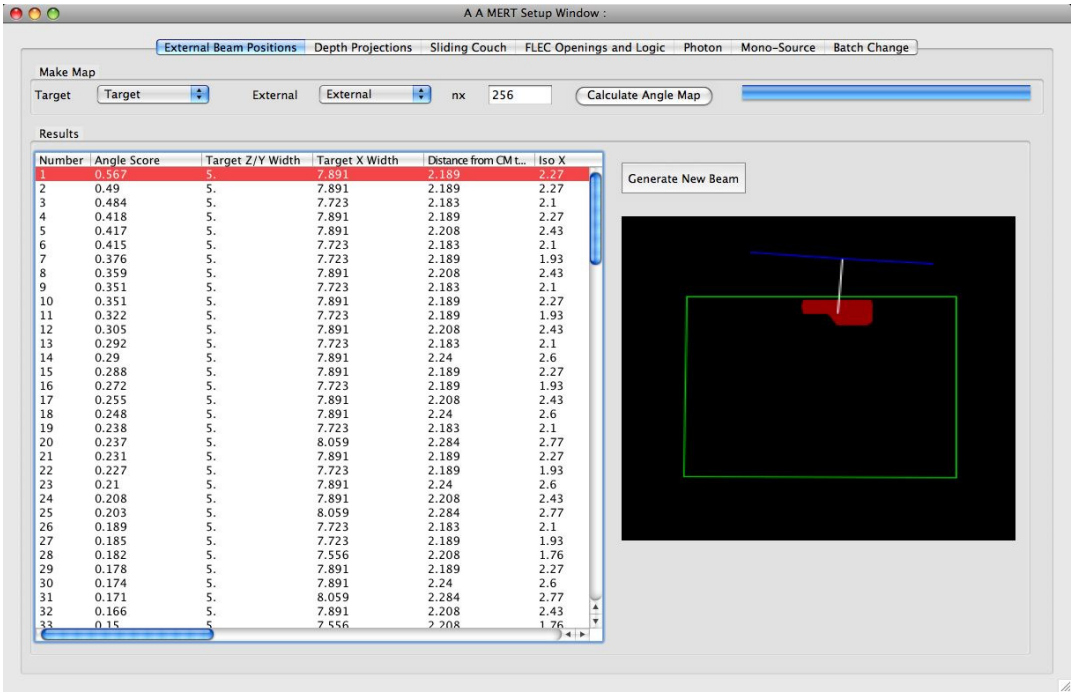

Figure 4–7: MERT beam setup window showing external beam positioning tab

setup window (figure 4–7). The results are summarized and listed by score within a listbox where the user can review, visualize, and select a potential isocentre and gantry angle. Due to the limited depth range of electron beam and the high entrance dose of electron beam, the isocenter and gantry selection phase is of great importance. A judicious choice of the isocenter and gantry angle is required for high quality electron plans.

4.7.1 Beam Setup

Once an isocentre and gantry angle have been selected for use, the following step generates a set of electron beamlets. Four methods have been investigated to generate beamlets. The first two methods, raster and feathered, produce discrete

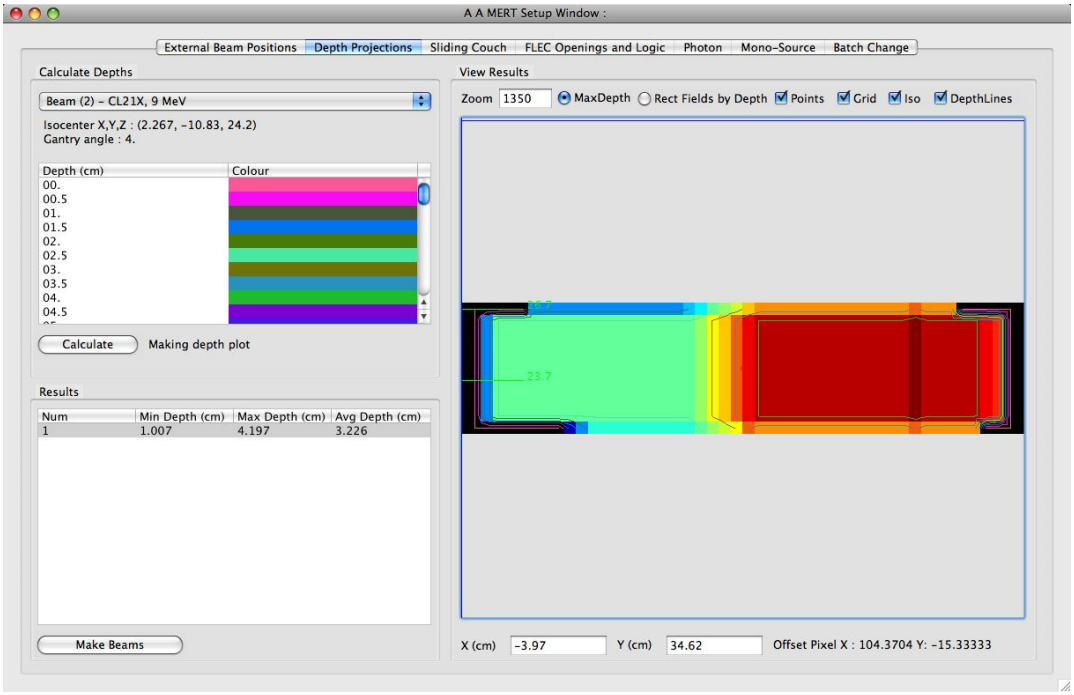

Figure 4–8: MERT beam setup window showing target depth plot. Isodepth contours are shown in colour lines surrounding the target volume. Isodepth legend is shown in the top left listbox. The colourwash displays the maximum target depth (red) to minimum (blue)

openings, which are frequently reused between patient plans. A raster pattern refers to abutting fields while the feathered pattern refers to fields that overlap each other. The MERT beam setup window allows the user to generate various sized abutting and feathered fields per incident electron beam. Feathered fields include an offset distance, which is often half the field size. Raster and feathered patterns produce a large number of beamlets and do not take patient specific geometric conditions into account. In an effort to reduce the number of beamlets and better conform the beamlets to the target geometry two additional methods, depth projection and sliding couch, were created. The depth projection method

generates isodepth contours of the target volume at the projection angle of the beam. This enables the user to generate fields based on depth. The user may choose to generate fields based on the maximum depth within the projection plane or generate a series of fields at various depth values. The isodepth contours of a simple target geometry are shown in figure 4–8, together with the maximum depth colourwash. The sliding couch method was created to accommodate larger elongated target volumes, which do not fit within the 8×8 cm^2 few leaf electron collimator (FLEC) but would fit within an $8 \times x$ cm^2 where x is in the direction of couch motion. A maximum sized field is created per x step size. Depending on the step size, neighbouring fields may overlap. The field size for a maximum sized field is determined by the maximum extent of the target projection width and height in each direction.

Once all the beamlet fields have been created, the next step is to assign electron energies. It has been common practice to assign all electron energies to each field which enables the optimization algorithm to filter out unsuitable electron energies based on the optimization objectives. If more control on the electron energy selection is required, the user has the choice of assigning which energies are applied to which field.

Electron beamlet dose calculation is performed within MMCTP using EGSnrc, XVMC or a combination of the two. The dose calculation includes the collimator scatter, bremsstrahlung from the FLEC leaves and the treatment head. The treatment head simulation may be stored as a phase-space file for repeated use or run within the patient specific dose calculation as a shared library source. Each

beamlet field of specific electron energy and FLEC segment, has a corresponding patient specific dose calculation.

4.7.2 Inverse Optimization

Once beamlets have been generated and dose distributions calculated, the plan is ready for inverse optimization. In general, the optimization algorithms optimize the dose distribution weights and all other parameters are fixed. The exception to the rule is the FLEC-DAO algorithm, which optimizes dose distribution weights and FLEC segments. The inverse optimization window (figure 4–9) facilitates the connection between MMCTP and the external C optimization programs. The window is divided into three components: pre-run settings, run, and run analysis.

The pre-run settings allow the user to edit organ and target constraints as well as control which dose distributions are included within the optimization run. Organ constraints consist of a dose limit, volume limit, and penalty value. Target constraints consist of a dose maximum and penalty value, and a dose minimum and penalty value. Structures defined within MMCTP are available as constraint volumes and the user has the option of assigning the constraint type.

The DDC properties tab consists of a large listbox and allows the user to control which dose distributions are included within each optimization run. The user may choose to include or exclude dose distributions based on previous runs, electron energy or field size. A secondary function of the DDC tab is to display the returned dose distribution weights. Each entry on the listbox stores the include

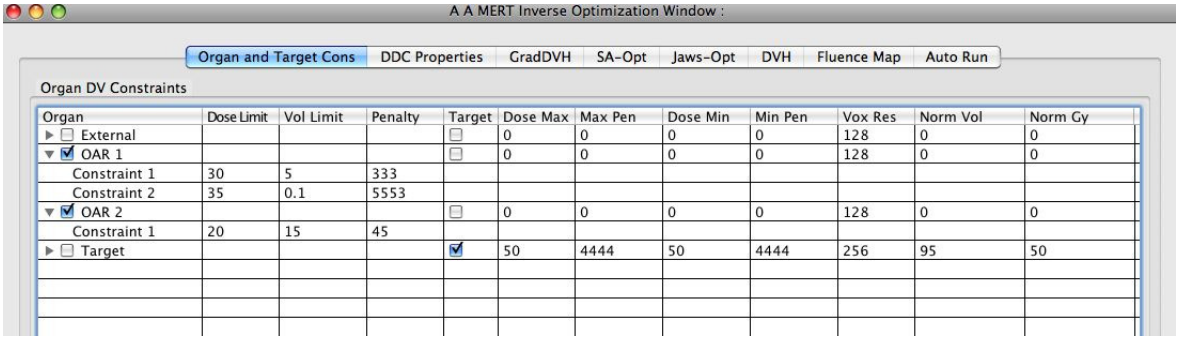

Figure 4–9: MERT inverse optimization window. The organ and target constraint tab allows the user to edit optimization constraints.

option, dose distribution name, weight, energy, field size, normalization value, beam number, gantry angle, isocentre, and beam mode.

The run component controls the optimization runs and is split into three sections for the separate C optimization programs: gradient, simulated annealing, and dynamic jaw. Each section consists of input options, a run button and an output feedback display. General input options include the number of iterations, maximum and minimum weight bounds, weight initialization, and dose normalization. In addition to general input options there are many program specific input options, which need to be carefully adjusted. The run button generates a program specific input file and launches the optimization program. A timer within the optimization window iteratively updates the program output and displays the context within the window.

The run analysis tabs consists of the DVH tab and the fluence tab. The DVH tab imports the optimization DVHs for viewing. As the optimization programs are DVH-based, it is essential to be able to visualize the DVHs throughout the

optimization process. The optimization algorithms use a single cost function value to critique the solution at each iteration. However, the cost function value is an oversimplification of the plan while the DVHs, which are generated and visualized at each iteration, offer a complete description of the solution. The iterative DVHs enable a limited amount of interactive capability to the system that permits the user to stop the process, make changes to the run options and continue the optimization process.

The fluence tab, shown in figure 4–10 provides a 2D map of the beamlet weights. Filtering options within the fluence tab enables the user to visualize the spatial relative beamlet intensity weight pattern per energy, isocentre, gantry angle, and beam mode.

The extent of run options within the optimization window allows for interactive planning. Interactive planning may include energy filtering, field position filtering, or optimization input changes. Run options will affect the results of the optimization run and a judicious choice of these parameters is required for high quality electron plans.

4.7.3 Optimization Results

The final component of the MERT toolkit consists of the output database window, which allows the user to save and compare optimization results. This feature allows direct comparison of DVHs between multiple runs. The optimization output is saved within a Real SQL database file. The file consists of records, which store the following information: cost function value, date, MERT optimization program name, optimization input file, dose distributions and weights, organ and

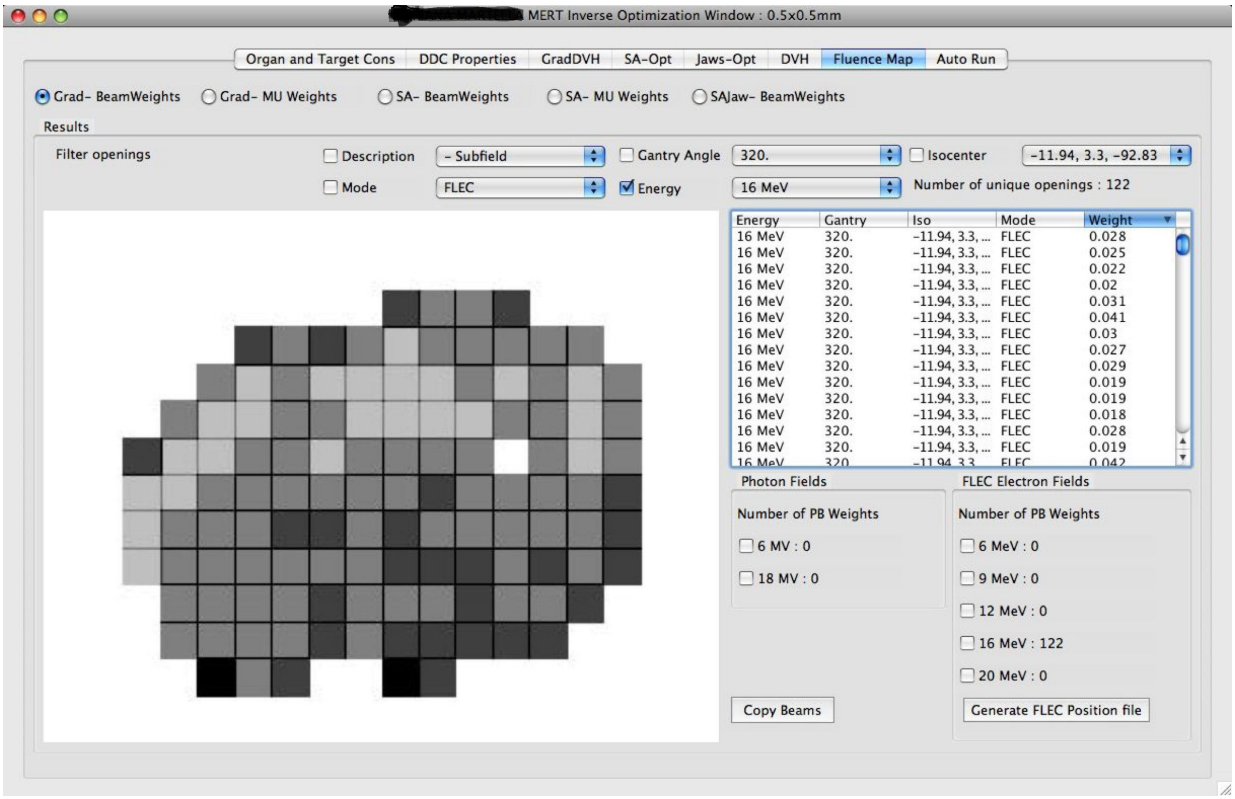

Figure 4–10: MERT inverse optimization window. The fluence tab allows the user to review the relative beamlet intensity map per beam mode, gantry angle, beam energy, or isocentre. The dimensions of the squares represent the FLEC leaf positions for each beamlet. The current display is filtered for 16 MeV beamlets. The grey scale represents beamlet weight (MU) normalized to the maximum beamlet weight shown in black.

target constraints, and notes. Each record stores the complete set of information required to reproduce an optimization result. As such, the database has been useful in determining the optimal input parameters required to arrive at acceptable plans. For example, it is not intuitive how one should assign target and organ

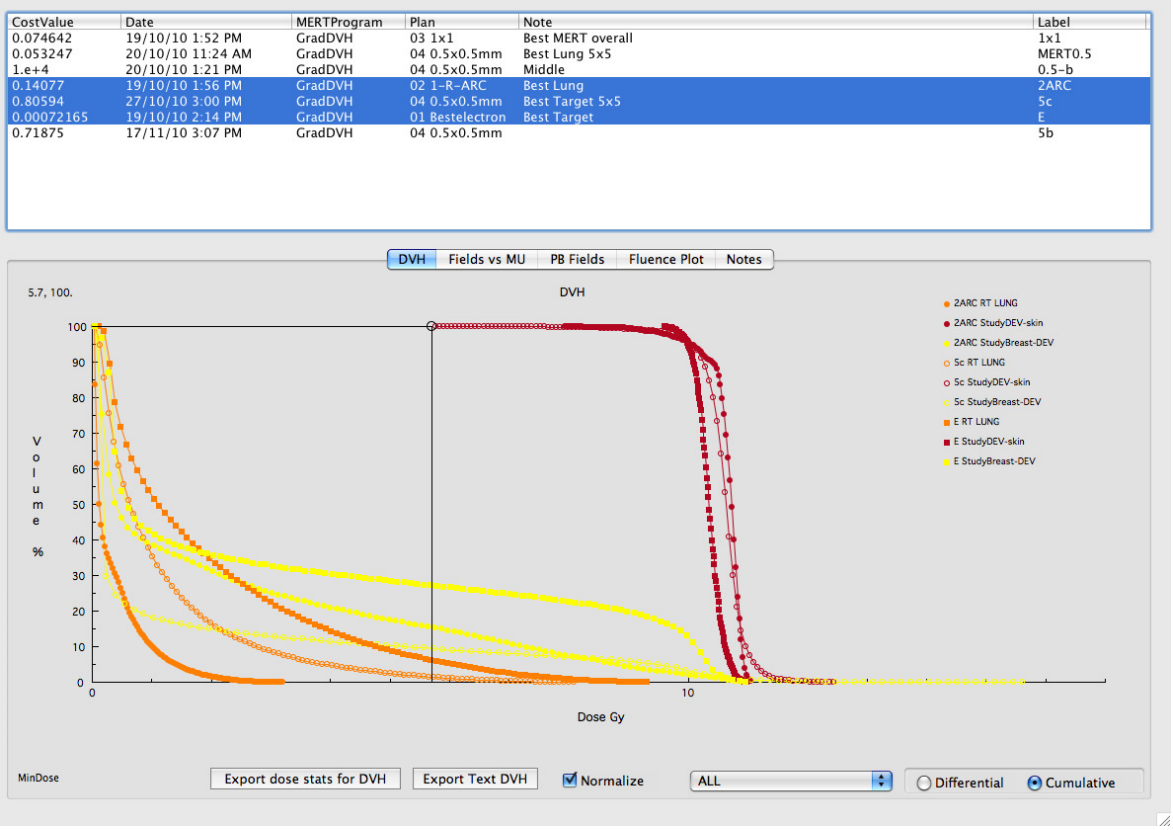

Figure 4–11: MERT output database window. The window allows the user to browse and review the details of each optimization run. A canvas plot allows for DVH comparisons between multiple plans. Plans are sorted within a listbox and summarized by a few key parameters.

constraint penalty values. It is common best practice to perform multiple runs with various penalty values in order to measure the sensitivity of each constraint

on the optimization outcome. The convenience of the output database allows the user to perform this task quickly and effectively. The DVH results of three different treatment modalities are shown in figure 4–11. In addition to the DVH graphs, the user has access to the list of dose distributions under the PB field tab. The list summarizes the properties of each dose distribution and the dose weight. The fluence tab displays a 2D fluence map and the notes tab displays the optimization input file, constraint file, optimization output file, and user notes.

4.8 References

[1] B R B Walters and I Kawrakow. A "HOWFARLESS" option to increase efficiency of homogeneous phantom calculations with DOSXYZnrc. *Med. Phys.*, 34(10):3794–807, 2007.

[2] D A Low, W B Harms, S Mutic, and J A Purdy. A technique for the quantitative evaluation of dose distributions. *Med. Phys.*, 25(5):656–661, 1998.

CHAPTER 5
Paper II: Patient comparison between the Analytic Anisotropic Algorithm and Monte Carlo dose calculation for head and neck patients treated with simultaneous integrated boost intensity-modulated radiation therapy

Andrew Alexander, Emilie Soisson, Line Comeau, and Jan Seuntjens

Phys. Med. Biol., Under review 2011

Contents

Following the development of MMCTP, there was an effort to train individuals at the McGill Medical Physics Unit on the use of MMCTP. These individuals provided feedback and contributed to the continued development of the system. In 2009, MMCTP was installed on a clinical workstation with the emphasis of training clinical physicists and dosimetrists on the use of MMCTP. In 2009, the clinical staff at McGill were a demographic with no experience in Monte Carlo treatment planning systems or Monte Carlo transport codes BEAMnrc and DOSXYZnrc. The following manuscript represents the first use of MMCTP within the clinic. A dosimetrist was trained to use MMCTP for an investigation into the dosimetric agreement between the AAA algorithm and Monte Carlo. The results from the dosimetric study were used in the validation of AAA for clinical use. The study represents a significant milestone in the development of MMCTP and it is a testament to the maturity of the system, as it is rare for research projects to cross into the clinical environment. The dosimetric results of the study provided evidence-based insight into dosimetric discrepancies observed in previous independent studies.

Abstract

The McGill Monte Carlo treatment planning system (MMCTP) is designed to allow non-Monte Carlo (MC) specialists access to MC dosimetry based on highly accurate, open source codes. The aim of this study was to evaluate dosimetric differences between the analytical anisotropic algorithm (AAA) and Monte Carlo (MC) of intensity-modulated radiation therapy (IMRT) plans with simultaneous

integrated boost (SIB) using MMCTP in a clinical setting. In this study, a dosimetrist performed the tasks of exporting Eclipse AAA plans and recomputing them in MMCTP using BEAMnrc and DOSXYZnrc. The dosimetrist evaluated AAA and MC dose distributions using dose-volume indices and isodose line displays. Analysis of the target volumes revealed close agreement between AAA and MC, as the range of results were within 5% and the mean less than 2% for all but the $D_{98\%}$ values. In general, dosimetric differences were limited to regions of high and low density, resulting in buildup, builddown, and lateral scattering effects. The parotids, which are in a region of lateral disequilibrium, showed the greatest deviation by as much as 20% from MC. The realization of this study suggests that MMCTP is an excellent research tool for clinical staff and non-MC experts to investigate dosimetric differences between clinical dose calculation algorithms and MC.

5.1 Introduction

Intensity-modulated radiation therapy (IMRT) is now the standard treatment for head and neck (HN) cancer. IMRT treatments have the ability to produce conformal radiation to irregularly shaped targets, while sparing critical structures directly adjacent to the planning target volumes (PTV). IMRT for HN cancer usually involves a simultaneous integrated boost (SIB) technique, which allows multiple target volumes to receive different prescribed doses. The technique allows for dose escalation to increase local tumour control probability over conventional IMRT [1, 2, 3, 4]. IMRT with SIB has been shown to increase conformality,

shorten the overall treatment course and limit the growth of squamous cell carcinoma [5, 6].

Due to the complexity of the multileaf collimator (MLC) pattern in IMRT, dosimetric accuracy and beam delivery verification are essential requirements for its use, as recommended by AAPM [7], to perform patient-specific quality assurance (QA). One such QA procedure involves the use of an independent system to calculate and verify the planned dose to a patient or a QA phantom. The McGill Monte Carlo treatment planning system [8] (MMCTP) was developed in part for this task. MMCTP can be used as an independent verification tool to evaluate the accuracy of clinical treatment plans. Unlike a commercial MC TPS, which is typically a "black box" closed system, the MC transport parameters within MMCTP are fully customizable to the end-user. Non-MC treatment planning systems (TPS) use advanced kernel based models, which contain inherent dosimetric limitations that affect accuracy under specific conditions [9]. These conditions, which are usually caused by inadequate modelling of secondary electron transport, include small fields ($< 4 \times 4$ cm^2) and tissue interfaces involving high density bone, low density lung or sinus air cavities [10, 11, 12, 13]. IMRT treatments present addition challenges for analytical model-based treatment planning systems, as MLC leakage and scattered radiation from the MLC play a larger role [14]. As a result, the dose predicted by the TPS and the actual dose received by the patient might differ considerably [15]. Monte Carlo simulations have the ability to model complex geometries both in the patient's inhomogeneous media and the linear accelerator's head. This includes the transport of particles

through the MLC leaves to account for scatter and leakage radiation. With these dosimetric benefits in mind, several investigators have reported on the implementation of MC simulations within clinical settings [16, 17, 18, 19, 20, 9, 21, 22].

Francescon *et al* [9] investigated the dose distribution calculation algorithm in the commercial treatment planning system PINNACLE (Philips Radiation Oncology Systems, Fitchburg, WI) for IMRT plans with 6 MV photon beams. The BEAMnrc [23] MC code was used to compare the distributions of PINNACLE. An output difference of 8% was observed for small field sizes and the isocentre dose difference was 2.9% for a HN IMRT plan.

Leal *et al* [20] investigated the use of MC calculations for routine QA procedures. IMRT plans from Plato (Nucletron, Veenendaal, Netherlands) TPS were recalculated using a MC system. In general, the authors observed acceptable agreement between Plato and MC; however, major differences were observed in regions of high heterogeneity.

Boudreau *et al* [22] evaluated the dose distributions for 11 HN IMRT plans using PEREGRINE (North American Scientific, Cranberry Township, PA), a MC dose-calculation code and the CORVUS (North American Scientific, Cranberry Township, PA) algorithm. They reported a reduction of 12% in the volume covered by the prescription isodose line for the CTV and a 4% and 6% increase in the mean dose for the parotid and brainstem. The observed differences were attributed to secondary electron fluence perturbations, which were not modelled

in CORVUS, issues of organ outlining, and differences in reporting dose to water versus dose-to-medium.

Sakthi *et al* [18] evaluated the dosimetric accuracy of convolution-superposition (CS) with MC calculations for thirty-one HN IMRT with SIB treatments. On average, their MC results agreed with CS in the patient geometry; however, dose-index deviations of greater than 5% were common. The authors call attention to these deviations, as they can impact dose escalation protocols by shifting treatment dose levels.

Dogan *et al* [24] investigated the dosimetric differences between CS and MC for twenty-two prostate plans treated with SIB IMRT. Differences greater than 5% were observed in the organs at risk (OAR) while, on average, the targets agreed to within 2%. The authors concluded that for some patients, the magnitude of these dose differences would place patients in dose levels that no longer satisfied the intended protocol dose requirements.

The purpose of this study was to evaluate the dosimetric differences between HN IMRT plans calculated using the analytical anisotropic algorithm (AAA) within Eclipse TPS (Version 8.6, Varian Medical Systems, Palo Alto, CA), and those calculated using the MC codes BEAMnrc and DOSXYZnrc [25] within MMCTP. In recent years, there have been many reports on the accuracy of AAA [26, 27, 28, 29, 30], but few that have reported on the dosimetric comparison between AAA and MC in a large set of patients. The results of this comparisons will allow for a quantitative assessment on the accuracy of HN SIB IMRT patient

plans calculated using AAA. In addition, this study provides an opportunity to evaluate the usability of MMCTP as a QA tool for clinical staff and researchers.

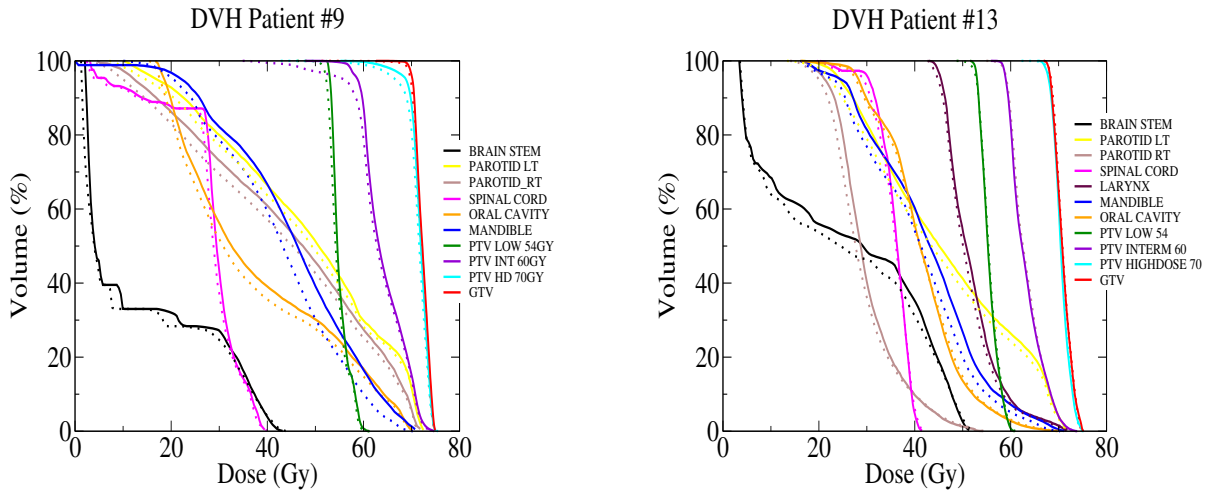

(a) (b)

Figure 5–1: DVH graphs for two patient plans 9 (a) 13 (b), AAA (solid line) and MC (dotted). (a) low dose region of PTV60 Gy shows a large difference between AAA and MC (b) all target graphs agree well.

5.2 Materials and Methods

5.2.1 Patient Selection

Eighteen previously planned and treated HN patients were selected for the study. All patients had undergone SIB-IMRT treatment on a Varian 21EX linac (Varian Medical Systems, Palo Alto, CA). The HN cases were comprised of three unknown primary, four tonsil carcinomas, four tongue carcinomas, one floor of mouth carcinoma, and six squamous cell carcinomas of the larynx. All patients underwent a CT simulation in the supine position for planning purposes.

A thermoplastic mask was used for HN immobilization. The CT slices were reconstructed at 3 mm intervals.

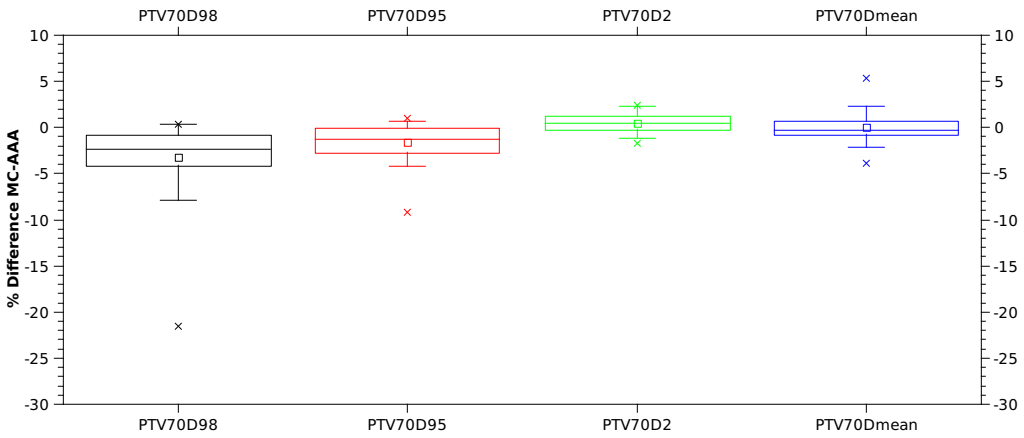

Figure 5–2: Box plot for percent difference between MC and AAA for PTV70 dose-volume indices. Max and min difference (diagonal cross), 95%-5% confidence interval (whiskers) 25-75 percentile (box) mean (rectangle) median (line).

5.2.2 Target Volumes

All target volumes were outlined by a radiation-oncologist. The outlined targets consisted of the gross tumour volume (GTV70 Gy), defined as the gross observable extent of the malignant tumour, and any positive lymph nodes. The clinical target volume (CTV60 Gy) and nodal clinical target volumes (CTV nodes 54 Gy - 56 Gy) consisted of all subclinical and microscopic disease around the primary tumour, as well as high risk lymph nodes in the neck region. CTV nodes included all lower risk nodal areas. The CTV was obtained by expanding the GTV by 1 cm in all three dimensions except in volumes that involved bone, air, and critical structures. The planning target volumes (PTV) included a 3-5 mm margin

around each CTV to account for setup uncertainties and organ motion. PTVs were cropped 5 mm from the edge of the skin for most of the cases.

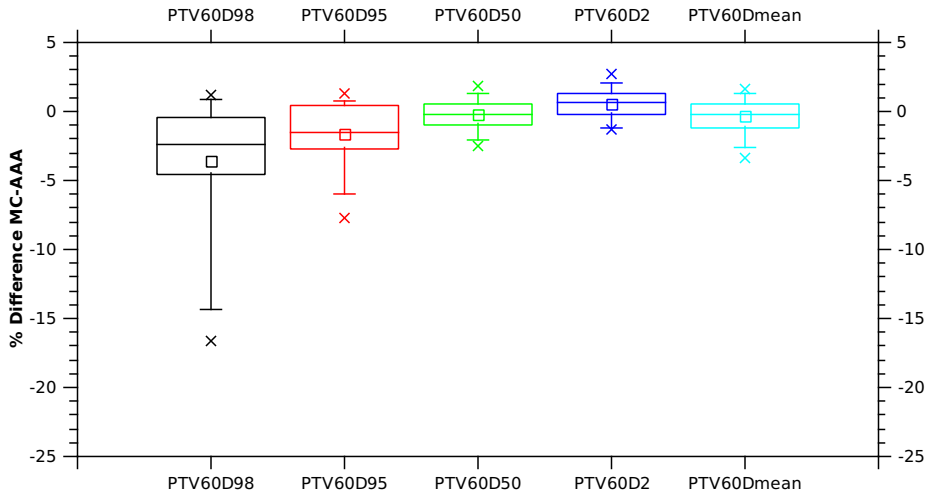

Figure 5–3: Percent difference of all 18 plans for PTV60. Max and min difference (diagonal cross), 95%-5% confidence interval (whiskers) 25-75 percentile (box) mean (rectangle) median (line).

The prescription doses were; 70 Gy to the PTV primary, 60 Gy to the PTV high risk and 54 Gy - 56 Gy to PTV nodal low risk delivered simultaneously in 33 or 35 fractions. The treatment goals aimed to achieve adequate coverage of all PTVs with the target volume receiving at least 95% of the prescribed dose and a maximum dose of less than 107%.

5.2.3 Critical Structures

Contoured critical structures for the patient set included the spinal cord, cochlea, esophagus, larynx, eyes, optic nerve, optic chiasm, submandibular gland, brainstem, mandible, oral cavity, larynx, and parotid gland. A subset of these

structures are included in the discussion. The planning constraints were as follows: The maximum dose was limited to $\leq$ 45 Gy for the spinal cord, 55 Gy for the brainstem and 70 Gy for the mandible. Volume constraints were to limit the dose to 50% of the larynx $\leq$ 40 Gy ($D_{50\%}$=40 Gy) and to limit the mean parotid dose to below 26 Gy. If the constraints could not be met for both parotids, at least one of the parotids was to be spared as much as possible without compromising the target. However, due to the close proximity of the parotids to the 70 Gy target volume, it was difficult to meet this constraint.

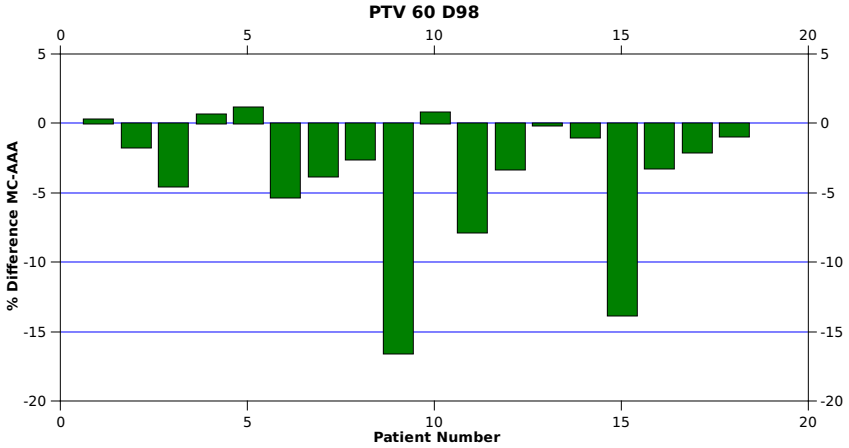

Figure 5–4: PTV60 $\Delta_{\%}D_{98\%}$ percent difference plotted per patient. Negative values signify a MC underestimate versus AAA.

5.2.4 IMRT Optimization and Treatment Planning

Each IMRT plan was created using seven fixed non-coplanar 6 MV photon beams. The beam arrangements were at fixed gantry angles of 0, 50, 105, 155, 205,

255, and 310 degrees. The IMRT plan was created for dynamic MLC beam delivery with a Varian 21EX linear accelerator equipped with a 120-leaf millennium MLC (Varian Medical Systems, Palo Alto, CA).

Plan optimization and dose calculation was performed on the Eclipse TPS with a dynamic MLC sliding window technique. After optimization, the TPS performed a final dose calculation on the deliverable MLC leaf sequence pattern. The original plans were calculated and approved for treatment using the PB dose engine. For the purpose of this study, the approved plans were then recalculated using the AAA algorithm with heterogeneity correction turned on and with the original number of monitor units (MUs), to represent a more realistic estimate of the delivered dose distribution.

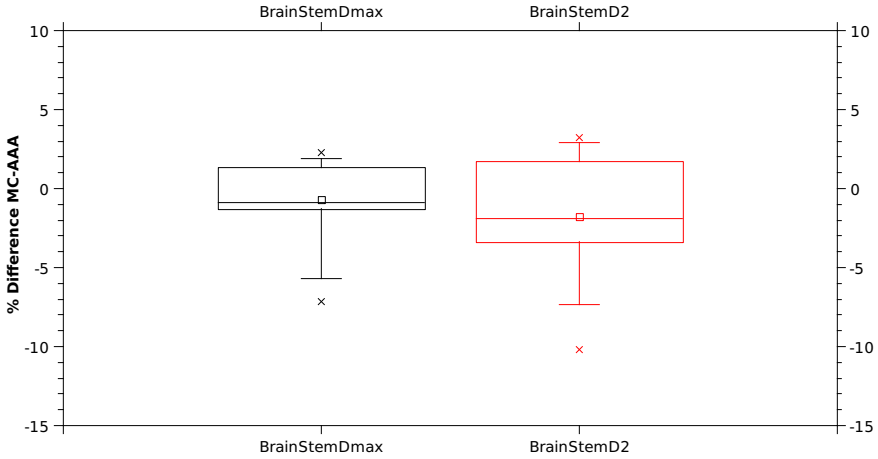

Figure 5–5: Box plot for percent difference between MC and AAA for brainstem dose-volume indices. 25-75 percentile is centered around 0. Brainstem $D_{2\%}$ mean is located at -1.8% and 95%-5% confidence interval is between +3% and -7%. Max and min difference (diagonal cross), 95%-5% confidence interval (whiskers) 25-75 percentile (box) mean (rectangle) median (line).

5.2.5 Monte Carlo

MC simulations were used to investigate the dosimetric accuracy of the eighteen SIB-IMRT plans. DICOM files were exported from Eclipse and imported into MMCTP for MC recalculations. The DICOM set included images, structures, plans, and dose distributions. MMCTP is an automated research tool, which interfaces with MC user codes BEAMnrc and DOSXYZnrc. BEAMnrc and DOSXYZnrc are widely considered as the gold standard in dosimetric accuracy of radiation transport for radiotherapy. BEAMnrc was used to model the particle fluence exiting the linac, while DOSXYZnrc was used to transport the particle fluence from the linac and calculate dose to the patient. DOSXYZnrc patient models were generated on a voxel resolution of $3 \times 3 \times 3$ mm^3. The models were created from the DICOM CT images and a CT ramp model that included four materials: air, lung, soft tissue, and bone. The MC simulations were performed on two dual quad-core 2.26 GHz Intel Xeon xservers. MC simulations were run to an average statistical uncertainty of 1%. The MC codes within MMCTP have been commissioned to match measured PDDs, profiles and output values for the 21EX linac. The entire recalculation task, from exporting DICOM files to analysis of the MC DVHs, was carried out by an experienced clinical dosimetrist (but who had no prior MC expertise). The MMCTP workstation was stationed within the treatment planning area for routine clinical MC analysis of flagged patient plans. The user interaction time was limited to a 5 minute task of DICOM import.

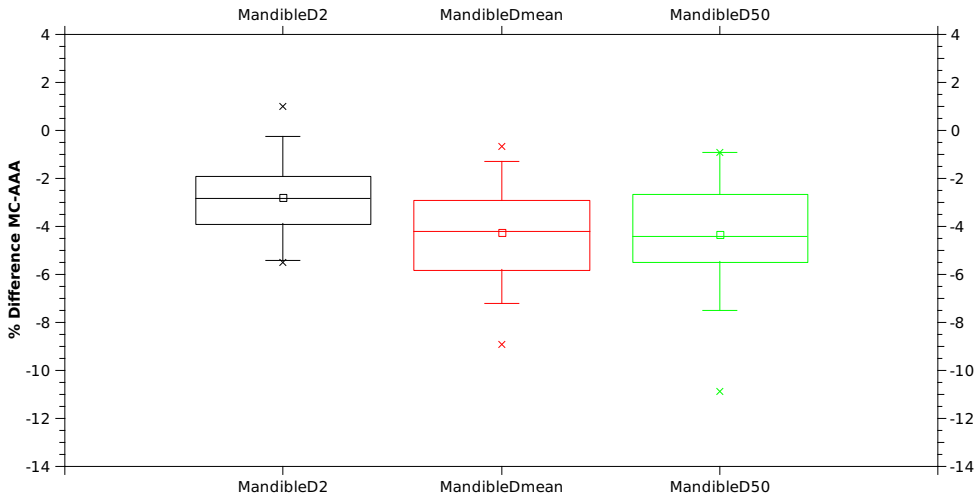

Figure 5–6: Mandible displays a trend of lower predicted MC dose. Max and min difference (diagonal cross), 95%-5% confidence interval (whiskers) 25-75 percentile (box) mean (rectangle) median (line).

5.2.6 Plan Evaluation

All patient plans, PB with no heterogeneity correction, AAA with heterogeneity correction, and MC calculated plans, were evaluated using dose volume-based indices. PB calculations were included in this study as a point of reference, as these patients were planned and treated with a PB plan. However, results are focused on the difference between AAA and MC, as PB differences are dominated by a failing to account for tissue heterogeneities. Previous studies have already established the superiority of AAA heterogeneity corrections over PB [31, 32, 33, 34, 35, 26]. In addition, the comparison between AAA and MC was part of AAA's clinical commissioning at the McGill University Health Centre.

All results were analyzed within MMCTP. This ensures a common algorithm for DVH calculations and for isodose displays between Eclipse and MC dose

distributions. Although isodose displays and DVHs give valuable information about the plan, the following endpoints were evaluated to quantitatively assess each plan: GTV and PTVs were evaluated at the minimum dose received by 98% of the volume ($D_{98\%}$), the dose received by 95% of the volume ($D_{95\%}$), the maximum dose received by 2% of the volume ($D_{2\%}$), the dose received by 50% of the volume ($D_{50\%}$), and the mean dose (D_{mean}). Critical structures were evaluated at the maximum dose (D_{max}) and $D_{2\%}$ for the spinal cord and brainstem. Parotid glands were evaluated at $D_{90\%}$, $D_{50\%}$, and D_{mean}. For the mandible, oral cavity and larynx, $D_{2\%}$, $D_{50\%}$, and D_{mean} were evaluated. As recommended in ICRU Report 83, the $D_{2\%}$ index was used to evaluate the maximum dose, as it is less prone to statistical fluctuations [18].

The dosimetric data was analyzed for statistical differences using one-way ANOVA (SAS Inst., Inc, Cary, NC. 9.2, 2008). Post-hoc testing was assessed using the Bonferroni multiple comparison test. Data was expressed as mean ± SD. Differences were considered significant if $p < 0.05$. For each comparison, differences between the MC plans were calculated with respect to the local point of interest AAA, using the formula,

$$\Delta_{\%}(D_x) = \frac{D_x^{MC} - D_x^{AAA}}{D_x^{AAA}} \times 100 \tag{5.1}$$

where x is a particular dose-volume index. In addition to dose-volume indices, the plans were compared qualitatively using isodose lines.

Table 5–1: Summary of results for eighteen HN plans; showing dose-volume indexes associated mean value with standard deviation, relative % difference between MC and AAA, and P-value

Index	Index	PB (Gy)	AAA (Gy)	MC (Gy)	Relative % diff
GTV	$D_{98\%}$	70.7 ± 0.8	69.2 ± 1.3	68.9 ± 1.2	-0.5 ($p > 0.05$)
	$D_{95\%}$	71.0 ± 0.7	69.7 ± 1.3	69.5 ± 1.1	-0.2 ($p > 0.05$)
	$D_{2\%}$	74.8 ± 1.3	74.4 ± 1.7	74.8 ± 1.6	0.5 ($p > 0.05$)
	D_{mean}	72.7 ± 0.8	71.8 ± 1.2	71.9 ± 1.1	0.2 ($p > 0.05$)
PTV70	$D_{98\%}$	69.3 ± 1.5	67.7 ± 1.9	65.6 ± 4.6	-3.2 ($p > 0.05$)
	$D_{95\%}$	70.1 ± 0.5	68.7 ± 1.0	67.6 ± 1.9	-1.6 (**$p < 0.05$**)
	$D_{2\%}$	74.7 ± 1.2	74.6 ± 1.5	75.0 ± 1.6	0.5 ($p > 0.05$)
	D_{mean}	72.3 ± 0.4	71.2 ± 1.3	71.2 ± 1.0	0.05 ($p > 0.05$)
PTV60	$D_{98\%}$	59.6 ± 1.1	58.2 ± 1.4	56.1 ± 3.6	-3.6 ($p > 0.05$)
	$D_{95\%}$	60.5 ± 0.6	59.1 ± 0.9	58.3 ± 1.6	-1.5 (**$p < 0.05$**)
	$D_{2\%}$	71.3 ± 0.8	70.9 ± 0.9	71.3 ± 1.4	0.6 ($p > 0.05$)
	D_{mean}	64.2 ± 0.6	63.6 ± 0.8	63.4 ± 1.0	-0.3 ($p > 0.05$)
PTV56	$D_{98\%}$	55.5 ± 1.2	53.9 ± 1.6	51.0 ± 4.4	-5.4 ($p > 0.05$)
	$D_{95\%}$	56.2 ± 1.1	54.9 ± 1.0	53.3 ± 2.2	-2.9 ($p > 0.05$)
	$D_{2\%}$	65.8 ± 8.1	65.34 ± 3.3	64.8 ± 3.4	-0.7 ($p > 0.05$)
	D_{mean}	59.2 ± 0.4	58.0 ± 1.4	57.3 ± 1.6	-1.2 ($p > 0.05$)
PTV54	$D_{98\%}$	54.3 ± 0.4	52.6 ± 0.7	51.1 ± 4.2	-2.7 ($p > 0.05$)
	$D_{95\%}$	54.8 ± 0.3	53.1 ± 0.6	52.4 ± 2.9	-1.1 ($p > 0.05$)
	$D_{2\%}$	63.6 ± 3.8	62.9 ± 3.7	63.5 ± 3.9	0.8 ($p > 0.05$)
	D_{mean}	57.5 ± 0.6	56.3 ± 0.9	56.4 ± 1.2	0.2 ($p > 0.05$)

5.3 Results and Discussion

The dosimetric results are summarized in tables 5–1 and 5–2. With the exception of two dose indices, the mean differences between AAA and MC did not reach statistical significance. This is in part due to the large variability between patient plans, as evident in the standard deviations. A few individual cases displayed large differences (> 5%) between the two algorithms.

Table 5–2: Summary of results for eighteen HN plans; showing dose-volume indexes associated mean value with standard deviation, relative % difference between MC and AAA, and P-value

Index	Index	PB (Gy)	AAA (Gy)	MC (Gy)	Relative % diff
Cord	D_{max}	42.2 ± 1.9	41.6 ± 1.8	41.8 ± 1.7	0.3 ($p > 0.05$)
	$D_{2\%}$	40.4 ± 1.8	39.8 ± 1.8	39.6 ± 2.0	-0.6 ($p > 0.05$)
Brainstem	D_{max}	45.3 ± 6.3	43.9 ± 6.0	43.6 ± 6.6	-0.7 ($p > 0.05$)
	$D_{2\%}$	40.9 ± 7.4	39.7 ± 7.1	39.2 ± 7.9	-1.7 ($p > 0.05$)
RT Parotid	$D_{90\%}$	21.8 ± 9.3	21.5 ± 8.5	20.3 ± 11.0	-5.5 ($p > 0.05$)
	D_{mean}	39.9 ± 10.2	39.5 ± 9.7	39.3 ± 11.7	-0.3 ($p > 0.05$)
LT Parotid	$D_{90\%}$	21.2 ± 8.1	21.1 ± 7.7	18.9 ± 7.7	-10.3 ($p > 0.05$)
	D_{mean}	41.4 ± 8.1	40.9 ± 7.7	39.6 ± 8.3	-3.3 ($p > 0.05$)
Mandible	$D_{2\%}$	68.7 ± 5.9	68.6 ± 5.7	66.7 ± 5.8	-2.7 ($p > 0.05$)
	D_{mean}	49.8 ± 7.5	48.8 ± 7.4	46.8 ± 7.4	-4.2 ($p > 0.05$)
Oral Cavity	$D_{2\%}$	67.8 ± 5.7	66.6 ± 5.4	66.6 ± 5.7	-0.0 ($p > 0.05$)
	D_{mean}	48.7 ± 9.8	47.0 ± 8.4	47.1 ± 10.1	0.0 ($p > 0.05$)
Larynx	$D_{2\%}$	71.2 ± 4.8	71.5 ± 5.1	71.7 ± 5.7	0.3 ($p > 0.05$)
	D_{mean}	59.8 ± 9.7	59.5 ± 9.7	60.0 ± 9.6	0.8 ($p > 0.05$)

5.3.1 Target Volumes

Target volumes include the GTV and PTV70, PTV60, and low (PTV56-54). The GTV results were in excellent agreement. The average relative differences for $D_{98\%}$, $D_{95\%}$, $D_{2\%}$, and D_{mean} were within 0.5%. The range of the individual differences were within 2%, with the exception of patient 15. The MC PTV70 and PTV60 results displayed a greater deviation from AAA. The mean $\Delta_{\%}D_{95\%}$ index was -1.6% for PTV70 and -1.5% for PTV60. These differences were found to be statistically significant. Figures 5–2 and 5–3 display the local percent differences: $\Delta_{\%}D_{98\%}$, $\Delta_{\%}D_{95\%}$, $\Delta_{\%}D_{2\%}$, and $\Delta_{\%}D_{mean}$ for PTV70 and PTV60. The PTV70 results were within the 5% limit, while the PTV60 results included four $\Delta_{\%}D_{98\%}$ values that were outside of the 5% limit, as shown in figure 5–4.

The MC dose indices for patient 15 were consistently lower than AAA. Upon examination of patient 15, it is believed that these large differences are the result of high and low density heterogeneity regions surrounding the GTV and PTVs. In addition, the extent of the GTV volume includes areas within the buildup region of the 6 MV beam.

The GTV and PTV70 dose indices of patient 9 agreed well with MC. However, the same can not be said for $D_{98\%}$ of PTV60. The MC low dose region of PTV60 (figure 5–1(a)) is 15% lower than AAA. An isodose comparison between AAA and MC is shown in figure 5–7 and the PTV60 structure is shown in cyan. Within this figure, the 63 Gy isodose line for MC (dashed) and AAA (solid), deviate from each other in the top right and left corners. This deviation is believed to be caused by the mandible bone adjacent to the PTV60. This scenario repeats itself in other patient plans, such as patient 11, and highlights the type of observable dosimetric differences between AAA and MC calculations.

5.3.2 Organs at Risk

Dosimetric agreement between AAA and MC varied for each specific OAR. Examination of table 5–2 revealed no systematic differences between the two algorithms. The mandible D_{mean} was -4.3% lower than AAA; an indication that mandible MC dose was consistently lower than AAA dose.

The parotid dose difference displayed the largest deviation from AAA, as evident in table 5–2 with the mean difference for $\Delta_{\%}D_{90\%}$ situated at -10%. $D_{90\%}$ values are a measure of the low dose component within the parotid volume. The relative percent difference plot for both parotids is shown in figure 5–8. MC dose

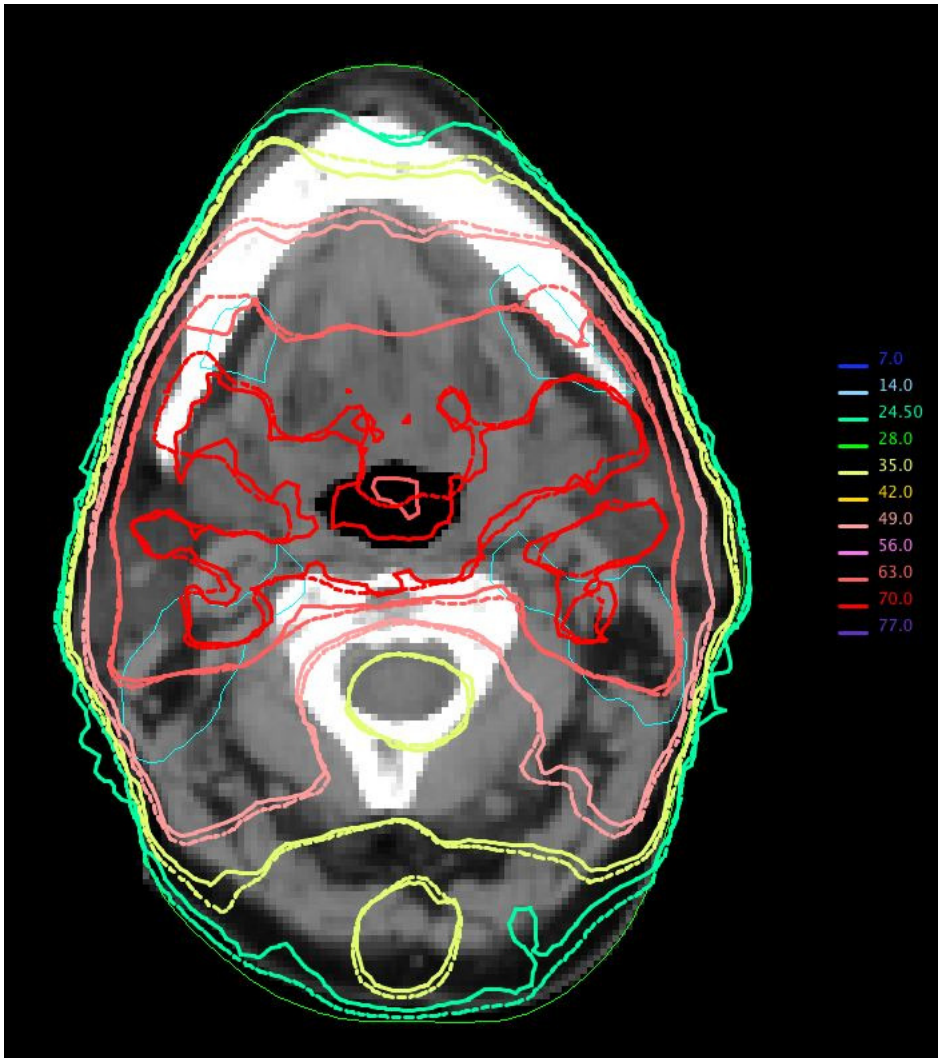

Figure 5–7: Isodose line comparison between AAA (dashed lines) and MC (solid lines) for Patient 9. The PTV60, shown in cyan color, is surrounded by regions of high and low density materials. The MC 63 Gy isodose line deviates from the AAA isodose line in the top right corner. The deviation is believed to be caused by the high density mandible bone adjacent to the PTV60 structure.

indices were consistently lower than AAA by 5% or more. A patient's isodose plot displaying both dose distributions is shown in figure 5–9. Within the figure,

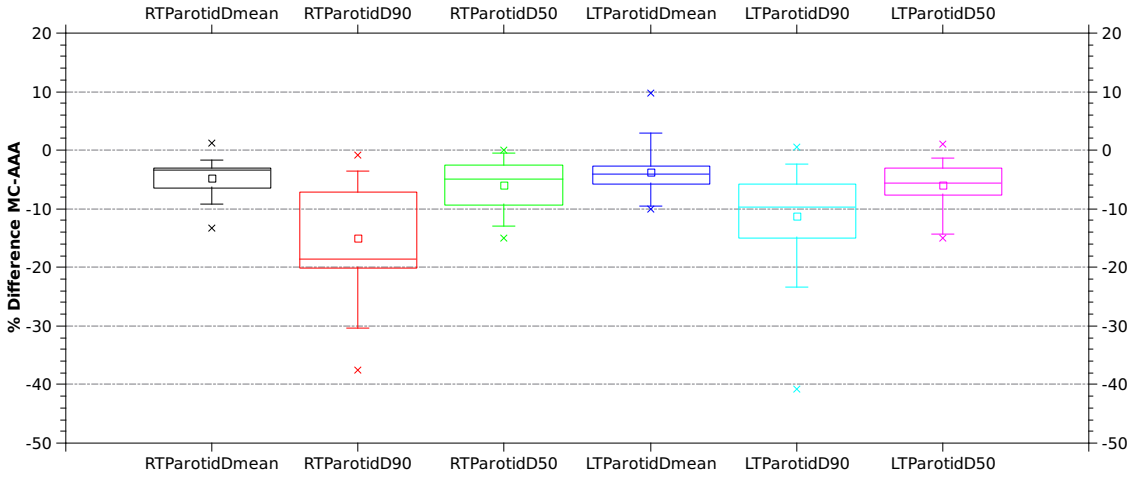

Figure 5–8: Parotid percent difference displays a trend of lower predicted MC dose.

there is a noticeable gap between the two isodose lines throughout the parotid structure. The gap is especially noticeable within the lower valued isodose lines. A contributing factor to the separation gap could be due to a limitation of AAA in the buildup and lateral falloff region. The effects are highlighted due to the tangential components of the treatment fields within this region. Another source of discrepancy could be attributed to the boundary voxels of the patient model. These voxels could be slightly offset to a maximum difference of half a voxel (1.5 mm) due to rounding of the dose grid voxels between the two dose engines; although, the net effect of rounding errors over many patients should be null.

A recent RapidArc (Varian Medical Systems, Palo Alto, CA) HN planning study by Bush *et al* [36], which examined the dosimetric differences between AAA and MC, concluded that AAA overestimates the parotid dose by 4.5-7.0%. A study by Gagne *et al* [37] concluded that AAA overestimates the parotid dose

by about 9%. Bush suggests that the reported dose difference is likely due to the close proximity of the parotids to the MLC field edge and due to the presence of air pockets within the parotid contours. The large dose difference observed in the parotids is consistent with AAA's inability to appropriately model dose near and in the penumbra defined by the MLC.

The mean parotid dose is often used as a clinical endpoint in the assessment of xerostomia; results of the mean parotid dose difference are shown in figure 5–8. The right parotid mean MC dose is centered 5% lower than AAA with all MC values within 2σ below the AAA values. The left parotid mean MC dose is centered 5% lower than AAA with all MC values within 1σ below the AAA values. This result represents a significant dosimetric discrepancy and warrants further investigation to asses a potential error in dosimetric reporting. The impact of this investigation could shift the parotid tolerance dose value in the quantitative analysis of normal tissue effects in the clinic (QUANTEC) [38] for reduced saliva function.

5.3.3 Dose to Water

The MC calculations within this study calculated and reported dose to medium while AAA calculated and reported dose to water. In order to evaluate the impact of this discrepancy, a small number of MC plans were recalculated in a heterogeneous water-density phantom. For the target volumes, the MC water calculations improved the agreement to AAA to within 1%. The original MC DVH for patient 9 is shown in figure 5–1(a) while the MC water DVH for patient 9 is shown in figure 5–10. The improvement in target agreement between MC

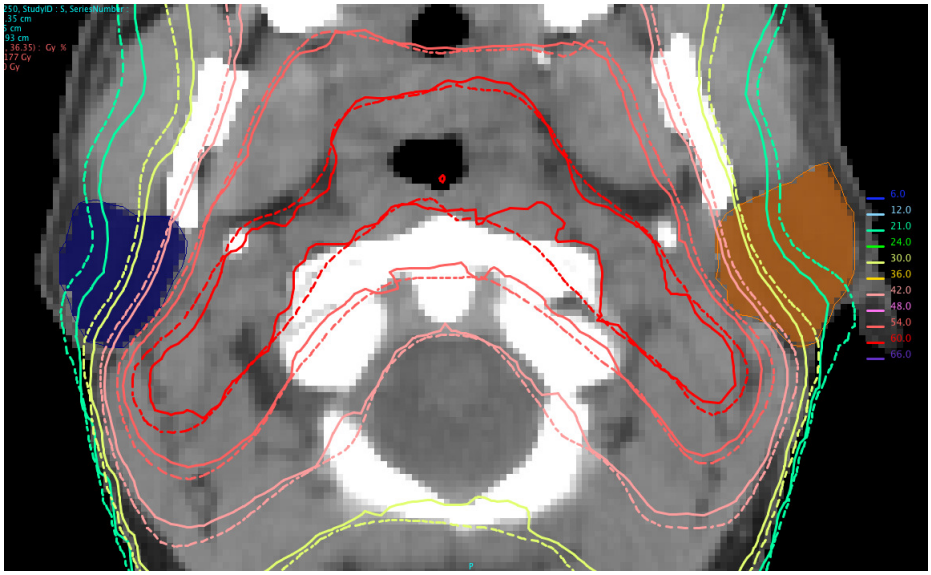

Figure 5–9: Typical parotid isodose plot MC (solid), AAA (dashed). The volume of low dose isodose lines is lower for MC than AAA. The AAA buildup gradient is larger than MC.

water and AAA suggests that particle transport through various materials was the dominant factor for observed dosimetric differences in the target volumes. With regards to the OAR, some MC water indices were closer to the AAA values, while others displayed no change. This suggests that other factors, such as accuracy of the beam model within the penumbra region and MLC scatter/leakage contributed to these differences.

For consistency, MC studies should compare both dose to water and dose to medium when comparing plans with conventional dose to water based systems. The necessity of comparing both methods will continue until dose to water or dose to medium is shown to correlate more closely with clinical outcome [39]. The

observed difference between dose to medium and dose to water was consistent with Siebers *et al* [40] conversion ratios.

5.3.4 MMCTP

In addition to the dosimetric results presented above, this study provided an opportunity to evaluate the feasibility of MMCTP as a clinical tool for dosimetric analysis. With the exception of commercially available clinical MC systems, research based MC simulations are often considered lengthy, cumbersome, and impractical in a clinical setting. The clinical environment requires a simple to use system with minimal user knowledge of the underlying processes. In this study, MMCTP was used by a clinical dosimetrist with no prior experience in MC simulations. With training and experience, the MMCTP GUI was considered equivalent in it's easy-to-use interface as a commercial TPS. The amount of user interaction time was minimal for importing DICOM patients and launching the MC simulations. The dominant inefficiency in the system was the MC simulation time, however, this time can be reduced with the use of fast GPU Monte Carlo codes or XVMC [41]. XVMC for photon dose calculations has been shown to be 80 times more efficient than DOSXYZnrc simulations [42]. In addition, patient plans could be processed in parallel using multiple instances of MMCTP to maintain 100% CPU load over a 24 hour period.

5.4 Conclusions

Open source MC codes such as BEAMnrc and DOSXYZnrc have an important role to play in clinical radiotherapy research. These codes, interfaced within MMCTP, have enabled clinical staff to investigate and report on dosimetric

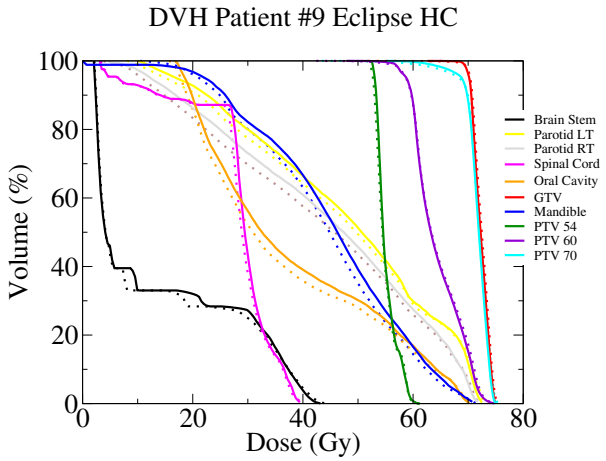

Figure 5–10: DVH graphs for patient 9, AAA (solid line) and MC water (dotted). The MC water calculation matches the AAA calculation for PTV60.

differences between AAA and MC. The observed dosimetric differences in this study were limited to regions of high and low density, which can be attributed to radiation transport differences in buildup, builddown, as well as lateral scattering. Specific OAR, such as the parotids, which are located near the beam buildup region, showed the greatest deviation from MC. The parotids $\Delta_{\%}D_{90\%}$ mean was as high as 10% with individual plans being overestimated in AAA by as much as 20%. OAR overestimations may not negatively impact clinical patients, however, this trend will bias clinical studies. Target volumes were better matched to MC results as the range of results were within 5% and the mean was within 2% for all but the $D_{98\%}$ values. For the eighteen patient plans, PTV70 and PTV60 $D_{95\%}$ values were found to be statistically significant with a mean difference of -1.6% and -1.5%. These systematic deviations in the target dose indicate that the intended target coverage was not achieved. Target dosimetric differences of as little as 2%

can affect dose protocol levels, and these deviations may have clinical implications. Target discrepancies were largely the result of reporting dose to material, as dose to water calculations provided excellent agreement. As a component of AAA's clinical commissioning, this study provided acceptable dosimetric confidence in AAA.

Throughout this study, MMCTP has demonstrated to be a valuable tool for radiotherapy research, as a trained dosimetrist with no prior experience in MC simulations was able to use MMCTP for all MC calculations. The role of MMCTP is to provide the radiotherapy community with an independent dose calculation algorithm for improved insight when assessing dosimetric differences between clinical treatment planning systems and measurements. This study paved the way for clinical personnel to use MMCTP for MC investigations and prompted a followup study to investigate dosimetric differences between AAA and MC for lung stereotactic body radiation therapy (SBRT).

5.5 Acknowledgements

The authors thank Wamied Abdel Rahman (Ph.D.) for the installation and support of the clinical MC cluster and Sarah Finch for assistance with SAS. Financial support from The Terry Fox Foundation Strategic Initiative for Excellence in Radiation Research for the 21st Century (EIRR21) at CIHR. Work was partially supported by NSERC RG-PIN 298191.

5.6 References

[1] Frank C S Wong, Alice W Y Ng, Victor H F Lee, Collin M M Lui, Kwok-Keung Yuen, Wing-Kin Sze, To-Wai Leung, and Stewart Y Tung. Whole-field

simultaneous integrated-boost intensity-modulated radiotherapy for patients with nasopharyngeal carcinoma. *Int. J. Radiat. Oncol. Biol. Phys.*, 76(1):138–145, 2010.

[2] K K Fu, T F Pajak, A Trotti, C U Jones, S A Spencer, T L Phillips, A S Garden, J A Ridge, J S Cooper, and K K Ang. A Radiation Therapy Oncology Group (RTOG) phase III randomized study to compare hyperfractionation and two variants of accelerated fractionation to standard fractionation radiotherapy for head and neck squamous cell carcinomas: first report of RTOG 9003. *Int. J. Radiat. Oncol. Biol. Phys.*, 48(1):7–16, 2000.

[3] S Wu, C Xie, X Jin, and P Zhang. Simultaneous modulated accelerated radiation therapy in the treatment of nasopharyngeal cancer: a local center's experience. *Int. J. Radiat. Oncol. Biol. Phys.*, 66(4):S40–S46, 2006.

[4] D Kwong, J Sham, and L Leung. Preliminary results of radiation dose escalation for locally advanced nasopharyngeal carcinoma. *Int. J. Radiat. Oncol. Biol. Phys.*, 64(2):374–381, 2006.

[5] A Lauve, M Morris, R Schmidt-Ullrich, and Q Wu. Simultaneous integrated boost intensity-modulated radiotherapy for locally advanced head-and-neck squamous cell carcinomas: II–clinical results. *Int. J. Radiat. Oncol. Biol. Phys.*, 60(2):374–387, 2004.

[6] R Mohan, Q Wu, M Manning, and R Schmidt-Ullirch. Radiobiological considerations in the design of fractionation strategies for intensity-modulated radiation therapy of head and neck cancers. *Int. J. Radiat. Oncol. Biol. Phys.*, 46(3):619–630, 2000.

[7] Gary A Ezzell, James M Galvin, Daniel Low, Jatinder R Palta, Isaac Rosen, Michael B Sharpe, Ping Xia, Ying Xiao, Lei Xing, Cedric X Yu, IMRT subcommitte, and AAPM Radiation Therapy committee. Guidance document on delivery, treatment planning, and clinical implementation of IMRT: report of the IMRT Subcommittee of the AAPM Radiation Therapy Committee. *Med. Phys.*, 30(8):2089–2115, 2003.

[8] A Alexander, F Deblois, G Stroian, K Al-Yahya, E Heath, and J Seuntjens. MMCTP: a radiotherapy research environment for Monte Carlo and patient-specific treatment planning. *Phys. Med. Biol.*, 52(13):N297–308, 2007.

[9] P Francescon, S Cora, and P Chiovati. Dose verification of an IMRT treatment planning system with the BEAM EGS4-based Monte Carlo code. *Med. Phys.*, 30(2):144–157, 2003.

[10] M Arnfield, C Siantar, J Siebers, P Garmon, and L Cox. The impact of electron transport on the accuracy of computed dose. *Med. Phys.*, 27(6):1226–1238, 2000.

[11] A Bergman, K Bush, M Milette, I Popescu, and K Otto. Direct aperture optimization for IMRT using Monte Carlo generated beamlets. *Med. Phys.*, 33(10):3668–3679, 2006.

[12] S Cardoso, V Alves, L da Rosa, and L Campos. Monte Carlo simulation of bony heterogeneity effects on dose profile for small irradiation field in radiotherapy. *PLoS one*, 5(5):e10466, 2010.

[13] I Das, G Ding, and A Ahnesjö. Small fields: nonequilibrium radiation dosimetry. *Med. Phys.*, 35(1):206–215, 2008.

[14] R Mohan, M Arnfield, S Tong, Q Wu, and J Siebers. The impact of fluctuations in intensity patterns on the number of monitor units and the quality and accuracy of intensity modulated radiotherapy. *Med. Phys.*, 27(6):1226–1238, 2000.

[15] G Cranmer-Sargison and W Beckham. Modelling an extreme water–lung interface using a single pencil beam algorithm and the Monte Carlo method. *Phys. Med. Biol.*, 49(8):1557–1567, 2004.

[16] Margarida Fragoso, Ning Wen, Sanath Kumar, Dezhi Liu, Samuel Ryu, Benjamin Movsas, Ajlouni Munther, and Indrin J Chetty. Dosimetric verification and clinical evaluation of a new commercially available Monte Carlo-based dose algorithm for application in stereotactic body radiation therapy (SBRT) treatment planning. *Phys. Med. Biol.*, 55(16):4445–4464, 2010.

[17] J Yang, J Li, L Chen, and R Price. Dosimetric verification of IMRT treatment planning using Monte Carlo simulations for prostate cancer. *Phys. Med. Biol.*, 50(5):868–878, 2005.

[18] N Sakthi, P Keall, I Mihaylov, Q Wu, and Y Wu. Monte Carlo-based dosimetry of head-and-neck patients treated with SIB-IMRT. *Int. J. Radiat. Oncol. Biol. Phys.*, 63(3):968–977, 2006.

[19] C M Ma, T Pawlicki, S Jiang, and J Li. Monte Carlo verification of IMRT dose distributions from a commercial treatment planning optimization system. *Phys. Med. Biol.*, 45(9):2483–2495, 2000.

[20] A Leal, F Sánchez-Doblado, and R Arráns. Routine IMRT verification by

means of an automated Monte Carlo simulation system. *Int. J. Radiat. Oncol. Biol. Phys.*, 56(1):58–68, 2003.

[21] N Dogan, J V Siebers, P J Keall, F Lerma, Y Wu, M Fatyga, J F Williamson, and R K Schmidt-Ullrich. Improving IMRT dose accuracy via deliverable Monte Carlo optimization for the treatment of head and neck cancer patients. *Med. Phys.*, 33(11):4033–4043, 2006.

[22] C Boudreau, E Heath, and J Seuntjens. IMRT head and neck treatment planning with a commercially available Monte Carlo based planning system. *Phys. Med. Biol.*, 50(5,):878–890, 2005.

[23] D W O Rogers, B A Faddegon, G X Ding, C M Ma, J We, and T R Mackie. BEAM: A Monte Carlo code to simulate radiotherapy treatment units. *Med. Phys.*, 22(5):503–524, 1995.

[24] N Dogan, I Mihaylov, Y Wu, and P Keall. Monte Carlo dose verification of prostate patients treated with simultaneous integrated boost intensity modulated radiation therapy. *Radiat. Oncol.*, 4(18):1–17, 2009.

[25] B Walters, I Kawrakow, and D W O Rogers. *DOSXYZnrc Users Manual*. Ionizing Radiation Standards, National Research Council of Canada, 2007.

[26] S Davidson, R Popple, G Ibbott, and D Followill. Heterogeneity dose calculation accuracy in IMRT: Study of five commercial treatment planning systems using an anthropomorphic thorax phantom. *Med. Phys.*, 35(12):5434–5439, 2008.

[27] G Ding, D Duggan, B Lu, D Hallahan, A Cmelak, A Malcolm, J Newton, M Deeley, and C W Coffey. Impact of inhomogeneity corrections on dose

coverage in the treatment of lung cancer using stereotactic body radiation therapy. *Med. Phys.*, 34(7):2985–2994, 2007.

[28] E Sterpin, M Tomsej, B De Smedt, N Reynaert, and S Vynckier. Monte Carlo evaluation of the AAA treatment planning algorithm in a heterogeneous multilayer phantom and IMRT clinical treatments for an Elekta SL25 linear accelerator. *Med. Phys.*, 34(5):1665–1677, 2007.

[29] H Neuenschwander, R Mini, and E Born. Collapsed cone and analytical anisotropic algorithm dose calculations compared to VMC++ Monte Carlo simulations in clinical cases. *Journal of Physics*, 74, 2007.

[30] Irina Fotina, Peter Winkler, Thomas Künzler, Jochen Reiterer, Isabell Simmat, and Dietmar Georg. Advanced kernel methods vs. Monte Carlo-based dose calculation for high energy photon beams. *Radiother. Oncol.*, 93(3):645–653, 2009.

[31] I Gagne and S Zavgorodni. Evaluation of the analytical anisotropic algorithm (AAA) in an extreme water-lung interface phantom using Monte Carlo dose calculations. *J. Appl. Clin. Med. Phys.*, 18(1):33–46, 2006.

[32] A Van Esch, L Tillikainen, J Pyykkonen, M Tenhunen, H Helminen, S Siljamaki, J Alakuijala, M Paiusco, M Lori, and D P Huyskens. Testing of the analytical anisotropic algorithm for photon dose calculation. *Med. Phys.*, 33(11):4130–4148, 2006.

[33] G Ding, D Duggan, and C Coffey. Comment on "Testing of the analytical anisotropic algorithm for photon dose calculation"[Med. Phys., 4130–4148 (2006)]. *Med. Phys.*, 34(8):3414, 2007.

[34] C Bragg and K Wingate. Clinical implications of the anisotropic analytical algorithm for IMRT treatment planning and verification. *Radiother. Oncol.*, 82(2):276–284, 2008.

[35] V Panettieri, P Barsoum, M Westermark, L Brualla, and I Lax. AAA and PBC calculation accuracy in the surface build-up region in tangential beam treatments. Phantom and breast case study with the Monte Carlo code PENELOPE. *Radiother. Oncol.*, 93(1):94–101, 2009.

[36] K Bush, S Zavgorodni, and I Gagne. Monte Carlo evaluation of RapidArc^{TM} oropharynx treatment planning strategies for sparing of midline structures. *Phys. Med. Biol.*, 55(16):4465–4479, 2010.

[37] I Gagne, W Ansbacher, and S Zavgorodni. A Monte Carlo evaluation of RapidArc dose calculations for oropharynx radiotherapy. *Phys. Med. Biol.*, 53(24):7167–7185, 2008.

[38] L B Marks, E D Yorke, A Jackson, R K T Haken, L S Constine, A Eisbruch, S M Bentzen, J Nam, and J O Deasy. Use of normal tissue complication probability models in the clinic. *Int. J. Radiat. Oncol. Biol. Phys.*, 76(3 Suppl):S10–19, 2010.

[39] N Dogan, J Siebers, and P Keall. Clinical comparison of head and neck and prostate IMRT plans using absorbed dose to medium and absorbed dose to water. *Phys. Med. Biol.*, 51(19):4967–4980, 2006.

[40] J V Siebers, P J Keall, A E Nahum, and R Mohan. Converting absorbed dose to medium to absorbed dose to water for Monte Carlo based photon beam dose calculations. *Phys. Med. Biol.*, 45(4):983–995, 2000.

[41] M Fippel. Fast Monte Carlo dose calculation for photon beams based on the VMC electron algorithm. *Med. Phys.*, 26(8):1466–1475, 1999.

[42] I Kawrakow and M Fippel. Investigation of variance reduction techniques for Monte Carlo photon dose calculation using XVMC. *Phys. Med. Biol*, 45(8):2163–2183, 2000.

CHAPTER 6
Paper III: Toward automatic field selection and planning using Monte Carlo-based direct aperture optimization in modulated electron radiotherapy

Andrew Alexander, François DeBlois, and Jan Seuntjens

Phys. Med. Biol., 55(16):4563-4576, 2010

Contents

MERT has been proposed to deliver highly conformal treatments to superficial targets, with improved sparing of OAR dose. However, this statement is often drawn from initial MERT studies where the alternative modality is direct electrons or conformal photon therapy. Over the past ten years, there has been an enormous amount of development in photon therapy such as IMRT and volumetric arc therapy. These advanced techniques challenge the opening statement and the

usefulness of MERT in today's advanced cancer centres. In order to compete with current photon techniques, MERT planning demands inverse optimization and MERT comparisons should be referenced to standard practice techniques.

Previous work by Khalid Al-Yahya at the McGill Medical Physics Unit resulted in the construction of the few leaf electron collimator (FLEC). The FLEC serves as a tertiary electron add-on to the clinical accelerators installed at the Montreal General Hospital. The main objectives of Al-Yahya's work was to build the FLEC and validate Monte Carlo models of the electron accelerator. The current chapter builds on these two objectives with the development of an automated system for inverse MERT planning and delivery. The system is built within MMCTP and is seen as an essential tool for clinical MERT viability. The following manuscript describes the automated MERT planning process as developed within the McGill Monte Carlo treatment planning system (MMCTP).

Abstract

Modulated electron radiotherapy (MERT) has been proven to produce optimal plans for shallow tumours. This study investigates automated approaches to the field determination process in generating optimal MERT plans for few-leaf electron collimator (FLEC) based MERT, by generating a large database of pre-calculated beamlets stored as phase-space files. Beamlets can be used in an overlapping feathered pattern to reduce the effect of abutting fields, which can contribute to dose inhomogeneities within the target. Beamlet dose calculation was performed by Monte Carlo (MC) simulations prior to direct aperture optimization (DAO). The second part of the study examines a preliminary clinical comparison

between FLEC-based MERT and helical TomoTherapy. A MERT plan for spinal irradiation was not able to conform to the PTV dose constraints as closely as the TomoTherapy plan although the TomoTherapy plan was taken as is, i.e., not Monte Carlo re-calculated. Despite the remaining gradients in the PTV, the MERT plan was superior in reducing the low-dose bath typical for TomoTherapy plans. In conclusion, the FLEC-based MERT planning techniques developed within the study produced promising MERT plans with minimal user input. The phase-space database reduces the MC calculation time and the feathered field pattern improves target homogeneity. With further investigations, FLEC-based MERT will find an important niche in clinical radiation therapy.

6.1 Introduction

Electron beams with energies from 4-25 MeV are ideal for treating shallow tumours and are available for routine clinical use in the vast majority of radiotherapy departments. A 2005 publication by Mu *et al* [1] suggests that if proton therapy is not available, advanced electron therapy such as modulated electron radiotherapy (MERT) may provide a better alternative to IMRT for reduced risk of radiation-induced secondary cancers. Despite the availability and historical significance of electron therapy within radiation oncology, current practice of electron therapy is underutilized [2].

Current clinical electron techniques such as the use of cutouts and bolus date back 20 years and are seen as labour intensive with limited conformity. The underuse of electrons is partially due to clinical considerations but also to the lack of sophisticated system for advanced electron therapy. In order to reinvigorate

clinical electron therapy treatments, the clinic requires an automated system, similar to IMRT for advanced photon therapy. This system would encompass an automated field-shaping device, Monte Carlo (MC) treatment planning system and beamlet optimization processes. The optimization process for few-leaf electron collimator (FLEC) [3] based MERT is investigated in this work.

Current techniques in electron therapy date back to the 1980s with the use of compensating bolus for increased target dose homogeneity. In 1996, Hyödynmaa *et al* [4] published their work on optimization of conformal electron therapy using energy and fluence-modulated beams. The published technique used pencil beams generated from a spot scanning racetrack microtron of energies from 5-25 MeV to modify the energy deposition with depth in a controlled manner as an alternative to bolus. Since 1996 there have been many attempts to adapt this technique on a clinical radiotherapy accelerator as an advanced alternative to bolus. The main difference between a racetrack microtron and a clinical accelerator is the scattering foil within the accelerator used to produce a large flat beam. To produce fluence-modulated beams on a clinical accelerator requires an additional beam collimation device. The use of the photon multi-leaf collimator (MLC) as an electron shaping device has been studied by Klein [5, 6], Plessis [7], Jin [8] and Salguero [9]. An alternative to the photon MLC would be a dedicated electron multileaf collimator located somewhere between the photon MLC and the patient's skin. This approach has been studied by Lee [10], Blomquist [11], Ravindran [12], Hogstrom [13], Gauer [14], and Vatanen [15]. The FLEC which currently rests within the Varian electron applicator also falls into this category of tertiary electron collimators.

Previous MERT studies have investigated the feasibility and dosimetric characteristics of electron collimators. Dose optimization processes for MERT is an underinvestigated area as it strongly depends on the details of the delivery device. Within our own FLEC-based MERT studies [3, 16], there was some arbitrariness in the initial choice of the fields which subsequently affected the quality of the optimized plan. A recent publication by Engel *et al* [17] describes the optimization process for advanced MLC based electron irradiation. Engel's process details the issues associated with generating a set of initial conformal beams, breaking this set into a subset of smaller fields, estimating the dose within the subset and optimization of the final fields. The challenges with MERT planning comes from the tradeoffs between using a large set of initial beams to increase the solution set within the optimization process at the cost of lengthy Monte Carlo calculation time or using a limited number of initial beams where the success of the optimization process is more sensitive to the geometric placement of the beams. Engel and others have described methods to estimate the dose from subsets or beamlets within a large field which is an excellent approach to increase the solution set at a slight cost to dosimetric accuracy within the optimization process. Current methods of MLC based MERT vary between groups, however, the results are quite similar. A slightly different approach is required for FLEC-based MERT due to the physical size (8×8 cm^2) and rectangular collimation.

The present study investigates an automated field determination and optimization process in generating optimal FLEC-based MERT plans. An automated algorithm determines the optimal beam incidence angles and maximum field size.

The optimization process directly adjusts the weights of the apertures, a process called direct aperture optimization (DAO) [18]. The challenge for this work was to generate a discrete set of apertures, which will be used as input to the DAO code to produce MERT plans that compete with available alternative treatment modalities. Within this study, we present the optimization results from a simple target geometry to determine the effect of abutting fields and feathered fields on target homogeneity and examine a clinical comparison between a MERT and a TomoTherapy plan.

6.2 Materials and Methods

The first step in investigating DAO optimization strategies was the generation of a large database of pre-calculated electron phase-space-based beamlets. Phase-space files contain particle information for all particles at a specific location below the treatment head. Unlike with IMRT, where a large field sized (20×20 cm^2) phase-space file can be divided into beamlets (1×1 cm^2) while ignoring collimation or leaf sequencing effects, electron fields are highly sensitive to the electron collimation device. In addition to the requirement of many phase-spaces, each electron MC calculation is computationally demanding. A series of field openings were generated using an overlapping feathered pattern. A feathered pattern was chosen to reduce the effect of abutting electron fields, which can contribute to dose inhomogeneities within the target. Dose distributions are calculated for each field and the optimization algorithm determines field weights. With the use of a large database of phase-space files, FLEC-based MERT plans should be superior to previous generations of FLEC-based MERT plans, where a small number of fields

were manually generated using the cross sectional area of the target volume and gantry angle.

The motorized few-leaf electron collimator (FLEC) has been characterized in previous articles by Al-Yahya [3, 16, 19]. A Monte Carlo model was commissioned for accurate dose calculations using BEAMnrc [20] and DOSXYZnrc [21] codes. The first part of this study examines the effect of beamlet size and position on target dose homogeneity. Target homogeneity can be evaluated from the cost function of the optimization algorithm, target dose volume histogram, and the isodose plot. The goals of the study will be to establish ideal parameters for MERT planning. In the second part of the study, these parameters will be applied to a clinical case where MERT treatments could potentially be used as an alternative treatment modality. Section 6.2.1 describes the entire process for developing FLEC-based MERT plans while section 6.2.2 investigates the size and placement of subfields, and section 6.2.3 describes the application of MERT planning on a clinical case.

6.2.1 FLEC-based MERT Planning

The MERT planning process is outlined in figure 6–1. The process can be divided into two phases, the planning phase and the optimization phase. After the optimization phase, the optimized plan parameters including the final dose distribution are evaluated within MMCTP (McGill Monte Carlo treatment planning software [22]). In the event that the final plan does not pass the evaluation, phase 1 can be revisited. The focus of the study is to examine the effect of subfield parameters (step 4) on optimization results.

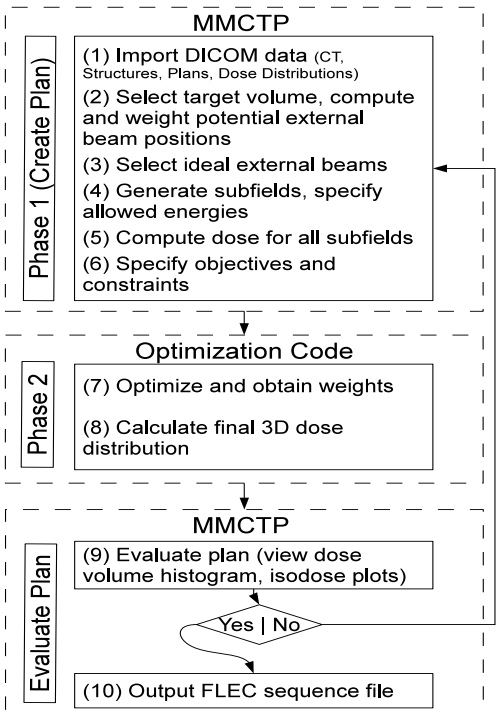

Figure 6–1: Entire FLEC-based MERT optimization process. Data transfer between MMCTP and optimization code is by ASCII files.

Phase 1 consists of six steps performed within MMCTP in the following flow:

1. DICOM patient data was imported into MMCTP
2. The target volume and external body contour were selected to compute and weight potential external beam positions. An algorithm generated ideal large field external beams based on physical geometric constraints such as patient orientation and proximity of the electron applicator cone to the patient's skin. The algorithm ranked the "best" possible beam position by: target symmetry, target projection width, target depth, and source to surface distance (SSD)

3. One or more open beams were selected from step 2 to cover the target volume.
4. The large open beams selected in step 3 were broken down into subfields and their dose distribution calculated. Without a conformal aperture which conforms closely to the shape of the target, it was necessary to modulate the open beams with smaller beamlets. It was hypothesized that these smaller beamlets will produce better target coverage and reduce the normal tissue dose. The size and spatial distribution of the beamlets were varied in a systematic process to determine the optimal parameters for ideal treatments. The maximum FLEC opening is 8×8 cm^2. It was determined to use 2×2 cm^2 beamlets as a tradeoff between higher resolution and lower dose output from the accelerator. Gauer and colleagues suggested a minimum opening of 3×3 cm^2 [14]. The size of the beamlets and the offset between beamlets were used to generate a large number of subfields. The total number of subfields in one dimension depends on the initial beam opening, size of the beamlets, and offset between beamlets, as calculated from equation 6.1.

$$Total_{x,y} = \frac{\mathrm{FLEC}_{\mathrm{opening_{x,y}}} - \mathrm{FLEC}_{\mathrm{beamlet_{x,y}}}}{\mathrm{FLEC}_{\mathrm{offset_{x,y}}}} + 1 \tag{6.1}$$

For example, an 8×8 cm^2 field with 2×2 cm^2 beamlets and a 0.5 cm offset between beamlets produces a total of 169 fields per energy. As the number of broad beams increase, the total number of beamlets quickly climbs into the thousands. It is important to remember that each beamlet requires a patient specific dose calculation. The size, position, and number of beamlets

significantly impact the total dose calculation time and the optimization results.

5. On average, the MC calculation time for one phase-space file was approximately 1 hour on a 2.7 GHz CPU cluster with 40 nodes. The specific calculation time for a complete linac head simulation of a 2×2 cm^2 9 MeV phase-space with 4,000,000 particles in the scoring plane was 70 minutes. The complete a linac head simulation began with a point source of electrons exiting the linac waveguide and finished at a scoring plan just beyond FLEC leaves at a distance of 95.01 cm from the electron source with a geometry radius of 15 cm throughout the linac head. These preparatory calculations represent the bulk of the work within MERT planning and it was essential to develop strategies to reduce the calculation time and to streamline the handling of many files. To this end, a phase-space database was introduced within MMCTP to reduce the impact of MC calculations. The database maintained a record of calculated phase-space files to limit the number of electron BEAMnrc simulations. The record stored the FLEC leaf positions, electron energy, and location of the phase-space file. An electron phase-space database was possible because of the repetitive nature of the beamlet sizes and positions generated during MERT planning. For each new beamlet calculation, the database was scanned for a match. If the matching process failed, the beamlet calculation proceeded and the database was updated with a new entry. The transport parameters used in EGS simulations were ECUT = AE = 700 keV cutoff for electron transport, PCUT = AP = 10 keV for

photon transport, and PRESTA-II as the electron stepping algorithm. A master phase-space file above the jaws was created as the source for each beamlet BEAMnrc simulation. The beamlet phase-space file was then transported through the patient geometry using DOSXYZnrc. The patient was modelled by converting the CT data into an EGSPhant file within MMCTP. The dimensions and voxel size of the EGSPhant file should be appropriate to the volume of interest. The DOSXYZnrc simulation creates a beamlet-specific dose distribution reported in absorbed dose to tissue per particle. A DOSXYZnrc calibration value normalizes the dose to absorbed dose per monitor unit. DOSXYZnrc simulations were run to an average percent error of 1% on dose values greater than 50% of the maximum dose. The specific calculation time for a DOSXYZnrc simulation with a 2×2 cm^2 9 MeV beam within a $3\times3\times3$ mm^3 EGSPhant file was 10 minutes.

6. The objective variables for the target included, a maximum and minimum dose limit and a corresponding dose penalty value. The organs at risk variables included a dose-volume constraint and a penalty value.

With the completion of phase 1, phase 2 begins externally to MMCTP in the following flow:

7. The optimization software was originally written in the visual software environment AVS (AVS5.4, AdvancedVisualSystems, MA) as described by Al-Yahya [16]. It has since been re-written in C language and interfaced within MMCTP. In general, the software has not changed and is only outlined to provide completeness to the study. The software uses a combination

of gradient and simulated annealing optimization, which uses DDCs and dose volume constraints to adjust the number of monitor units (MU) per beam and generate an optimal plan. DDCs are truncated MC dose distribution files which relate the dose contribution from each subfield to each voxel within a specific target or organ volume. Optimization parameters such as minimum and maximum MU per beam, gradient step size, and maximum number of iterations can be adjusted per run. The user defines a set of target and dose volume constraints, which are used to create a dose volume cost function. Target constants include a maximum and minimum dose and penalty value. Organ constraints include a penalty value for each dose and corresponding volume limit. The user can define more than one organ constraint for each organ.

The dose volume cost function is a quantitative measure of target and organ dose values, which fall outside of the desired dose range. The function is represented by equation 6.2, where **w** stands for the array of beamlet weights, $F_{TV}^{D}(\mathbf{w})$ represents the dose-based target objective term and $F_{OAR}^{V}(\mathbf{w})$ represents the volume-based organs at risk (OAR) objective term.

$$F^{DV}(\mathbf{w}) = F_{TV}^{D}(\mathbf{w}) + F_{OAR}^{V}(\mathbf{w}) \tag{6.2}$$

The objective terms are represented by equations 6.3 and 6.4

$$F_{TV}^{D}(\mathbf{w}) = \pi_{TV}^{max} \sum_{p \in TV} \Theta(D_{TV,p(\mathbf{w})} - D_{TV}^{max}) \left[\frac{D_{TV,p(\mathbf{w})} - D_{TV}^{max}}{D_{TV}^{max}} \right]^2 + \pi_{TV}^{min} \sum_{p \in TV} \Theta(-D_{TV,p(\mathbf{w})} + D_{TV}^{min}) \left[\frac{-D_{TV,p(\mathbf{w})} + D_{TV}^{min}}{D_{TV}^{min}} \right]^2 \tag{6.3}$$

$$F_{OAR}^{V}(\mathbf{w}) = \pi_{OAR_l} \sum_{l} \left[\frac{\sum_{p \in OAR_l} \Theta(D_{OAR_l,p(\mathbf{w})} - D_{OAR_l}^{max}) dV - V_{OAR_l}^{max}}{V_{OAR_l}} \right]^2 \tag{6.4}$$

where π_{TV}^{max} and π_{TV}^{min} refer to the penalty parameters of the target maximum and minimum dose constraints, respectively, Θ defines the Heaviside function, and $D_{TV,p(\mathbf{w})}$ is the dose deposited to point p of the target (denoted by TV) which contains a total of N_{TV} dose points. The dose to the target volume is constrained by the user-specified maximum and minimum dose D_{TV}^{max} and D_{TV}^{min} and relevant dose-volume relations for critical organs are specified by the dose-volume constraints of $(D_{OAR_l}^{max}, V_{OAR_l}^{max})$, where l labels all the organ constraints. dV is the elemental volume in the OAR. Each constraint in the OAR is assigned a penalty value π_{OAR} that weighs the individual penalty contribution to the overall objective function.

The gradient optimization algorithm makes use of a simple steepest descent algorithm, developed by Hristov [23] to satisfy the dose volume constraints. The simulated annealing algorithm, proposed by Sait [24], uses random numbers to adjust the beam weights and satisfy the dose volume constraints. Gradient optimization algorithms are generally orders of magnitude faster than stochastic

algorithms, however they may become trapped within a local minimum. In order to escape local minima, the results of the gradient optimization were input into the stochastic algorithm to determine if additional beam weight optimization was possible. Depending on the initial number of beams, and the total number of dose points per target and organ at risk, the optimization time can vary from minutes to hours. Optimization output includes an array of beam weights and a combined final dose distribution.

6.2.2 Establish Ideal Parameters for MERT Planning

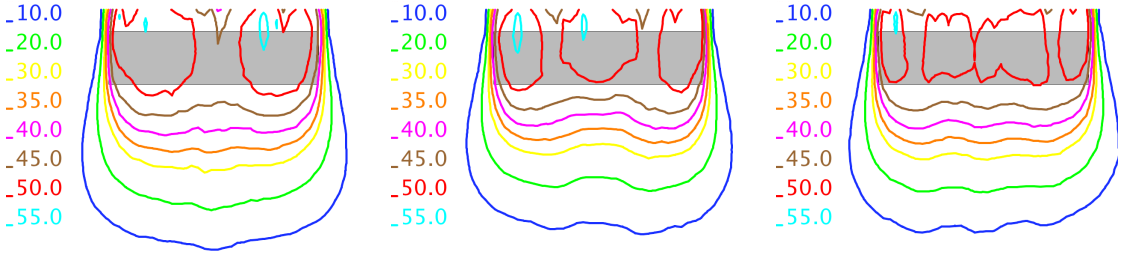

Figure 6–2: Slab geometry with isodose lines plotted in Gy values for various beamlet sizes. (a) 4×2 cm^2 beamlets (b) 2.66×2 cm^2 beamlets (c) 2×2 cm^2 beamlets

Virtual Slab:

A virtual target geometry was used to quantify the effect of feathered subfields. The geometry was a rectangular slab of thickness 1 cm. The slab was located 1 cm below the external contour with a width of 5 cm and thickness of 1 cm. The purpose of this was to limit the field selection to one dimension. Results in one dimension will be equally valid in two dimensions. Beamlet sizes of 4×2 cm^2, 2.66×2 cm^2, and 2×2 cm^2 were planned in an abutting pattern

Table 6–1: Virtual slab beamlet size

Beamlet size (cm^2)	Total # of Beamlets	# Used	Final Cost function
4×2	10	3	1
2.66×2	15	7	0.91
2×2	20	10	0.54

technique to determine which beamlet size resulted in the best target coverage. The size and number of beamlets are summarized in table 6–1.

The 2×2 cm^2 beamlet size was selected for the remainder of this study as it provided the best target coverage. In addition to determining the optimal beamlet size, the virtual slab was also used to determine a sufficient offset value between adjacent fields for feathered field coverage. The offset can be considered as the transverse displacement of one field to the next.

Beamlets of field size 2×2 cm^2 were planned using a feathered pattern technique with feather offset values of 20, 10, 5, 2.5, and 1 mm. Electron beam energies of 6, 9, 12, 16, and 20 MeV were used for all subfields. Table 6–2 summarizes the total number of subfields for each offset value used. The optimization software calculated subfield weights for each plan. The target constraints were set at target maximum dose of 50 cGy and target minimum dose of 50 cGy. There were no organs at risk considered for this part of the study. Target homogeneity was evaluated using the resulting DVH, final optimization cost function value, and dose profiles.

Virtual Case:

A virtual case was designed on a 3D homogeneous water phantom to evaluate our planning technique. The target geometry was scaled to fit within an 8×8 cm^2

Table 6–2: Virtual slab beamlet offset

Offset value (mm)	Total # of Beamlets	# Used	Final Cost function
20	21	10	1
10	36	14	0.84
5	66	17	0.77
2.5	126	19	0.74
1	306	20	0.71

Table 6–3: Virtual plan constraints

Volume	Dose (Gy)	Volume (%)	Penalty value
Target	50 max	100	1
Target	50 min	100	2
Organ 1	40	2	0.3
Organ 1	30	10	0.3
Organ 2	40	2	0.3
Organ 2	30	10	0.3

field. Critical structures were drawn surrounding the target volume. The depth of the target varied laterally to ensure the need of multiple energies. An open beam was placed at a gantry angle of zero degrees, as determined within the MERT planning process, step 3. Subfields of 2×2 cm^2 with a feathered offset of 0.5 cm were generated and their dose components calculated. The total number of subfields for this plan was 845. The resolution of the dose distributions and the optimization was $5 \times 5 \times 5$ mm^3. The optimization constraints, summarized in table 6–3, along with the dose distributions were input into the optimization algorithm for plan optimization.

6.2.3 Clinical Application of MERT Planning

In the second part of the study, a patient undergoing craniospinal irradiation (CSI) on TomoTherapy was imported into MMCTP for direct comparison with a

MERT generated plan. For the purpose of this study, the cranial irradiation was omitted within the MERT plan, the PTV structure was truncated to omit the cranial geometry. The diameter of the PTV is roughly 2 cm, and the depth varies from 1 to 2 cm from the patient's skin. The patient's position on the treatment couch was kept constant between the two plans as there was only the DICOM image set from TomoTherapy for treatment planning. Ideally, the patient's position would have been tailored for MERT deliveries. The MERT plan was constructed from four external beam positions to cover the entire length of the PTV. For each beam position, the x and y isocentre values were held constant and the z value (slice) varied, a delivery that could be realized by performing a longitudinal translation of the couch. In this case, the y value of the isocentre determined the SSD distance. The difference in SSD from the inferior to superior was +6 cm. Each beam position used a feathered field technique to generate subfield openings of 2×2 cm^2 for 6, 9, 12, 16, and 20 MeV beams. The resolution of the DOSXYZnrc dose distribution was $3 \times 3 \times 3$ mm^3. DOSXYZnrc simulations were run to an average percent error of 1% on dose values greater than 0.5 of the maximum dose. In general, the simulation time on a dual quad core Intel machine was 15 minutes per dose distribution. With the use of multiple machines, the time required for all dose calculations was 4 days. In comparison to clinical planning systems, this may seem extreme. However, no attempts were made to reduce the calculation time, as this falls outside the scope of the article. Nonetheless there are different avenues that could be followed to reduce the calculation time including the use of beam models. The MERT optimization used similar target and OAR

constraints, shown in tables 6–4, 6–5, as were used in TomoTherapy. The clinical prescription was 96% of the PTV volume receives at least 5.4 Gy. After importing the TomoTherapy dose distribution and recalculating the truncated PTV DVH, it was observed that the 96% volume receives only 5.2 Gy. We decided to match the MERT PTV DVH at 96%, 5.2 Gy to establish an equivalent clinical target coverage.

6.3 Results

6.3.1 Virtual Slab

A virtual target geometry was used to quantify the effect of beamlet size, and feathered subfields. The geometry was a rectangular slab of thickness 1 cm. The slab was located 1 cm below the external contour with a width of 5 cm.

Beamlet size:

Abutting beamlets of sizes 4×2, 2.66×2, and 2×2 cm^2 were positioned on the virtual slab to examine the effect of beamlet size on target homogeneity after dose weight optimization. Table 6–1 summarizes the number of initial beamlets, the number of beamlets chosen after optimization, and the relative cost function value normalized to the 4×2 cm^2 value. As the beamlet size decreases from 4 to 2 cm, the number of beamlets used increases and the final cost function decreases. There is a significant reduction in cost function value between the 2.66×2 and the 2×2 cm^2 beamlets, resulting in a more homogeneous target coverage as shown in figure 6–2. The 2×2 cm^2 size beamlets were deemed to be the most useful and were selected for the remainder of this study.

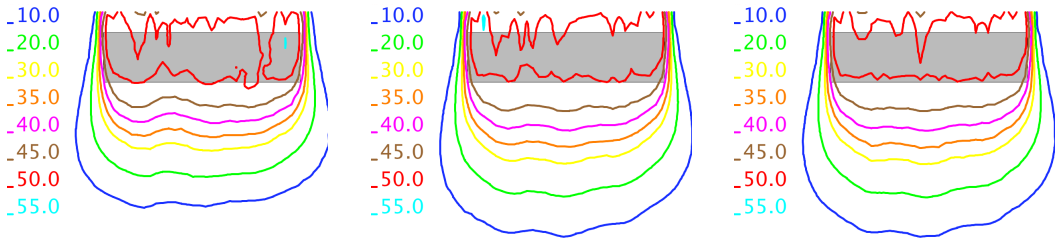

(a) (b) (c)

Figure 6–3: Slab geometry isodose lines plotted in Gy values for 2×2 cm^2 beamlet with various feathered offset distances. Target coverage improved with decreasing offset value. (a) 10 mm (b) 5 mm (c) 1 mm

Feathering offset value:

The feathering offset value can be considered as the transverse displacement from one field to the next. An offset value less than the width of the beamlet size will result in feathered fields with an overlapping component. Table 6–2 summarizes the number of initial beamlets, the number of beamlets chosen after optimization, and the relative cost function value normalized to the 20 mm offset value. The 20 mm offset value is equivalent to positioning abutting beamlets, as 20 mm is equal to the width of the beamlet. As the offset value decreases, the optimizer uses more beamlets to conform to the target constraints, and the cost function value decreases. There is a significant cost function decrease between abutting (20 mm) and feathered (10 or 5 mm) beamlets. As the offset value decreases from 5 mm to 1 mm, the difference is less significant. The isodose plots for 10, 5, and 1 mm feathered beamlets are shown in figure 6–3. The feathered beamlets are able to conform closer to the target constraints than the abutting beamlets. A feathering offset of 5 mm seems to be adequate for improved target

conformity when using 2 × 2 cm^2 beamlets. To compare between abutting and feathering fields, a midline profile through the optimized plan of each field placement technique is shown in figure 6–4. Figure 6–4 clearly demonstrates the benefit to target homogeneity that the feathering technique can provide.

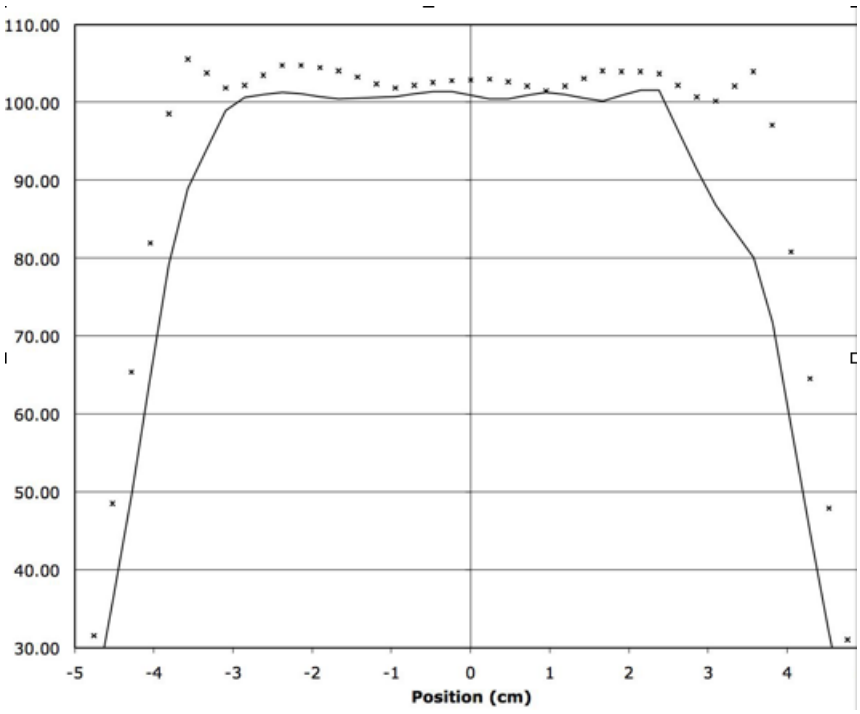

Figure 6–4: Profile through target volume of virtual slab geometry at midline depth for 2×2 cm^2 abutting junctions (points) and 2×2 cm^2 feathered with 5 mm offset junctions (line)

6.3.2 Virtual Case

A virtual MERT case was used to test our planning technique with feathered beamlets. The target and OAR geometries are shown in figure 6–5(a). A total of 846 beamlets were generated using 2×2 cm^2 beamlets with a 5 mm offset and five electron energies. The DAO algorithm selected 135 beamlets out of the

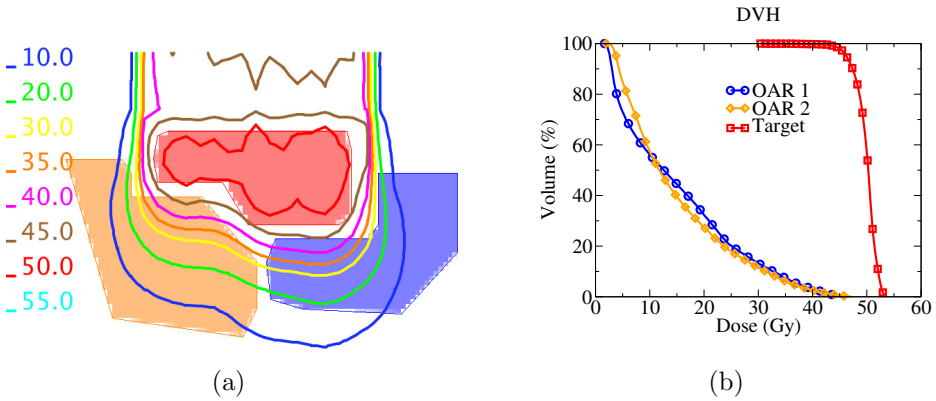

(a) (b)

Figure 6–5: Virtual case geometry and MERT optimization results. Target shown in red, two organs at risk shown in orange and blue (a) Axial isodose lines plotted in Gy values for optimized case through the isocentre slice (b) DVH graphs for target and two organs at risk.

possible 846. The isodose plot and DVH graphs of the optimized MERT plan are shown in figure 6–5. In general, the conformity of the target coverage is excellent. However, it appears as though the edges of the target volume are underdosed. This is explained by the isodose plotting algorithm and the 5 mm dose resolution, which is lower than the 1.68 mm image or structure resolution. The algorithm uses surrounding dose grid points to linearly interpolate the location of each isoline. A low resolution dose grid is subject to larger dose gradients between adjacent points and a larger estimate of the actual isodose line. A higher resolution dose grid would improve the isodose line uncertainty, and increase the MC dose calculation time. DVH graphs of both the target and OAR closely resemble the initial dose volume constraints. The minimum target dose is 40 Gy and the maximum is 54 Gy while the average is 50 Gy. The presence of hot and cold spots within the target volume point to limitations of using fields with finite feathering offsets. A

Table 6–4: Clinical TomoTherapy plan target constraints

Name	Importance	Max Dose (Gy)	Max Dose Pen.	DVH Vol (%)	DVH Dose (Gy)	Min Dose (Gy)	Min Dose Pen.
PTV	100	5.4	100	96	5.4	5.4	100

Table 6–5: Clinical TomoTherapy plan OAR constraints

Name	Importance	Max Dose (Gy)	Max Dose Pen.	DVH Vol (%)	DVH Dose (Gy)
Kidney LT	80	3	1	5	2
Kidney RT	80	3	1	5	2
Lung LT	80	5	1	10	2
Lung RT	80	5	1	10	2
Heart	70	2.5	10	5	2
Rectum	60	3	10	20	2
Intestine	1	1	1	1	1
Bladder	1	1	1	1	1
Liver	1	1	1	1	1

comparison between these results and a similar FLEC-based MERT plan published in 2005 demonstrate an overall improvement in target dose homogeneity, and OAR sparing [3].

6.3.3 Clinical MERT Plan

The MERT plan was not able to conform to the PTV dose constraints as closely as the TomoTherapy plan. It should be noted that the TomoTherapy plan was used as-is, without Monte Carlo recalculation or independent accuracy verification. The broader MERT PTV DVH, which was matched at 96%, has a lower minimum and higher maximum dose. Figure 6–6 compares the isodose lines between the two plans. DVH graphs between the TomoTherapy and MERT plan are shown in figure 6–7. Despite the disagreement between the PTV DVHs, the

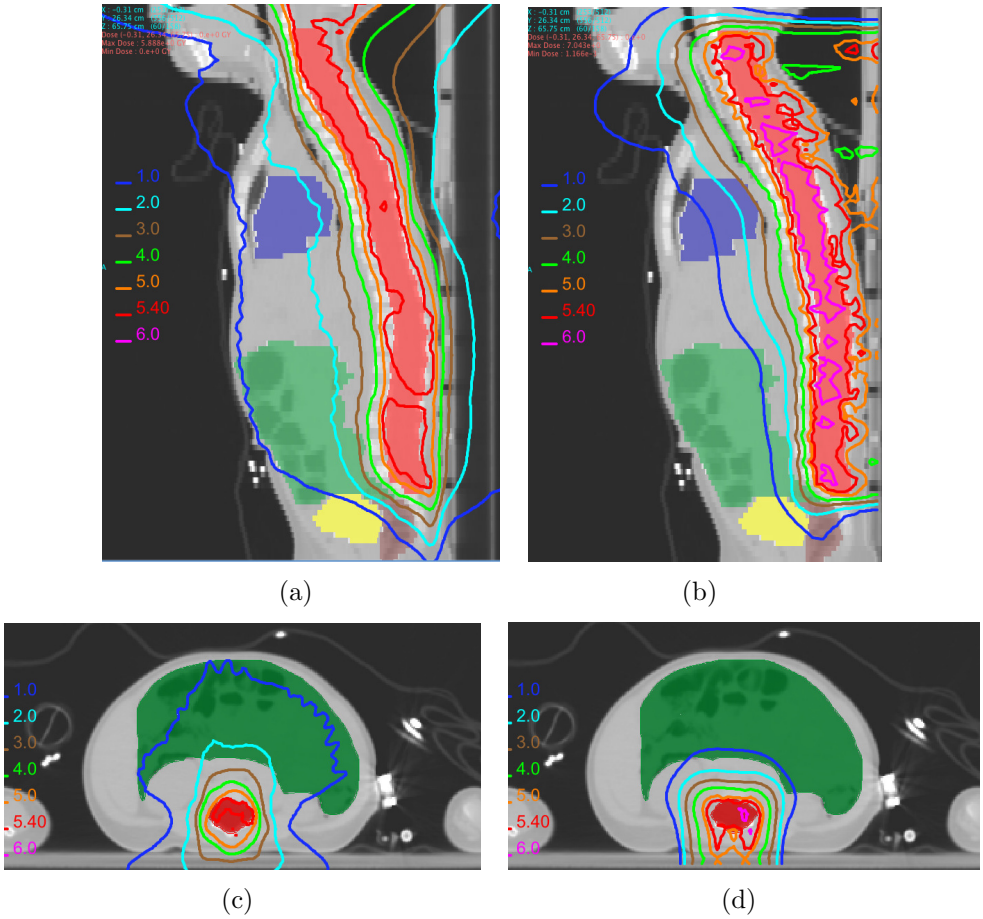

Figure 6–6: Sagittal and axial isodose lines of a TomoTherapy plan (a, c) MERT plan (b, d). PTV is outlined in red. The red isodose line corresponds to 5.4 Gy, which was the prescribed target dose. The MERT plan irradiated less tissue than the TomoTherapy plan. The 1 Gy isodose line is shown in blue.

MERT plan was able to reduce the dose to surrounding tissue. The reduction is most pronounced for organs located beyond the practical electron range such as the intestines, liver, and low dose component of the lungs. Tables 6–6 and 6–7 summarize the results of each plan. In general, the average MERT organ at risk

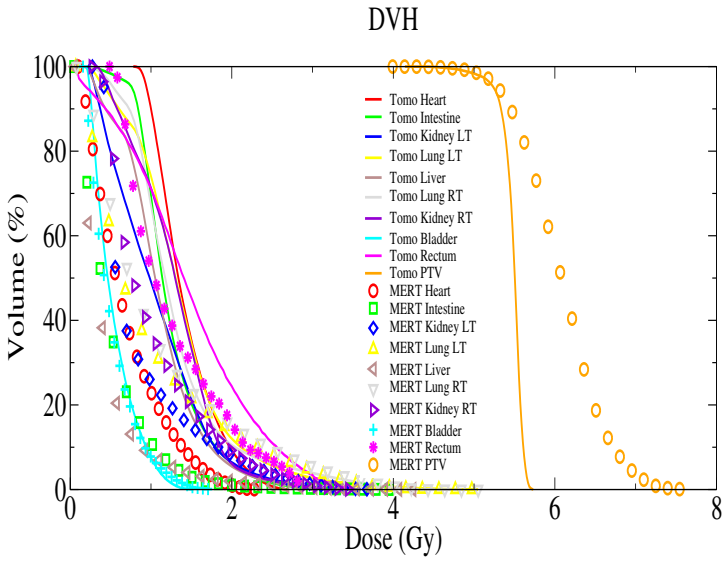

Figure 6–7: DVH comparison between TomoTherapy and MERT. PTV coverage is matched at 96%

Table 6–6: Clinical target results

Name	Max Dose (Gy)	Min Dose (Gy)	Avg Dose (Gy)	96% Dose (Gy)
TomoTherapy PTV	5.7	4.4	5.5	5.2
MERT PTV	7.6	4.0	6.0	5.2

dose is lower compared to TomoTherapy. However, the majority of the OAR constraints failed for both MERT or TomoTherapy.

The complexity of this case can be summarized by the number of voxels for all organs and the number of dose distributions. Large organs such as the spine, lungs, and intestines had a significant impact on the calculation time for each optimization iteration. The complexity of the case, along with the iterative nature of assigning cost function weights to the OAR and the desire to match the PTV

Table 6–7: Clinical plan OAR results

Name	Avg Dose Tomo (Gy)	Avg Dose MERT (Gy)	DVH Vol (%)	DVH Dose Tomo (Gy)	DVH Dose MERT (Gy)
Kidney LT	1	0.87	5	2.1	2.3
Kidney RT	1.2	1.0	5	2.0	2.3
Lung LT	1.3	0.97	10	2.1	2.3
Lung RT	1.3	1.1	10	2.0	2.4
Heart	1.4	0.7	5	2.1	1.6
Rectum	1.4	1.2	20	2.4	1.5
Intestine	1.2	0.5	1	2.6	2.0
Bladder	0.53	0.50	1	1.3	1.4
Liver	1.1	0.43	1	2.6	2.5

DVH at 96%, which requires several optimization runs, resulted in a lengthy optimization process of a few days.

6.4 Conclusion

This study has made an attempt at addressing the difficulties in plan optimization for FLEC-based MERT. A phase-space database has been created to eliminate the time consuming process of MC electron beam calculations and to address the arbitrariness in assigning beamlets for MERT optimization. In addition, a feathered field pattern technique was evaluated to minimize dose inhomogeneities from abutting electron fields. It has been demonstrated using virtual target geometries, that the feathered field technique can improve dose homogeneity throughout the target volume. A clinical CSI case was planned using our MERT planning technique and compared against a TomoTherapy plan. The TomoTherapy PTV DVH appeared narrow in comparison to the MERT DVH, however the former was calculated using a convolution/superposition (C/S) algorithm while the latter was

calculated using the Monte Carlo models BEAMnrc/DOSXYZnrc. Despite the differences in the calculation model, the results and conclusions are still valid as this study is a validation of our planning technique and not a dosimetric study. At the cost of the PTV coverage, the MERT plan reduced the dose to the organs at risk. This was evident within the DVH graphs, isodose plots, and dose metrics within table 6–7. Notable drawbacks to the technique would be the dose calculation time and the optimization time. The combined time should be on the order of a few hours for the system to be clinically viable. Additional studies will investigate the use of fast MC models, and adaptive optimization algorithms where apertures can be modulated within the optimization algorithm. Arc treatments would be an additional area of interest, albeit with a modified FLEC design. In conclusion, the FLEC-based MERT planning techniques developed within the study produced promising MERT plans with minimal user input. With further investigations, FLEC-based MERT will find an important niche in clinical radiation therapy.

6.5 References

[1] X Mu, T Björk-Eriksson, S Nill, U Oelfke, K Johansson, G Gagliardi, L Johansson, M Karlsson, and B Zackrisson. Does electron and proton therapy reduce the risk of radiation induced cancer after spinal irradiation for childhood medulloblastoma? a comparative treatment planning study. *Acta Oncol*, 44(6):554–562, 2005.

[2] K R Hogstrom and P R Almond. Review of electron beam therapy physics. *Phys. Med. Biol.*, 51(13):R455–489, 2006.

[3] K Al-Yahya, M Schwartz, G Shenouda, F Verhaegen, and Jan Seuntjens.

Energy modulated electron therapy using a few leaf electron collimator in combination with IMRT and 3D-CRT: Monte Carlo-based planning and dosimetric evaluation. *Med. Phys.*, 32(9):2976–2986, 2005.

[4] S Hyödynmaa, A Gustafsson, and A Brahme. Optimization of conformal electron beam therapy using energy- and fluence-modulated beams. *Med. Phys.*, 23(5):659–666, 1996.

[5] E Klein. Modulated electron beams using multi-segmented multileaf collimation. *Radiother. Oncol.*, 48(3):307–311, 1998.

[6] E E Klein, M Mamalui-Hunter, and D A Low. Delivery of modulated electron beams with conventional photon multi-leaf collimators. *Phys. Med. Biol.*, 54(2):327–339, 2009.

[7] F C P du Plessis, A Leal, S Stathakis, W Xiong, and C M Ma. Characterization of megavoltage electron beams delivered through a photon multi-leaf collimator (pMLC). *Phys. Med. Biol.*, 51(8):2113–2129, 2006.

[8] L Jin, C M Ma, J Fan, A Eldib, R A Price, L Chen, L Wang, Z Chi, Q Xu, M Sherif, and J S Li. Dosimetric verification of modulated electron radiotherapy delivered using a photon multileaf collimator for intact breasts. *Phys. Med. Biol.*, 53(21):6009–6025, 2008.

[9] F J Salguero, B Palma, R Arrans, J Rosello, and A Leal. Modulated electron radiotherapy treatment planning using a photon multileaf collimator for post-mastectomized chest walls. *Radiother. Oncol.*, 93(3):625–632, 2009.

[10] M C Lee, S B Jiang, and C M Ma. Monte carlo and experimental investigations of multileaf collimated electron beams for modulated electron radiation

therapy. *Med. Phys.*, 27(12):2708–2718, 2000.

[11] M Blomquist, M G Karlsson, B Zackrisson, and M Karlsson. Multileaf collimation of electrons–clinical effects on electron energy modulation and mixed beam therapy depending on treatment head design. *Phys. Med. Biol.*, 47(7):1013–1024, 2002.

[12] B Paul Ravindran, I Rabi Raja Singh, S Brindha, and S Sathyan. Manual multi-leaf collimator for electron beam shaping–a feasibility study. *Phys. Med. Biol.*, 47(24):4389–4396, 2002.

[13] K R Hogstrom, R A Boyd, J A Antolak, M M Svatos, B A Faddegon, and J G Rosenman. Dosimetry of a prototype retractable eMLC for fixed-beam electron therapy. *Med. Phys.*, 31(3):443–462, 2004.

[14] T Gauer, J Sokoll, F Cremers, R Harmansa, M Luzzara, and R Schmidt. Characterization of an add-on multileaf collimator for electron beam therapy. *Phys. Med. Biol.*, 53(4):1071–1085, 2008.

[15] T Vatanen, E Traneus, and T Lahtinen. Enhancement of electron-beam surface dose with an electron multi-leaf collimator (eMLC): a feasibility study. *Phys. Med. Biol.*, 54(8):2407–2419, 2009.

[16] K Al-Yahya, D Hristov, F Verhaegen, and J Seuntjens. Monte Carlo based modulated electron beam treatment planning using a few-leaf electron collimator—feasibility study. *Phys. Med. Biol.*, 50(5):847–857, 2005.

[17] K Engel and T Gauer. A dose optimization method for electron radiotherapy using randomized aperture beams. *Phys. Med. Biol.*, 54(17):5253–5270, 2009.

[18] D M Shepard, M A Earl, X A Li, S Naqvi, and C Yu. Direct aperture

optimization: a turnkey solution for step-and-shoot IMRT. *Med. Phys.*, 29(6):1007–1018, 2002.

[19] K Al-Yahya, F Verhaegen, and J Seuntjens. Design and dosimetry of a few leaf electron collimator for energy modulated electron therapy. *Med. Phys.*, 34(12):4782–4791, 2007.

[20] D W O Rogers, B A Faddegon, G X Ding, C M Ma, J We, and T R Mackie. BEAM: A Monte Carlo code to simulate radiotherapy treatment units. *Med. Phys.*, 22(5):503–524, 1995.

[21] B Walters, I Kawrakow, and D W O Rogers. *DOSXYZnrc Users Manual*. Ionizing Radiation Standards, National Research Council of Canada, 2007.

[22] A Alexander, F Deblois, G Stroian, K Al-Yahya, E Heath, and J Seuntjens. MMCTP: a radiotherapy research environment for Monte Carlo and patient-specific treatment planning. *Phys. Med. Biol.*, 52(13):N297–308, 2007.

[23] D Hristov, P Stavrev, E Sham, and B G Fallone. On the implementation of dose-volume objectives in gradient algorithms for inverse treatment planning. *Med. Phys.*, 29(5):848–856, 2002.

[24] S M Sait and H Youssef. *Iterative Computer Algorithms with Applications in Engineering: Solving Combinatorial Optimization Problems*. IEEE Computer Society Press, 1999.

CHAPTER 7
Paper IV: Comparison of modulated electron radiotherapy to conventional electron boost irradiation and volumetric modulated photon arc therapy for treatment of tumour bed boost in breast cancer

Andrew Alexander, Emilie Soisson, Tarek Hijal, Arman Sarfehnia, and Jan Seuntjens

Radiother. Oncol., 100(2):253-258, 2011

Contents

The following manuscript describes a dosimetric plan comparison between few leaf electron collimator (FLEC)-based modulated electron radiotherapy

(MERT) to conventional direct electron (DE) and volumetric modulated photon arc therapy (VMAT) for the treatment of tumour bed boost in breast cancer. Subsequent to the development of the MERT planning system within MMCTP, we proceeded with a clinical significance study on the role of MERT within tumour bed boosts in breast cancer. The philosophy behind this study was to evaluate the reproducibility and quality of MERT plans in tumour bed boost over a patient data-set. The MERT plans were benchmarked to DE and photon VMAT plans. This is the first study to examine MERT plan reproducibility within one treatment site and compare MERT plans with Varian's RapidArc technique.

Abstract

Background and purpose: To compare few leaf electron collimator (FLEC)-based modulated electron radiotherapy (MERT) to conventional direct electron (DE) and volumetric modulated photon arc therapy (VMAT) for the treatment of tumour bed boost in breast cancer.

Materials and Methods: Fourteen patients with breast cancer treated by lumpectomy and requiring post-operative whole breast radiotherapy with tumour bed boost were planned retrospectively using conventional DE, VMAT, and FLEC-based MERT. The planning goal was to deliver 10 Gy to at least 95% of the tumour bed volume. Dosimetry parameters for all techniques were compared.

Results: Dose evaluation volume (DEV) coverage and homogeneity were best for MERT ($D_{98\%}$=9.77 Gy, $D_{2\%}$=11.03 Gy) followed by VMAT ($D_{98\%}$=9.56 Gy, $D_{2\%}$=11.07 Gy) and DE ($D_{98\%}$=9.81 Gy, $D_{2\%}$=11.52 Gy). Relative to the DE plans, the MERT plans predicted a reduction of 35% in mean breast dose ($p <$

0.05), 54% in mean lung dose ($p < 0.05$), and 46% in mean body dose ($p < 0.05$). Relative to the VMAT plans, the MERT plans predicted a reduction of 24%, 36%, and 39% in mean breast dose, heart dose, and body dose respectively ($p < 0.05$).

Conclusions: MERT plans were a considerable improvement in dosimetry over DE boost plans. There was a dosimetric advantage in using MERT over VMAT for increased DEV conformity and low-dose sparing of healthy tissue including the integral dose; however, the cost is often an increase in the ipsilateral lung high-dose volume.

7.1 Introduction

The current standard of care for most patients diagnosed with early-stage breast cancer consists of breast conserving surgery, followed by whole breast radiotherapy (RT) and a boost to the tumour bed [1, 2, 3, 4]. Boost planning and delivery is traditionally sequential to whole breast RT with the use of electrons, photons, or a combination of both [1, 4, 5].

MERT is an electron radiation delivery modality, similar to intensity modulated radiotherapy (IMRT) for photon beams, that utilizes inverse planning techniques to generate a sequence of electron fields. MERT fields are comprised of mono or multi-energy electron beams which improve the target coverage conformity while minimizing the dose to surrounding OARs. The main advantage of MERT comes from the defined electron range. With conventional accelerators and for a subset of clinical treatment sites, MERT has the potential to deliver a conformal target dose to the tumour with less dose to normal tissue compared with conformal photon radiotherapy [6, 7, 8, 9, 10, 11, 12, 13]. Previous MERT

studies have focused on the development of electron collimators or plan comparison. Overall, MERT planning studies suffer from a small sample size without statistical significance testing, questionable target dose normalization points or through "dated" alternative planning techniques. A modern planning study which compared helical photon IMRT to MLC-based MERT for three treatment sites, concluded that MERT is superior to photon IMRT [13]. However, with only one plan per site, the comparison is limited to the quality of a single plan and may not reflect a global trend. Plan comparisons also depend critically on the type of collimation device used for the MERT solution proposed. As such, the aforementioned MLC-based studies cannot be generalized to another type of MERT solution.

Historically, electron beam radiation has been the most commonly used modality to deliver the tumour bed boost. The delivery method is a direct electron (DE) field, collimated through a custom cutout; however, the role of electron beam radiation for tumour bed boost will likely be diminished as alternative optimized photon beams have been shown to improve the overall plan quality for deep-seated tumours ($\geq$ 4 cm) [14].

The volumetric modulated arc therapy (VMAT) technique is an extension of conventional IMRT, in which an optimized treatment plan is delivered in one or more gantry arcs of 360° or less. Advantages to this technique are a substantial reduction in delivery time and reduction in doses to organs at risk (OAR) by spreading out the dose over a large number of segments [15, 16].

In the present study we compare the dosimetry of the three aforementioned modalities in the delivery of tumour bed boost: few leaf electron collimator

(FLEC)[8]-based MERT, conventional DE irradiation, and VMAT. The automated FLEC delivery system has been previously dosimetrically characterized [17]. This is the first study to examine FLEC-based MERT plan quality and reproducibility with fourteen patients and provide statistical significance testing.

7.2 Materials and Methods

7.2.1 Patient Selection and Evaluation

Fourteen consecutive patients treated at the McGill University Health Centre and requiring whole breast radiation and tumour bed boost after breast conserving surgery for early-stage breast cancer were selected for this comparative planning study. The patients were treated according to our standard institution protocol, but their imaging was retrospectively used for the study.

7.2.2 Image Acquisition

A treatment planning computed tomography (CT) scan was performed after the surgery, and before initiating radiotherapy. Patients were placed in the supine position, on a breast board, with both arms abducted alongside the head. The palpable breast tissue contour and the surgical scar were delineated with radio-opaque wires. Images were acquired from the mid-neck to the mid abdomen, using a 5 mm slice thickness and separation. The CT data was transferred to a commercial treatment planning system (TPS) (Eclipse, Varian Medical Systems Inc., Palo Alto, USA).

7.2.3 Definition of Target Volumes and Organs at Risk

The whole breast volume was defined as the tissue delineated by the aforementioned radio-opaque wire. In practice, on each transverse slice, the breast

volume extended from the pectoralis major muscle to the skin, excluding the pectoralis muscle, ribs or the first 5 mm of skin. The tumour bed volume was defined using the planning CT as well as the preoperative and operative reports. In practice, it included the surgical clips, as well as any hematoma, seroma, or other surgery-induced changes considered to be a part of the lumpectomy cavity. Tumour bed dose evaluation volume (DEV) was defined as the tumour bed with a 1.5 cm margin, but excluding the pectoralis muscle, ribs or the first 5 mm of skin. The 1.5 cm margin takes into account any microscopic disease, as well as setup and motion margins. Removal of the first 5 mm removes the buildup region of the beam, which are inherent to high-dose gradients, from the DEV volume.

The breast-minus-DEV contour represents normal tissue within the breast volume. The heart was contoured from the level of the pulmonary trunk to the apex, and included the pericardium but not the major vessels. Both lungs and the contralateral breast were also delineated.

7.2.4 Treatment Goals

The goal of the treatment was to deliver a dose of 10 Gy in 4 fractions to the tumour bed DEV, with the aim of covering at least 95% of the target volume with 100% of the prescription dose. Furthermore, an effort was made to reduce the treatment volume receiving more than 107% of the dose to a minimum. Similarly, an effort was made to keep the dose received by the normal breast, defined as the breast volume minus the DEV, to a minimum.

7.2.5 MERT Planning

MERT plans were created within the MMCTP TPS [18] using XVMC [19] as the dose calculation engine and an in-house developed inverse optimization system as described by Alexander et al. [20]. MMCTP has been modified to include MERT tools that are specific to FLEC-based MERT for choosing ideal gantry angles and isocentre positions. MERT plans were limited to one modulated incident beam angle. Delivery of a plan requires the motorized FLEC [17]. The MERT field was divided into beamlets of field size 0.5×0.5 cm^2 using an abutting field pattern technique.

With five electron energies; 6, 9, 12, 16, and 20 MeV, the total number of beamlets was 1280. For each beamlet, the XVMC simulation was run to an average statistical uncertainty of less than 0.5% on dose values greater than 50% of the maximum dose. The dose distributions were used as input for direct aperture optimization (DAO) [21] to derive beamlet weights. The objective variables for the target included a maximum and minimum dose limit, and a corresponding dose penalty value. The OAR variables included a dose-volume constraint and a penalty value. Planning constraints for the target and OAR were adjusted as needed to generate optimal plans.

7.2.6 DE Planning

Direct electron (DE) plans were created using forward planning techniques within the Eclipse TPS. The electron Monte Carlo (eMC) algorithm of the TPS was used to calculate the dose for each plan. The plans were manually optimized

by adjusting the electron cutout shape, electron beam energy, gantry angle, collimator angle, and couch angle.

7.2.7 VMAT Planning

VMAT plans were created within the Eclipse RapidArc (Varian Medical Systems Inc., Palo Alto, CA) TPS using two 6 MV photon arcs. A planning ring structure, comprised of a 1 cm margin around the tumour bed DEV was created. Dose constraints were then specified for the tumour bed DEV and the ring structure. The planning goals were set to achieve uniform target coverage while avoiding the heart and lung. The AAA algorithm of the TPS was used to calculate the dose for each VMAT plan. AAA was the only non-MC dose calculation method used in this study, and there could be some bias in the direction of favourable VMAT results due to analytical approximations particularly in regions of heterogeneity [22] and the surface buildup dose [23].

7.2.8 Plan Evaluation

All plans were evaluated using MMCTP planning tools to ensure a common platform for DVH calculations and isodose line plots. DE and VMAT plans were imported into MMCTP through the use of DICOM files. The DEV target was evaluated at the 'near minimum dose' [24] received by 98% of the volume ($D_{98\%}$), the dose received by 90% of the volume ($D_{90\%}$), 'near maximum dose' [24] received by 2% of the volume ($D_{2\%}$) and mean dose (D_{mean}). Critical structures were evaluated at the maximum dose (D_{max}), D_{mean}, and the volume receiving 5, 2, and 1 Gy (V_{5Gy}, V_{2Gy}, V_{1Gy}). The integral dose was evaluated for the body volume, and calculated as the mean dose times the volume. Lastly, the average DVHs were

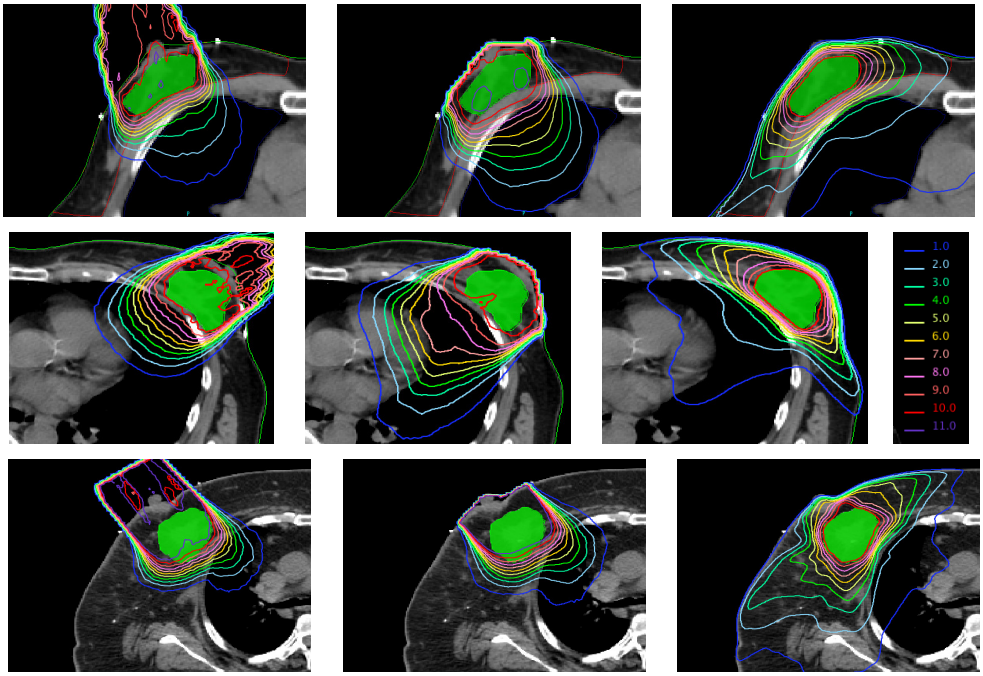

Figure 7–1: Isodose plots for shallow (row 1), mid-range (row 2), and deep (row 3) seated tumours, using MERT (column 1), DE (column 2), VMAT (column 3). The isodose value legend is shown in row 2 column 4

calculated to illustrate the trend of each technique. Data was analyzed for the effects of dosimetric differences using one-way ANOVA (SAS Inst., Inc, Cary, NC. 9.2, 2008). Post-hoc testing was assessed using the Bonferroni multiple comparison test. Differences were considered significant if $p < 0.05$.

7.3 Results

Table 7–1 reports the dose based numerical results, such as $D_{98\%}$ and D_{mean} for the target and organs at risk. Table 7–2 reports the volume based numerical results for the organs at risk. All plans were normalized such that $D_{95\%}$ received 10 Gy. Fig. 7–2 shows the average DVH plots for the DEV, lung, breast-minus-DEV, and body. Dose distributions for a shallow, mid-range and deep seated

Table 7–1: Summary of results for 14 boost plans; showing dose-volume indices associated mean value with standard deviation, ΔD^{DE}, ΔD^{VMAT} and p-value

Volume	Index	MERT Gy	DE Gy	ΔD^{DE} %	VMAT Gy	ΔD^{VMAT} %
DEV	$D_{98\%}$	9.77	9.81	-0.3	9.56	+2.3
		± 0.14	± 0.13	$p > 0.05$	± 0.12	$p = 0.001$
	$D_{90\%}$	10.17	10.23	-0.6	10.3	-1.3
		± 0.11	± 0.17	$p > 0.05$	± 0.07	$p = 0.007$
	$D_{2\%}$	11.03	11.52	-3.9	11.07	-0.3
		± 0.46	± 1.01	$p > 0.05$	± 0.21	$p > 0.05$
	D_{mean}	10.55	10.81	-2.3	10.7	-1.5
		± 0.28	± 0.6	$p > 0.05$	± 0.14	$p > 0.05$
Lung	D_{mean}	0.44	1.29	-54	0.37	+21
		± 0.23	± 0.75	$p < 0.0001$	± 0.14	$p > 0.05$
Breast-DEV	D_{mean}	1.39	2.1	-35.1	1.78	-23.8
		± 0.60	± 0.65	$p = 0.009$	± 0.51	$p > 0.05$
Heart	D_{mean}	0.34	0.33	+15.0	0.73	-36.4
		± 0.04	± 0.11	$p > 0.05$	± 0.56	$p > 0.05$
Body	D_{mean}	0.15	0.31	-45.7	0.25	-38.8
		± 0.05	± 0.15	$p = 0.0004$	± 0.07	$p = 0.03$

$\Delta D_x^{DE,VMAT}(\%) = \frac{D_x^{MERT} - D_x^{DE,VMAT}}{D_x^{DE,VMAT}} \times 100$

tumour depth with average depths of 2.2, 3.5, and 6.5 cm, respectively, are shown in Fig. 7–1 and the DVHs in Fig. 7–3.

The best DEV conformity was obtained with MERT, while the worst was obtained with DE. The average $D_{98\%}$, which represents the near minimum of the DEV coverage and $D_{2\%}$, which represents the near maximum of the DEV coverage was closest to 10 Gy for MERT. The MERT plans improved the VMAT $D_{98\%}$, $D_{90\%}$, and D_{mean} values by +2.3% ($p < 0.05$), -1.3% ($p < 0.05$), and -1.5%. Ipsilateral lung sparing was best with VMAT followed by MERT and worst with DE. The VMAT plans provided greater high-dose volume sparing than MERT or DE. When comparing DE and MERT, MERT consistently provided reduced lung dose indices ($p < 0.05$). The breast-minus-DEV illustrates the trade-off between direct vs. arc therapy. VMAT spared high-dose volume over low-dose volume, while MERT and DE spared low-dose volume over high-dose volume. The breast-minus-DEV D_{mean} was best with MERT followed by VMAT and worst with DE. The three volume indices, V_{5Gy}, V_{2Gy}, and V_{1Gy} reported were on average -30% ($p < 0.05$) lower with MERT compared to DE; in addition, MERT predicted lower V_{5Gy}, V_{2Gy}, and V_{1Gy} by -12%, -44% ($p < 0.05$), and -46% ($p < 0.05$) compared to VMAT. With regards to the body dose, V_{1Gy} and $V_{0.5Gy}$ values were examined as they present the 10% and 5% isodose volumes. There was surprisingly little difference between DE and VMAT for these volumes. MERT reduced these low-dose volumes by -50% in comparison to DE or VMAT. Regarding D_{mean} and subsequent integral dose to healthy tissue, MERT plans were the lowest. Overall, MERT plans succeeded to combine the best DEV coverage, the lowest dose to

Table 7–2: Summary of results for 14 boost plans; showing dose-volume indices associated mean value with standard deviation, ΔV^{DE}, ΔV^{VMAT} and p-value

Volume	Index	MERT (%)	DE (%)	ΔV^{DE} (%)	VMAT (%)	ΔV^{VMAT} (%)
Lung	V_{5Gy}	1.23 ± 1.41	6.09 ± 5.39	-66 $p = 0.0008$	0.01 ± 0.04	-
	V_{2Gy}	6.11 ± 4.2	20.75 ± 13.38	-58 $p < 0.0001$	3.0 ± 3.25	+340 $p > 0.05$
	V_{1Gy}	12.3 ± 6.82	35.27 ± 20.61	-53 $p < 0.0001$	11.5 ± 5.93	+21 $p > 0.05$
Breast-DEV	V_{5Gy}	12 ± 4.9	17.8 ± 5.61	-33 $p = 0.03$	14.2 ± 5.23	-12 $p > 0.05$
	V_{2Gy}	16.32 ± 6.23	23.3 ± 6.86	-31 $p = 0.05$	28.6 ± 7.0	-44 $p = 0.0002$
	V_{1Gy}	19.33 ± 7.1	27.97 ± 8.1	-32 $p = 0.03$	35.6 ± 8.6	-46 $p < 0.0001$
Heart	V_{2Gy}	5.4 ± 0.54	4.5 ± 1.8	+33 $p > 0.05$	9.6 ± 6.5	-27 $p > 0.05$
	V_{1Gy}	10.2 ± 1.9	6.7 ± 2	+64 $p > 0.05$	30 ± 27	-47 $p > 0.05$
Body	V_{1Gy}	2.74 ± 0.97	5.51 ± 2.91	-43.9 $p = 0.001$	4.64 ± 1.36	-38.8 $p = 0.02$
	$V_{0.5Gy}$	3.85 ± 1.38	8.54 ± 4.61	-46.9 $p = 0.0009$	8.64 ± 2.56	-52.5 $p = 0.0002$

$\Delta V_x^{DE,VMAT}(\%) = \frac{V_x^{MERT} - V_x^{DE,VMAT}}{V_x^{DE,VMAT}} \times 100$

the breast-minus-DEV, and a 2× reduction in integral dose over DE and a 1.7× reduction over VMAT. In terms of OAR sparing between MERT and DE, the MERT plan substantially improved lung, breast, and body dose. In terms of OAR sparing between MERT and VMAT, MERT improved the body dose, lung low-dose volume, and breast-minus-DEV dose below 6 Gy.

7.4 Discussion

This dosimetric study compared three techniques for the delivery of tumour bed boost in breast cancer, DE, the standard of care in most institutions, FLEC-based MERT, and VMAT. Our results showed that DE plans were inferior to MERT or VMAT. The quality of DE plans was shown to fluctuate between patients and was likely affected by a set of patient-specific geometrical properties. Inter-patient geometric variations, such as beam obliquity, target shape, and depth, were less of a factor on plan quality for MERT and were even less influential on plan quality for VMAT. Due to the high electron energy required for target coverage, the DE plans overdosed all OAR. This result agrees with previous work by Toscas et al. [14] which suggests that VMAT techniques are preferred to DE in tumour bed boost.

In terms of DEV coverage, MERT is an improvement over VMAT. Lung sparing was realized in VMAT plans through the use of tangential beams and intensity modulation to avoid the lung volume. On an individual patient basis, MERT lung sparing could compete with VMAT plans specifically in the low-dose region of the DVH curve. As a result, these MERT plans are globally preferred over VMAT. The use of tangential electron beams for MERT was unsuitable as the increased electron path length to the target volume and entrance dose to the surrounding breast volume would deteriorate the overall plan quality. MERT plans did produce hot-spots within the breast volume due to the use of a single beam angle; however all of the examined dose-volume indices were lower with MERT

than VMAT. MERT in combination with a limited arc delivery, (volumetric-MERT) could potentially reduce the occurrence of hot-spots within the breast volume and spread-out the skin dose, at a cost of increased low-dose volume.

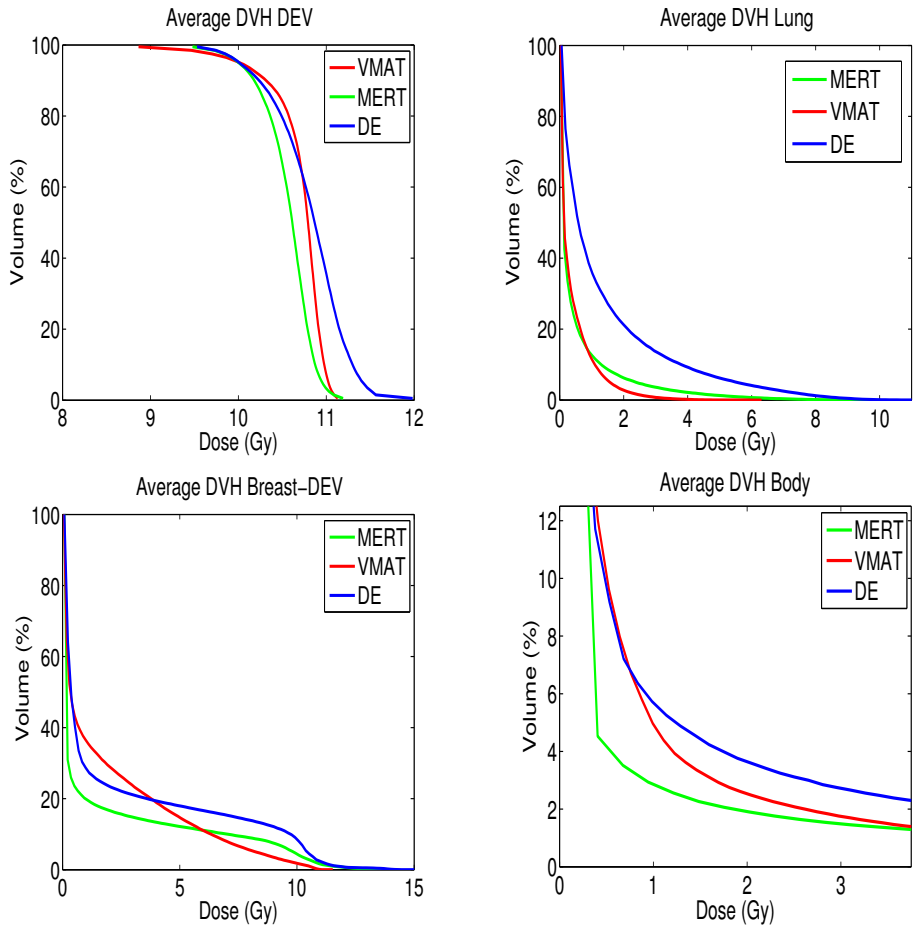

Figure 7–2: Average cumulative DVH for DEV, Lung, Breast-DEV, and Body

With regards to sparing of the low-dose body volume, the isodose plots of Fig. 7–1 present a clear trend of significant MERT low-dose volume reduction. The body dose or peripheral dose is often used to evaluate a potential risk factor for the development of secondary malignancies due to an increase in normal tissue

dose. Risk estimations are of great interest to the radiation oncology community, despite the fact that there remains considerable debate in the calculation of secondary malignancies risk [25]. Patient integral dose could be used within a risk calculation for increased risks of radiation-induced secondary malignancies [26]. A secondary risk calculation based on a linear radiobiological model and total body integral body dose, places MERT plans at a -46% reduction in radiation risk over conventional DE plans and a -39% reduction in radiation risk over VMAT plans. Toscas et al. [14] and Mu et al. [27] both agree that proton therapy reduces the greatest amount of total body dose in comparison with photon IMRT or VMAT. Thereafter, MERT provides the second best choice [27] followed by photon optimization, which is in agreement with our results. Due to the high cost of proton centers and the fact that MERT would be an add-on to most linear accelerators, MERT should be considered when total body integral body dose is a priority.

Three patient cases are discussed in detail to illustrate the inter-patient variability between plans through analysis of the target depth, isodose plots and DVHs. In the shallow tumour depth case, the MERT target coverage and integral dose advantage may be outweighed by superior VMAT lung sparing. In the mid-range tumour depth case, the MERT and VMAT lung doses were very similar. As such, MERT would be considered to be the best plan due to its advantages in target coverage and integral dose. However, the extreme DEV depth for the deep-seated case resulted in a gradient throughout the target volume for DE and MERT. MERT and DE applications clearly have their limitations in breast tumour

boost. Despite the majority of target depths in the mid-level range between 2.5 and 4.5 cm, not all plans in this range were as competitive as the mid-range case presented. This case exemplified the pairing of available electron energies with the distal edge of the target volume.

The success of MERT plans was found to be dependent on the available energy selection grid, target depth, patient geometry, and tumour size. Ideally, one would continuously vary the beam energy to allow for greater flexibility in depth control. In addition to target depth, a larger range of target voxel depths per beamlet position negatively affected target homogeneity. As such, thinner targets produced the most competitive MERT plans. MERT treatments, like any new treatment modality would require department policies on when MERT plans would be created and these plans would likely be compared against alternative modalities. Departments would likely set a cutoff depth for MERT planning and tumours beyond that depth would be planned using VMAT. The decision of which treatment modality is best will depend on the priorities of a specific case.

Based on the favourable comparisons shown in our work it is reasonable to suggest that there are clear advantages with MERT plans over VMAT plans. Due to inter-patient variability, these advantages are not always reproducible and readers should be cautious when interpreting small scale MERT planning studies. Another issue with previous planning studies is the dose normalization point. Plans were often normalized at the mean target dose which is potentially clinically unacceptable due to dose gradients within the target volume. Competitive comparisons should be matched at the prescription point of $D_{95\%}$ as matching

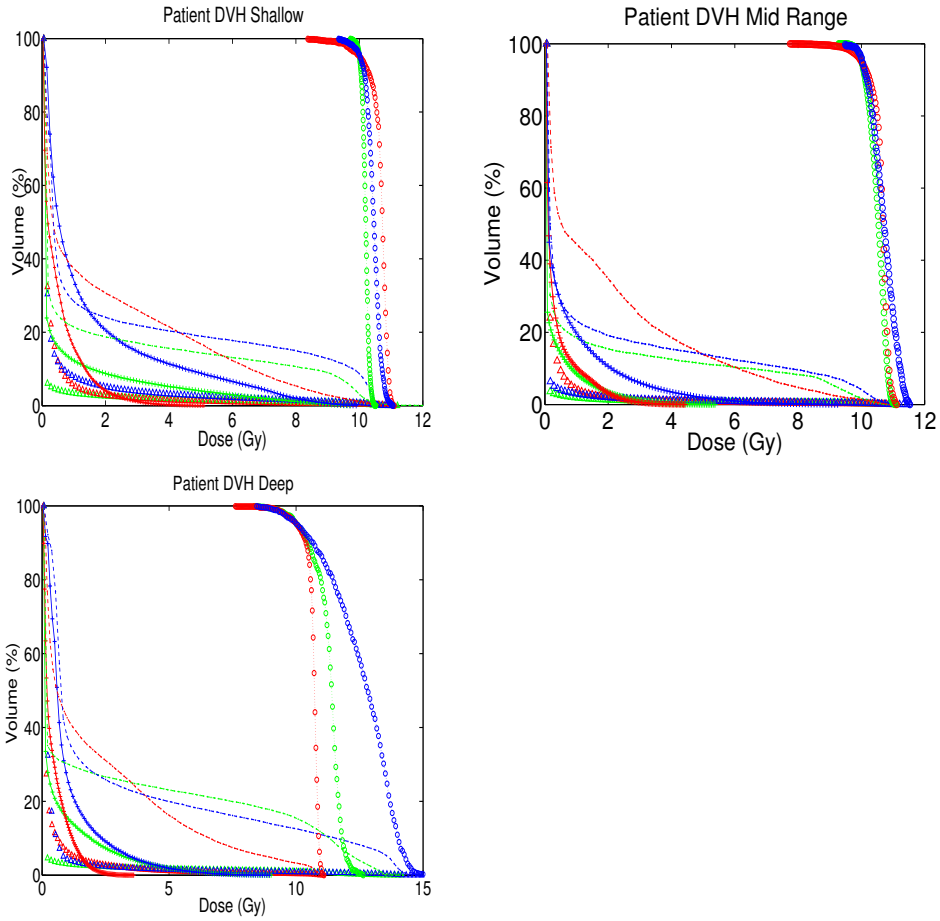

Figure 7–3: Patient DVHs for various target depths. MERT in green, DE in blue and VMAT in red. Symbols: DEV ◯, Lung +, Breast-minus-DEV - - and Body △.

the mean target coverage favours the MERT dose volumes within the organs at risk over the photon plans. It would be interesting to extend Gauer et al. [13] and other breast planning studies [28, 6, 9, 10, 29] with more patients to investigate the reproducibility of MERT in full course breast radiation therapy.

7.5 Conclusions

This is the first study to compare FLEC-based MERT, DE, and VMAT techniques in a large patient data-set. MERT is superior over conventional DE for the delivery of tumour bed boost in breast cancer. In an overall comparison of all three modalities, MERT produced the best plans in terms of target coverage, homogeneity, and integral dose. Lung sparing was superior in VMAT, while the MERT plans reduced the low-dose component of the breast-minus-DEV. Geometric properties of the target volume and body contour, in conjunction with the selection of available electron energies, were shown to influence the quality of the DE and MERT plans. In contrast, the VMAT plans were highly reproducible or independent of these geometric properties. For the delivery of tumour bed boost in breast cancer, MERT is a prospective alternative to DE, and may be preferred to VMAT for increased DEV conformity, low-dose sparing of healthy tissue, and integral dose.

Acknowledgments

The authors acknowledge Sarah Finch for assistance with SAS. Financial support from The Terry Fox Foundation Strategic Initiative for Excellence in Radiation Research for the 21st Century (EIRR21) at CIHR. Work partially supported by operating grants from NSERC RG-PIN 298191 and from CIHR MOP 102550.

7.6 References

[1] P Romestaing, Y Lehingue, and C Carrie. Role of a 10-Gy boost in the conservative treatment of early breast cancer: results of a randomized clinical

trial in Lyon, France. *J. Clin. Oncol.*, 15(3):963–968, 1997.

[2] B Fisher, S Anderson, and J Bryant. Twenty-year follow-up of a randomized trial comparing total mastectomy, lumpectomy, and lumpectomy plus irradiation for the treatment of invasive breast cancer. *N Engl J Med*, 16(347):1233–1241, 2002.

[3] Early Breast Cancer Trialists' Collaborative Group. Effects of radiotherapy and of differences in the extent of surgery for early breast cancer on local recurrence and 15-year survival: an overview of the randomised trials. *Lancet*, 366(9503):2087–2106, 2005.

[4] H Bartelink, J Horiot, and P Poortmans. Impact of a Higher Radiation Dose on Local Control and Survival in Breast-Conserving Therapy of Early Breast Cancer: 10-Year Results of the Randomized Boost Versus No Boost EORTC 22881-10882 Trial. *J. Clin. Oncol.*, 22(25):3259–3265, 2007.

[5] Y Kirova, N Fournier-Bidoz, V Servois, and F Laki. How to boost the breast tumor bed? a multidisciplinary approach in eight steps. *Int. J. Radiat. Oncol. Biol. Phys.*, 72(2):494–500, 2008.

[6] C M Ma, M Ding, J S Li, M C Lee, T Pawlicki, and J Deng. A comparative dosimetric study on tangential photon beams, intensity-modulated radiation therapy (IMRT) and modulated electron radiotherapy (MERT) for breast cancer treatment. *Phys. Med. Biol.*, 48(7):909–924, 2003.

[7] L Olofsson, Xi Mu, S Nill, U Oelfke, B Zackrisson, and M Karlsson. Intensity modulated radiation therapy with electrons using algorithm based energy/range selection methods. *Radiother. Oncol.*, 73(2):223–231, 2004.

[8] K Al-Yahya, D Hristov, F Verhaegen, and J Seuntjens. Monte Carlo based modulated electron beam treatment planning using a few-leaf electron collimator—feasibility study. *Phys. Med. Biol.*, 50(5):847–857, 2005.

[9] L Jin, C M Ma, J Fan, A Eldib, R A Price, L Chen, L Wang, Z Chi, Q Xu, M Sherif, and J S Li. Dosimetric verification of modulated electron radiotherapy delivered using a photon multileaf collimator for intact breasts. *Phys. Med. Biol.*, 53(21):6009–6025, 2008.

[10] F J Salguero, B Palma, R Arrans, J Rosello, and A Leal. Modulated electron radiotherapy treatment planning using a photon multileaf collimator for post-mastectomized chest walls. *Radiother. Oncol.*, 93(3):625–632, 2009.

[11] E E Klein, M Mamalui-Hunter, and D A Low. Delivery of modulated electron beams with conventional photon multi-leaf collimators. *Phys. Med. Biol.*, 54(2):327–339, 2009.

[12] F J Salguero, R Arráns, B A Palma, and A Leal. Intensity- and energy-modulated electron radiotherapy by means of an xMLC for head and neck shallow tumors. *Phys. Med. Biol.*, 55(5):1413–1427, 2010.

[13] T Gauer, K Engel, A Kiesel, and D Albers. Comparison of electron IMRT to helical photon IMRT and conventional photon irradiation for treatment of breast and chest wall tumours. *Radiother. Oncol.*, 94(3):313–318, 2010.

[14] J I Toscas, D Linero, I Rubio, A Hidalgo, R Arnalte, L Escudé, L Cozzi, A Fogliata, and R Miralbell. Boosting the tumor bed from deep-seated tumors in early-stage breast cancer: a planning study between electron, photon, and proton beams. *Radiother. Oncol.*, 96(2):192–198, 2010.

[15] A Clivio, A Fogliata, and A Franzetti-Pellanda. Volumetric-modulated arc radiotherapy for carcinomas of the anal canal: A treatment planning comparison with fixed field IMRT. *Radiother. Oncol.*, 92(1):118–124, 2009.

[16] L Cozzia, K A Dinshawc, S K Shrivastavac, U Mahantshettyc, R Engineerc, D D Deshpandec, S V Jamemac, E Vanettia, A Clivioa, G Nicolinia, and A Fogliataa. A treatment planning study comparing volumetric arc modulation with RapidArc and fixed field IMRT for cervix uteri radiotherapy. *Radiother. Oncol.*, 89(2):180–191, 2008.

[17] K Al-Yahya, F Verhaegen, and J Seuntjens. Design and dosimetry of a few leaf electron collimator for energy modulated electron therapy. *Med. Phys.*, 34(12):4782–4791, 2007.

[18] A Alexander, F Deblois, G Stroian, K Al-Yahya, E Heath, and J Seuntjens. MMCTP: a radiotherapy research environment for Monte Carlo and patient-specific treatment planning. *Phys. Med. Biol.*, 52(13):N297–308, 2007.

[19] M Fippel, W Laub, B Huber, and F Nusslin. Experimental investigation of a fast Monte Carlo photon beam dose calculation algorithm. *Phys. Med. Biol*, 44(12):3039–3054, 1999.

[20] A Alexander, F DeBlois, and Jan Seuntjens. Toward automatic field selection and planning using Monte Carlo-based direct aperture optimization in modulated electron radiotherapy. *Phys. Med. Biol.*, 55(16):4563–4576, 2010.

[21] D M Shepard, M A Earl, X A Li, S Naqvi, and C Yu. Direct aperture optimization: a turnkey solution for step-and-shoot IMRT. *Med. Phys.*, 29(6):1007–1018, 2002.

[22] E Sterpin, M Tomsej, B De Smedt, N Reynaert, and S Vynckier. Monte Carlo evaluation of the AAA treatment planning algorithm in a heterogeneous multilayer phantom and IMRT clinical treatments for an Elekta SL25 linear accelerator. *Med. Phys.*, 34(5):1665–1677, 2007.

[23] V Panettieri, P Barsoum, M Westermark, L Brualla, and I Lax. AAA and PBC calculation accuracy in the surface build-up region in tangential beam treatments. Phantom and breast case study with the Monte Carlo code PENELOPE. *Radiother. Oncol.*, 93(1):94–101, 2009.

[24] International Commission on Radiation Units and Measurements (ICRU). *Prescribing, Recording, and Reporting Photon Beam Intensity Modulated Radiation Therapy*. ICRU Report 83, 2010.

[25] Eric J Hall and Cheng-Shie Wuu. Radiation-induced second cancers: the impact of 3D-CRT and IMRT. *Int. J. Radiat. Oncol. Biol. Phys.*, 56(1):83–88, 2003.

[26] D Verellen and F Vanhavere. Risk assessment of radiation-induced malignancies based on whole-body equivalent dose estimates for IMRT treatment in the head and neck region. *Radiother. Oncol.*, 53(3):199–203, 1999.

[27] X Mu, T Björk-Eriksson, S Nill, U Oelfke, K Johansson, G Gagliardi, L Johansson, M Karlsson, and B Zackrisson. Does electron and proton therapy reduce the risk of radiation induced cancer after spinal irradiation for childhood medulloblastoma? a comparative treatment planning study. *Acta Oncol*, 44(6):554–562, 2005.

[28] C M Ma, T Pawlicki, M C Lee, S B Jiang, J S Li, J Deng, B Yi, E Mok, and

A L Boyer. Energy- and intensity-modulated electron beams for radiotherapy. *Phys. Med. Biol.*, 45(8):2293–2311, 2000.

[29] K Engel and T Gauer. A dose optimization method for electron radiotherapy using randomized aperture beams. *Phys. Med. Biol.*, 54(17):5253–5270, 2009.

CHAPTER 8
Paper V: Dynamic jaw optimization for FLEC-based MERT and mixed beam radiotherapy

Andrew Alexander, Emilie Soisson, Marc-André Renaud, and Jan Seuntjens

Med. Phys., Under review 2011

Contents

The success of the previous two MERT planning studies reaffirm the potential role of MERT for clinical radiotherapy. However, the previous studies focused on generating high quality plans without regard for practical delivery aspects. As a result, the plans created within the previous two studies may only represent idealized cases. The previous studies made use of many small sized apertures to generate plans and this approach is accompanied with lengthy treatment times. The following manuscript describes a novel approach to MERT optimization, in which the aperture shapes and weights are adjusted iteratively. The philosophy behind this study was to reduce the number of beamlet apertures required to generate ideal MERT plans, which in turn will reduce the MERT delivery time. The approach greatly reduced the number of MERT fields, although at a slight cost to the target dose homogeneity. As a result of the loss in target dose homogeneity the MERT plan was re-optimized with the addition of photon beamlets. Consequently, this is the first study to combine FLEC-based MERT plan optimization with photon beamlet optimization for the creation of mixed beam radiotherapy plans.

Abstract

Despite promising research in modulated electron radiotherapy (MERT), an applicator to produce modulated electron beams and associated treatment planning software is still not commercially available. This work investigated an optimization process in treatment planning for the McGill few leaf electron

collimator (FLEC) MERT delivery device. In addition, the possibility of combining MERT with photon fields was examined to investigate mixed beam radiotherapy.

A FLEC direct aperture optimization optimization (DAO) method (FDAO), in which FLEC apertures and weights were iteratively optimized was created. We evaluated the performance of FDAO against our previous technique for generating FLEC plans and with commercially available photon beam optimization algorithms using a basic target and organ at risk geometry. We applied the FDAO technique on a sarcoma treatment to evaluate clinical parameters. Lastly, we examined the merit of mixing the FDAO generated FLEC electron fields with photon fields to improve the dosimetry of the sarcoma treatment.

In relation to the alternative plans, the FDAO generated sarcoma MERT plan was competitive in its ability to reduce the dose to OAR but weaker in its ability to highly conform the dose to the target volume. The addition of photon fields improved the quality of the MERT plan in terms of OAR sparing and target conformality.

The FDAO approach yielded deliverable FLEC-based MERT plans with a limited number of fields. The approach combined with photon optimization added flexibility, where the mutual benefits of each radiation type was used in unison to improve plan quality.

8.1 Introduction

Modulated electron radiotherapy (MERT) is an emerging electron modality that has been shown to deliver conformal dose to shallow targets [1, 2, 3]. The main advantage of MERT comes from the physical properties of electron beam

therapy such as the defined electron range, which limits the dose to organs at risk (OAR). Dose conformity has been achieved through the combination of energy modulation in the direction of the beam and lateral uniformity and conformity by intensity modulation via the electron collimator [4]. The first studies which explored MERT [5, 1, 6, 7, 8] used microtron based scanned electron beam systems. Narrow electron beamlets generated from microtron based systems can be easily controlled in energy and intensity and these studies have shown MERT to be of great value. However, most radiotherapy departments do not have access to a microtron for electron radiotherapy. As such, studies have evaluated the feasibility and dosimetry of various linac based electron collimator devices for potential MERT applications [9, 10, 11, 12, 13, 14, 15, 16, 17, 18, 19, 20, 21, 22, 23, 24, 25, 26, 27, 28, 29, 30, 31]. These studies examined the dosimetric characteristics of tertiary electron collimators. Planning studies have attempted to provide the community with a robust methodology for MERT planning [32, 4, 8, 17, 33, 34, 35, 36, 37]. The combination of these two areas of focus has resulted in subsequent studies which have demonstrated dosimetric advantages under clinical situations for the application of MERT [38, 39, 16, 34, 40, 36, 41].

Despite the positive results from previous studies, commercial vendors have yet to provide the radiation therapy community with an integrated system to produce and optimize intensity modulated electron beams. We propose a system that would encompass an automated field-shaping device, Monte Carlo (MC) treatment planning system (TPS), and field optimization. As our field-shaping device and MC system has been adequately studied, the focus of this work was

limited to electron field optimization. In addition, electron beamlets were paired with photon beamlets for an investigation into mixed beam (photon-electron) optimization. Mixed beam optimization has been suggested as the most promising avenue for MERT implementation in the clinical setting [16, 42], however, detailed studies and automated all-inclusive systems are lacking.

The automated field-shaping device selected for this study was the few leaf electron collimator (FLEC) [17] developed at McGill University (Montreal, Quebec, Canada). Previous FLEC-based studies by Al-Yahya *et al* [17, 16] relied on manual selection of openings and inverse planning, while more recent studies by Alexander *et al* [35, 41] utilized a large number of small regularly spaced beamlets to generate dosimetrically competitive plans. Unfortunately, small electron beamlets contain a few inherently negative properties such as: a loss in output [22, 24, 25, 30], loss in energy dependence of therapeutic range [8, 24], and increase in bremsstrahlung contamination photons [22, 29, 31]. With regards to the design and use of the FLEC, the relative increase in bremsstrahlung contamination photons was a result of a loss in output. Due to the technical configuration of the FLEC and linac controller, the delivery mode was limited to step and shoot. The delivery time required to deliver a large number of FLEC beamlets quickly becomes unreasonable and compromises clinical feasibility.

Previous MLC-based MERT planning techniques include an inverse planning study by Lee *et al* [4], in which an MLC leaf sequence pattern was generated from beamlet dose weights. To account for scatter and leakage from the leaf ends, the MLC leaf sequence was recalculated using MC and the plan re-optimized by

adjusting MLC segment weights. Lee's approach is a 2 step method for generating deliverable MLC electron segments for inverse MERT planning. The technique was used within a comparative dosimetric study by Ma *et al* [38] for the creation of four MERT breast plans. A study by Salguero *et al* [36] used a similar 2 step approach in generating deliverable electron beam sequences. Engel *et al* [33] described the optimization process for advanced MLC based electron irradiation. The study relied on field segmentation and randomization to achieve the best results. A forward planning MERT optimization process has been described by Surucu *et al* [37]. In Surucu's work, the target geometry was divided into electron energy bins based on target distal depth. The spatial size of each bin corresponded to a MLC segment and subsequent dose distribution. Dose distribution weights were then manually adjusted.

The combination of MERT with photon beams for mixed beam radiotherapy (MBRT) has been previously discussed within the context of the FLEC for improved target uniformity [16] and within the wider community for MERT and unmodulated electron and photon radiotherapy [6, 43, 44, 7, 45, 3, 46, 38, 15, 47, 39, 48, 49, 36, 37, 50]. The study by Al-Yahya *et al* [16] proposed a method that combined 3D conformal photon fields or pre-optimized photon IMRT fields with manually selected electron beamlets. The proposed method to integrate electron and photon beamlets was straight-forward and may not be the best approach for generating high quality MBRT plans as the specifics of the IMRT fields where generated without consideration of the electron fields. In addition, the selection of manual electron beamlets was labour-intensive and without careful

analysis could result in suboptimal plans. In 2010, Surucu *et al* [37] investigated the combination of an equally weighted MERT and IMRT plan. The MERT segments were generated based on the target depth and weights were manually adjusted for each segment. An independent IMRT plan was generated separately from the MERT plan. The equally weighted MERT and IMRT plan represented a simplistic hybrid plan whereby the photon component was generated without any interplay with its corresponding electron component. A recent study by Ge *et al* [50] investigated the combination of forward planned electron fields with photon IMRT. The flexibility of the study was limited due to the use of Pinnacle (Philips Radiation Oncology Systems, Fitchburg, WI), which prevented the ability to modulate individual electron beamlets within the MBRT inverse optimization stage. The manually selected electron beamlets were treated as a single fixed dose distribution within Pinnacle and scaled with weight against the photon 1×1 cm^2 beamlets. Despite the laborious task of manually creating the electron component of the MBRT plan, the dosimetry of the MBRT plans were an improvement over the IMRT benchmark comparisons. For the studies presented, there were considerable differences within the methodology for generating MBRT plans. In addition, no study directly optimized the photon and electron beamlets in conjunction. Without a systematic study to investigate the best method for generating high quality MBRT plans, the potential quality of all MBRT plans remains in question. Thus far, MBRT studies have separated inverse photon and electron beamlet optimization. This is likely due to the lack of a flexible optimization system for combined inverse MBRT optimization. The approach

investigated in this study involves an inverse optimization process that combines decoupled photon and electron beamlets.

This work investigated a dynamic aperture optimization process, which directly optimized the FLEC aperture shapes and weights using direct aperture optimization (DAO). This process was analogous to the jaw-only IMRT optimization described by Earl *et al* [51]. In this study, the performance of the optimization algorithm, FDAO, was evaluated for the application of FLEC-based MERT. This work presents the benchmark results of a FDAO plan compared against the previous 2×2 cm^2 technique for generating FLEC-based MERT plans [35] and clinical photon inverse optimization systems. The previous technique comparison provided end point differences, such as the number of fields and dosimetric values. While the clinical system comparison was included to establish a competitive reference point. The FDAO benchmark plan was created on a virtual phantom under ideal conditions such as a constant source to surface distance and a multilevelled target and organ at risk geometry. To evaluate the clinical application of FDAO, a FDAO MERT plan was generated for a rhabdomyosarcoma case and quantitatively compared against clinical photon and electron treatment plans. The sarcoma case represented a real clinical scenario with a complex geometry. Quantitative dosimetric comparisons of the sarcoma case are representative of a realistic clinical comparison. Lastly this work explored the topic of MBRT. Photon beamlets were added to the FDAO MERT sarcoma plan to evaluate the merit of FLEC-based MBRT in an optimization process that decoupled photon and electron beamlets.

8.2 Materials and Methods

DAO is an iterative inverse optimization technique where aperture shapes and weights are adjusted to satisfy the optimization goals [52]. The technique incorporates the full dosimetric properties of each aperture shape to provide dosimetric accuracy within the optimization stage. DAO was first designed for photon step and shoot IMRT delivery, where it was shown to reduce the number of beam segments, reduce the number of monitor units, and produce efficient treatment deliveries that maintain the full dosimetric benefits of IMRT. The technique is transferable to MERT where the perturbation effects of electron beam shaping devices are included within the optimization phase to maintain dosimetric accuracy and minimize optimization convergence errors [53]. An alternative optimization method would be to apply aperture-based corrections or full MC simulations to the preliminary plan and subsequently readjust relative weights within a post-optimization run.

8.2.1 Previous 2×2 cm^2 FLEC-Based MERT Technique

A previous FLEC-based MERT planning study [35] that examined beamlet sizes recommended that the use of 2×2 cm^2 beamlets in a feathered offset pattern produced favourable plans in terms of target homogeneity and quantity of beamlets. The technique can be summarized as follows: (1) the delivery angles and isocenters were chosen; (2) 2×2 cm^2 beamlets were generated in a feathered offset pattern for each external beam position; (3) CT derived patient-specific dose distributions of all energies available were computed for each beamlet; (4)

the treatment goals were defined; (5) the optimization was performed; (6) the final plan was analyzed.

8.2.2 New FLEC-Based DAO MERT technique

The FDAO MERT technique was an extension from previous optimization strategies at McGill whereby aperture shapes were optimized alongside beam weights. FDAO was integrated into our in-house Monte Carlo (MC) treatment planning system, (MMCTP) [54]. The MMCTP planning system utilizeds the MC codes BEAMnrc [55], DOSXYZnrc [56], and XVMC [54] for patient-specific dose calculation. A MERT toolkit was added to MMCTP in order to streamline the entire process. The planning process is outlined in figure 8–1 and can be divided into two phases: (1) treatment planning, and (2) FDAO.

The treatment planning phase consists of five steps:

Step 1: An algorithm generated a list of potential external beam positions (isocenter and gantry angle) using the target volume and external body contour based on: target symmetry, target projection width, target depth, and source to surface distance (SSD).

Step 2: One or more open beams were selected from step 1 to cover the target volume.

Step 3: The beams selected in step 2 were divided into subfield beamlets based on the beams eye view projection of the target distal depth below the surface of the patient. All available beam energies were assigned to each subfield.

Step 4: The patient-specific dose distributions were computed using BEAMnrc, DOSXYZnrc or XVMC.

Step 5: The planning goals were defined (target maximum and minimum, organ at risk dose volume limits).

The FDAO phase consists of two steps:

Step 6: The beamlet aperture and weight optimization was performed using a simulated annealing type algorithm.

Step 7: The optimized plan was transferred to MMCTP for planning analysis. If the plan satisfied the planning goals, then it is finalized. Otherwise the process was repeated with modifications.

The patient-specific dose distributions, together with the planning goals, were input into the FDAO code for optimization. Beam weights and apertures were directly modified within FDAO. A pseudo random number was used to determine if a beam weight or aperture would be adjusted. Each aperture adjustment required a new patient-specific dose calculation. The objective function, which is a mathematical representation of the planning goals and current beam weights, was evaluated iteratively. The objective function within this study has been presented in previous work [35]. If the new objective function value was lower than the previous iteration, the iteration was labeled as a successful iteration and the current change was accepted. If the value was higher than the previous value, the solution was worse than the previous iteration and the change was accepted with probability p. Accepting worse solutions based on a probability value is a characteristic of a simulated annealing method and is useful in avoiding local

minima. The probability value p decreased according to the following equation:

$$p = B\frac{1}{(n_{succ}+1)^{1/T_0^{prob}}}, \tag{8.1}$$

where B was the probability at the start of the optimization, n_{succ} was the number of successful iterations that decreased the cost function, and T_0^{prob} was a constant that dictated the rate at which the probability value p decreased. As the optimization progressed, $n_{succ} \to \infty$, $p \to 0$, and the algorithm was less likely to accept worse solutions. For each beamlet weight or aperture adjustment, a change of random size was sampled from a Gaussian distribution. The width of the Gaussian decreased according to the following equation:

$$\sigma = A \times e^{-n_{succ}/T_0^{step}}, \tag{8.2}$$

where A was the width of the Gaussian at the beginning of the optimization and T_0^{step} was a cooling constant [57] that quantified the rate at which the width of the Gaussian decreased [51]. The value of σ was directly related to the magnitude of beam weight and aperture changes at each iteration. As $n_{succ} \to \infty$, $\sigma \to 0$. A minimum cutoff value for σ was used to terminate the optimization process. The degrees of freedom within FDAO code consisted of beamlet weight and the four leaf positions (X1, X2, Y1, Y2). The collimator angle, gantry angle, and couch angle were not adjusted within the mechanics of FDAO. A few initial boundary conditions were required within FDAO to restrict the motion of the FLEC leaves to the geometric limits of the FLEC. The initial σ width of beam weight changes ($A_{weights}$) and FLEC leaf displacements ($A_{aperatures}$), initial probability value B,

and constants T_0^{step} and T_0^{prob}, were all determined systematically. Throughout this study, the minimum field size was set at 2 cm, as the goal of this work was to create plans that utilized large subfields. The initial sigma width A, constants T_0^{step} and T_0^{prob}, and initial probability value B were all closely intertwined and had to be mutually selected. The rate of convergence to the solution increased with lower values of T_0^{step} and T_0^{prob}. A larger σ value, was found to produce a series of worse solutions and required a small probability value p to avoid a cascade of accepting worse solutions. The values of A, T_0^{step}, and T_0^{prob} could not be determined *a priori* and required a systematic trial and error procedure to identify appropriate values. The values selected for this study were $A_{weights} = 2$, $A_{apertures} = 2$ cm, $T_0^{step} = 120$, $T_0^{prob} = 2$, and $B = 5\%$.

Monte Carlo FLEC simulations

Feasibility testing of DAO with MERT required a fast electron MC code for quick electron field calculations. XVMC was selected as the electron dose engine and was used to simulate both the beam and patient. The XVMC beam model was commissioned to match measured central axis PDDs at $R_{100\%}$ and $R_{50\%}$, and the rectangular aperture collimation of the FLEC with respect to field size. The XVMC beam model was simplistic and did not adequately model the out of field scattered dose, penumbra region or relative output factors. However, an accurate representation of a clinical electron field was not required or essential in order to evaluate the mechanics and feasibility of FDAO. The XVMC models were used within the FDAO evaluation component of this work

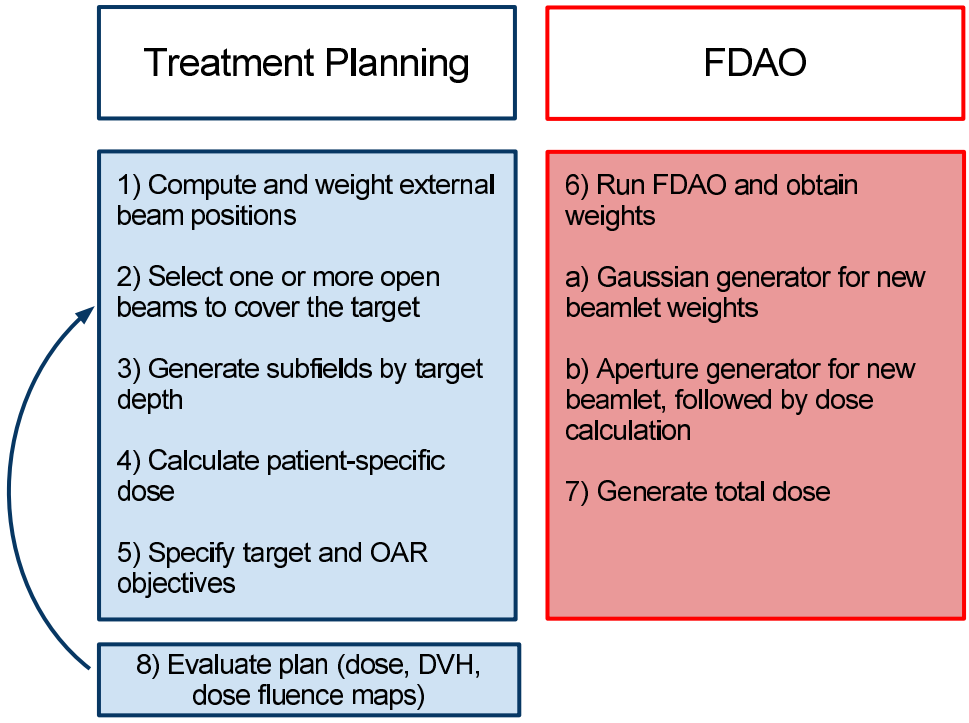

Figure 8–1: FLEC-based MERT FDAO process within MMCTP. If the optimized plan does not meet the planned objectives, the process is repeated with modifications to step 2 or 5.

Full treatment head BEAMnrc Varian CL21EX FLEC electron models for 6, 9, 12, 16, and 20 MeV have been previous commissioned to an accuracy of 2%/2 mm in comparison to measured PDD and profiles throughout the field size range of the FLEC [31]. These electron beam models accurately model the bremsstrahlung production within the linac head and lateral scattering of electrons from the FLEC leaves. The electron beam models were run within DOSXYZnrc using source 9 when used with FDAO to simply the MC process. The DOSXYZnrc simulations were run down to an average percent error of 0.5% on dose values greater than 50% of the maximum dose. The transport parameters used in EGSnrc simulations were ECUT = AE = 700 keV cutoff for electron transport, PCUT = AP = 10 keV for photon transport and PRESTA-II as the electron step algorithm. The EGSnrc models were used within the FDAO clinical application and MBRT component of this work.

8.2.3 FDAO Evaluation

The Eclipse TPS (Varian Medical Systems Inc., Palo Alto, USA) was used to created a digital water phantom with a superficial target volume and two organs at risk surrounding the target volume. The details of the phantom include: 67 axial slices of 0.3 cm thickness and a 30×20 cm^2 rectangular water phantom centered on each slice. The proximal edge of the target volume paralleled the external contour at a depth of 1.5 cm. The target volume spanned 6 cm in axial slice thickens and it's shape was tapered at each slice end. Laterally, the target volume was 6 cm wide and consists of two distal depths, 1.5 cm and 3.5 cm. Two organs at risk surrounded the distal edge of the target volume with a separation

gap of 0.5 cm between the target volume and organs at risk. The separation gap between the organs at risk was 0.5 cm. The phantom can been seen in figure 8–3 with all structures labeled. OAR 1 was positioned 2 cm from the external contour in depth while OAR 2 was positioned 1.5 cm in depth from the external contour. Both OAR volumes spanned 9 cm in the direction normal to the axial slices and their shape wrapped around the extent of the target volume in the axial direction. The target volume was 92 cm^3, OAR 1 volume was 180 cm^3, while OAR 2 volume was 220 cm^3. The phantom and structures were exported to Helical TomoTherapy (HT) (Tomotherapy, Madison, USA) and MMCTP. The IMRT and VMAT-RapidArc^{TM} (Varian Medical Systems Inc., Palo Alto, USA) plans were created in Eclipse.

The optimization goals were: 50 Gy minimum and maximum target dose, with a dose normalization point of 50 Gy to 98% of the volume; 40 Gy to 2% of the OARs; 30 Gy to 10% of the OARs. The optimization goals were matched as best as possible to all systems.

To first order, the success or failure of an optimization system in radiotherapy is the ability to adequately conform the dose to the target while minimizing the dose to neighbouring normal structures. The complex clinical systems selected in this study were chosen to provide us with a benchmarking point, to which we can compare the results of FDAO. The FDAO plan was also compared to the previously developed 2×2 cm^2 MERT planning technique [35]. If the domestic quality of the FDAO plan was as good as the clinical systems and the 2×2 cm^2 MERT

planning technique, we can assume that FDAO produces clinically acceptable plans. Quality was assessed based on a variety of dose volume metrics.

The clinical optimization systems created plans that met the planning objectives in a matter of minutes (excluding the beamlet dose calculation time for HT). Each clinical plan was created by an experienced planner with the goal of creating a high quality plan. The final plans were exported to MMCTP for analysis.

8.2.4 FDAO Clinical Application

A head and neck rhabdomyosarcoma case was used to evaluate the capabilities of FDAO for a single beam orientation irradiation setup. The goal of the treatment was to deliver a dose of 36 Gy to the PTV, with the aim of covering 95% of the target volume with 100% of the prescription dose. A single forward planned direct electron (DE) 9 MeV cutout field had been previously created in Eclipse for clinical treatment. For the purpose of this study, two additional plans, a five field 6 MV IMRT plan and a three arc 6 MV VMAT-RapidArc^{TM} plan were created to provide benchmark references for the FDAO plan.

All plans modelled the patient anatomy as homogeneous water to minimize the number of parameters that affect plan comparisons between treatment planning systems. As such, the Eclipse plans were exported to MMCTP and recalculated using BEAMnrc and DOSXYZnrc. The Varian CL21EX 9 MeV electron BEAMnrc beam model and the Varian CL21EX 6 MV photon BEAMnrc beam model has been previously commissioned to an accuracy of 2%/2 mm. The electron cutout simulation made use of an in-house EGSnrc user code called

cutout [58], to transport particles through the cutout aperture. The DOSXYZnrc EGSPhant model also modelled the patient anatomy as homogeneous water using the same voxel resolution of ($2.5\times2.5\times3$ mm^3) as Eclipse, ensuring a consistent patient geometry model between MMCTP and Eclipse. The VMAT-RapidArc^{TM} calculation made use of a recent modification to DOSXYZnrc, which enabled multiple gantry angle index simulations [59]. The DOSXYZnrc simulations were run down to an average percent error of 0.5% on dose values greater than 50% of the maximum dose. The transport parameters used in EGSnrc simulations were ECUT = AE = 700 keV cutoff for electron transport, PCUT = AP = 10 keV for photon transport and PRESTA-II as the electron step algorithm.

8.2.5 Mixed Photon and Electron Therapy

MBRT combines photon and electron fields into a single plan. The electron beamlets, created within the FDAO optimization phase of the MERT sarcoma plan were reused and combined with two tangental photon beams placed 180 degrees apart. The photon beams were divided into MLC collimated beamlets of 1×1 cm^2. The dose distribution for each beamlet was calculated using BEAMnrc and DOSXYZnrc within MMCTP. The electron and photon beamlet weights were optimized using a previously described gradient optimization algorithm [35]. For clinical delivery of MBRT, the 1×1 cm^2 photon beamlets would require post processing segmentation to generate a finite and sufficiently small number of photon IMRT segments. Photon beamlets were not segmented within this study.

Table 8–1: Number of beamlets per energy per MERT mode for virtual phantom geometry.

MERT Mode	6 MeV	9 MeV	12 MeV	16 MeV	20 MeV	Total
2×2 cm^2 Feathered	26	53	101	117	115	412
FDAO	13	7	10	3	0	33

8.3 Results

8.3.1 FDAO Evaluation

The MERT phantom plan was created using a single beam orientation and five isodepth subfields. The process resulted in a total of 25 beamlets: five subfields times five available electron energies (6, 9, 12, 16, and 20 MeV). The FDAO code generated an additional one thousand beamlets. The final FDAO plan consisted of 33 beamlets. The beams eye view of external-surface-to-distal tumour depth projection plane and intensity maps of the plan are shown in figure 8–2. A visual comparison between the beams eye view and intensity maps confirm the paring of distal tumour depth with electron beam energy.

Results of the FDAO code and clinical systems are shown in figures 8–3 and 8–4. The best target coverage was obtained with HT, followed by IMRT, VMAT-RapidArc^{TM}, and lastly MERT. All plans were normalized at the near minimum, $D_{98\%}$. The MERT near maximum $D_{2\%}$ dose was 2.1 Gy (4%) higher than HT. Despite the increased heterogeneity observed within the MERT target, the plan was superior in reducing the low dose bath, which is typically seen in IMRT, VMAT and HT, as shown in the isodose lines of figure 8–3. DVH graphs of the OARs highlight the benefits and downsides of the FDAO-MERT plan. The FDAO algorithm was able to reduce the low dose regions of the OARs below that

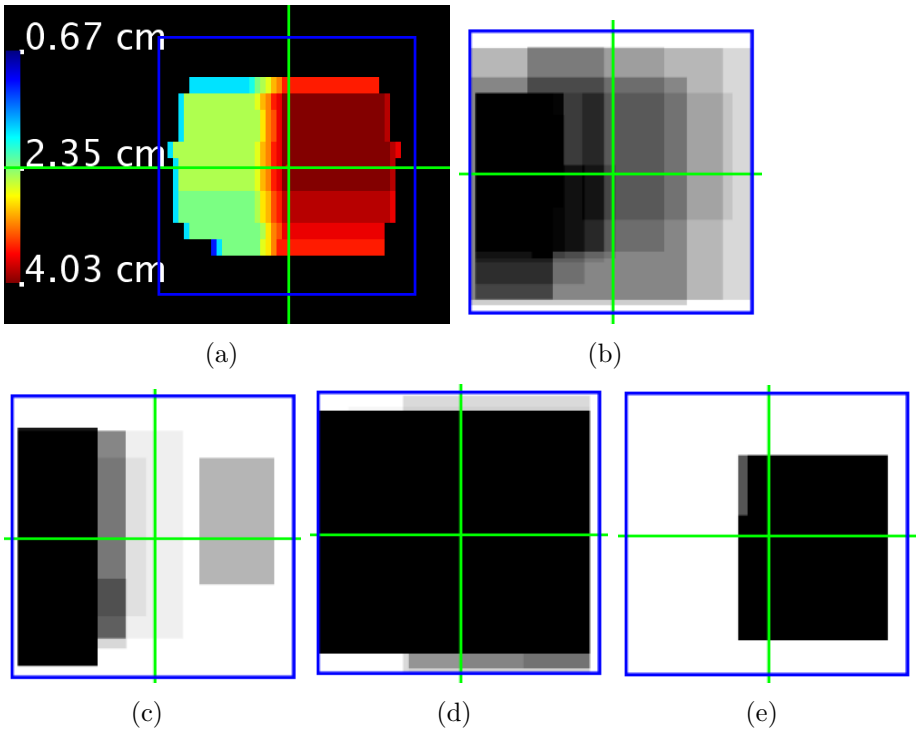

Figure 8–2: Beams eye view of external-surface-to-distal tumour depth projection plane (a), and FDAO relative intensity maps for each beam energy: 6 MeV (b), 9 MeV (c), 12 MeV (d), and 16 MeV (e). The isocenter is marked by the crosshairs and the 8×8 cm^2 maximum FLEC field size by the outlined square. Darker beamlets indicate higher weights than lighter beamlets. Intensity maps were normalized to the maximum weight for each energy.

of the clinical systems. However, the technique could not match the OAR high dose volume levels of the clinical systems.

8.3.2 FDAO Comparison with 2×2 cm^2 Beamlets

The benchmarking FDAO plan was compared with the previous technique. The result of this comparison is summarized in table 8–1 and DVHs in figure 8–5. The FDAO plan matched target coverage and improved OAR sparing with the use of less beamlets. The FDAO plan was an overall substantial improvement in MERT planning in terms of clinical and technical objectives. A reduction in the number of beamlets was desired as this translates into shorter treatment times and QC procedures. In addition to the previous two benefits, the dosimetry of the FDAO plan was preferred in terms of a higher output per MU ratio over the smaller 2×2 cm^2 beamlet fields which reduced the photon bremsstrahlung component.

8.3.3 FDAO Clinical Application

The FDAO MERT plan was created, as outlined above using a single beam orientation. The process created a total of 70 beamlets, fourteen subfields times five available electron energies; 6, 9, 12, 16, and 20 MeV. Dose distributions for the 70 beamlets were calculated using BEAMnrc electron models and the homogeneous water patient anatomy DOSXYZnrc EGSPhant model. The FDAO code ran for a total of 500 iterations, which includes the BEAMnrc and DOSXYZnrc simulation of an additional 250 beamlets. The final FDAO plan consisted of 37 beamlets of energies 6 and 9 MeV.

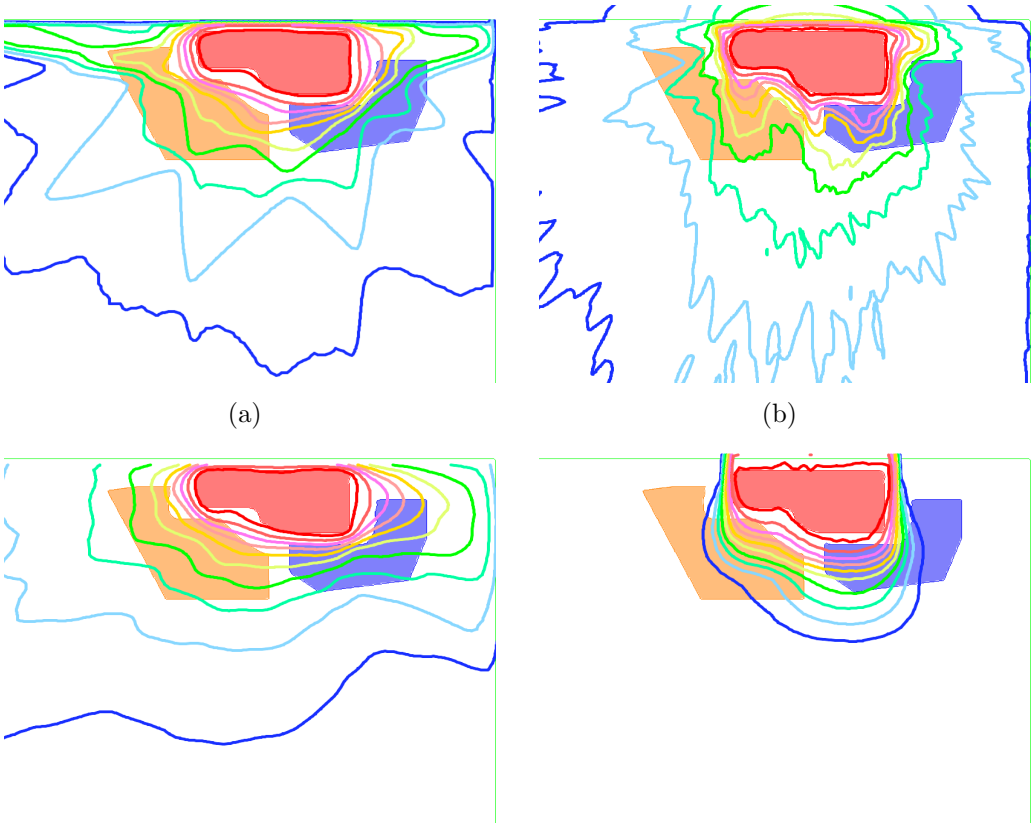

Figure 8–3: Geometry of virtual phantom, external contour (green line), target (red), OAR1 (blue) and OAR2 (orange), and isodose line distribution per plan: Eclipse IMRT (a), HT (b), Eclipse RapidArc™ (c), and FDAO MERT (d). The FDAO MERT plan irradiated the least amount of tissue by a considerable margin. Isodose lines represented: 10%, 20%, 30%, 40%, 50%, 60%, 70%, 80%, 90%, and 100%.

Table 8–2: Summary of FDAO sarcoma plan.

Assesment	6 MeV	9 MeV	12 MeV	16 MeV	20 MeV
# of beamlets	14	23	0	0	0
min aperture size (cm^2)	4.1	4.9	-	-	-
max aperture size (cm^2)	33.3	26.5	-	-	-
mean aperture size (cm^2)	17.3	15.3	-	-	-
fractional weight (%)	37	63	0.0	0.0	0.0

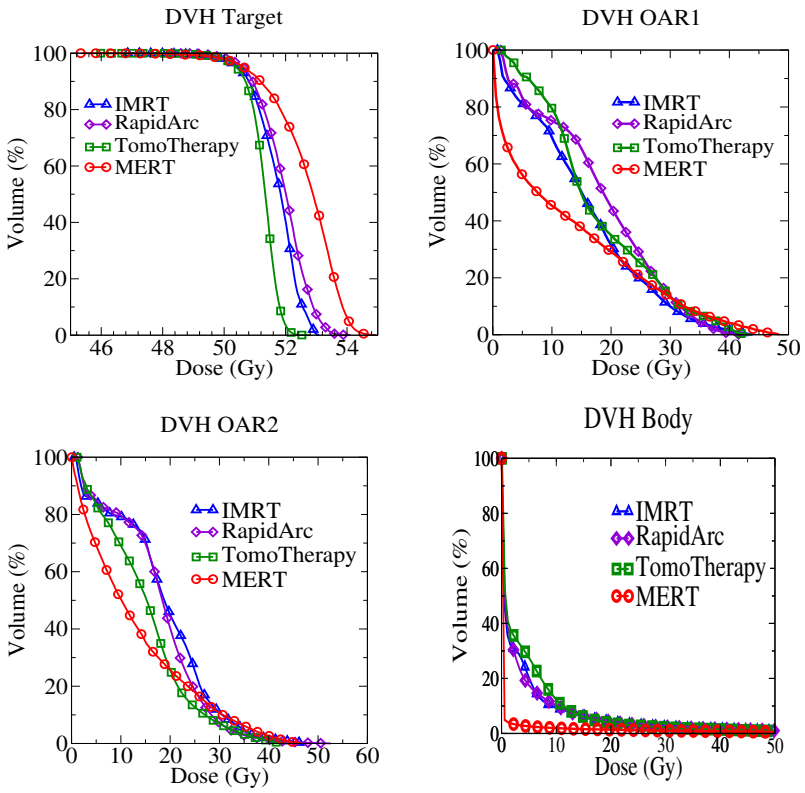

Figure 8–4: Optimization results of target, OAR1, OAR2, and body. FDAO-MERT plan was not able to conform the dose to the target (50 Gy, $D_{98\%} = 50$ Gy) as well as the clinical systems. The FDAO code was superior in sparing the low dose regions of the OARs; however, the clinical systems were superior in dose sparing in the high dose regions.

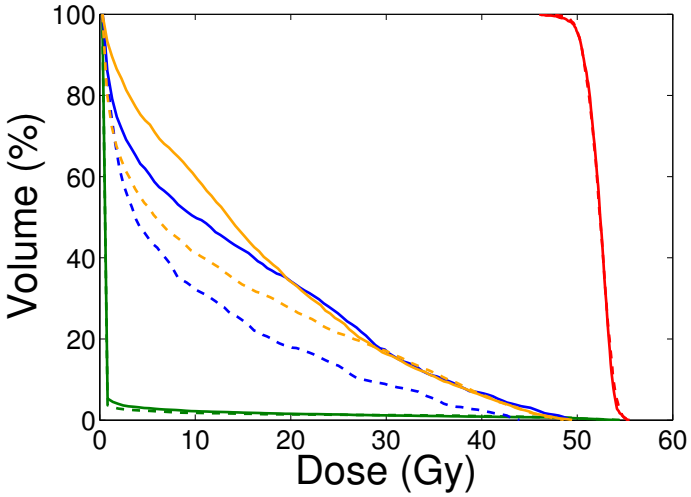

Figure 8–5: Dose volume histogram for the virtual phantom geometry. Volumes include: target (red), OAR1 (blue), OAR2 (orange), and body (green). Solid lines denote 2×2 cm^2 feathered plan (412 beamlets), whereas dashed lines denote FDAO plan (33 beamlets). 98% of the target volume was to receive 50 Gy.

DVH results of the sarcoma case are shown in figure 8–6, isodose plots in figure 8–7, a summary of the beamlets in table 8–2, and dose metrics in table 8–3. The best target homogeneity was achieved with photon IMRT or VMAT. FDAO target homogeneity was similar to DE target homogeneity. As expected, with regards to OAR sparing, the FDAO plan was an improvement in OAR sparing over the DE plan. In addition, the FDAO plan reported lower OAR mean dose in comparison to the photon IMRT or VMAT plan. With regards to the mean body dose and the isodose volume surrounding 2 and 5 Gy, the electron plans (FDAO and DE) reported lower doses than the IMRT or VMAT plans.

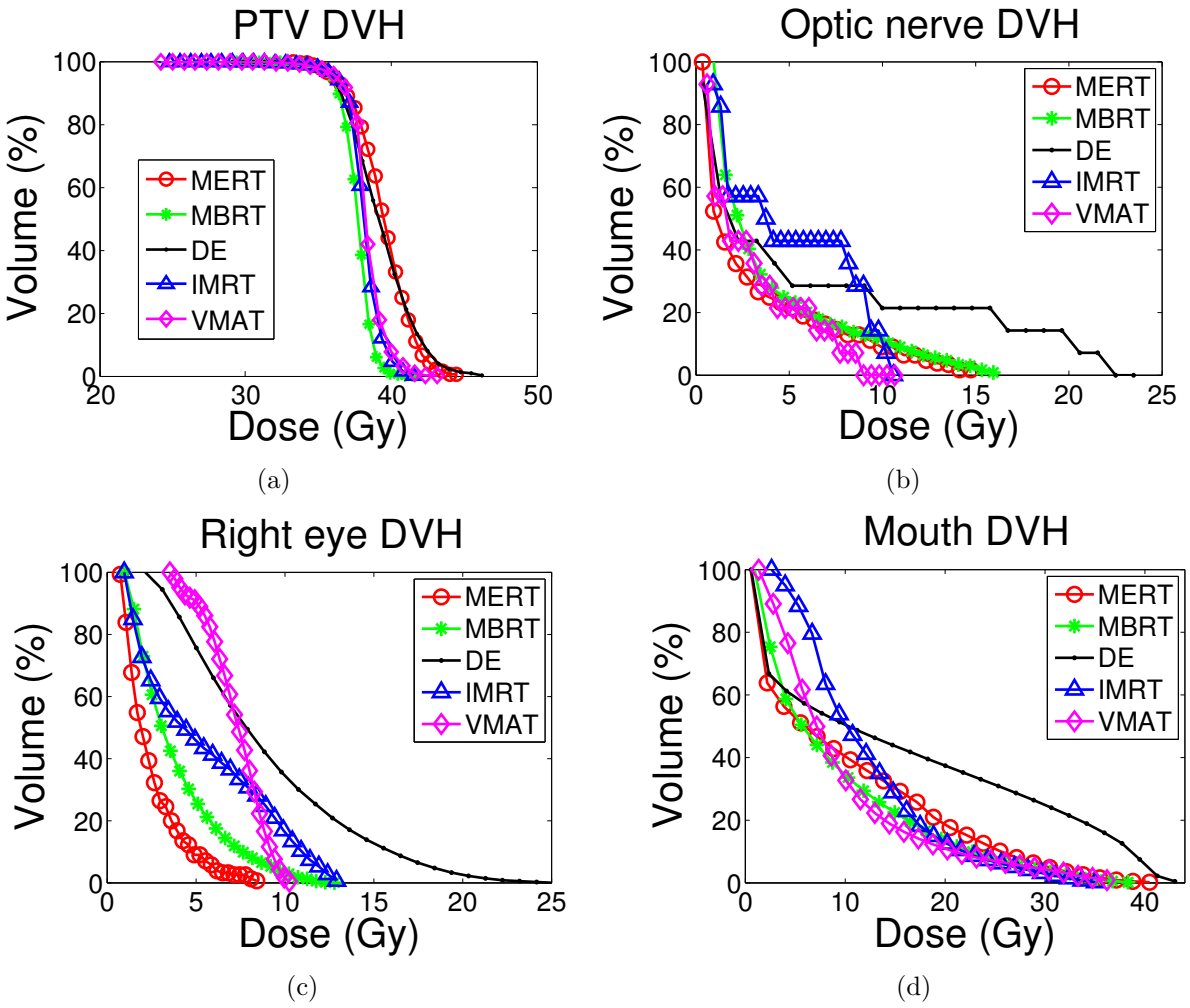

Figure 8–6: Dose volume histogram for the clinical case. PTV coverage was normalized at $D_{95\%} = 36$ Gy.

Table 8–3: Summary of dose-volume indices for sarcoma plan. Prescription dose of 36 Gy to 95% of the PTV.

Volume	Index	MERT	DE	IMRT	VMAT	MBRT
PTV	$D_{98\%}$ (Gy)	33.5	34.2	35.1	34.9	34.8
	$D_{2\%}$ (Gy)	44.1	44.5	40.5	40.9	39.6
	D_{mean} (Gy)	40.1	39.3	38.0	38.2	37.6
Mouth	D_{mean} (Gy)	9.7	15.5	12.0	9.5	8.7
Ipsilateral optic nerve	D_{mean} (Gy)	2.9	6.0	4.7	3.1	1.6
Contralateral eye	D_{mean} (Gy)	1.7	8.8	5.3	7.2	0.9
Contralateral lacrimal	D_{mean} (Gy)	0.30	2.2	0.79	1.6	0.30
Body	D_{mean} (Gy)	1.0	1.3	1.8	1.5	1.0
Body	V_{2Gy} (cm^3)	429	436	1258	1036	451
Body	V_{5Gy} (cm^3)	318	340	777	503	296

8.3.4 Mixed Photon and Electron Therapy

The two tangential photon beams divided into beamlets of 1×1 cm^2 were added to the previous MERT plan in an effort to improve target homogeneity. The photon beamlets added an additional 450 dose distributions to the solution space. The gradient optimization algorithm made use of the same FDAO constraint values. The final MBRT plan consisted of 19 MERT beamlets and 95 photon beamlets.

Results of the MBRT plan are shown in figure 8–6, isodose plots in figure 8–7, a summary of the beamlets in table 8–4, and dose metrics in table 8–3. The MBRT plan was an improvement in target homogeneity compared to MERT and the clinical systems. In addition, the MBRT plan reduced dose to the organs at risk. In fact, the only OAR MBRT metric increase was within the low dose isodose volume of the body contour.

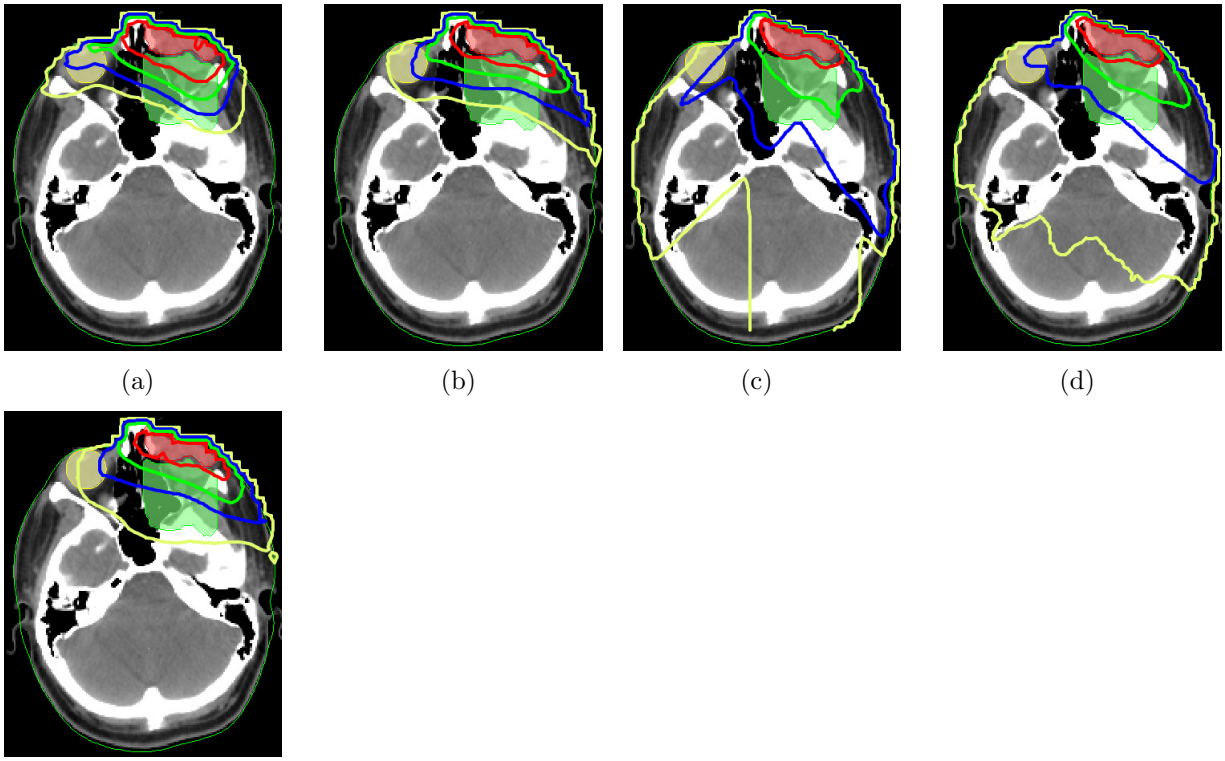

(a) (b) (c) (d) (e)

Figure 8–7: Clinical comparison of isodose distributions between DE (a), FDAO MERT (b), IMRT (c), VMAT (d), and MBRT (e). The 1.8, 9, 21, and 36 Gy lines are shown (corresponding to the prescription dose of 5%, 25%, 60%, and 100%).

Table 8–4: Summary of MBRT sarcoma plan.

Assesment	6 MeV	9 MeV	12 MeV	16 MeV	20 MeV	6 MV
# of beamlets	7	4	0	2	6	95
min aperture size (cm^2)	5.7	4.9	-	8.8	10.4	1.0
max aperture size (cm^2)	25.0	8.5	-	30.1	27.5	1.0
mean aperture size (cm^2)	12.6	7.0	-	19.6	20.0	1.0
fractional weight (%)	24.5	2.5	0.0	3.0	39.4	30.6

8.4 Discussion

8.4.1 FDAO Evaluation

This study has benchmarked the FDAO code for inverse MERT planning against clinical optimization systems and our previous technique for FLEC-based MERT planning. The clinical systems provided a realistic reference point to which a FDAO plan could be compared. The difference in target coverage between the photon plans and the electron FDAO plan may be partially explained by particle type and inherent gradients of electron beams. In addition, it may be unrealistic to assume that FDAO can match the target coverage of clinical systems, due to the use of relatively large electron fields. The clinical systems used beamlets on the order of 0.5×0.5 cm^2. Perspective studies, comparing IMRT photons to intensity modulated protons (IMPT) [60, 61, 62], demonstrated the same trend with proton plans unable to conform to target homogeneity as closely as photon optimization. OAR sparing and total body dose was superior with MERT. The reduction was attributed to the use of a single beam orientation and the limited penetration depth of electron beams. In the high-dose region of the OAR, the MERT plan was inferior to the clinical systems. This effect may be reduced with the use of a limited MERT arc, to spread-out the high dose volume.

In the MERT-MERT comparison of FDAO versus 2×2 cm^2 feathered beamlets, the FDAO plan improved normal tissue dose sparing with the use of less beamlets. Despite previous studies showing promising plans using regularly spaced

beamlets, practical considerations such as treatment delivery time and total number of MUs are a deterrent to clinical implementation. A FDAO-MERT plan now meets the clinical requirement of efficient treatment delivery.

In general, the FDAO code for FLEC-based MERT demonstrates great potential in its ability to reduce the low-dose irradiated volume including the low dose to the OAR at a slight but clinically acceptable cost in target coverage. A notable drawback to this technique would be the lengthy optimization time. However, the dominating inefficiency rests with the MC dose calculations and not the technique itself. Fast MC codes or analytical models would substantially improve the optimization time. In addition, the optimization process could be parallelized and run on a GPU. In addition, the selection of optimization parameters was not straightforward and this could lead to situations where the parameters would have to be re-adjusted to achieve a good result. Lastly, it is possible that the FDAO generated FLEC-based MERT plans may not represent the full potential of FLEC-based MERT due to sub-optimal termination of the algorithm. As such, our results should not be viewed as an upper limit on the quality of FLEC-based MERT.

8.4.2 FDAO Clinical Application

The rhabdomyosarcoma case represented a clinical situation where FLEC-based MERT would be considered. The total number of MERT beamlets was within reason and would be deliverable within an acceptable time frame. In a comparison with the clinical treatment options, the MERT plan reported less integral body dose, improved OAR dose sparing with the exception of the mouth

volume, and slightly worst but clinically acceptable target homogeneity when compared to the photon modalities. Dose sparing was most pronounced for volumes located at depth or distant from the target. In comparison to the DE plan, which consisted of a single 9 MeV cutout field, the MERT plan consisted of two electron energies, 6 and 9 MeV. The improved OAR sparing seen within the MERT plan in comparison to the DE plan was partially attributed to the use of a lower electron beam energy in the plan. These results are consistent in comparison to other MERT studies such as the one by Ma *et al* [38], which concluded that IMRT photons provided the best target coverage while MERT provided significant OAR sparing.

The poorer MERT target homogeneity was attributed to the use of large rectangular electron fields. Moreover, the choice of when to terminate the FDAO code was arbitrary and could have led to a suboptimal solution. The optimization time for the clinical case was substantially higher than the benchmarking case due to the increase in calculation time with BEAMnrc and DOSXYZnrc simulations versus XVMC. The FDAO code was terminated after the generation of 250 additional beamlets, or four times less than the benchmarking case. Despite the lengthy calculation time, an optimization scheme utilizing full MC models avoids problems associated to fluence based beamlet optimization, which require post-modelling of the collimator scatter and perturbation corrections. The full MC model was chosen as it provides the highest level of dosimetric plan accuracy within the optimization process. If accuracy is less important, simplistic beam

models could have been used to calculate dose for a substantial reduction in calculation time.

In order to reduce the impact of dosimetric differences in the beam or patient model, the clinical plans were recalculated within MMCTP using homogeneous water as the patient material. The MERT plan was calculated with the same patient model. Minimizing the dosimetric transport differences allows us to compare the fundamental plan differences due to the optimization mode and particle type. Despite the fact that the clinical plans were originally calculated in homogeneous water a recalculation in MMCTP introduced an uncertainty to this comparison as the exact geometry of the MMCTP patient model could be slightly different than the geometry within Eclipse. These differences are attributed to partial volume effects in the determination of patient edge voxels. Due to the target's close proximity to the skin, it is possible that these effects could have negatively influenced the target coverage for the clinical plans. The impact of partial volume effects was evaluated by examining the MMCTP target coverage DVH against the Eclipse DVH. The DVHs agreed well and we can assume that any partial volume effects had a minimal influence for this case.

8.4.3 FDAO MERT with Photon Beamlets

MERT target coverage may be improved with multiple beam angles or a limited arc. However, due to the close proximity of the FLEC to the patient's body, multi-angled FLEC beams may not be achievable. A simpler approach for FLEC-based MERT (due to the physical presence of the electron applicator) would be to combine the MERT field with multiple photon beam orientations

for improved target homogeneity. The proposed MBRT planning method, using the FDAO derived MERT beamlets, has been shown to improve both target homogeneity and OAR sparing. These results are consistent with previous MBRT studies [43, 45, 16, 49, 37, 50]. The photon fields could be sequenced to deliver step and shoot segments or a sliding window type sequence. For the purpose of this study, the photon beamlets were not sequenced into segments.

It is interesting to note that the summary of electron beamlets used within the MBRT plan and the MERT plan were different. The MERT plan used only 6 and 9 MeV beamlets, while the MBRT plan utilized 6, 9, 16, and 20 MeV beamlets. Despite the use of higher energy electron beamlets, the OAR sparing was better within the MBRT plan. For this case, the preferred percentage of electron dose contribution was 70%, which is higher than the 50% value as reported from previous studies [48, 37, 50]. The relative increase in electron dose observed within this work could be due to the specific geometry of this case or due to the increased flexibility within our optimization system to integrate and re-weight individual electron and photon beamlets. In addition, the specific location of the photon beamlets is of interest in relation to the target volume. The focus of the photon beamlets was determined to be within the perimeter of the target volume. The role of the photon beamlets appears to be for sharping the dose gradient surrounding the target volume. This is interesting as it is a 3D application to a previous study by Korevaar *et al* [44] which combined photon fields with electron fields to sharpen the penumbra of electron profiles with depth. A study by Das *et al* [39] concluded that the role of electrons and photons in

MBRT varied by treatment site and that further investigations are required to establish a definitive conclusion.

Practical considerations of clinical MBRT, such as number of isocenters and patient setup, have yet to be investigated and discussed. Despite excellent improvement in the clinical case, the absence of a larger dataset of MBRT patient plans limits the predictive power of this comparison. The quality of the MERT and MBRT plan is likely influenced by a series of patient-specific parameters. In the case of FLEC-based MERT, target size is an important factor while target depth is an important factor for MERT in general. For the sarcoma case, the dosimetric cost of additional photon beams was likely diminished due to the convex geometry of the area of interest. Photon beams directed towards the center of the patient body would contain a higher dosimetric cost to the organs at risk and body dose. Future MBRT studies could investigate the pairing of suitable FLEC-based MERT combined with linac-based VMAT.

8.5 Conclusions

This study examined a new technique and optimization code called FDAO for the development of FLEC-based MERT plans. The FDAO benchmarking example using a simplified electron beam model produced a competitive FLEC-based MERT plan in comparison to HT, VMAT and IMRT. The example demonstrated that FDAO can reduce the number of beamlets to a deliverable level and reduce the dose to the OAR over previous FLEC-based optimization without compromise to the target coverage. MERT target coverage was not as conformal as the clinical

systems. This was likely a side effect of large electron beamlets in comparison to the small photon beamlets utilized in photon plan optimization.

A clinical FDAO MERT plan was created and benchmarked against clinical electron and photon planning systems to illustrate its merit. The MERT plan was competitive in its ability to reduce dose to organs at risk and internal dose; however, the plan suffered from poorer target conformality in comparison with the photon planning techniques.

For the application of clinical FLEC-based MERT, target coverage may supersede the benefits associated to OAR sparing. Under these conditions we have shown that target coverage can be improved with a limited number of photon fields. The MBRT plan shown in this study combined the best target coverage with the greatest amount of OAR sparing with only a slight increase in the low dose isodose volume compared with the MERT plan. The plan represents the first generation of simultaneous electron and photon beamlets optimization for the creation of FLEC-based MBRT.

8.6 Acknowledgments

The authors thank Tanner Connell at McGill University for providing us with commissioned BEAMnrc electron models and Dr. Elaine Conneely at the National University of Ireland for providing us with a commissioned BEAMnrc 6 MV photon model. Financial support from The Terry Fox Foundation Strategic Initiative for Excellence in Radiation Research for the 21st Century (EIRR21) at CIHR. Work was partially supported by NSERC RG-PIN 298191.

8.7 References

[1] S Hyödynmaa, A Gustafsson, and A Brahme. Optimization of conformal electron beam therapy using energy- and fluence-modulated beams. *Med. Phys.*, 23(5):659–666, 1996.

[2] C M Ma, T Pawlicki, M C Lee, S B Jiang, J S Li, J Deng, B Yi, E Mok, and A L Boyer. Energy- and intensity-modulated electron beams for radiotherapy. *Phys. Med. Biol.*, 45(8):2293–2311, 2000.

[3] M Blomquist, M G Karlsson, B Zackrisson, and M Karlsson. Multileaf collimation of electrons–clinical effects on electron energy modulation and mixed beam therapy depending on treatment head design. *Phys. Med. Biol.*, 47(7):1013–1024, 2002.

[4] M C Lee, J Deng, J Li, S B Jiang, and C M Ma. Monte carlo based treatment planning for modulated electron beam radiation therapy. *Phys. Med. Biol.*, 46(8):2177–2199, 2001.

[5] E P Lief, A Larsson, and J L Humm. Electron dose profile shaping by modulation of a scanning elementary beam. *Med. Phys.*, 23(1):33–44, 1996.

[6] B Zackrisson and M Karlsson. Matching of electron beams for conformal therapy of target volumes at moderate depths. *Radiother. Oncol.*, 39(3):261–270, 1996.

[7] M Asell, S Hyödynmaa, S Söderström, and A Brahme. Optimal electron and combined electron and photon therapy in the phase space of complication-free cure. *Phys. Med. Biol.*, 44(1):235–252, 1999.

[8] L Olofsson, X Mu, S Nill, U Oelfke, B Zackrisson, and M Karlsson. Intensity modulated radiation therapy with electrons using algorithm based energy/range selection methods. *Radiother. Oncol.*, 73(2):223–231, 2004.

[9] D D Leavitt, J R Stewart, J H Moeller, and W L Lee. Electron arc therapy: design, implementation and evaluation of a dynamic multi-vane collimator system. *Int. J. Radiat. Oncol. Biol. Phys.*, 17(5):1089–1094, 1989.

[10] E E Klein, Z Li, and D A Low. Feasibility study of multileaf collimated electrons with a scattering foil based accelerator. *Radiother. Oncol.*, 41(2):189–196, November 1996.

[11] M A Ebert and P W Hoban. Possibilities for tailoring dose distributions through the manipulation of electron beam characteristics. *Phys. Med. Biol.*, 42(11):2065–2081, 1997.

[12] M G Karlsson, M Karlsson, and C Ma. Treatment head design for multileaf collimated high-energy electrons. *Med. Phys.*, 26(10):2161–2167, 1999.

[13] M C Lee, S B Jiang, and C M Ma. Monte Carlo and experimental investigations of multileaf collimated electron beams for modulated electron radiation therapy. *Med. Phys.*, 27(12):2708–2718, 2000.

[14] J Deng, M C Lee, and C M Ma. A Monte Carlo investigation of fluence profiles collimated by an electron specific MLC during beam delivery for modulated electron radiation therapy. *Med. Phys.*, 29(11):2472–2483, 2002.

[15] K R Hogstrom, R A Boyd, J A Antolak, M M Svatos, B A Faddegon, and J G Rosenman. Dosimetry of a prototype retractable eMLC for fixed-beam electron therapy. *Med. Phys.*, 31(3):443–462, Mar 2004.

[16] K Al-Yahya, M Schwartz, G Shenouda, F Verhaegen, and J Seuntjens. Energy modulated electron therapy using a few leaf electron collimator in combination with IMRT and 3D-CRT: Monte Carlo-based planning and dosimetric evaluation. *Med. Phys.*, 32(9):2976–2986, 2005.

[17] K Al-Yahya, D Hristov, F Verhaegen, and J Seuntjens. Monte carlo based modulated electron beam treatment planning using a few-leaf electron collimator—feasibility study. *Phys. Med. Biol.*, 50(5):847–857, 2005.

[18] L Olofsson, M G Karlsson, and M Karlsson. Effects on electron beam penumbra using the photon MLC to reduce bremsstrahlung leakage for an add-on electron MLC. *Phys. Med. Biol.*, 50(6):1191–1203, 2005.

[19] L Olofsson, M G Karlsson, and M Karlsson. Photon and electron collimator effects on electron output and abutting segments in energy modulated electron therapy. *Med. Phys.*, 32(10):3178–3184, 2005.

[20] F C P du Plessis, A Leal, S Stathakis, W Xiong, and C-M Ma. Characterization of megavoltage electron beams delivered through a photon multi-leaf collimator (pMLC). *Phys. Med. Biol.*, 51(8):2113–2129, 2006.

[21] T Gauer, D Albers, F Cremers, R Harmansa, R Pellegrini, and R Schmidt. Design of a computer-controlled multileaf collimator for advanced electron radiotherapy. *Phys. Med. Biol.*, 51(23):5987–6003, 2006.

[22] K Al-Yahya, F Verhaegen, and J Seuntjens. Design and dosimetry of a few leaf electron collimator for energy modulated electron therapy. *Med. Phys.*, 34(12):4782–4791, 2007.

[23] T Vatanen, E Traneus, and T Lahtinen. Dosimetric verification of a Monte

Carlo electron beam model for an add-on eMLC. *Phys. Med. Biol.*, 53(2):391–404, January 2008.

[24] T Gauer, J Sokoll, F Cremers, R Harmansa, M Luzzara, and R Schmidt. Characterization of an add-on multileaf collimator for electron beam therapy. *Phys. Med. Biol.*, 53(4):1071–1085, 2008.

[25] E E Klein, M Vicic, C Ma, D A Low, and R E Drzymala. Validation of calculations for electrons modulated with conventional photon multileaf collimators. *Phys. Med. Biol.*, 53(5):1183–1208, 2008.

[26] L Jin, C-M Ma, J Fan, A Eldib, R A Price, L Chen, L Wang, Z Chi, Q Xu, M Sherif, and J S Li. Dosimetric verification of modulated electron radiotherapy delivered using a photon multileaf collimator for intact breasts. *Phys. Med. Biol.*, 53(21):6009–6025, 2008.

[27] E E Klein, M Mamalui-Hunter, and D A Low. Delivery of modulated electron beams with conventional photon multi-leaf collimators. *Phys. Med. Biol.*, 54(2):327–339, 2009.

[28] T Vatanen, E Traneus, and T Lahtinen. Enhancement of electron-beam surface dose with an electron multi-leaf collimator (eMLC): a feasibility study. *Phys. Med. Biol.*, 54(8):2407–2419, 2009.

[29] J Mihaljevic, M Soukup, O Dohm, and M Alber. Monte Carlo simulation of small electron fields collimated by the integrated photon MLC. *Phys. Med. Biol.*, 56(3):829–843, 2011.

[30] T P O'Shea, Y Ge, M J Foley, and B A Faddegon. Characterization of an extendable multi-leaf collimator for clinical electron beams. *Phys. Med. Biol.*,

56(23):7621–7638, 2011.

[31] T Connell, A Alexander, M Evans, and J Seuntjens. An experimental feasibility study on the use of scattering foil free beams for modulated electron radiotherapy. *Phys. Med. Biol.*, 57:1–15, 2011.

[32] E Klein. Modulated electron beams using multi-segmented multileaf collimation. *Radiother. Oncol.*, 48:307–311, 1998.

[33] K Engel and T Gauer. A dose optimization method for electron radiotherapy using randomized aperture beams. *Phys. Med. Biol.*, 54(17):5253–5270, 2009.

[34] F J Salguero, B Palma, R Arrans, J Rosello, and A Leal. Modulated electron radiotherapy treatment planning using a photon multileaf collimator for post-mastectomized chest walls. *Radiother. Oncol.*, 93(3):625–632, 2009.

[35] A Alexander, F DeBlois, and Jan Seuntjens. Toward automatic field selection and planning using monte carlo-based direct aperture optimization in modulated electron radiotherapy. *Phys. Med. Biol.*, 55(16):4563–4576, 2010.

[36] F J Salguero, R Arráns, B A Palma, and A Leal. Intensity- and energy-modulated electron radiotherapy by means of an xMLC for head and neck shallow tumors. *Phys. Med. Biol.*, 55(5):1413–1427, 2010.

[37] M Surucu, E E Klein, M Mamalui-Hunter, D B Mansur, and D A Low. Planning tools for modulated electron radiotherapy. *Med. Phys.*, 37(5):2215–2224, 2010.

[38] C M Ma, M Ding, J S Li, M C Lee, T Pawlicki, and J Deng. A comparative dosimetric study on tangential photon beams, intensity-modulated radiation therapy (IMRT) and modulated electron radiotherapy (MERT) for breast

cancer treatment. *Phys. Med. Biol.*, 48(7):909–924, 2003.

[39] S K Das, M Bell, L B Marks, and J G Rosenman. A preliminary study of the role of modulated electron beams in intensity modulated radiotherapy, using automated beam orientation and modality selection. *Int. J. Radiat. Oncol. Biol. Phys.*, 59(2):602–617, June 2004.

[40] T Gauer, K Engel, A Kiesel, and D Albers. Comparison of electron IMRT to helical photon IMRT and conventional photon irradiation for treatment of breast and chest wall tumours. *Radiother. Oncol.*, 94(3):313–318, 2010.

[41] A Alexander, E Soisson, T Hijal, A Sarfehnia, and J Seuntjens. Comparison of modulated electron radiotherapy to conventional electron boost irradiation and volumetric modulated photon arc therapy for treatment of tumour bed boost in breast cancer. *Radiother. Oncol.*, 100(2):253–258, 2011.

[42] R Weinberg, J Antolak, G Starkschall, R Kudchadker, and K Hogstrom. Electron intensity modulation for mixed-beam radiation therapy with an x-ray multi-leaf collimator. In *AAPM Annual Meeting Program*, page 2985. Med. Phys., AAPM, June 2008.

[43] T Jansson, H Lindman, K Nygård, C V Dahlgren, A Montelius, C Oberg-Kreuger, S Asplund, and J Bergh. Radiotherapy of breast cancer after breast-conserving surgery: an improved technique using mixed electron-photon beams with a multileaf collimator. *Radiother. Oncol.*, 46(1):83–89, 1998.

[44] EW Korevaar and BJM Heijmen. Mixing intensity modulated electron and photon beams: combining a steep dose fall-off at depth with sharp and depth-independent penumbras and flat beam profiles. *Phys. Med. Biol.*, 44,

1999.

[45] J G Li, L Xing, A L Boyer, R J Hamilton, D R Spelbring, and J V Turian. Matching photon and electron fields with dynamic intensity modulation. *Med. Phys.*, 26(11):2379–2384, November 1999.

[46] B Faddegon, M Svatos, M Karlsson, L Olofsson, and J Antolack. Treatment head design for mixed beam therapy. In *AAPM Annual Meeting, Montreal, Canada*, volume 29, page 1285. AAPM, 2002.

[47] X Mu, L Olofsson, M Karlsson, R Sjögren, and B Zackrisson. Can photon IMRT be improved by combination with mixed electron and photon techniques? *Acta. Oncol.*, 43(8):727–735, 2004.

[48] M F Chan, Y Song, and C Burman. The Treatment of Extensive Scalp Lesions Combining Electrons with Intensity-Modulated Photons. *Int. Conf. of the IEEE Engineering in Medicine and Biology Society*, 1:152–155, 2006.

[49] J Krayenbuehl, S Oertel, J Davis, and I Ciernik. Combined photon and electron three-dimensional conformal versus intensity-modulated radiotherapy with integrated boost for adjuvant treatment of malignant pleural mesothelioma after pleuropneumonectomy. *Int. J. Radiat. Oncol. Biol. Phys.*, 69(5):1593–1599, 2007.

[50] Y Ge and B A Faddegon. Study of intensity-modulated photon-electron radiation therapy using digital phantoms. *Phys. Med. Biol.*, 56(20):6693–6708, 2011.

[51] M Earl, M Afghan, C Yu, and Z Jiang. Jaws-only imrt using direct aperture optimization. *Med. Phys.*, 34(1):307–314, 2007.

[52] D M Shepard, M A Earl, X A Li, S Naqvi, and C Yu. Direct aperture optimization: a turnkey solution for step-and-shoot IMRT. *Med. Phys.*, 29(6):1007–1018, 2002.

[53] I B Mihaylov and J V Siebers. Evaluation of dose prediction errors and optimization convergence errors of deliverable-based head-and-neck IMRT plans computed with a superposition/convolution dose algorithm. *Med. Phys.*, 35(8):3722–3727, 2008.

[54] A Alexander, F Deblois, G Stroian, K Al-Yahya, E Heath, and J Seuntjens. MMCTP: a radiotherapy research environment for Monte Carlo and patient-specific treatment planning. *Phys. Med. Biol.*, 52(13):N297–308, 2007.

[55] D W O Rogers, B A Faddegon, G X Ding, C M Ma, J We, and T R Mackie. BEAM: A Monte Carlo code to simulate radiotherapy treatment units. *Med. Phys.*, 22(5):503–524, 1995.

[56] B Walters, I Kawrakow, and D.W.O Rogers. DOSXYZnrc Users Manual. *NRC Report PIRS 794*, Jun 2007.

[57] S Kirkpatrick, C Gelati, and M Vecchi. Study of intensity-modulated photon-electron radiation therapy using digital phantoms. *Science*, 220(4598):671–680, 1983.

[58] J Last. A stand-alone software system to calculate output factors for arbitrarily shaped inserts with monte carlo technique. Master's thesis, McGill University, 2008.

[59] A Alexander, M Renaud, and J Seuntjens. All-Inclusive DOSXYZnrc Source for Monte Carlo QA of External Beam Radiotherapy. In *AAPM 2011 Meeting*

Program (Vancouver, Canada), pages SU–D–BRB–3. Med. Phys., 2011.

[60] X Mu, T Björk-Eriksson, S Nill, U Oelfke, K Johansson, G Gagliardi, L Johansson, M Karlsson, and B Zackrisson. Does electron and proton therapy reduce the risk of radiation induced cancer after spinal irradiation for childhood medulloblastoma? a comparative treatment planning study. *Acta Oncol*, 44(6):554–562, 2005.

[61] L Widesott, A Pierelli, C Fiorino, I Delloca, S Broggi, G M Cattaneo, N D Muzio, F Fazio, R Calandrino, and M Schwarz. Intensity-modulated proton therapy versus helical tomotherapy in nasopharynx cancer: planning comparison and NTCP evaluation. *Int. J. Radiat. Oncol. Biol. Phys.*, 72(2):589–596, 2008.

[62] A Fogliata, S Yartsev, G Nicolini, A Clivio, E Vanetti, R Wyttenbach, G Bauman, and L Cozzi. On the performances of Intensity Modulated Protons, RapidArc and Helical Tomotherapy for selected paediatric cases. *Radiat. Oncol.*, 4(2):1–19, 2009.

CHAPTER 9
Conclusions

Contents

The main issues that have been addressed have surrounded the development of an advanced, research based, Monte Carlo treatment planning system for re-calculation studies and modulated electron radiotherapy. The MMCTP software environment provides researchers with a flexible framework for treatment planning, Monte Carlo dose calculation and dose evaluation studies. A modulated electron radiotherapy toolkit was successfully incorporated into MMCTP to advance the development of MERT at McGill University. We interfaced three inverse optimization algorithms within MMCTP for the generation of high quality MERT and mixed beam photon and electron plans. We proposed various planning techniques and time saving measures for automated MERT planning. We developed the FLEC linac override control software for the delivery of MERT fields. We proposed a method to combine FLEC-based MERT plans with photon beamlets for mixed beam therapy. We have demonstrated through planning studies and comparisons

with alternative treatment modalities that FLEC-based MERT plans contain inherent advantages to direct electron therapy and advanced photon therapy modalities. Specifically, FLEC-based MERT has been shown to increase target homogeneity for shallow target sites and reduce the integral body dose.

9.1 MMCTP

The MMCTP system allows for Monte Carlo treatment planning, outcome analysis and future research implementations. The system processes DICOM patient data and converts the data into an internal file format. The format is flexible and allows for modern planning techniques such as volumetric modulated arc therapy. Three Monte Carlo codes have been incorporated into MMCTP to streamline the generation, transfer, and submission of input files. Input files can be edited within MMCTP to tweak simulation parameters. The CT images are converted to mass density and material data for DOSXYZnrc and XVMC Monte Carlo codes. MMCTP contains an internal queuing system and logic scripts to handle large scale Monte Carlo simulations on multiple hosts. The system is autonomous and flexible with a hierarchy of user interfaces to meet the needs of basic clinical users as well as advanced researchers.

A version of MMCTP is installed within the Department of Radiation Oncology at the McGill University Health Centre. The system is capable of calculating a wide array of treatment techniques and machines. This includes Varian CL21EX accelerators from electron cutout fields to photon RapidArc fields, Siemens conformal photon therapy and TomoTherapy. MMCTP has been the topic or been discussed in over 23 international conference presentations. We

have hosted an international MMCTP users course at McGill University to teach users on the features and uses of MMCTP, with the hope that the community will contribute to the future development of this advanced treatment planning software.

9.2 MERT and Inverse Planning within MMCTP

A large number of features were added to MMCTP to enable inverse optimization. These features ease the process of creating quality plans and can be divided into three groups: beam setup, inverse optimization, and optimization results. Beam setup provides the user with an interface to generate and choose ideal beam incidence angles based on the target geometry and external body contour. Subsequently, field size setup provides the user with options on the size of the subfields. Subfields can be generated from a raster pattern for photon beams or based on the target depth for electron beams. Inverse optimization provides the user with an interface to control the three optimization algorithms linked to MMCTP. Parameters such as the dose volume constraints, number of iterations and cooling rate are within the users control. The output of the optimization runs are piped back into MMCTP for analysis. Optimization results can be saved within a database file for DVH comparisons between competing plans. In addition, the database file contains the optimization input file used to create the plan. It is important to save these input files as initial conditions affect the outcome. In addition, this allows us to create a Pareto surface of optimal solutions to visualize the clinical trade-offs between optimal plans with various specified clinical goal criteria. A database to store plans and accompanying software to compare plans is a powerful feature in itself, which has yet to become available in the majority of commercial treatment

planning systems. The planning tools have allowed us to fine tune the planning process and meticulously compare the influence of initial beam placement and subfield parameters on the final optimization results.

The inverse planning tools within MMCTP are extremely useful and were used extensively for the generation of MERT plans within this work. The tools are general enough to allow for the creation of photon beamlets for inverse photon optimization and for the creation of mixed beam photon and electron plan optimization.

9.3 MERT Planning Techniques

We investigated three inverse MERT planning techniques. The feathered field technique was shown to improve overall plan quality versus raster fields. Subsequently, the dynamic jaw technique was shown to further improve plan quality and reduce the number of treatment fields. These planning techniques are integrated into MMCTP to streamline the generation of MERT fields, MERT field dose calculation and MERT optimization. The MERT planning techniques developed here will help shape the policies for automated MERT planning at McGill University.

9.4 FLEC-Based MERT Plans

We investigated MERT plan quality in comparison studies for three treatment sites. The first of which was spinal irradiation where we demonstrated a dosimetric advantage in organ at risk sparing versus helical TomoTherapy. A sequential study examined plan quality and reproducibility for breast boost irradiation. The study compared FLEC-based MERT to direct electron and 6 MV photon VMAT. In an

overall comparison of all three modalities, MERT produced the best plans in terms of target coverage, homogeneity, and integral dose. Although, geometric properties of the target volume and body contour, in conjunction with the selection of available electron energies, were shown to influence the quality of the MERT plan. The final study compared MERT plan quality to direct electron, photon IMRT and VMAT for a head and neck sarcoma irradiation. The MERT plan was considerably better in sparing of total healthy tissue, however the cost was inferior target homogeneity. With the addition of two tangential photon fields the MERT sarcoma plan drastically improved in terms of target coverage without cost to the organ at risk sparing. The MERT plans developed here are clinically acceptable and provide dosimetric alternatives to the standard properties of inverse photon plans. The success of these MERT plans warrants the continued development of MERT for the eventual realization of a new niche modality in clinical radiation therapy.

9.5 FLEC Control Software

The FLOC program ties together the MMCTP-MERT optimized fields, the FLEC, the FLEC 4 axis controller, and the linac. The program greatly reduces the tedious task of setting field sizes, beam energies or the number of monitor units. In addition to the MERT sequence file, the FLOC program can be used interactively to drive the FLEC for use under the radiation field or for quality assurance measurements of the collimator leaves. The FLOC program meets the needs of FLEC-based step and shoot delivery and is flexible enough to support more advanced delivery techniques such as dynamic deliveries.

9.6 Outlook and Future Work

Further improvements and developments are required before FLEC-based MERT becomes realized. Despite our advances in FLEC-based MERT planning and the FLEC controller software, the FLEC itself requires additional research for encoder alternatives. The inability to use the FLEC under radiation has hindered the progress in the development of QC procedures for FLEC-based MERT plans. The original encoders were never designed for exposure to ionizing radiation. Their technology included a MOSFET transistor which failed after the first irradaition. Although not confirmed, it is expected that the lethal dose to these encoders was less than 1 Gy. Prior to clinical use the MERT plans will require extensive validation studies. Anthropomorphic phantoms would be ideal for these studies where detectors can be placed within for *in vivo* measurements. The anthropomorphic phantoms would provide end-to-end testing of MERT planning and delivery.

Additional improvements could be investigated on the planning side. The dose calculation time is currently one bottleneck for large scale MERT planning. A fast macro-MC technique could provide an acceptable balance between accuracy and speed to improve the planning process. The optimization algorithms can also be parallelized or ported over to a GPU-based platform. Treatment time or total number of electron beamlets could be incorporated as a parameter to the cost optimization function. The delivery time could also be decreased with optimization on the beamlet chronological sequence to minimize time between beamlet positioning. Dynamic delivery of beamlet sequences similar to photon

sliding window could be investigated. Lastly, the FLEC holder, which is currently a 15×15 cm^2 electron applicator, could be redesigned to add flexibility for arc deliveries with a retractable FLEC.

Appendix A
FLEC linac override control software (FLOC)

FLEC linac override control software (FLOC)

The following technical note describes the flew leaf electron collimator (FLEC) controller. The controller consists of the motorized FLEC, a PIII CPU PC equipped with a National Instruments (NI) (National Instruments, Austin, TX) PCI-7330 controller board connected to a NI MID-7604 integrated four axis controller, NI-Motion libraries, a KVM (Keyboard, Video, and Mouse) switch and the C++ FLEC control program called FLOC (FLEC linac override control). The PC, NI controller and KVM switch are visible in figure 9–1, while the FLEC is visible in figure 9–2.

FLOC Introduction

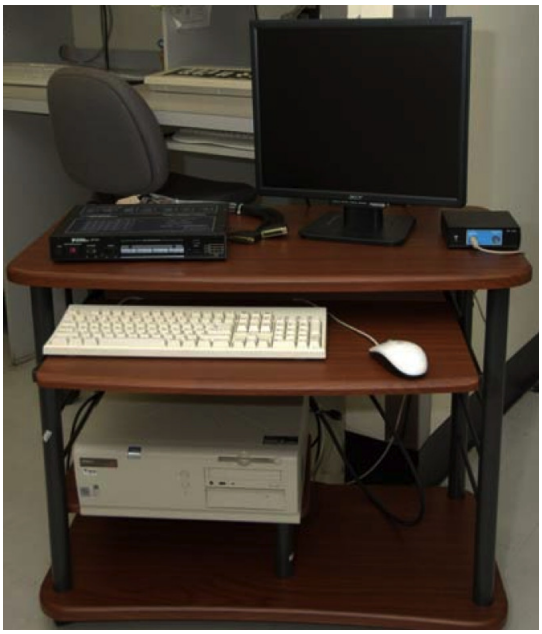

Figure 9–1: FLEC controller consists of a PC, national instrument four axis controller and a KVM switch [1].

The FLEC allows us to collimate electron fields at 95 cm SAD for the application of modulated electron radiotherapy (MERT). However, a typical

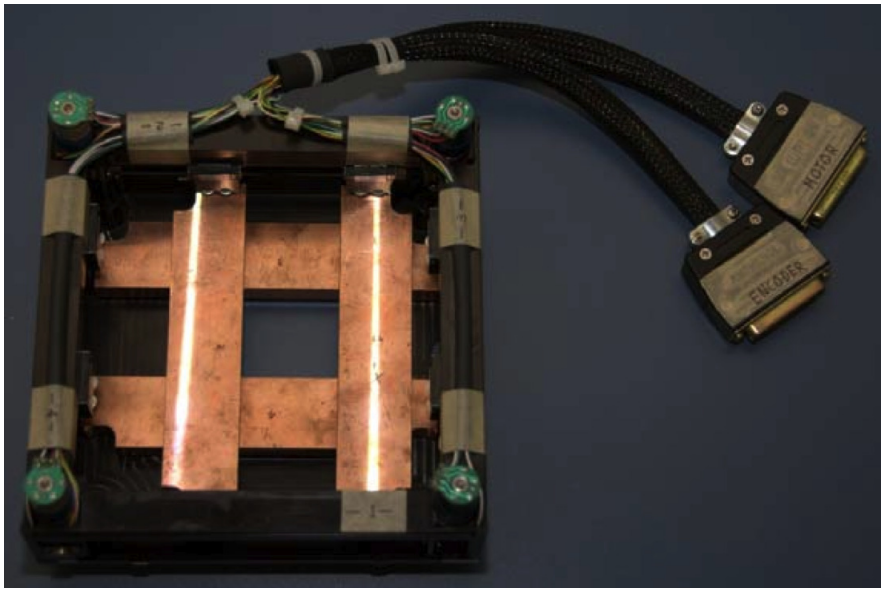

Figure 9–2: Motorized FLEC with connections to the NI MID-7604 integrated four axis controller [1].

MERT plan may consist of many electron fields, which sets the requirement for a dynamic electron collimator. As such, the FLEC has been outfitted with stepper motors to enable automatic FLEC motion. The FLEC consists of four copper leaves, where each leaf is attached to a drive screw. The drive screws are driven by stepper motors connected through right angled gearheads and monitored by encoders attached to the drive screw. The ends of the drive screw contain limit switches. A CAD view of the FLEC and these devices is shown in figure 9–3. Communications between the FLEC and the NI controller are carried through shielded cables that run from the treatment room to the console area. Communication with the linac is through the KVM switch that is connected to the console's keyboard. Controlling the linac through keyboard stokes is not ideal as it does not allow for information to pass back from the linac to the control program. However, it allows the control of the linac with minimal modifications to the clinical system. Input and output feedback from these devices are handled within the NI controller or KVM switch and processed within the FLOC program.

The FLOC program contains the logic and motion control settings used to move the FLEC leaves and linac settings. FLOC is a command line interface program, written within Microsoft Visual C++ version 6.0. The program workspace consists of a main C++ file, which is currently 1500 lines of code, with references

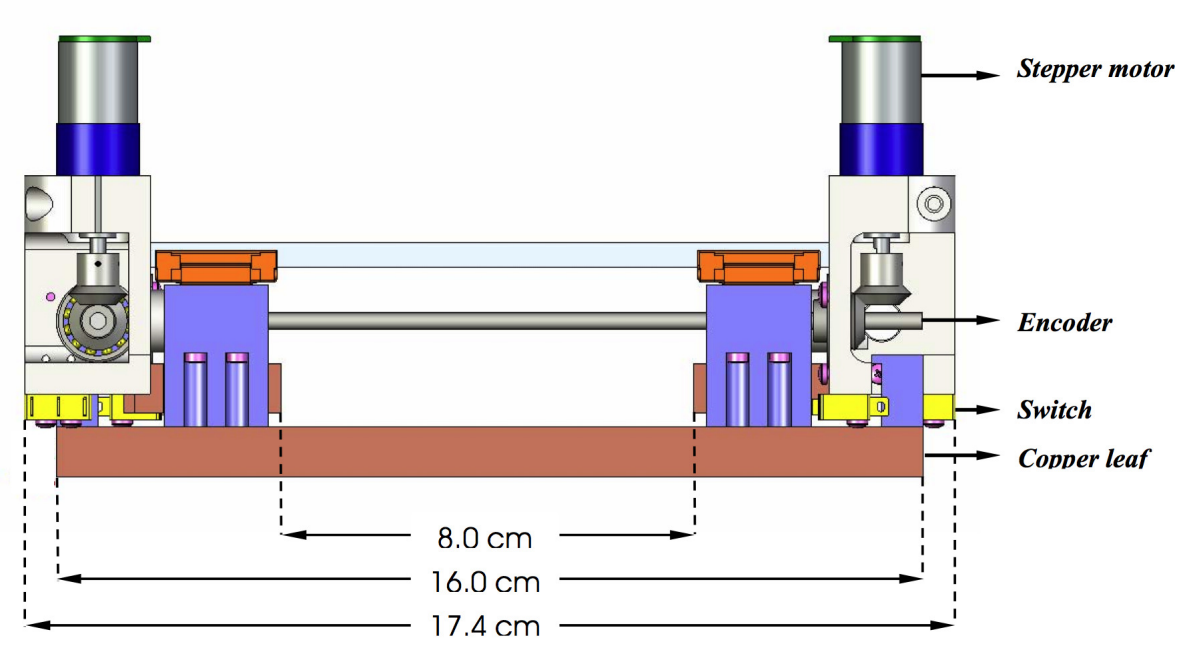

Figure 9–3: CAD design drawing for side view of FLEC

to flecmotn and standard libraries. The FLOC program is divided into three main sections: FLEC properties, Field settings, and FLEC plan sequence. Each section is described below.

FLEC Properties

The FLEC properties section allows the user to run an initialization test on the device. The user is required to initialize the device after a system restart, if the FLEC is disconnected or if the system has detected a fault on an axis. The initialization process sets the controller to a known state based on predefined configuration settings stored within a file. The initialization parameters include attributes such as, the axis configuration, which map DAC resources to an axis and configures the axes for servo or stepper control, motor type, limit switch polarity, maximum velocities, etc. After initialization, the program checks for modal errors with a call to read the status of the Communication Status Register (CSR) on the NI-7330 board. The second test within FLEC properties is labelled as "Find Home". This test can be run on all axis or individually. The goal of the test is to find the home position, which represents the fully retracted position of the leaf. The test establishes a repeatable reference position for the motion system. The home position is identified by activation of the limit switch. The limit

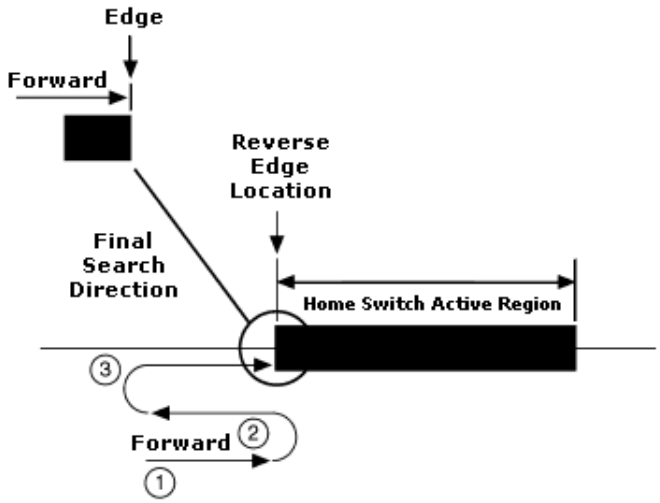

Figure 9–4: Find home sequence for the forward direction (1). When the home input is found, the reverse edge (2) is located. When the reverse edge is located, the edge is approached in the forward direction (3). [2]

switch is a closed loop contact device, which upon activation, opens the contact loop. Initiating the home search begins a sequence of events, which are illustrated in figure 9–4. Following the home search, an axis offset is applied. The offset, which is unique to each axis, moves the leaf to the absolute correct position of the retracted 4 cm from central axis position. This new position, which will have an associated reference position, is now initialized to zero. Due to the complexity of this sequence, the test may fail in its ability to identify the edge of the home switch. The test may fail due to erratic triggering of the limit switch, or due to the chosen velocity of the leaf motion. If the test fails repeatedly, the limit switch signal should be examined.

The offset positions used for each axis are currently hard coded into FLOC. These offsets were determined with the aid of high precision calipers. In addition to these position offsets, the number of encoder steps per millimetre was measured and is currently hard coded to 2708 steps/mm. Ideally these values would be tested routinely within a semi-automated FLOC quality control (QC) test and updated within the FLEC properties. The QC method would require the user to perform a series of caliper measurements at set leaf positions. The method used to obtain the current values was performed external to the FLEC properties section

of FLOC. In an overall evaluation of absolute FLEC positioning and positioning reproducibility, we can safely report an uncertainty of less than 0.5 mm.

Field Settings

The field settings section allows the user to move the FLEC leaves to a defined location. This section provides the user with complete control over the FLEC leaves and would be useful for QA measurements or FLEC motion testing. The section begins with an option to "Move Field" or "Move Axis". "Move Field" will move an axis x or y to a symmetric value entered by the user. "Move Axis" will move a specific axis by a value entered by the user. Once an axis is selected for movement, the program prompts the user for a new position in mm. The new position is checked to ensure a collision will not occur with the corresponding leaf. If the position is accepted, FLOC sets up the trajectory for motion with calls to load operation mode, s-curve, acceleration, velocity, target position, and finally, start motion. While the axis is in motion, a feedback loop updates the live position of the axis and checks for model errors. If an error is detected, FLOC sends a command to kill all motion. Move axis will move one axis at a time, while move field will move two axes simultaneously. Simultaneous motion of the X or Y field requires additional checks to ensure both axes move at the same speed such that one axis does not collide into the other during motion.

The coordinate system of the FLEC is similar to the linac with leaf travel beyond the central axis reported as a negative position. The "Move Field" option will assume a positive value and the corresponding leaf positions will be moved to half of the field value. An asymmetric field can only be defined by moving individual axes. During "Move Axis", the user may enter a positive or negative value to define an arbitrary field.

FLEC Plan Sequence

The FLEC plan sequence section is for the automated delivery of MERT fields. Unlike the previous two sections of FLOC, this section interacts with other moving components in the linac through the use of the KVM switch. The section begins with a request for a beamlet file. The beamlet files are generated within MMCTP upon completion of an optimization run. FLOC will browse a local directory housing beamlet sequence files; the user selects the correct file to load. An example file is shown in figure 9–5. Once selected, FLOC will read-in the file and generate an array of beamlet sequences. MERT beamlets, which share the same X and Y field settings, are grouped into a fieldlet. Each fieldlet is checked to ensure that the positions do not exceed the limits of the FLEC, that the positions do not cause a collision, and that the field widths are above the tolerance opening of 2 mm. If the file passes read-in checks, the sequence is ready for delivery.

```
NumberOfFieldlets=6
40., -20., 10., 10., 4.5, -1.5, 1.5, 1.5 - 16 MeV(12), 20 MeV(13)
30., -10., 10., 10., 3.5, -0.5, 1.5, 1.5 - 6 MeV(6)
25., -5., 10., 10., 3., 0., 1.5, 1.5 - 9 MeV(34), 16 MeV(4)
20., 0., 10., 10., 2.5, 0.5, 1.5, 1.5 - 16 MeV(67), 20 MeV(3)
15., 5., 10., 10., 2., 1., 1.5, 1.5 - 16 MeV(4), 20 MeV(2)
10., 10., 10., 10., 1.5, 1.5, 1.5, 1.5 - 20 MeV(8)
```

Figure 9–5: Example FLOC beamlet text file exported from MMCTP. The number of fieldlets represents the number of unique openings. The format of the file is FLEC $X1$, $X2$, $Y1$, $Y2$ in mm followed by linac jaw $X1$, $X2$, $Y1$, $Y2$ in cm followed by the linac electron energy and in brackets the number of MUs.

Delivery requires initialization of the KVM switch and constant flushing of stdin (standard input stream) to remove padded strings. The first command moves the linac jaws to the correct location. As there is no feedback from the KVM switch, the user is required to press "enter" when the jaws have finished moving. When complete, FLOC will proceed to move the FLEC jaws. Once all jaws have been positioned, FLOC will initialize the linac to the correct beam energy, number of monitor units, and prompt the user for an "enter" command to begin treatment after these settings have been made. Lastly, the user is again required to press "enter" once the treatment has finished. For the current fieldlet position, FLOC will loop through all energies. The process is then repeated for all fieldlets.

Application

The FLOC program has yet to be used during the delivery of an optimized MERT treatment plan, due to an unforeseen design flaw with the FLEC position feedback encoders. The technology within these encoders contained MOSFET switches, which are known to be radiation sensitive. The encoders were damaged during the first exposure to radiation. However, due to the extremely stringent design of the FLEC, we have not been able to find a suitable BJT (bipolar junction transistor) type encoder, which fits within the FLEC structure. Efforts are now ongoing to develop a potentiometer feedback mechanism to monitor the steps of the FLEC drive screws. Alternatively, the FLOC program could be modified to operate in "open loop mode", which eliminates the requirement of a position feedback signal. These modifications would be straight-forward and would allow for immediate use of the FLEC, albeit in a less precise mode.

Conclusion

The FLOC program ties together the MMCTP optimized beamlets, the FLEC, and the linac settings. The program greatly reduces the tedious task of setting field sizes, beam energies or the number of monitor units. Despite its ability to set fields sizes, the program is not autonomous and requires the user to "push" FLOC from task to task in the delivery of a beamlet sequence file. Efforts can be made to incorporate a linac feedback mechanism to FLOC with the current Varian CL21EX accelerators; however, recent Varian accelerators such as TrueBeam, offer the end-user a developer mode to enable user-specific deliveries. This mode empowers clinical physicists and researchers with an elegant method to test new treatment and imaging techniques. The FLOC could be modified to communicate with the developer mode of TrueBeam to truly test the delivery efficiency of FLEC-based MERT beamlets.

References

[1] K Al-Yahya. *Energy modulated electron therapy: design, implementation, and evaluation of a novel method of treatment planning and delivery.* PhD thesis, Physics Department – McGill University, Montreal, Quebec, Canada, 2007.

[2] National Instruments Corporation. *NI Motion Function Help*, 6.0 edition, 2003.

List of Abbreviations and Symbols

2D: Two Dimensional

3D: Three Dimensional

AAPM: American Association of Physicists in Medicine

BJT: Bipolar Junction Transistor

CM: Component Module (BEAMnrc)

CPU: Central Processing Unit

CRT: Conformal Radiation Therapy

CS: Convolution Superposition

CSI: Cranio Spinal Irradiation

CT: Computerized Tomography

CTV: Clinical Target Volume

$D_{2\%}$: Dose received by 2% of the volume

$D_{90\%}$: Dose received by 90% of the volume

$D_{95\%}$: Dose received by 95% of the volume

$D_{98\%}$: Dose received by 98% of the volume

D_{max}: Maximum dose received by volume

D_{mean}: Mean dose received by volume

D_{min}: Minimum dose received by volume

DAC: Digital-to-Analog Converter

DAO: Direct Aperture Optimization

DBS: Directional Bremsstrahlung Splitting

DDC: Dose Deposition Coefficient

DE: Direct Electron

DEV: Dose Evaluation Volume

DICOM RT: DICOM with extensions for radiation therapy

DICOM: Digital Imaging and Communications in Medicine

DJO: Dynamic Jaw Optimization

DMX: Density Matrix

DNA: Deoxyribonucleic Acid

DPE: Dose Prescription Error

DVH: Dose Volume Histogram

ECUT: Electron cutoff energy

EMET: Energy Modulated Electron Therapy

FLEC: Few Leaf Electron Collimator

FLOC: FLEC Linac Override Control

GPU: Graphical Processing Unit

GTV: Gross Tumour Volume

GUI: Graphical User Interface

HN: Head and Neck

HU: Hounsfield Unit

ICRU: International Commission on Radiation Units

IMRT: Intensity Modulated Radiotherapy

KVM: Keyboard Video Mouse

Linac: Linear accelerator

MBRT: Mixed Beam Radiotherapy

MC: Monte Carlo

MCO: Multi-criteria Optimization

MCTP: Monte Carlo Treatment Planning

MERT: Modulated Electron Radiotherapy

MeV: Megaelectron volt

MLC: Multi-leaf Collimator

MMCTP: McGill Monte Carlo Treatment Planning software package

MOSFET: Metal Oxide Semiconductor Field-Effect Transistor

MRI: Magnetic Resonance Imaging

MU: Monitor Unit

NI: National Instruments

NLP: Nonlinear Programming

NRC: National Research Council

NTCP: Normal Tissue Control Probability

OAR: Organ At Risk

OCE: Optimization Convergence Errors

OOP: Object-oriented Programming

OS: Operating System

PB: Pencil Beam

PCUT: Photon cutoff energy

PEGS: Preprocessor for EGS

PET: Positron Emission Tomography

PTV: Planning Target Volume

QA: Quality Assurance

QUANTEC: Quantitative Analyses of Normal Tissue Effects in the Clinic

Real SQL: SQL in Real Studio

RFA: Radiation Field Analyzer

RT: Radiation Therapy

RTOG: Radiation Therapy Oncology Group

SIB: Simultaneous Integrated Boost

SQL: Structured Query Language

SSD: Source to Surface Distance

TCP: Tumour Control Probability

TPS: Treatment Planning System

US: Ultrasound

V_{1Gy}: Volume receiving at least 1 Gy of dose

V_{2Gy}: Volume receiving at least 2 Gy of dose

V_{5Gy}: Volume receiving at least 5 Gy of dose

VMAT: Volumetric Modulated Arc Therapy

VR: Value Representation (DICOM)

XVMC: X-ray Voxel Monte Carlo

Definitions

D: Dose, nominal SI units of Gy

μ_{en}/ρ: Mass energy absorption coefficient cm^2/g

m: Mass kg

AAA: Analytical Anisotropic Algorithm developed by Varian Medical Systems for MV photon dose calculation

BEAMDP: BEAM Data Processor used to analyze the phase-space parameters

Beamlet: Small-sized beam of collimated radiation

BEAMnrc: Monte Carlo simulation system for modelling radiotherapy sources

Bolus: Water/tissue equivalent material which can be used in electron treatments for tissue compensation or beam modulation

Chi-squared: The sum of the squares, to test variance of a normally-distributed population

DOSXYZnrc: An EGSnrc-based Monte Carlo simulation code for calculating dose distributions in a rectilinear voxel phantoms

Eclipse: Treatment planning software developed by Varian Medical Systems

EGSnrc: Electron Gamma Shower Monte Carlo code for particle transport of coupled electron-photon

EGSPhant: a DOSXYZnrc file type for containing phantom properties

Field: An area covered by a radiotherapy beam

Fractionation: When the total dose of radiation is divided into several, smaller doses over a period of several days

Gantry: A device for rotating the radiation delivery beam around the patient

Hypoxia: A condition in which an area or region of the body is deprived of adequate oxygen supply

Isocentre: A point in space where the central axis of rotation exist. The mechanical isocentre is the point where the gantry, collimator, and couch rotation intersect.

Normal cells and healthy tissue: All disease free cells and tissues

Pareto surface: A solution that cannot be further improved in any volume of interest without worsening another volume of interest

Phase-space: Information relating to particle position, direction, and charge

$R_{90\%}$: Therapeutic range of an electron field, defined at the 90% dose level

RapidArc: Advanced mode of MV photon treatments which utilize 360° arcs for delivery of VMAT on Varian linacs, developed by Varian Medical Systems

REALBasic: Object-oriented language developed by Real Studio

TomoTherapy System: Advanced mode of 6MV photon treatments which utilize a 360° helical fan-beam mode for delivery of VMAT. Owned by Accuray

X-ray: Proton radiation emitted by electrons outside nucleus

XVMC: X-ray Voxel Monte Carlo code for photon and electron particle transport in rectilinear phantoms

Index List